TG 371-5
May 1963

PROCEEDINGS of the THIRD MEETING

TECHNICAL PANEL ON SOLID PROPELLANT COMBUSTION INSTABILITY

Held at the Applied Physics Laboratory
Silver Spring, Maryland
March 4 and 5, 1963

APPLIED PHYSICS LABORATORY • THE JOHNS HOPKINS UNIVERSITY

TG 371-5
May 1963
Copy No.

133

Proceedings of the Third Meeting

Technical Panel on Solid Propellant Combustion Instability

Held at the Applied Physics Laboratory
Silver Spring, Maryland
March 4 and 5, 1963

THE JOHNS HOPKINS UNIVERSITY
APPLIED PHYSICS LABORATORY
8621 Georgia Avenue, Silver Spring, Maryland

Operating under Contract NOw 62-0604-c with the
Bureau of Naval Weapons, Department of the Navy

BLANK PAGES
IN THIS
DOCUMENT
WERE NOT
FILMED

INTRODUCTION

The 3rd Meeting of the Panel on Solid Propellant Combustion Instability (SPIC) was held March 4-5, 1963 at the Applied Physics Laboratory, The Johns Hopkins University. In view of overlapping membership and in order to economize on participants' time, it was scheduled jointly, as in the previous year, with the 5th AFOSR Contractor's Meeting on Solid Propellant Combustion.

One of the important functions of the Panel is to bring together active workers and research administrators approximately once a year; to schedule informal reports on research findings and plans; and to emphasize those points where detailed discussion can prove illuminating.

The papers in this report represent, in various degrees of condensation, results acquired during 1962. Since these Panel meetings are primarily intended to provide opportunities for the exchange of information on work in progress, the contributions are not to be judged by the standards of papers submitted for publication in professional journals. Rather, they are summaries of status reports whose principal purpose is to elicit comments and to indicate the direction in which the more promising lines of work are pointing.

The vigor of the research effort in the field of combustion instability is undeniable. The experimental programs, in particular, are beginning to "zero in" on quantitative measurements of the acoustic admittance of burning propellants, a goal that was only dimly visible three years ago. Attention is directed to the papers on the exploitation of the self-excited resonance tube technique (reported in more detail in the Proceedings of the Ninth Symposium on Combustion in contributions from NOTS, BRL, and the University of Utah). In addition, Dr. S. N. Foner described two novel measuring techniques which, if successful, would lend themselves to meaningful determinations of the amplification characteristics of propellants burning within cavities, without the limitation that the propellant system produce "spontaneous" oscillations.

The intricacies of the instability phenomena (and, in particular, the difficulty of performing proper experimental measurements) are well demonstrated in the comments of Dr. R. Cantrell on the corrections to be applied to admittance determinations in a T-burner. This interplay between experiment and theoretical interpretation (which is repeated again in the discussion of "entropy waves" by Summerfield et al.) represents one of the most fruitful aspects of the Combustion Instability research program.

Altogether, more than ten papers addressed themselves to measurements of acoustic admittance. Others dealt with observations on nonlinear and nonresonant instabilities, the fluid dynamics of the flow process, the interaction of oscillation with the ballistic properties of the propellant, viscoelastic properties, etc. The amount of stimulating work was such that the technical sessions extended late into the afternoons. Thanks are due to the authors for their prompt effort in making available their condensed remarks.

The papers included in these Proceedings are the ones dealing specifically with Combustion Instability problems. A complete listing of all papers presented at the joint meeting is given on pages 187 to 189.

The following newly appointed Panel Members attended: Professor A. O. Converse (Carnegie Institute; Pittsburgh, Pa.), Dr. I. Dyer (Bolt. Beranek and Newman; Boston, Mass.), Dr. G. R. Leader (Thiokol; Elkton, Md.).

The financial assistance of the Advanced Research Projects Agency, Chemistry Office, in support of the SPIC Panel is gratefully acknowledged.

TABLE OF CONTENTS

THE LARGE SOLID MOTOR PROGRAM

William Cohen
Chief, Solid Propulsion Systems
Office of Manned Space Flight
NASA

In November of 1962, a solid motor feasibility program was jointly accepted by Administrator, NASA, and Secretary of Defense. The program will establish the feasibility of solid propellant motors with capabilities for use in very large launch vehicles for massive space missions. The motors to be evaluated will have thrust capability in the range of 6 to 10 million pounds each, will be approximately 23 feet in diameter by 100 feet long, and will contain over 3 million pounds of propellant.

The authorized program involves the manufacture and test of a total of six motors of this class. The first four will be of the full diameter but approximately half-length. The last two will be of full performance characteristics. The motors will be made in one piece.

As sub-scale tools for the evaluation of nozzle materials and thrust vector control, segmented motors 156" in diameter will be made and fired. In general, these will contain no more than 400,000 pounds of propellant and probably will consist of one or two center segment designs. At least one of these motors will contain propellant with burning rate and charge design to produce 3 million pounds of thrust for duration of approximately 60 seconds. The purpose of this motor is to evaluate the full diameter nozzle of the half-length 260" motor.

The most probable application of the motors in the 6 million pound thrust class is in booster stages of very large launch vehicles with payload capability of approximately 1 million pounds in earth orbit. Upper stages of such vehicles will probably consist of liquid-hydrogen, liquid-oxygen motors. The solid propellant motors will probably be used in clusters of four, producing stage thrust of 25 to 35 million pounds.

The dimensions of the solid motor may result in fundamental oscillatory modes which can induce or maintain combustion instability, with all its detrimental effects. These might extend beyond the motor itself into the relatively fragile liquid propellant stages and possibly into the human payload. This possibility must be reduced to the vanishing point; but the high cost of the motors (perhaps $10 million each) will limit the numbers available for development and testing. Thus, the advent of very large solid propellant motors for space launch vehicles raises conflicting conditions; high reliability and compatibility with manned payloads and liquid stages must be established, but extensive test and development programs are not possible.

PROGRESS OF WORK AT SUMMERFIELD RESEARCH STATION AND THE UNIVERSITY OF SHEFFIELD, ENGLAND

G. F. P. Trubridge
Imperial Chemical Industries

and

G. Sotter
University of Sheffield, England

At Summerfield Research Station, which is managed by Imperial Metal Industries Limited (a subsidiary of Imperial Chemical Industries Limited) on behalf of the Ministry of Aviation, work is carried out involving combustion research and the design, development and production of solid propellant rocket motors for the Services.

In the present report emphasis is placed on the research effort devoted to the elucidation of the phenomena associated with combustion instability. With this objective, programmes of theoretical and experimental investigations are being pursued at Summerfield Research Station and at the University of Sheffield under a Ministry of Aviation contract.

During the three years of activity of the Solid Propellant Combustion Instability Panel, considerable advances have been made towards an understanding of the general problems of instability. The output of theoretical and experimental papers has been prolific, so that the task involved in interpreting these contributions to the state of knowledge and obtaining the results in an effective form suitable for use by the designers of rocket motors, has now become a major problem of communication.

As some contribution towards bridging the gap between the basic research and applied fields, the author has carried out a detailed examination of the theory of unstable combustion developed by the group at the Applied Physics Laboratory, under the general direction of Dr. F. T. McClure. Expanded versions of the five principal papers have been prepared, which will be circulated to members of the Panel. (1) to (5). These five papers comprise Parts 2 to 6 of a general report. Part 1, which is in preparation, will provide a general survey of the whole field of investigation on unstable combustion in non-mathematical terms. Further parts on already published work are in preparation, and additional parts will be prepared should the need arise.

In these expanded versions all formulae developed in the original papers have been derived in full and a certain amount of relevant background material has been included. The text of the original papers has been closely followed and expansions of the material have only been made where these might help the reader towards attaining a proper appreciation of the physical, chemical and mathematical principles involved, without undue effort and absorption of time.

The present author has reserved for future reports any comments on his excursions into the many supplementary issues raised by

studying the theory developed at the Applied Physics Laboratory. He is also not unaware of the many other valuable contributions, both theoretical and experimental, which have been made by a number of investigators, but some selection has to be made by each individual from the vast amount of material available in this intriguing field of study.

The programme on instability at Sheffield University under the direction of Prof. M. W. Thring, and conducted by Mr. J. Swithenbank and Mr. G. Sotter is now under way. The principal objectives are to obtain a better understanding of the details of the chemical processes occurring in the combustion zones by spectroscopic and other methods, and to determine the processes involved in the "coupling" between "oscillatory" and "irregular" burning.

The emission spectra from a leaded double-base propellant are being studied under stable conditions, and in particular the 2596 Å band of nitric oxide has been selected for investigation under unstable conditions. The work, however, is still in an early stage; a full report will be presented later for circulation to the Panel members.

Changes in mean chamber pressure in rocket motors departing from the expected value are referred to as "irregular burning". This phenomenon is generally accepted as being "triggered" in some way by small amplitude oscillatory pressure variations. High speed cine photos (1000 to 3000 frames per second) have been taken, which show that at least some of the pressure peaks arising in unstable burning are associated with vortices in the flow. This phenomenon has been known about, at least qualitatively, for over twenty years and has been mentioned by a number of investigators. Detailed references to this work will, however, be deferred for a full report on the subject which is in preparation.

At the Panel meeting a cine film was presented of the unstable burning of a six-inch slotted radial burning charge in a non-aluminized cast double-base propellant, which was photographed through the transparent (4-inch "Perspex") end of a window motor. At three stages during the firing, which lasted six seconds, a single vortex was formed which filled the entire chamber. The duration of each vortex was about one tenth of a second, and the times of occurrence correlated with irregular peaks in the pressure time record. From visual observation, the rotational gas speed has been estimated to be about Mach 0.2 at the forward end of the motor. This type of instability can be expected to produce barrelling in the conduit, which has been observed in interrupted firings by Trubridge (6).

This single vortex shows velocity profiles for acoustic streaming associated with the first transverse travelling mode. (See Plates 1A and 1B.) Acoustic streaming is a classical phenomenon which has been discussed by Rayleigh (7) and Moore and Maslen (8) among others. In the case of a solid propellant rocket motor, the flow is altered by transpiration of mass and energy on the propellant

surface. The rotating gases are forced towards the centre, increasing their speed of rotation to conserve angular momentum. The theoretical treatment of the phenomena involves solution of three-dimensional compressible viscous flow equations and boundary layer equations with mass and energy added and is under active investigation.

Much of the instability of the propellant-motor combination under review has, however, been associated with the first and second standing transverse modes (9). Streaming diagrams for these modes are given in Plates 2A, 2B, 3A and 3B. The prints on these plates show smoke patterns produced by solid particles in the combustion products, which have been transported to the center following the streamlines shown, and have begun to cool as they travel back towards the propellant surface. Both the oval and the cruciform shapes are relatively stable, remaining in one orientation for several tenths of a second; they may, however, rotate slowly. In the film in which these shapes were observed, at one period the oval could be seen oscillating between two orthogonal positions; this was apparently an attempt by the second transverse mode to establish itself, for the cruciform shape appeared shortly thereafter. The eight vortices formed by the second transverse mode should tend to erode the propellant in eight places around its inner circumference late in the firing; this has in fact been observed in interrupted firings of similar charges by Trubridge (6).

A film was made for a charge with a six-point star configuration and suggested the presence of small vortices in the points of the star.

In the development of the theory of instability of solid propellant rocket motors, recourse has had to be made to empirical laws for the pressure rate of burning, where the velocity of flow of the propellant gases over the burning surface is negligibly small, and for the erosive rate of burning, where the velocity of flow of the gases is relatively large. Well founded theories for both pressure and erosive rate of burning under stable conditions, especially if they included the treatment of transient (time dependent) behaviour,would be very valuable in improving the basic concepts underlying current theories of instability. Several investigators have tackled the problem of development of a theory of the pressure rate of burning under stable conditions with some limited success, but much more work is needed.

The present author, in parallel with the studies at the Armour Research Foundation (10), is making continued efforts to develop a quantitative theory of erosive burning based on fundamental principles of the change of combustion rates by heat transfer and chemical reaction processes from a high speed, high temperature, accelerating compressible gas mixture, through the boundary layers and reaction zones of the burning propellant. Studies of current theories of erosive burning involving simplified treatment of the boundary layer equations,with transpiration, have been made, but

these are by no means satisfactory from the point of view of applying them to instability problems, even though the authors claim good agreement with some experimental results after fitting values for the available free parameters. The theories should also include, but do not, an interpretation of the so-called "negative" erosion, in which the erosive burning rate is smaller than the corresponding pressure burning rate. So far the chemical, physical and analytical difficulties arising, especially these associated with the interaction of the boundary layer flow itself and the combustion zones, and with the degree of laminar or turbulent flow in the main gas stream, have proved insurmountable.

One of the many significant deductions from the theory of instability developed by the group at the Applied Physics Laboratory is the importance of considering the whole acoustic field of the rocket motor, and in particular the acoustic features of the solid propellant itself. A small group has been set up at Summerfield Research Station to study the visco-elastic behaviour of propellants, including the dynamic response phenomena. It is hoped to obtain experimental results which can be used in the theoretical investigations on instability.

REFERENCES

1. Expanded version of "Combustion Instability: Acoustic Interaction with a Burning Propellant Surface", by R. W. Hart and F. T. McClure. J. Chemical Physics 30, 1501-1514, 1959.

2. Expanded version of "Acoustic Resonance in Solid Propellant Rockets", by F. T. McClure, R. W. Hart and J. F. Bird. J. Applied Physics 31, 884-896, 1960, and Solid Propellant Rocket Research (edited by M. Summerfield), p. 295, 1960.

3. Expanded version of "The Influence of Erosive Burning on Acoustic Instability in Solid Propellant Rocket Motors", by R. W. Hart, J. F. Bird and F. T. McClure. Solid Propellant Rocket Research, p. 423, 1960.

4. Expanded version of "Effect of Propellant Compressibility on Acoustic Instability", by J. F. Bird, L. Haar, R. W. Hart and F. T. McClure. J. Chemical Physics 32, 1423-29, 1960.

5. Expanded version of "On Amplification and Attenuation of Sound by Burning Propellants", by R. W. Hart and R. H. Cantrell, Applied Physics Laboratory SPIC 50, 1962.

6. "Unstable Burning in Solid Propellant Rocket Motors", by G. F. P. Trubridge. 2nd Rocket Propulsion Symposium, Cranfield, 1962.

7. "Theory of Sound" by Lord Rayleigh, 1878-1896, Dover edition, Vol.II, p. 333, 1954.

8. "On Strong Transverse Waves without Shocks in a Circular Cylinder", by S. H. Maslen and F. K. Moore. J. Aero. Sciences 23, 583-593, 1956.

9. "Investigation of Combustion Instability in Solid Propellant Rocket Motors", by G. Sotter. Progress Report No. 3, University of Sheffield, Department of Fuel Technology and Chemical Engineering (1963).

10. Analytical Investigation of Combustion Instability in Solid Propellant Rockets, by W. J. Christian. Armour Research Foundation ARF Project D244, SPIC 61, 1962.

Plate 1A - PRINT OF FRAME FROM HIGH-SPEED CINEFILM TAKEN DURING IRREGULAR BURNING IN SLOTTED RADIAL BURNING CHARGE IN CAST DOUBLE-BASE PROPELLANT. (DIAMETER OF BURNING ZONE IS ABOUT 3½ INCHES. ROTATION IS COUNTER-CLOCKWISE. THE MOTOR, WITH A FORE END OF PERSPEX, WAS DEVELOPED AND SUPPLIED BY THE SUMMERFIELD RESEARCH STATION OF IMPERIAL METAL INDUSTRIES LIMITED.

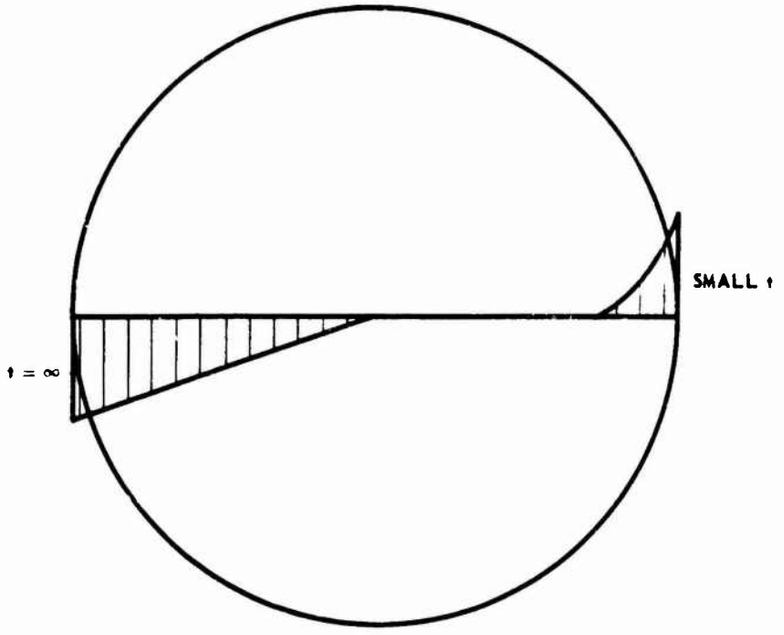

Plate 1B - VELOCITY PROFILE WITH RESPECT TO RADIUS AND TIME (t) FOR ACOUSTIC STREAMING ASSOCIATED WITH FIRST TRAVELLING TANGENTIAL MODE.

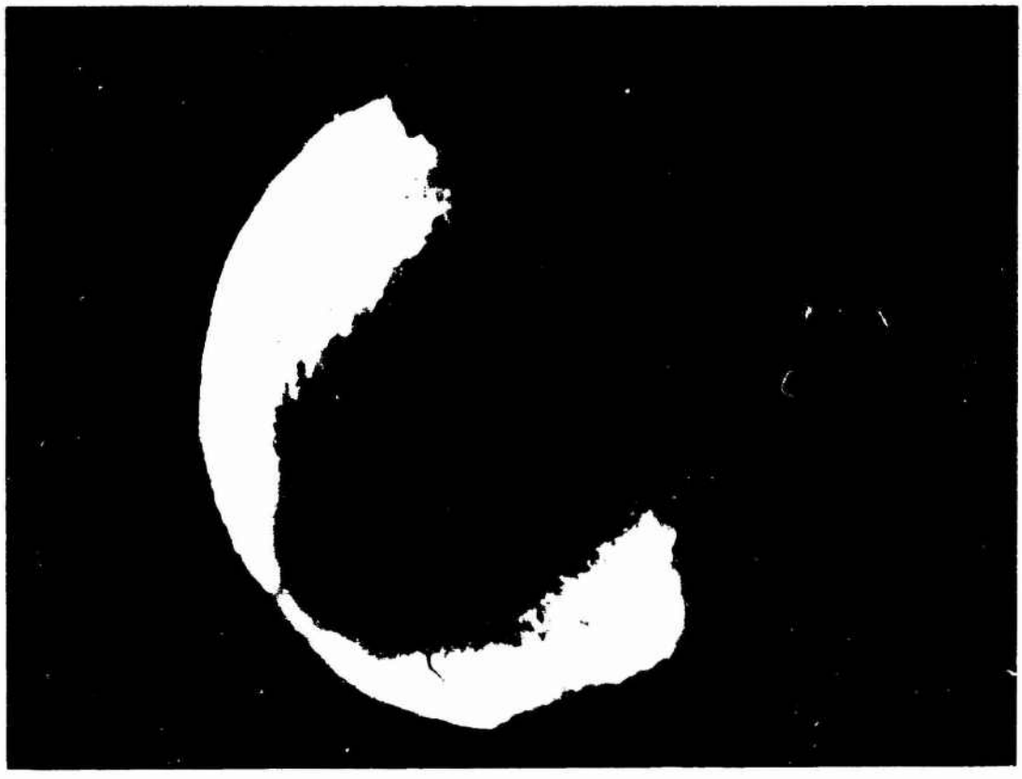

Plate 2A - OVAL-SHAPED SMOKE PATTERN (PARTLY OBSCURED BY BLACKENING OF WINDOW) OBSERVED IN HIGH-SPEED CINEFILM. CIRCULAR AXIAL PERFORATION IS ABOUT 4 INCHES IN DIAMETER.

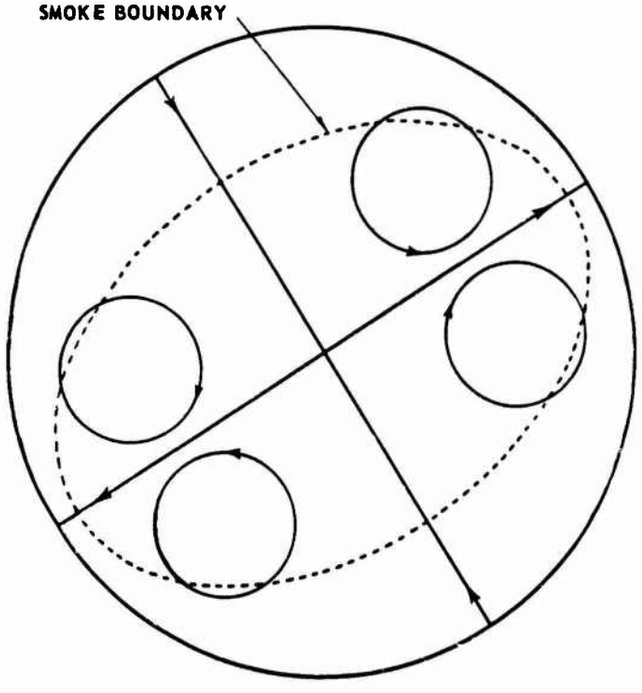

Plate 2B - ACOUSTIC STREAMING PATTERN ASSOCIATED WITH FIRST STANDING TANGENTIAL MODE INCLUDING MASS TRANSFER EFFECTS.

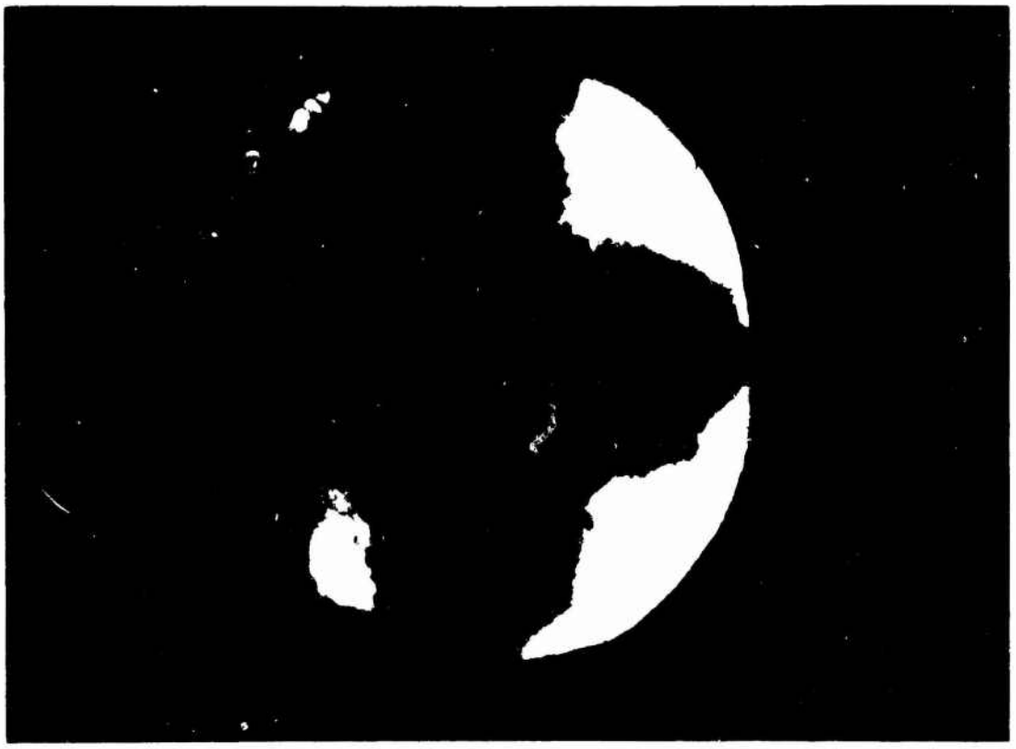

Plate 3A - CRUCIFORM SMOKE PATTERN (PARTLY OBSCURED BY BLACKENING OF WINDOW) OBSERVED LATER IN FIRING FROM WHICH *Plate 2A* PHOTOGRAPH WAS TAKEN. CIRCULAR AXIAL PERFORATION IS ABOUT 4½ INCHES IN DIAMETER.

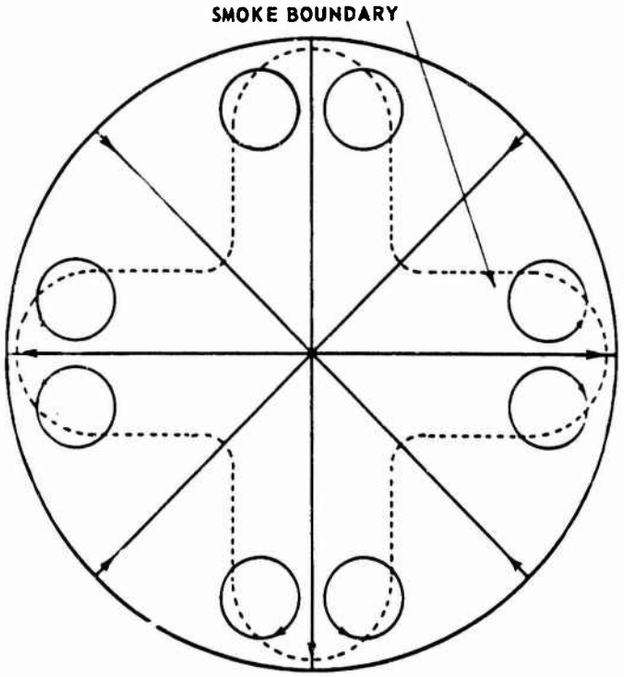

Plate 3B - ACOUSTIC STREAMING PATTERN ASSOCIATED WITH SECOND STANDING TANGENTIAL MODE INCLUDING MASS TRANSFER EFFECTS.

APL EXPERIMENTAL PROGRAM*

S. N. Foner
Applied Physics Laboratory
The Johns Hopkins University

I. INTRODUCTION

The experimental program on combustion instability at the Applied Physics Laboratory is concerned principally with measurements of acoustic interactions with solid propellants, and, in particular, with the measurement of the acoustic admittance of a burning solid propellant surface.

Two rather promising methods for the measurement of acoustic admittances of burning propellant surfaces have been devised. Both methods employ resonant acoustic cavities to attain high sensitivity. In one method, the burning propellant serves as a random noise source to excite various resonances in the cavity. From measurements of the power spectral density distribution for any particular mode it is possible, in principle at least, to determine the bandwidth and, therefore, the Q of the cavity, which in turn is a function of the admittance of the burning surface. There are a number of attractive features in this system; namely, the apparatus is simple, the system is self-tuning, and several modes may be excited simultaneously, permitting admittance measurements to be made at several frequencies. The major disadvantage is that the analysis of the data involves a complex computational program consisting of digitizing the data, computing the correlation function $\psi(\tau)$, and then calculating the cosine transform,

$$W(f) = r\int_0^\infty \psi(\tau)\cos 2\pi f\tau \, d\tau$$

to obtain W(f), the power spectrum as a function of frequency. A complication is introduced by the fact that the resonant frequencies are not constant, but change with time due to regression of the burning surface and to variations in the temperature and composition of the propellant gases.

In the second method, the acoustic cavity is used as the frequency-determining element of an oscillator, with energy being

*The work reported was carried out in collaboration with R. L. Hudson and B. H. Nall.

supplied by an external phase-locked mechanical driver. A simplified schematic diagram of such a system is shown in Fig. 1. The mechanical driver excites the cavity at a selected resonant frequency. The signal is picked up by a microphone, amplified, filtered, phase-shifted appropriately, and fed back to the driver in such a way as to keep the system oscillating at resonance. The problem remaining is to design an electronic scheme for measuring the bandwidth or Q of the resonance. As we shall discuss later, a practical system for carrying out these measurements requires rather elaborate electronic instrumentation.

In comparing the two methods it will be noted that in the first method, the instrumentation is relatively simple and the heavy load is placed on the data analysis phase of the program; in the second method, while the electronic instrumentation is complicated, there is no requirement for a complex computational program. In contrast to admittance measurement techniques which use unstable propellant systems and determine the rates of growth and decay of pressure oscillations, both methods described here are applicable to stable propellant systems.

II. EXPERIMENTAL APPARATUS

The acoustic cavity used is essentially a steel pipe 2.0 in. ID by 20 in. long which has approximately 200 holes 1/16 in. diameter drilled in the midplane to exhaust the propellant gases. The cavity is mounted vertically inside a pressurized vessel. This arrangement results in pressure equalization between the inside and outside of the acoustic cavity and thereby permits the use of sensitive microphones for sound pressure measurements. For the experiments in which the propellant serves as a noise source, two water-cooled Altec-Lansing high intensity type 21BR-180 and 21BR-200 microphones are mounted in the top of the cavity. In the phase-locked driver experiments, the top of the cavity is replaced by the driver assembly and only one microphone is used. A modified torpedo flask connected to the pressure vessel serves as a ballast tank and limits the overall pressure rise during a run to about 10 psi.

The experiments to date have been carried out with a composite double base propellant (DQO) furnished to us by T. A. Angelus of the Allegany Ballistics Laboratory. The propellant is 2.00 in. in diameter and 1.00 in. long and is mounted in the bottom of the cavity. Figure 2 shows the cavity loaded with a propellant prior to being lowered into the pressure vessel. The array of exhaust holes for the propellant gases are clearly visible in the photograph. The propellant is ignited by switching a 110 volt ac line across a zig-zag nichrome wire in contact with the propellant surface which has been sprinkled lightly with black powder. The

system is pressurized to 200 psi with super-dry nitrogen prior to firing. Burning time for the 1 in. length propellants used is about 9 seconds.

III. NOISE EXCITATION OF CAVITY RESONANCES

The noise spectrum generated by the burning propellant was recorded on a multi-channel tape recorder and given a preliminary analysis by playback through a Raytheon Rod Spectrum Analyzer. Some rather interesting effects were observed. On ignition a series of modes were excited. The fundamental was the strongest signal throughout the run. Starting at about 340 cps, its frequency moved up to an equilibrium value of about 740 cps in about 3 seconds and then remained approximately constant. A more careful measurement on the frequency of the fundamental showed that it was actually decreasing slowly during the last half of the run, as expected, due to regression of the propellant surface and consequent increase in cavity length.

In addition, excitation of the second and third harmonics, as well as the lowest Helmholtz frequency, were observed. A mode splitting phenomenon was noted in the case of the second and third harmonics. This effect presumably occurs because of temperature differences in the cavity. The lower half of the cavity which is being swept out by the propellant gases is at a considerably higher temperature than the upper half of the cavity which relies principally on convection for heat transfer. One way of considering the mode splitting effect is to treat the cavity as a coupled system consisting of two parts having different physical properties, and, therefore, capable of simultaneous excitation at two somewhat different frequencies.

The data from this experiment are being analyzed by a computer program in an effort to determine the power spectra associated with the resonances. Since noise levels during stable propellant burning are generally too low to be measured by conventional instrumentation, the actual sound levels encountered may be of some interest. In the run described, the two microphones recorded an average sound level of 115 db or about 100 dynes/cm^2.

IV. PHASE-LOCKED OSCILLATOR SYSTEM

The phase-locked acoustic oscillator system uses a tracking filter to follow frequency changes and employes a phase modulation scheme for rapid determination of bandwidth. A simplified block diagram of the apparatus is shown in Fig. 3. The driver excites

the audio cavity containing the propellant at a selected resonant frequency. The signal is picked up by the microphone, amplified, and sent to a phase-lock tracking filter which contains a voltage controlled oscillator (VCO) and crystal oscillator whose signals when combined in a mixer produce an audio signal at the driver frequency. A power amplifier closes the feedback loop. A phase modulation technique is employed to center the frequency precisely on the resonance maximum and to measure the bandwidth of the system. For this purpose, a low frequency modulation (33 cps) is injected into the phase modulator. If the system is being driven off resonance, this will be detected as AM modulation and will be observed on the phase shift indicator. The phase shifter is adjusted to bring the indicator reading to zero. The bandwidth is obtained from the output of a phase detector which measures the amplitude of the sidebands produced by the low frequency (33 cps) modulation. For a cavity of very high Q, the sideband amplitude (or phase modulation) received at the microphone will be very small, while for a low Q cavity the sideband amplitude will be large. This arrangement provides a very convenient means for rapid measurement of the Q of systems whose frequencies are varying with time. An additional phase detector compares the audio output from the microphone with the signal driving the cavity and thus gives a direct readout of signal amplitude.

The complete phase-locked acoustic analyzer system was successfully tested in an experiment with a burning propellant. Some of the salient features of the experiment are shown in Fig. 4. Prior to ignition the oscillator was locked onto the fundamental mode ($\lambda = 2L$) at a frequency of 350 cps. The measured Q of the system was 200, corresponding to a bandwidth of 1.75 cps. On firing, the tracking oscillator moved up in frequency, but inadvertently locked onto a Helmholtz resonance at about 500 cps. This is a low Q mode, as is evident from the small amplitude of the signal. During this period, the bandwidth was so large that the amplifier used in making the recording trace in Fig. 4 was overloaded. At about 4 sec. after ignition, lock-on to the fundamental mode at 740 cps was achieved. No particular loss of data was incurred by the failure to achieve lock-on earlier, since the system requires a few seconds to reach temperature equilibrium. The bandwidth after attaining lock-on at the fundamental frequency was about 0.5 cps, corresponding to a cavity Q of about 1400. An independent confirmation of this rather high Q was obtained from calculations based on the rate of growth of the signal amplitude following lock-on. It will be noted that substantial variations in amplitude and bandwidth occur during burning, indicating that some physical parameter in the system, most likely the propellant response, is fluctuating. The frequency plot also shows some irregularities, but the effect is considerably smaller than in the case of amplitude or bandwidth. The decrease in cavity frequency due to propellant regression can be seen on the frequency plot. When the propellant burns out, the frequency drops, the bandwidth increases, and the amplitude at first decreases and then is followed by an increase due to the higher efficiency of the acoustic driver at lower frequencies.

A rather unexpected effect on the damping of the cavity was observed after propellant burnout. About 3 seconds after the run, the amplitude started to go down accompanied by an increase in bandwidth. At about 8 seconds, the Q of the cavity was degrading rapidly. It reached a minimum at about 30 seconds and then recovered slowly. At the minimum in cavity Q, the amplitude had dropped by a factor of 12 compared to pre-run conditions, corresponding to a decay constant α of about 65 sec^{-1}. It has been suggested by R. W. Hart and R. H. Cantrell that the observed damping is due to condensation of water vapor in the cavity to form droplets, and calculations have been made to show that the magnitude of the damping can be accounted for with reasonable choice of parameters.

Further analysis of the data from this test is in progress. In order to obtain meaningful values of the propellant admittance from the experimental data on the cavity Q, it will probably be necessary to put in corrections for gas flow and for the non-uniform temperature distribution in the cavity with the resulting displacement of the exhaust holes from the nodal plane.

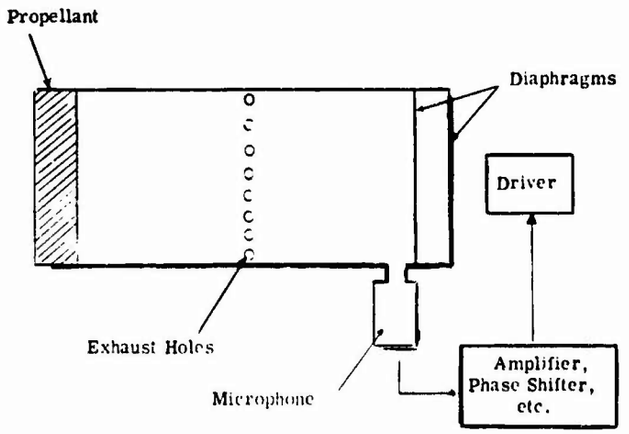

Fig. 1 SCHEMATIC DIAGRAM OF AN ACOUSTIC OSCILLATOR WITH CAVITY AS FREQUENCY-DETERMINING ELEMENT

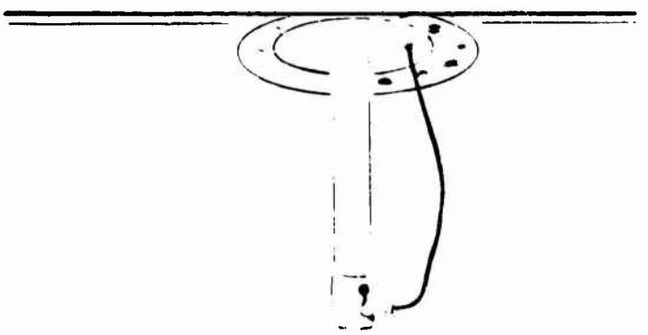

Fig. 2 CAVITY ASSEMBLY PRIOR TO BEING LOWERED INTO PRESSURE TANK

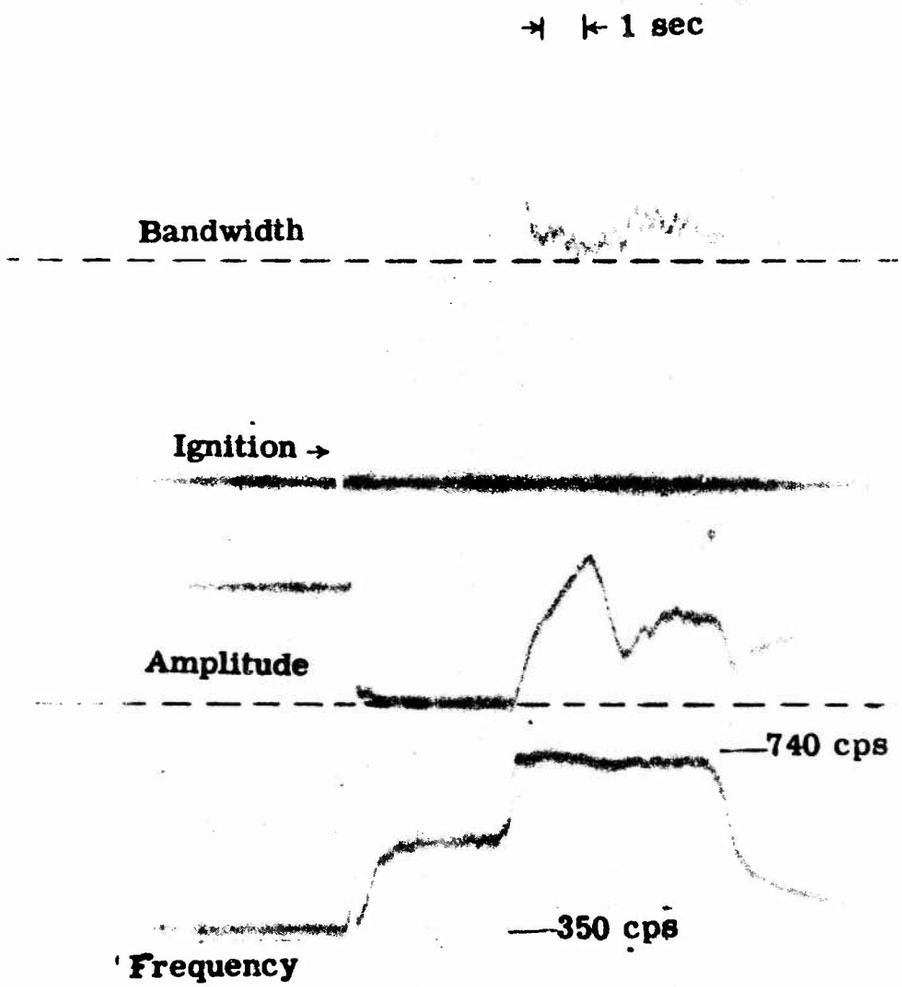

Fig. 4 EXPERIMENTAL RESULTS OF TEST WITH BURNING PROPELLANT

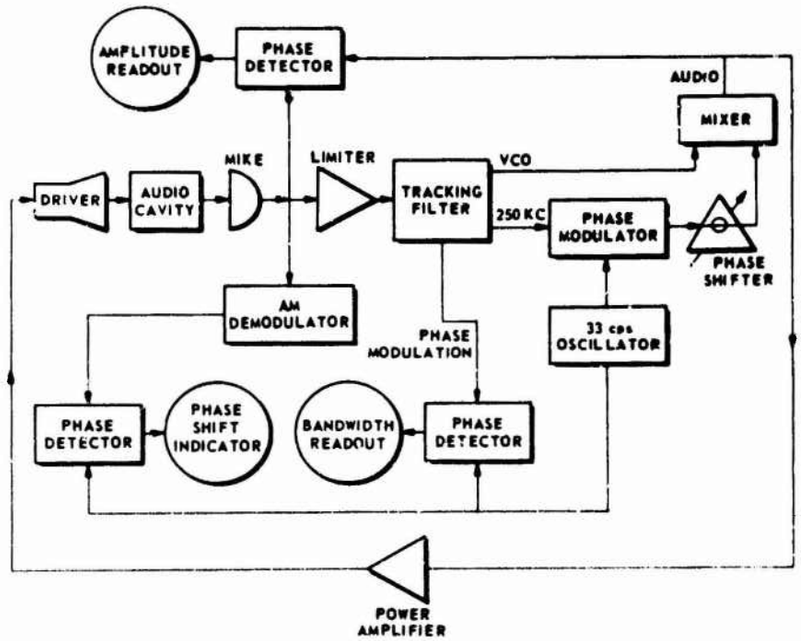

Fig. 3 SCHEMATIC DIAGRAM OF PHASE-LOCKED ANALYZER SYSTEM

EFFECT OF PROPELLANT VARIABLES ON RESPONSE FUNCTION*

M. D. Horton
U. S. Naval Ordnance Test Station
China Lake, California

This program used a self-excited double-end burner to study the effect of several propellant variables upon the response function of the combustion zone of a propellant at 200 psig. A PBAA-AP composite propellant was used for the study and the variables involved were ammonium perchlorate particle size, the effect of one percent copper chromite as an additive, and the effect of one percent LiF as an additive.

The propellants tested and their designations are listed in Table I. Figure 1 shows the response functions of the propellants. The results speak for themselves as to the complexity of the problem. At this time there seems to be no general explanation of the trends.

Table I

Propellant designation	Polybutyl acrylic acid copolymer (%)	80μ Ammonium perchlorate (%)	15μ Ammonium perchlorate (%)	Copper chromite added (%)	LiF added (%)
A-13	24	76	0	0	0
A-14	24	0	76	0	0
A-15	24	76	0	1	0
A-16	24	0	76	1	0
A-17	24	76	0	0	1
A-18	24	0	76	0	1

*Sponsored by Special Projects Office of Bureau of Naval Weapons.

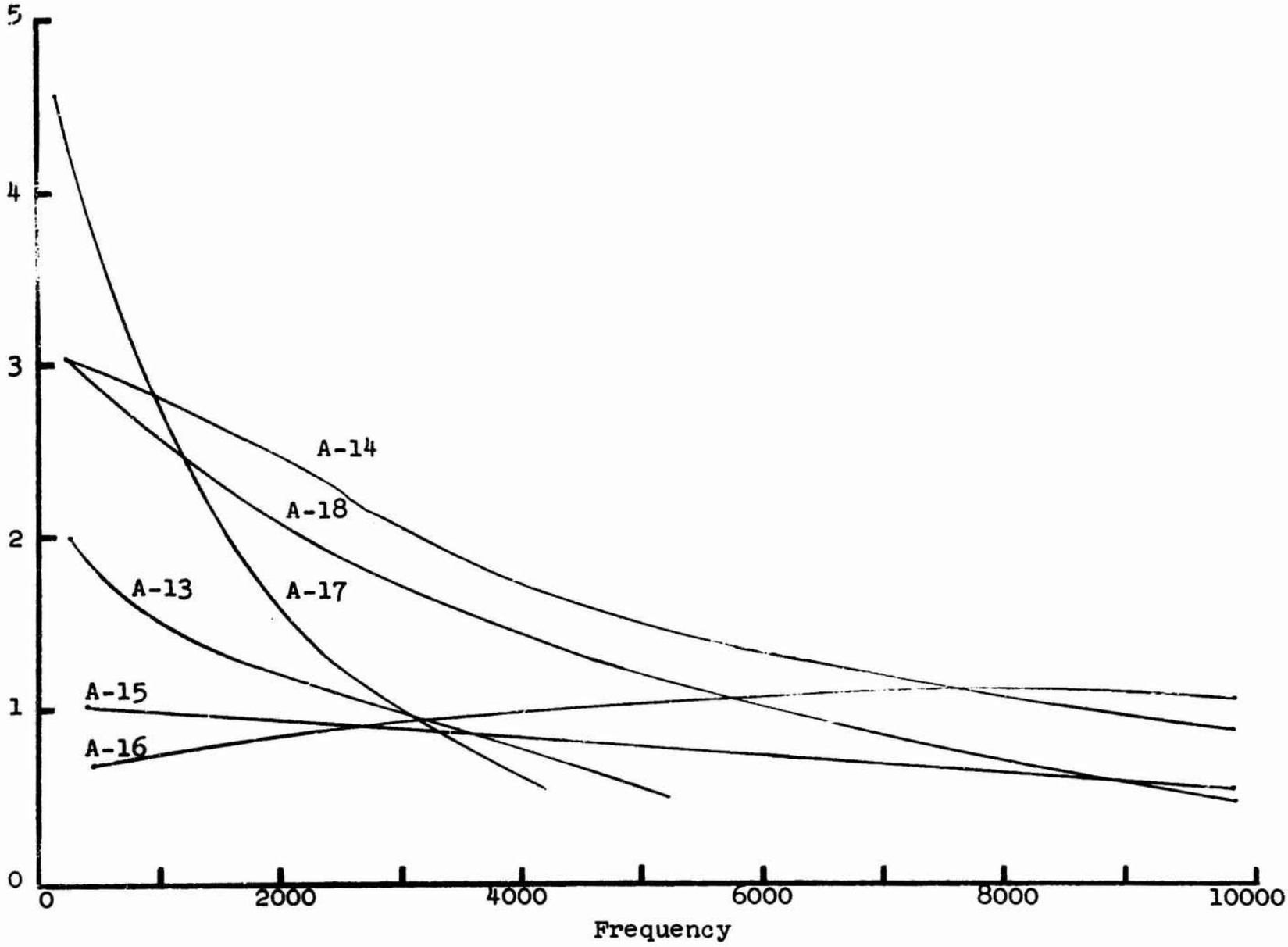

Fig. 1 RESPONSE FUNCTIONS OF THE PROPELLANTS LISTED IN TABLE I.

MECHANISM OF SUPPRESSION OF OSCILLATORY BURNING BY ALUMINUM ADDITIVES*

M. D. Horton
U. S. Naval Ordnance Test Station
China Lake, California

In this series of experiments, a self-excited, double-end burner was used to study the oscillatory behavior of several variations of a PBAA-AP composite propellant. These variations were identical except that some contained small amounts of aluminum or alumina as an additive. Oscillatory tests were made with each propellant over the frequency range of 1,500 to 10,000 cps at 200 psig. From each oscillatory test record, the exponential growth decay constants of the oscillations were determined. These exponential growth constants were then used to calculate the response functions of the combustion zones of the propellants and, within the accuracy of the method, it was observed that all of the variations had the same response function-frequency curve.

Observation of the growth and decay constants showed that the oscillations generally grew less rapidly when the propellant contained an additive and the oscillations decayed more rapidly after burnout. For the aluminum additives, the suppression increased directly with concentration (for concentrations of 0, 0.5, 1.0, and 1.5%), decreased with the particle size of the aluminum (for the 25μ, 5μ, and 0.2μ aluminum tested), and increased with pressure (400 psig compared to 200 psig). At the same concentration level, the alumina was roughly half as effective as the 25μ aluminum.

Inasmuch as the Al and Al_2O_3 did have a suppressive action on the oscillations of the additive-containing propellants and yet seemed not to affect the response function of the combustion zone, it was believed that the additives functioned through a damping mechanism. The theory of Epstein and Carhart treats the viscous damping action of particles suspended in a gas and this theory was used to examine the data. It was found that, under reasonable assumptions, the increased viscous damping caused by the condensed-phase particles introduced into the combustion gas by the additive would qualitatively explain the experimental results. The conclusion was therefore drawn that the viscous damping action of alumina droplets in the combustion gas accounted for at least a large fraction of the stabilizing influence of these additives in this propellant.

* Sponsored by the Special Projects Office of the Bureau of Naval Weapons.

ACOUSTIC WALL LOSS THEORY

R. H. Cantrell
Applied Physics Laboratory
The Johns Hopkins University

INTRODUCTION

The usual acoustic theory of wall losses (Ref. 1, for example) is not appropriate for the conditions found in rocket motor or test apparatus cavities. This theory is applicable to cavities with no mean flow and with rigid isothermal walls where the wall temperature and undisturbed gas temperature are identical. In a rocket cavity, there is a steady state flow in the absence of acoustic disturbance, and the wall temperature may be different from that of the gas core. This paper reports a theoretical investigation of the wall losses for a rocket cavity and applies the results to the interpretation of T-burner experiments to determine the acoustic admittance of burning solid propellant surfaces. An analysis is made of the frequently used hypothesis that the inherent damping during the oscillation growth period of T-burners is identical to the damping measured after burnout. To obtain the inherent damping from the measured damping, a significant correction is often indicated.

THEORY

The flow conditions which prevail in many rockets are shown in Fig. 1. There is an essentially uniform flow in the core of the cavity, and near the walls there is a steady state velocity boundary layer. When the wall temperature is different from the gas core temperature, the steady state temperature profile is similar to the velocity profile, and the steady state thermal and velocity boundary layers are of comparable thickness. When a sound field is present, there is also an acoustic boundary layer adjacent to the wall. The acoustic boundary layer thickness is typically an order of magnitude less (except near a leading edge) than those of the steady state boundary layers for the usual velocities, temperatures, and frequencies encountered in solid propellant applications. In the present report, the wall is assumed isothermal, which is reasonable whenever a typical time for wall temperature change is long compared to the period of the acoustic oscillation.

The acoustic field in the rocket cavity assumes different forms in the gas core, steady state boundary layer, and the acoustic boundary layer is not identical to the gas core acoustic field as envisaged in the usual theory because the acoustic field is modified (from the gas core field) in the steady state boundary layer as well as in the acoustic boundary layer. Examination of the x-momentum equation of fluid dynamics shows the mechanism of modification in the steady state boundary layer. The x-momentum equation is

$$ik\tilde{\alpha} = - \left(\frac{\bar{T}}{T_c}\right) \frac{\partial \tilde{\epsilon}}{\partial x} \qquad (1)$$

where $k = \omega/c$, ω is the angular frequency, c is the gas core sound speed, $\tilde{\alpha}$ is the dimensionless Fourier acoustic velocity coefficient defined implicitly by $v_{ac} = \mathrm{Re}[c\tilde{\alpha}\, e^{i\omega t}]$, $\tilde{\epsilon}$ is the dimensionless Fourier acoustic pressure coefficient, T is the temperature, the subscript c indicates gas core conditions, and the overbar indicates a steady state value. When the wall is colder than the gas, Eq. (1) shows that the acoustic velocity in the steady state boundary layer is less than the gas core value since the acoustic pressure gradient is essentially independent of distance from the wall. Thus, for a fixed core temperature, the viscous acoustic wall loss should be somewhat less for a cold wall than for a wall at core temperature because of the diminished velocity amplitude at the edge of the acoustic boundary layer (within which the loss occurs). The viscous loss is also lessened for a cold wall because of a diminished viscosity in the acoustic boundary layer. Likewise, the thermal loss is less for a cold wall because the thermal conductivity decreases with temperature. It should be noted that the imaginary part of the acoustic frequency is a measure of the loss and is calculated from

$$\mathrm{Im}\ \omega = - \frac{1}{\langle E \rangle} \left\langle \frac{dE}{dt} \right\rangle \qquad (2)$$

where E is the acoustic energy within the cavity and $\langle\ \rangle$ denotes the time average. The preceding argument shows that $\langle dE/dt \rangle$ is lessened as the wall is cooled. In the determination of $\langle E \rangle$, the principal contribution arises from the acoustic field in the gas core and is almost independent of the various boundary layer modifications.

A detailed quantitative estimate of the acoustic wall loss for a cavity with steady state mean flow and thermal boundary layers is given in Ref. (2) and will not be repeated here. Ref. (2)

utilizes a variational method to find the complex eigenfrequencies of a cavity. The two principal advantages of the variational method are: (1) that it is relatively insensitive to the assumed form of the acoustic field (trial function) and (2) that it provides for the possibility of conversion of other forms of energy into acoustic energy in a region of steep gradients (this possibility turns out to be unimportant in present solid propellant applications). The geometry of the calculation is that of Fig. 1. It is chosen because there are no net gain or losses in the system due to flow, so the principal loss is at the wall. The primary result of the variational calculation for an axial mode in a half-wavelength cavity is

$$\text{Im } \omega = \frac{S}{2V} \left(\frac{T_w}{T_c} + \frac{\gamma - 1}{\sqrt{Pr}} \right) \left(\frac{\pi f \mu_w}{\rho_w} \right)^{1/2} \qquad (3)$$

where S is the wall surface, V is the cavity volume, γ is the specific heat ratio, Pr is the Prandtl number, f is the frequency, μ is the viscosity, ρ is the density and the subscript w indicates wall conditions. The result of Eq. (3) is shown in Fig. 2, where it is seen that the loss diminishes as the wall is cooled and the core temperature held constant. The insensitivity of the variational method to the choice of trial function is illustrated by the dashed line. In that case, there is no modification of the acoustic field trial function in the steady state boundary layer. The close agreement of the two calculations illustrates the power of the variational method.

APPLICATION OF THE THEORY

The results of the present method are applicable to the interpretation of T-burner experiments to determine the acoustic admittance [or response function $\text{Re}(\tilde{\mu}/\tilde{\epsilon})$] of a burning solid propellant surface. A T-burner as shown in Fig. 3 has a large wall area, so wall losses should usually be significant. Experiments with T-burners are described at this meeting in detail by several participants (Ref. 3, for example), so only those details essential to the present application will be repeated here. The propellant response function is calculated from the various measurements by the relation

$$\text{Re} \left(\frac{\tilde{\mu}}{\tilde{\epsilon}} \right) = \frac{\bar{p}}{4\bar{m}c} \left(\frac{\alpha_1 - \alpha_2}{f} \right)$$

where $\bar{p}$ is the steady state pressure, $\bar{m}$ is the steady state mass flux at the propellant surface, α_1 is the measured acoustic pressure amplitude growth rate, and α_2 is the inherent damping present during the oscillation growth period. (Note that the theoretical estimate for $\alpha_2 = -$ Im ω is given in Eq. [3].) Since the inherent damping cannot be directly measured, it is commonly assumed that the inherent damping is identical to that measured after burnout. This assumption has always been questioned, but used of necessity.

A difficulty in the foregoing interpretation arises because the resonant frequency of the cavity changes rapidly after burnout. By the time the oscillations are sufficiently small to use with the linearized theory, the frequency is about one-half the oscillation growth period frequency. The diminished frequency implies that the cavity core has become cold, so linear decay measurements are made at reduced frequencies and temperatures.

In a recent series of T-burner experiments at NOTS for several propellants with similar gas compositions (Ref. 4), the measured decay rate depends roughly on the square root of the frequency, indicating the dominance of wall damping. Accurate processing of these data according to the present method is impossible because the frequencies and temperatures at which the decay rate is measured are unknown. However, it is believed that the assumptions made below are sufficiently reasonable to indicate the magnitude of error involved in the identical damping hypothesis. Since the final frequencies are approximately one-half the frequency during the oscillation growth period, it is assumed that $f_f = f/2$, where the subscript f indicates a final value after burnout at small amplitude. The final core temperature is thus $T_{c,f} = T_c/4$. The wall temperatures during the oscillation growth period and after burnout are unknown, but it is assumed they are identical and $T_w = T_c/4$.

The NOTS data correlate roughly with $\alpha_{2,f} = -3.5\sqrt{f/100}$ for the series of tests where $\alpha_{2,f}$ is the measured damping. When it is assumed that the only losses are wall losses and that $\gamma = 1.2$, $Pr = 0.75$, and $T_c = 3000°K$, these data imply an effective wall viscosity $\mu_w = 15.7(10)^{-4}$ poise. This viscosity is large, but the high value could be due to wall roughness and scale deposit on the walls. When this value of viscosity is used in Eq. (3) with the other assumptions of this section, it is found that

$$\alpha_2 = (0.545)\,\alpha_{2,f} = -1.9\sqrt{f/100} \qquad (5)$$

The importance of this correction at low frequency is easily seen by comparison of two d ta-processing methods: the first uses the identical damping hypothesis and the general correlation ($\alpha_2 \equiv \alpha_{2,f} = -3.5\sqrt{f/100}$) while the second uses the correlated correction of Eq. (5). For the first method

$$\frac{\tilde{\mu}}{\tilde{\epsilon}} = \frac{\bar{p}}{4\bar{m}c}\left(\frac{\alpha_1}{f} + 3.5\sqrt{\frac{100}{f}}\right) \tag{6a}$$

and for the second

$$\frac{\tilde{\mu}}{\tilde{\epsilon}} = \frac{\bar{p}}{4\bar{m}c}\left(\frac{\alpha_1}{f} + 1.9\sqrt{\frac{100}{f}}\right) \tag{6b}$$

As an example, for one propellant in the NOTS series, $\alpha_1 = 5\ \text{sec}^{-1}$ at 620 cps. Eq. (6a) gives $(\tilde{\mu}/\tilde{\epsilon}) = (\bar{p}/4\bar{m}c)(1.41)$ while Eq. (6b) gives $(\tilde{\mu}/\tilde{\epsilon}) = (\bar{p}/4\bar{m}c)(0.77)$. Since the underlying assumptions for the result calculated by Eq. (6b) are believed to be reasonable (if not accurate), a significant correction to the measured damping is undoubtedly necessary to obtain accurate values of the inherent damping, especially at low frequency.

DISCUSSION

The calculations of the previous section indicate that the inherent damping may be significantly different from the damping measured after burnout. The validity of the calculations is limited by the lack of knowledge concerning the final frequency and wall temperatures during the growth period and after burnout. If these quantities are measured in future experiments, it is believed that the methods outlined in this paper can be used to obtain better values of α_2 from the measured decay rates. In applying the present theory, however, it must be ascertained that wall loss is the dominant loss and that other damping mechanisms (for example, particle damping) are not present. Alternatively, the extent of each type of damping must be known.

REFERENCES

1. Lambert, R. F., J. Acoust. Soc. Am. 25, 1068-1083 (1953).

2. Cantrell, R. H., McClure, F. T., and Hart, R. W., J. Acoust. Soc. Am. 35 (accepted for publication in April 1963 issue).

3. Horton, M. D., "Effect of Propellant Variables on Response Function", (this volume).

4. Horton, M. D., private communication, 1963.

ACKNOWLEDGMENT

The author wishes to thank Dr. M. W. Horton of NOTS for generously supplying much raw data on his experiments and for permission to discuss these data.

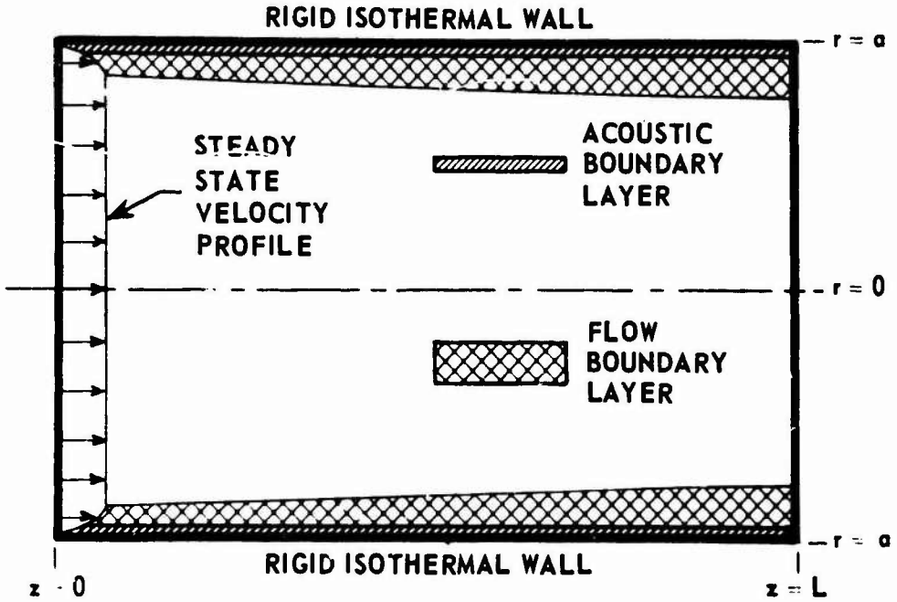

FIG. 1 SCHEMATIC REPRESENTATION OF ROCKET CAVITY SHOWING VELOCITY PROFILE AND ACOUSTIC BOUNDARY LAYER

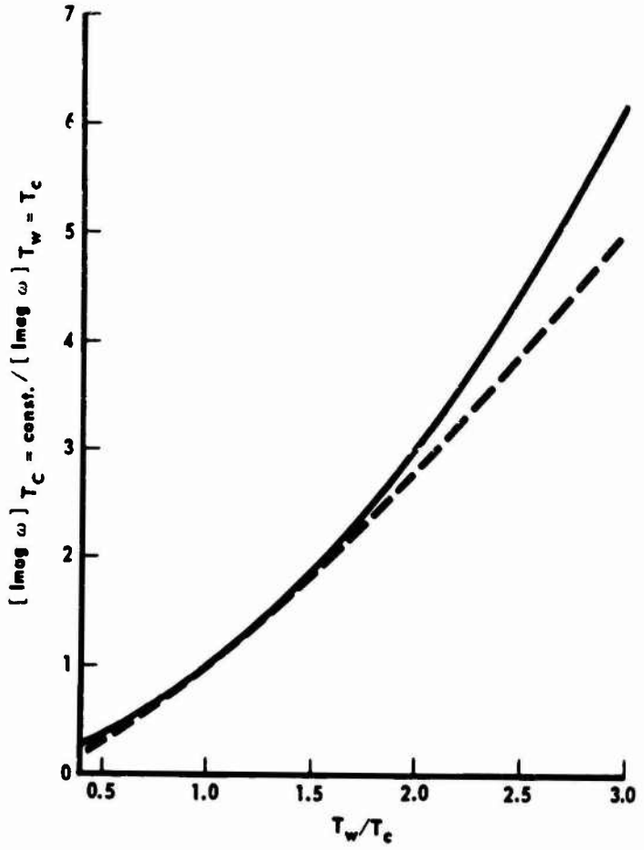

FIG. 2 RATIO OF $(\text{Im}\omega)$ FOR VARIOUS VALUES OF WALL TEMPERATURE T_w AND FIXED GAS CORE TEMPERATURE T_c TO $(\text{Im}\omega)$ FOR $T_w=T_c$. THE VISCOSITY TEMPERATURE RELATIONSHIP IS $\mu \sim T^{3/4}$ AND THE PRANDTL NUMBER $Pr=0.75$. THE SOLID LINE DISPLAYS THE RESULT OF Eq. (3), AND THE DASHED LINE DISPLAYS THE RESULTS OF THE VARIATIONAL METHOD FOR A TRIAL FUNCTION NOT MODIFIED IN THE STEADY STATE BOUNDARY LAYER.

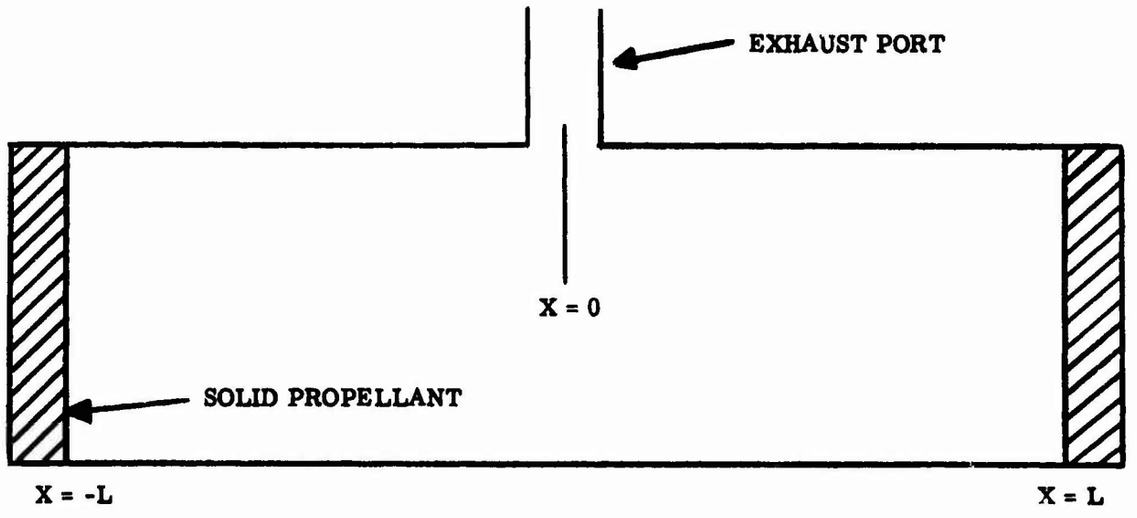

FIG. 3 SCHEMATIC DRAWING OF A T-BURNER

THE EXPERIMENT AT BRL ON ACOUSTIC ADMITTANCE MEASUREMENTS OF BURNING PROPELLANT SURFACES*

Richard C. Strittmater, Leland Watermeier, and Samuel Pfaff

Ballistic Research Laboratories
Aberdeen Proving Ground, Md.

The object of the work reported here was to improve the reproducibility and to decrease energy losses in the resonant tube experiment to measure the admittance of burning propellant surfaces. Much of the work has been concentrated in the following areas:

1. Improvement of coupling between gages and combustion tube.
2. Obtaining uniform ignition.
3. Reduction of thermal wall losses.
4. Improvement of exhaust conditions.

To determine the coupling characteristics between the combustion chamber and gages, a series of shock tube tests on the gages and coupling cavities were completed. These tests indicated the cavity resonant frequency to be very close to the range of fundamental frequencies being measured. Redesign of this cavity has eliminated this condition. The thermal isolation afforded by the redesigned cavity and grease still appears adequate and the resonant frequency of the coupling cavity is now 20,000 cps.

A new method has been developed for applying the resistance wire igniter to the propellant sample. This has improved the uniformity of ignition and gives promise of improving reproducibility in this experiment.

The inside wall of a combustion tube was coated with 6 mils of ZrO_2 in order to reduce thermal losses at the walls. The tube was 1 3/16" in diameter and was 2 1/4" long. The fundamental frequency was 8100 cps. Results indicated that there was no significant reduction of losses. The value of the admittance of the burning surface determined in the coated tube was the same as the value determined in the uncoated tube.

---

*This work is supported by the Army Materiel Command.

A new combustion chamber was built which vents the product gases through four holes instead of one. The idea behind this is as follows. In the "T Motor" experiments to determine the acoustic admittance, it is assumed that the acoustic losses during burning are the same as after burnout. This single assumption probably introduces more error into the experiment than any other. Therefore, it is important to reduce the losses wherever possible. It was believed that the losses would be reduced by venting the gases uniformly around the entire periphery of the tube, rather than through one hole as in original "T Motors".

At BRL an approximation to uniform venting has been designed in the form of a combustion tube that uses four drilled holes for venting the gases. The centers of the holes lie in the central transverse plane of the tube and the holes are 90° apart. The combined cross sectional area of the four orifices in the new burner is equal to the cross sectional area of the single orifice in the original T Motor. The central transverse cross section of the new chamber is shown in Fig. 1. Very few experiments have been completed with this chamber. However, on the basis of these experiments, a few remarks can be made:

1. None of the data taken at 3300 cps has shown the presence of the cusp-like mode described in the work of Hart, McClure,and Cantrell.

2. The admittance determined from the data taken in the 4-orifice burner agrees with the previous results obtained with the single orifice burner.

3. The losses measured in the 4-orifice burner are less than in the single orifice burner.

Our original plans to run comparative tests with Horton, Price; Ryan, Coates, and Baer (1) were side-tracked somewhat by the considerations discussed above. In the near future we hope to accomplish the original goal of comparative tests and to pursue the problem of minimizing the acoustic losses.

REFERENCE

1. Horton, M.D. and Price, E.W.; Ryan, N.W., Coates, R.L., and Baer, A.D., The Ninth Symposium (International) on Combustion. New York, Academic Press, Inc., to be published.

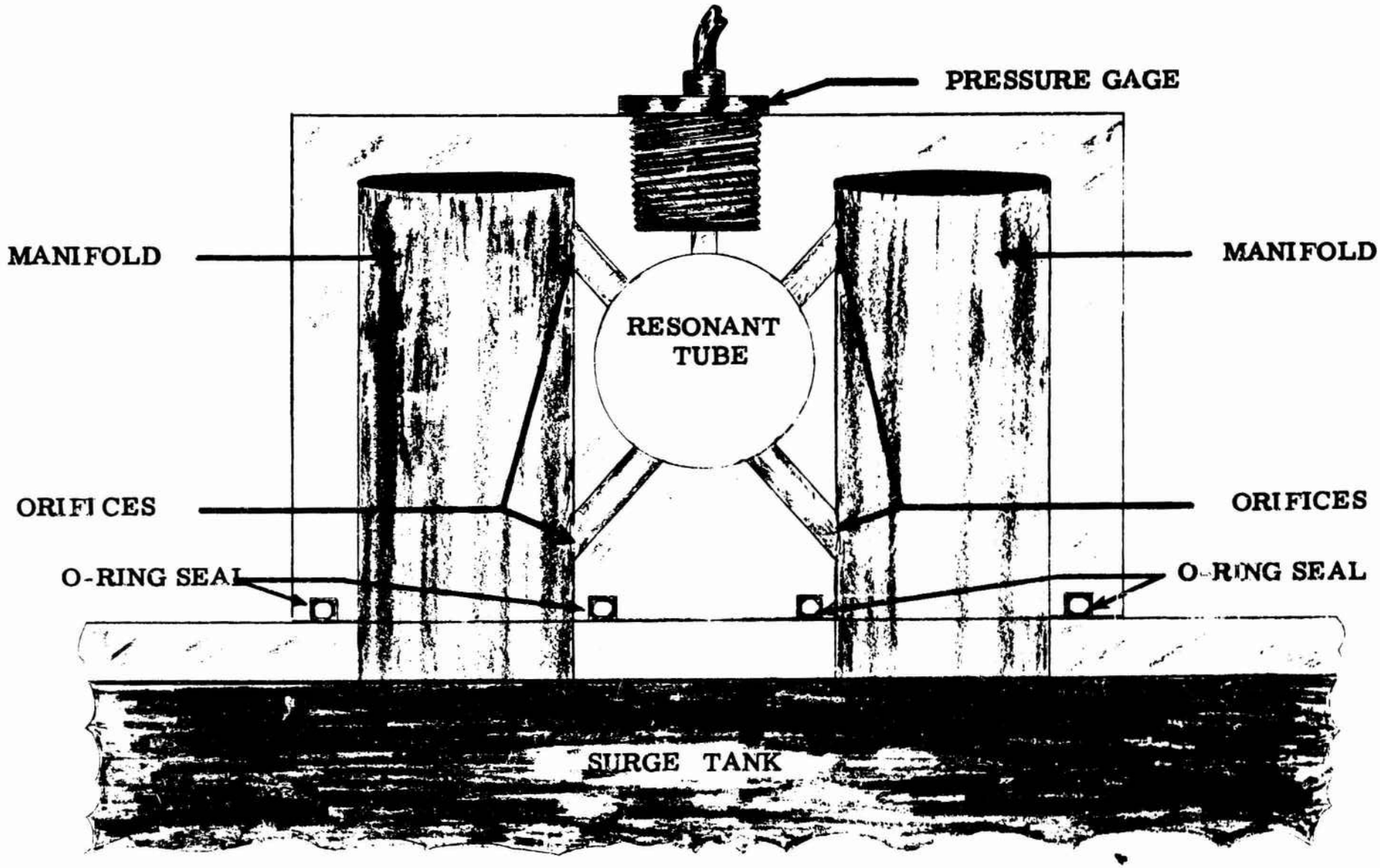

Fig. 1 CENTRAL TRANSVERSE CROSS-SECTION (at orifices) OF END BURNING COMBUSTION CHAMBER

COMBUSTION IRREGULARITIES OF SOLID PROPELLANTS*

Norman W. Ryan
Dept. of Chemical Engineering
University of Utah
Salt Lake City, Utah

At the University of Utah there have been two principal lines of attack on the oscillatory burning problem, both employing the side-vented end-burner. In one, the oscillation growth constants are determined from records of runs with short propellant grains burning first in only one end, then in each end. The constants obtained permit estimating both the acoustic admittance of the burning surface and the chamber losses. In the other attack, long grains are burned in only one end, the grain being advanced at the burning rate to maintain constant gas phase geometry. An attempt has been made to interpret the results observed in terms of the viscoelastic properties of the solid propellant.

Acoustic Admittance

If it is assumed that convective movement of the gas can be neglected and that losses in the gas column can be considered proportional to acoustic velocity, the wave equation can be solved to give the real part of the specific acoustic admittance of the burning surface and the loss coefficient in terms of the growth constants, α_2 for double-end run and α_1 for single-end run, as follows:

$$k_f = \frac{\alpha_2 - \alpha_1}{2f}$$

where f is the frequency, and

$$\frac{R-}{2\rho} = \alpha_2 - 2\alpha_1 \quad \text{sec.}^{-1} \quad .$$

Recent work on Utah F propellant has confirmed the growth constant-frequency correlation previously reported for single-end runs, but has led to a revision of the correlation for double-end runs. It is now believed that the relationship for double-end runs lies nearly half-way between that reported by R. L. Coates, then of the Utah laboratory, and that reported by M. D. Horton of N.O.T.S. Results, still regarded as tentative, computed according to the above equations indicate that the specific acoustic admittance varies inversely with the square root of the frequency and the loss coefficient is very nearly constant. The frequency range investigated was 600 to 7000 cps.

Participation of the Solid Phase

In the solution of the wave equation applied to the solid phase when a long grain is burned, the coefficient of the position parameter is taken as complex in order to introduce the attenuation constant,

which can then be related to the other viscoelastic properties of the solid. The time dependence is fixed by the sinusoidal pressure-time relationship at the supported end. The acoustic admittance of the free end is matched to the value computed, assuming that the difference between oscillation growth constants (determined in the gas phase) for short grains and for long grains represents the amount of acoustic energy pumped into, and dissipated within, the solid phase.

Provided viscoelastic properties are known and the liberties taken in the derivation are admissible, the resulting solution permits expressing, as a function of the grain length, each of the following: (1) ratio of pressure amplitudes at the end plates (solid end to gas end), (2) the phase difference between the two end pressure signals, and (3) the reduction in the value of the growth constant below the short-grain value. Unfortunately the viscoelastic properties are not known. Attempts to obtain the complex moduli pertinent to the particular process have not been unambiguously successful. Comparison of experimental results to values of the three variables above computed for arbitrarily assumed values of the quality factor, Q , indicates that the Q for Utah F propellant is about 5.

Attempts to produce oscillatory burning with highly aluminized modified double-base propellants, experiments in which Hercules (Bacchus) personnel participated,were unsuccessful. Much of the difficulty is now thought to have been due to inadequate ignition. When ignition was satisfactory, burning was normal and stable. The negative results do encourage future work. They included occasional chuffing and sometimes complete decomposition of the propellant, leaving a large residue of unburned, unmelted aluminum.

---

*This work supported by Advanced Research Projects Agency (ARPA).

EXPERIMENTS WITH A SOLID PROPELLANT ACOUSTIC OSCILLATOR*

J. F. Engler and W. Nachbar
Lockheed Missiles and Space Company
Research Laboratories
Palo Alto, California

Standing wave oscillations in the gas cavity above an end-burning solid propellant grain have been studied by using as test apparatus a side-vented rocket motor with a transparent combustion chamber. One-inch long, uninhibited grains of an 80%-20% ammonium perchlorate-polyurethane propellant are pressed tightly into one end of a quartz tube, 6" long and 1 1/2" I.D., which in turn forms one end of a cavity of adjustable total length. Pressure measurements are made using both high-and low-frequency response transducers, and high-frame-rate cameras are used to monitor the regression of the propellant surface under oscillatory and non-oscillatory operation.

Oscillations in chamber pressure of frequencies from 1000-2000 cps. were developed to 10 psi amplitude on a 200 psia average. Frequencies observed were inversely proportional to chamber length but 20% lower than calculated acoustic frequencies for the closed-closed tube. In addition, both frequencies and amplitudes were observed to be strongly dependent upon mean pressure in a consistent way. Higher amplitudes and lower frequencies were observed at lower pressures. Actual burning rates are measured from the motion picture record with the aid of a Vanguard Motion Analyzer. It was found that, within a calculated probable experimental error, the observed mean burning rate agreed with the strand test rate under both oscillatory and non-oscillatory conditions.

In an accidental experiment, it was shown that the burning propellant can be extinguished within 8 milliseconds by fracturing the quartz tube.

---

*This work was performed at the Lockheed Missiles & Space Company Research Laboratories, Palo Alto, California, under the sponsorship of the LMSC Independent Research Program.

A REVIEW OF EXPERIMENTAL WORK ON ACOUSTIC INSTABILITY IN DOUBLE BASE PROPELLANTS FOR THE PERIOD MARCH 1, 1962 TO MARCH 1, 1963

S. F. Mathews and T. A. Angelus
Hercules Powder Company
Allegany Ballistics Laboratory
Cumberland, Maryland

A program has been initiated at ABL to investigate low frequency (200-1000 cps) acoustic instability in composite modified double base (CMDB) propellants. The primary emphasis of recent work has been to develop a burner to operate in this frequency range. This approach has provided some unusual results which may lead to a better understanding of inherent losses in the system.

All firing tests have been performed in a side-vented six-foot-long "T-burner" with an inside diameter of 3 1/8 inches (Fig. 1). Two-inch-long grains are placed in both ends and ignited with bag igniters. All tests have been made with a nonaluminized CMDB propellant. The nozzle was sized for 400 psi chamber pressure and the resonant frequency corresponding to the calculated flame temperature of the propellant was 300 cps.

Typical performance of the T-burner with uninsulated walls is shown in Fig. 2. The pressure-time record of a round which was mechanically stabilized with chamber baffles is also shown for comparison. The burning range during instability is severely lowered and the observed frequency (170 cps) corresponds to a chamber gas temperature of about 1000°K, which is over 2000°K lower than the calculated temperature. The chamber wall temperature of the burner was measured during burning and heat balance calculations gave an equivalent drop in chamber gas temperature. This temperature drop was subtracted from the calculated flame temperature to estimate final gas temperatures of 1220°K for unstable operation and 2200°K for stabilized operation. The temperature for unstable operation agrees reasonably well with the temperature computed from the frequency and in both cases the heat loss to the walls can be used to explain the low operating pressure at the average burning rate of the firings.

The burner has been fired with two types of chamber insulation - nitrile rubber and asbestos phenolic. Firings with the insulated chamber produced significantly higher operating pressure (325-350 psi) and higher frequencies (260 cps). However, the oscillations in both cases were completely suppressed within 2.5 seconds and thereafter the rounds were stable.

The stabilizing effect of the insulation was considered due to increased acoustic losses and not due to a pressure dependence of the propellant admittance. Therefore, the sound absorption characteristics

of the insulation were measured in a standing wave apparatus. A hard termination was used in the end of the tube to eliminate reflection losses and the inside of the standing wave tube was lined with cylindrical samples of the insulation to simulate motor conditions. The acoustic pressure was compared to the unlined tube at constant input to the driver. The acoustic pressure loss of both types of insulation (including a fired sample of the nitrile rubber) was less than ten per cent in the frequency range of the T-burner oscillations. This level of absorption did not explain the stability of the insulated burner. The losses in the insulated T-burner are believed to be a result of viscous damping in the thick boundary layer formed by decomposition of the ablative insulation.

An additional experiment was carried out in the uninsulated T-burner in which chamber gas samples were collected and gas temperatures in the chamber were measured with bare junction thermocouples (platinum-platinum/10 per cent rhodium) Chemical analysis of gas samples, taken during stable and unstable burning, revealed no evidence of incomplete reaction. However, uncertainties in the sampling technique make the results questionable and the relation of combustion efficiency to the depressed burning rate remains a matter of conjecture. The temperature-time record is compared to the frequency and pressure history of the unstable round in Fig. 3. The gas temperature shows reasonably good agreement with the temperatures computed from frequency and the results also demonstrate the excessive heat loss in the system. The most interesting result, however, is the low temperature recorded six inches from the burning surface which indicates the temperature to be far below the flame temperature. During stabilized burning, the melting of the thermocouple located six inches from the burning surface (melting point of platinum is 2028°K), gives qualitative evidence that the local gas temperature near the burning propellant was much higher than that during unstable burning. These results offer a possible explanation for the depressed burning rate; i.e., the presence of the acoustic oscillations in the gas with a high temperature gradient (due to heat loss) causes the temperature in the vicinity of the burning surface to be lowered.

The proposed solution for the performance anomalies of the low frequency T-burner involves the use of a nonablative thermal insulator. Future work will include an evaluation of rigid ceramic material to reduce the thermal and acoustic losses. In addition, the mass flow rate will be increased in an attempt to minimize the effect of heat loss in the system.

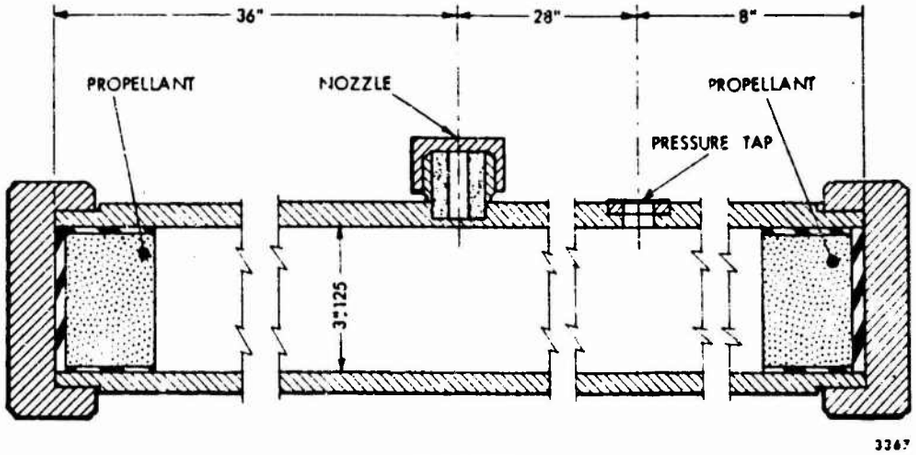

FIGURE 1
Prototype Motor (EM 54) for Unstable Combustion Studies

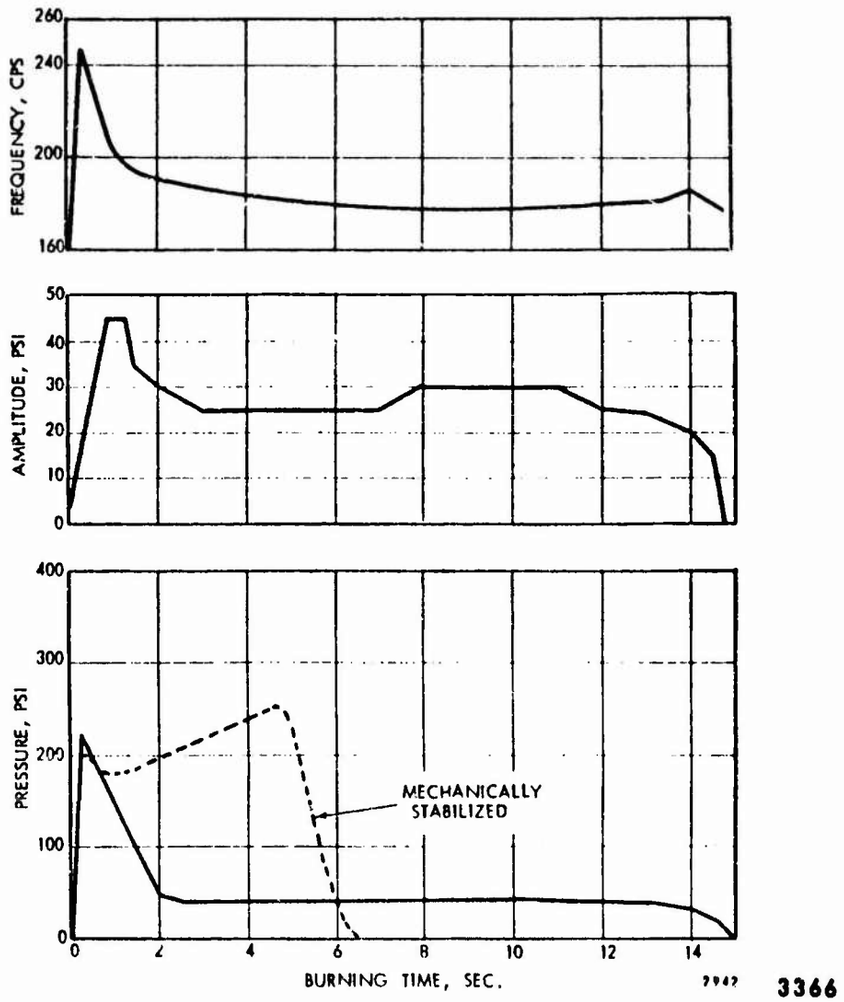

FIGURE 2
Frequency, Amplitude, Pressure vs. Time for EM-54 Double-End-Burner, Uninsulated

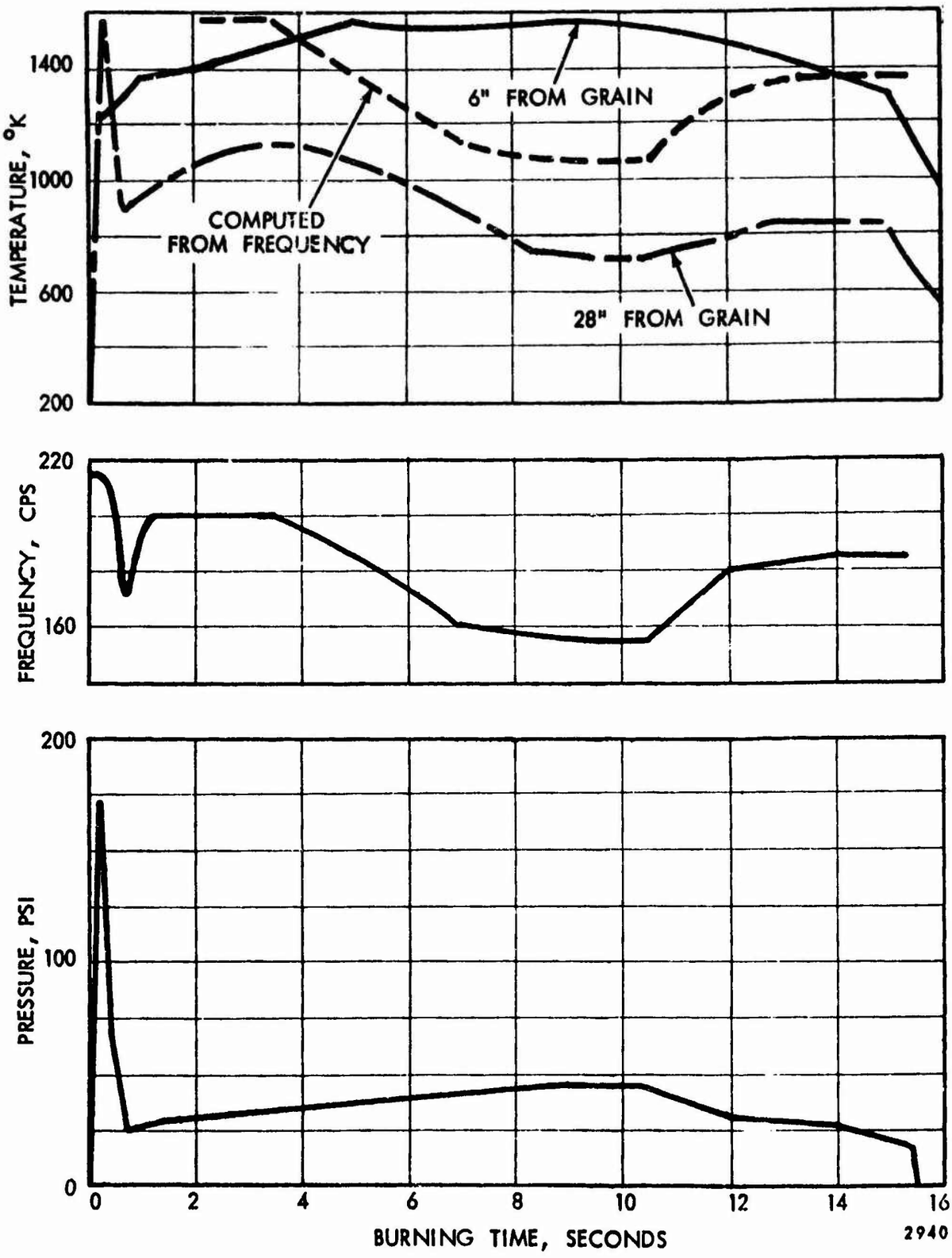

FIGURE 3
Effect of Transient Chamber Temperatures with Uninsulated EM-54 Double-End-Burner

DOUBLE-END BURNER EXPERIMENTS

R. L. Coates
Hercules Powder Company
Bacchus Works

The recent success of the use of side-vented, double-end motors to obtain quantitative data to characterize unstable combustion has prompted us to try to adapt these kind of tests to a motor development program. Even though absolute measurements of the more relevant property pertaining to combustion instability, the acoustic admittance, cannot yet be made with complete confidence, a quantitative comparison of different propellant compositions is possible. Measurements of the rate of growth of oscillation amplitude for different compositions when fired under identical conditions provides a quantitative measure of relative tendencies toward stable combustion.

Several improvements were made in the double-end burner technique to allow testing of rather stable burning propellants. To reduce acoustic losses, a larger motor (4.5" diameter) was constructed with all exposed internal surfaces covered with a phenolic-asbestos insulating material. To increase acoustic amplification, provision was made to use shallow cup-shaped grains as well as the ordinary end-burning grains, thus increasing the burning surface area.

Eleven firings have been made to date with this motor with a propellant containing a substantial amount of aluminum. End-burning grains were found to burn stably, but cup-shaped grains with tubular sections greater than 2" in length were found to produce oscillatory burning. Oscillations having peak-to-peak amplitudes as great as 150 per cent of the mean pressure were observed.

The use of grains with varying surface area presents an opportunity for a different approach to estimating burning surface admittance and the inherent motor losses. If the dimensions of the grains are such that the one-dimensional acoustic characteristics of the motor are preserved, a simplified analysis shows that the rate of growth of oscillations can be written as

$$\alpha = -\left\{ 2 \frac{\rho c^2}{L} \left(\frac{A}{Ae}\right) Yr + \alpha_2 \right\}, \qquad (1)$$

where ρ and c are the density and sound velocity of the propellant gas, L is the length of the motor, (A/Ae) is the ratio of actual burning surface area to that for an end-burning grain, Yr is the real part of the acoustic admittance of the burning surface, and α_2 represents a term due to inherent losses asscciated with flow and inert surfaces (the decay constant). Equation (1) shows that if a series of tests were made with varying burning-surface area ratio but the same propellant and motor length, and the measured values of α were then plotted versus A/Ae, the admittance, Yr, could be obtained from the slope and α_2 could be obtained from the intercept of a best fit line drawn through the data points.

To illustrate the analytical technique, data from four of the initial firings were analyzed. Although the data were rather poor, an estimate was made of the burning surface specific admittance and the damping constant. Values obtained from these data are $\rho c Y_r = 0.005$, and $\alpha_2 = -20$ sec^{-1}.

PHYSICAL PROCESSES OF SOLID PROPELLANT COMBUSTION*

R. B. Lawhead and L. W. Carlson
Rocketdyne
Canoga Park, California

Accurate measurements of the acoustic impedance of burning solid propellant grains are required if the current analytical theories of solid propellant rocket combustion are to be effectively evaluated. Conventional methods of measuring acoustic impedance using steady-state sinusoidal pressure waves require accurate pressure-amplitude measurements as a function of distance from the surface at discrete frequencies over the range of interest. With a burning solid propellant, the surface is constantly regressing at a fairly rapid rate. If conventional methods of measurement are to be used, it is necessary to employ elaborate experimental or analytical techniques to compensate for the changing surface position. Even then, a complete impedance-frequency response cannot be obtained with a single burning sample, but requires many tests, all under identical conditions.

The studies described here were undertaken to examine the possibility of obtaining a complete spectrum of impedance-frequency values from measurements of the pressure-time histories of a single shock wave, incident on and reflected from a burning propellant surface.

The studies under our original contract (AF 49(638) 1093) were completed last July and have been reported in Rocketdyne Report R3802. Studies have recently been resumed under a new AFOSR contract (AF 49 (638)-1208), using the results of the earlier studies as a guide for their direction.

The results of the earlier studies can be summarized as follows:

Nonburning Transient Technique Evaluation

1. A frequency-dependent transfer function which describes the response of a surface to a normal shock wave can be determined from measurements of the pressure-time history of the shock wave incident on and reflected from the surface, provided that very weak (pressure ratios less than C.02) shocks are used.
2. The transfer function is defined as the ratio of the Fourier transforms of the reflected pressure-time function to the incident pressure-time function and is obtained through an IBM 7090 program which evaluates the individual transforms and then computes the ratio of the complex values.
3. Computation of a transient impedance function which corresponds with a classical acoustic impedance value depends on demonstration that the transient transfer function is identical with the classical reflection coefficient.

*This work supported by Advanced Research Projects Agency (ARPA).

4. For a perfectly reflecting termination, the transient reflection coefficient (computed from observed pressure-time histories) was found to be within ± 3 percent of the classical value of 1.00.

5. No satisfactory comparison between the transient and classical reflection coefficients could be obtained with inert materials because the inert materials tested (e.g., cellulose sponge) exhibited nonlinear behavior, even at the very low shock strengths used.

6. Comparison of measured transient reflection coefficients with classical values for simple resistive impedances (e.g., tube area change) showed the transient values to be high by 5 to 15 percent, depending on the relative area change (the larger the area change, the better the agreement). This difference appears also to be due to some as yet undefined nonlinear behavior of the low but finite amplitude waves.

7. The observed nonlinear response of simple passive materials indicates that no one-to-one correspondence can be established between classical and transient reflection coefficients (and hence impedances). The response of burning propellant surfaces will probably be even more nonlinear than the passive elements.

8. A re-examination of the analytical treatments of instability will have to be made to determine the significance of the transient response function which can be determined by means of the weak shock experimental technique.

Application to Burning Propellants

1. Gross differences are measured in the pressure-time histories of weak shock waves incident on and reflected from different types of solid propellants burning at 450 psi. Only minute differences are observed between aluminized and nonaluminized samples of the same type of propellant.

2. The effects of the hot-gas region generated by the propellant combustion prevents determination of whether the observed differences in pressure-time are due to real differences in propellant response to the pressure wave or to differences in gas temperature gradients and product composition.

3. Pressure traces also show that a pressure wave is generated due to the shock wave interaction with the burning surface. This "wave" appears to be coincident with the reflected wave at the propellant surface, but travels at a speed about one-third the velocity of sound. Motion picture documentation shows an increase in luminosity of combustion originating at the surface which appears to be associated with this pressure wave.

4. To eliminate hot-gas effects and unusual wave propagation phenomena, it appears that the measurements of the incident and reflected waves should be made at the propellant surface rather than at a station some distance away from the surface.

5. A "wave-splitting" technique for making the pressure measurements of the surface of the material has been devised and cold-flow Schlieren pictures indicate that it is feasible.

The studies under our new contract are making use of the wave splitter technique since it appears that the best approach is to attempt to eliminate the effects of the hot-gas region from the primary measurements and to make the measurements at the surface of the propellant.

The wave splitter technique may be described as follows: A planar shock wave propagating through a hot-gas region is split into two parts by a partition separating the tube into two areas of flow. One part of the shock wave travels to a burning solid propellant surface and reflects from it. A pressure transducer located at the plane of the burning surface registers the combined input and reflected wave form. The other part of the shock wave travels down the other portion of the tube past another pressure transducer located in the same plane as the one by the burning surface; this wave continues to another termination before reflection. Solid propellant located at the second termination has been ignited simultaneously with the test sample to give a similar hot-gas region. The end of the tube is located at sufficient distance from the pressure transducer so that the pressure pulse reflection does not overlap the incoming wave. The distance required is merely greater than the quantity:

$$\text{Driver length} \times \frac{\text{sound speed in hot gas}}{\text{sound speed in driver gas}} .$$

Thus, this pressure transducer experiences separately only the incoming wave and an inconsequential reflected wave. The incoming wave can be aligned and subtracted electronically from the combined wave recorded by the other pickup. Thus, the input and reflected wave recorded at the propellant surface are available for analysis. There are a number of restrictions which apply to this scheme: (1) The wave-splitting device must have a sharp leading edge. Preliminary cold tests using Schlieren photography show that reflection from the leading edge can be made negligible. (2) The wave splitter must seal off the two wave passages so no interaction across this boundary occurs. This is not thought to be a difficult problem. (3) The wave splitter must be at least one-half the length of the pressure pulse traveling in the hot gas to be able to separate leakage between pickups around its tip. (4) Equivalent hot-gas sources must be provided on each side of the wave splitter. One of these sources must have a surface normal to the wave passage past the pressure transducer. (5) The shock wave must be planar and symmetrical with respect to the two transducers. This can be proven prior to testing by Schlieren pictures and pressure records sampling shock behavior.

Emphasis in the next few months will be placed on obtaining response function for normally incident shocks with various aluminized

and non-aluminized propellants using the wave splitting technique. In addition, grazing incident waves will be examined using a 6-in. diameter pancake-type chamber in which simultaneous high speed motion pictures and pressure records can be obtained under conditions of transverse modes of combustion oscillations.

ACOUSTIC ADMITTANCE MEASUREMENTS: REFLECTED-PULSE METHOD*

George M. Muller
Stanford Research Institute
Menlo Park, California

A reflected-pulse method for measuring the normal acoustic admittance of a burning propellant surface has been under investigation at Stanford Research Institute for about two years. This method involves sending a plane acoustic pulse (peak pressure less than 1% of ambient pressure) down a long tube terminated by the surface to be investigated, and observing the pressure-time profile of the pulse before and after reflection. By computing the Fourier transforms of the incident and reflected pulse, one can determine the complex reflection coefficient R and hence η, the real part of the complex admittance ratio $Y\rho c$[1], for a range of frequencies whose limits are set by the length and diameter of the tube and the shape of the pulse. It is more convenient to consider instead of η the related quantity $\eta^* = (1/2)(1 - |R|)$ which depends only on the absolute value of R; η is given in terms of η^* by $\eta = \eta^* + (\eta^*)^2$, an equation which is correct to terms of second order in the real and imaginary parts of 1 - R.

The values of η^* thus obtained contain two contributions: (1) the true η^* of the termination and (2) the tube η^*, representing losses or gains[2] which arise from the motion of the pulse through the tube between the point where the pressure is recorded and the termination. Previous work has shown that, for sufficiently small values of true η^* and tube η^*, these two contributions may be treated as independent. In the case of a cold sample, the tube η^* may be found by repeating the measurement with the tube terminated by a blank, i.e., a rigid surface whose η^* is zero. With an obvious notation we have, then,

$$\eta^*_{TRUE} = \eta^*_{SAMPLE} - \eta^*_{BLANK} \quad . \qquad (1)$$

During the past year, we conducted a systematic investigation of the precision and general internal coherence of this method when applied to cold samples. The samples were rigidly-backed, cylindrical columns of 1.2-mm-diameter lead spheres (No. 12 birdshot) contained in a steel cup designed to fit on the bottom end of a vertically mounted pulse tube. Considerable pains were taken in the

*Research reported in this publication was supported by the Advanced Research Projects Agency and technically monitored by the Air Force Office of Scientific Research, Contract No. AF 49(638)-565.

1. Y is the admittance/unit area; ρ and c are the density and sound speed of the gas in the tube.

2. Gains are due to nonlinear (finite-amplitude) effects.

machining of the joint between tube and cup in order to avoid the spurious disturbances which arise from mismatch or leakage. This particular type of sample was chosen because it is reproducible (the void fraction was 41 ± 1% for all column heights used), has a reflection coefficient close to unity, and allows this reflection coefficient (and hence η^*) to be varied systematically by changing the column height.

Initially, pulse records were obtained with the cup empty ("blank") and with 10, 12, and 13.5 mm columns of lead shot, at a peak pulse pressure of 0.0002 atm (Series I). The entire series was then repeated at a peak pulse pressure of 0.002 atm (Series II). In Fig. 1 we show the calculated values of η^*_{BLANK} and of η^*_{SAMPLE} for the 12 mm column, each value being the average obtained from three runs. The values of η^*_{TRUE} as determined at the two pressure levels fall so closely together that we merely indicate the total spread between the two curves. In the frequency range considered, the results for the 13.5 mm column were equally good, except at the upper end of the range where η^*_{SAMPLE} becomes so large that Eq.(1) can no longer be expected to hold. For the 10 mm column, agreement between the two curves was good everywhere except near the high-frequency end where the spread reached 0.006.

In view of the satisfactory results obtained, we extended the measurements to determine η^*_{TRUE} at column heights of 4.1, 5.5, and 7.9 mm; these measurements were only done at the lower pulse pressure level (Series III). The results obtained from Series I and III are summarized in Fig. 2; it should be noted that all curves were drawn so as to fall within 0.002 of the points calculated from the experimental data.

The internal precision among successive determination of η^* with the same termination and nominally identical pulses is indicated by Table 1. We have listed the mean values of η^*_{BLANK} for Series I, II, and III, together with the standard deviation. For each frequency we also give $|S_{-}(\omega)|$, the absolute value of the Fourier transform of the incident pulse normalized to have a value of unity at approximately the peak frequency. Actually, $|S_{-}(\omega)|$ at the maximum and minimum frequency listed will vary from run to run by several percent, and the peak pressure by as much as 20%; this variation seems to have only a negligible effect on the computed value of η^*. Note that in each series there is a range of frequencies, including the peak frequency, where the standard deviation is significantly smaller than the average for the entire range; this only confirms what one would expect intuitively. The standard deviations given in Table 1 are completely representative of those which occur in the determination of the various η^*_{SAMPLE}. Taking 0.0007 as typical for the "best" frequency and 0.002 as typical for the best octave, we obtain estimated standard deviations for η^*_{TRUE} by multiplying these numbers by $\sqrt{2}$, i.e., 0.001 for the best frequency and 0.003 for the best octave.

These measurements were made with the use of a low-pass filter to eliminate frequencies about 4 kc/s from the recorded microphone signal. In the light of recent investigations (for details see Quarterly Technical Summary Report No. 16 under Contract No. AF 49 (638)-565) it appears that the precision can probably be considerably improved by using a band-pass filter to eliminate from the signal frequencies below about two or three times ω_0, where $\omega_0 = (2T)^{-1}$, T being the length of the incident pulse. (With our present apparatus, T – 2 msec, ω_0 – 80 c/s.)

Table 1.

THREE DETERMINATIONS OF η^* AS A FUNCTION OF ANGULAR FREQUENCY; BLANK (ZERO-ADMITTANCE) TERMINATION

$\omega \times 10^{-4}$ (sec^{-1})	I: Runs 61-63 Peak pressure: 2×10^{-4} atm			II: Runs 81-83 Peak pressure: 2×10^{-3} atm			III: Runs 101-103 Peak Pressure: 2×10^{-4} atm		
	$\eta^*_{mean} \times 10^{-2}$	$\sigma \times 10^{-2}$	$\lvert S_-(\omega)\rvert$ (Run 61)	$\eta^*_{mean} \times 10^{-2}$	$\sigma \times 10^{-2}$	$\lvert S_-(\omega)\rvert$ (Run 81)	$\eta^*_{mean} \times 10^{-2}$	$\sigma \times 10^{-2}$	$\lvert S_-(\omega)\rvert$ (Run 101)
1.000	3.46	0.50	0.330	2.41	0.18	0.364	3.49	0.23	0.421
1.059	3.63	0.33	0.364	2.77	0.24	0.413	3.60	0.14	0.454
1.122	3.75	0.29	0.403	3.17	0.13	0.468	3.70	0.14	0.489
1.188	3.96	0.05	0.452	3.56	0.08	0.533	3.88	0.08	0.528
1.259	4.16	0.14	0.513	3.82	0.18	0.607	4.04	0.14	0.574
1.333	4.24	0.05	0.580	3.96	0.13	0.685	4.09	0.08	0.626
1.412	4.33	0.17	0.657	4.11	0.01	0.756	4.20	0.10	0.690
1.496	4.60	0.17	0.754	4.38	0.06	0.819	4.48	0.06	0.771
1.585	4.91	0.09	0.869	4.69	0.02	0.889	4.74	0.06	0.869
1.679	5.00	0.07	0.966	4.91	0.06	0.964	4.92	0.07	0.963
1.778	4.97	0.09	1.000	5.09	0.02	1.000	4.99	0.03	1.000
1.884	5.04	0.05	0.946	5.39	0.15	0.937	5.25	0.04	0.935
1.995	5.23	0.17	0.808	5.82	0.09	0.768	5.54	0.07	0.776
2.113	5.29	0.13	0.625	6.22	0.13	0.565	5.75	0.14	0.575
2.239	5.54	0.12	0.461	6.71	0.25	0.405	6.03	0.09	0.389
2.371	5.91	0.14	0.331	7.44	0.18	0.290	6.04	0.10	0.274

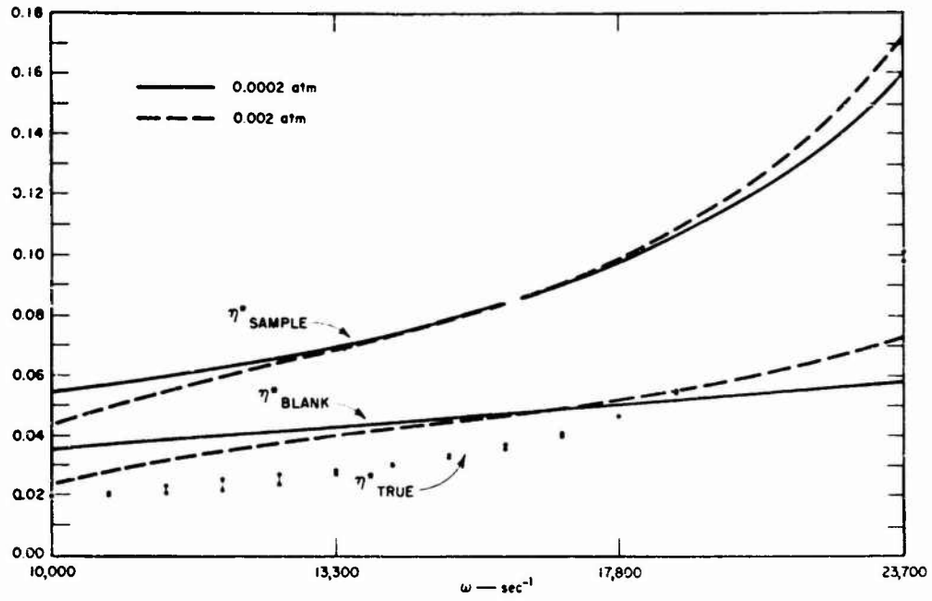

Fig. 1 η^* AS A FUNCTION OF ANGULAR FREQUENCY FOR A SOLIDLY-BACKED 12-mm COLUMN OF 1.2 mm- DIAMETER SPHERES

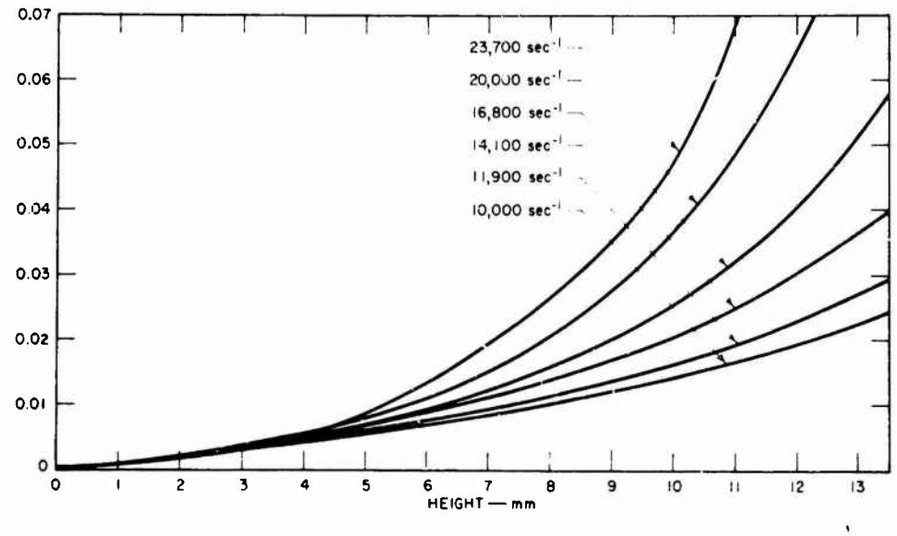

Fig. 2 η^* AS A FUNCTION OF HEIGHT FOR A SOLIDLY-BACKED COLUMN OF 1.2 mm-DIAMETER SPHERES

EXPERIMENTS FOR THE MEASUREMENT OF THE ACOUSTIC IMPEDANCE OF A BURNING SOLID PROPELLANT*

Dr. Gordon R. Leader
Thiokol Chemical Corporation
Elkton Division
Elkton, Maryland

INTRODUCTION

Studies have been made to determine the feasibility of the application of a method developed by O. K. Mawardi (1) for measurements of the acoustic impedance of a burning propellant surface. Measurements by this method, involving externally imposed sound oscillations, could usefully supplement and check data on acoustic impedance of burning propellant surfaces which are currently being obtained by other methods, and could aid in verification and further development of theoretical studies of the problem of combustion instability in solid propellant rocket motors.

EXPERIMENTAL METHOD

The Mawardi method is intended for measurement of the acoustic impedance of inert sound absorbing materials and uses for this purpose a small heavy walled solid chamber such as is shown in Fig. 1. Application of this chamber to measurements on burning propellant requires that the chamber be vented, and Fig. 1 shows in cross section, the manner in which nine radially distributed exhaust ports were provided for the chamber. The chamber is also fitted with a sound driver which supplies to the chamber a high sound intensity of a single frequency in the range 200 - 2000 cps. The sound input is delivered to the chamber through a wire packed source tube and an annular opening around a circular plug in the top of the chamber so as to give a high source impedance and a uniform sound pressure distribution in the chamber. A microphone is also connected to the chamber through a

*The major portion of this work was supported by the Office of Naval Research, Contract NOnr 3474(00), and ARPA Order # 23-62.

small diameter probe tube which is partially packed with steel wool to increase its impedance. A B and K Type 4134 condenser microphone has been used in all passive tests, but was replaced during active tests by an Astatic 151 ceramic microphone which was found better able to withstand the pressure surge and other effects which accompany propellant combustion. The sound chamber is constructed in three sections which can be bolted together when in use or disassembled to permit different types of samples, i.e. solid metal plate, sound absorbing material or propellant sample to be installed in the bottom of the chamber. Small size of the acoustic chamber is necessary to prevent acoustic resonance effects and satisfy other requirements of the Mawardi method. These requirements limit application of the 20 cc chamber to the frequency range 200 - 3000 cycles/sec. An even smaller chamber is required for higher frequencies.

The basic instrumentation used for measurements is shown in Fig. 2. With a given termination in the bottom of the test chamber, sound of a given frequency and at constant intensity is fed into the chamber. The resulting sound oscillations in the chamber are sensed by the microphone and are measured with respect to intensity by the B and K AF Spectrometer and with respect to Phase by the Ad-Yu phase meter. Measurements are read directly from these instruments in passive tests or are recorded on high speed strip recorders during active tests on burning propellant.

The tests on burning propellant must be conducted under pressure. For this purpose, a pressurized chamber of total volume 5.5 cu. ft., capable of withstanding pressures to 1000 psi and permitting the necessary electrical connections to be made to the sound chamber has been provided. (The interior walls of the chamber are lined with sound absorbing material.) Fig. 3 shows a schematic drawing of this pressurized chamber and its accessory equipment.

Each measurement of impedance by the Mawardi method involves comparison of the microphone response under two conditions: with rigid termination, and with sample termination in the bottom of the chamber. If the sound current is constant, and the sum of source and microphone impedance is large in respect to impedance of the chamber, the sample impedance Z_m is related to the impedance of the chamber by the expression

$$Z_m = \frac{Z_1}{\xi e^{j\varphi} - 1} \qquad (1)$$

where ξ is the ratio of microphone voltages and φ is the difference in phase angle shift for the two conditions. In each condition the phase difference between sound driver current and microphone voltage is determined.

When the source and microphone impedance are not sufficiently large to be neglected, a correction term for its effect must be added giving:

$$Zm = Z_1 \left(\frac{1}{\xi_e j\varphi - 1} \right) \left(\frac{1}{1 + \frac{Z_1}{Z_o}} \right) \tag{2}$$

Z_o = sum of source and microphone impedance in a solid chamber. It was found during work on this program that this same expression can also be applied to a vented chamber, where Z_o in this case signifies the sum of source, microphone and holes impedance. The correction term can be obtained as a numerical complex quantity s + tj for the solid chamber by conducting measurements with rigid termination at two different chamber volumes and obtaining at each frequency a value of voltage ratio ξ and phase angle difference φ for this situation. Where $V_1/V_2 = 1/2$

$$\frac{Z_o}{Z_1} = \frac{1 - \xi_e j\varphi}{\xi_e j\varphi - 2} \tag{3}$$

$$\frac{1}{1 + \frac{Z_1}{Z_o}} = \frac{\frac{Z_o}{Z_1}}{\frac{Z_o}{Z_1} + 1} = s + tj \tag{4}$$

It can be readily shown that $s = \xi \cos \varphi - 1$ and $t = \xi \sin \varphi$.

In similar fashion, the analogous correction term a + bj for the vented chamber can be derived by the same treatment of measurements made on the vented chamber with two different chamber volumes (20 and 40 cc volumes were used). The real part of the solid chamber correction term is near unity and the imaginary part is small so that the error introduced by neglect of this term is small, but for the vented chamber, the correction terms vary with frequency over a wide range of values and their use is essential in order to obtain correct impedance measurements.

The correction terms for the vented chamber are incorporated into the working equations which are used to calculate sample impedances from the acoustic data (comparison of rigid and sample termination). These are:

$$R_m = \frac{d(a\xi \sin\theta - b(\xi\cos\theta - 1))}{\xi^2 + 1 - 2\xi\cos\theta} \quad (5)$$

$$X_m = \frac{d(a(\xi\cos\theta - 1) + b\xi\sin\theta)}{\xi^2 + 1 - 2\xi\cos\theta} \quad (6)$$

$$Z_1 = \frac{-\gamma P j}{2\pi f V} \qquad \xi = \frac{Z_1 A}{\rho C} \quad (7)$$

where A = cross sectional area of the chamber and ρ C = characteristic impedance of the medium. The results are thus obtained as specific acoustic impedance ratios.

ACTIVE AND PASSIVE MEASUREMENTS

The validity of the experimental method has been demonstrated by measurements on passive samples. Tests on Johns Manville Airacoustic and other absorbing materials at 1 atm in the solid chamber gave results for real and imaginary parts of the acoustic impedance ratio which are in good agreement with reported values of the sound absorption coefficient for these materials (2), converted to specific acoustic impedance ratio as described by Beranek (3). Measurements in the vented chamber were checked against values obtained for the same passive sample in the solid chamber. Typical results of this comparison are shown in Table I which gives measurements made on a 1/2 inch fiber glass pad sample at ambient pressure. Similar measurements were made at 200 psi, using appropriate correction terms determined at this pressure. In this case, good agreement was again obtained for the imaginary component of impedance ratio between solid and vented chambers. The real components showed poorer agreement than at 1 atmosphere, but were sufficiently close to justify application of this method of calculation to data obtained from active shots (4).

Measurements on burning propellant have thus far been made using a non-aluminized, 82 percent loaded polyurethane propellant. The 20 cc_2 chamber with 9-1/8 inch vents, having a total port area of .11 in^2, is intended for use with a propellant sample 1/2 in. thick, weighing 24 g and having a total area of 2 inches. It has been shown that samples of this size can be burned in the chamber without causing a damaging temperature rise of the driver or microphone. Combustion of this amount of propellant in the pressurized

chamber increases pressure only from 500 to 528 psi and a pressure relief valve in the system operated to maintain the original pressure. The sample combustion causes a pressure surge of 2-3 psi in the sound chamber during burning. To minimize this effect and the amount of combustion noise, both of which can interfere with proper operation of the microphone and driver, samples of reduced surface area (1 in^2) have been used in most of the preliminary measurements.

Table I

SPECIFIC ACOUSTIC IMPEDANCE OF FIBER GLASS PAD (1 Atm)

	Real (R)		Imaginary (X)	
Frequency (K_c)	Solid	Vented	Solid	Vented
0.2	1.40	-6.7	-14.1	-11.7
0.3	0.99	0.30	- 9.7	- 8.6
0.4	1.05	0.44	- 7.3	- 6.7
0.5	1.30	0.51	- 5.9	- 4.0
0.6	1.18	0.65	- 5.1	- 4.9
0.7	1.07	0.60	- 4.4	- 4.2
0.8	0.99	0.59	- 3.8	- 3.9
0.9	0.84	0.46	- 3.35	- 3.40
1.0	0.69	0.61	- 3.20	- 3.14

In active shot measurements made thus far at 200 psi microphone voltage and phase angle shift have been successfully recorded during 4-5 seconds burning times. Interpretation of results was made difficult by the presence of combustion noise and by the effect of pressure surge during combustion on the driver and microphone. A 1/3 octave filter has been used to reduce the interference of combustion noise in most of these studies, but recent work has shown the need for an even better filter and one with a narrower band pass (5-10 cycles) will be employed in future work to improve both the voltage and phase angle recordings. The Astatic 151 ceramic microphone used during active shots has been shown to be able to accommodate the pressure surge during combustion without loss in performance. The seriousness of pressure surge effect on driver output was overlooked during preliminary measurements and appears to

invalidate the first results obtained. Correction of this effect has been made by providing larger ports for equalization of pressure on both sides of the driver diaphragm.

CONCLUSION

The means for overcoming the major experimental obstacles to obtaining significant data during active shots from which acoustic impedances can be calculated have thus been found. These will be applied in future work to studying in detail at various pressures and frequencies the acoustic impedance of the non-aluminized polyurethane propellant, and tests will then be extended to include other propellant types.

REFERENCES

1. Mawardi, O. K., "Measurement of Acoustic Impedance," J. Ac. Soc. Am. 21 84-91 (1949).

2. Tukasik and Nolle, "Handbook of Acoustic Noise Control", Volume I, Supplement 1, WADC Tech Report 52-204, April 1955.

3. Beranek, Acoustic Measurements, p. 869.

4. Thiokol Chemical Corporation, Elkton Division, "Experiments for Measurement of Acoustic Impedance of Burning Solid Propellant", Quarterly Reports 1-6, May 15, 1961 - Feb. 15, 1963, Contract Nonr 3473(00).

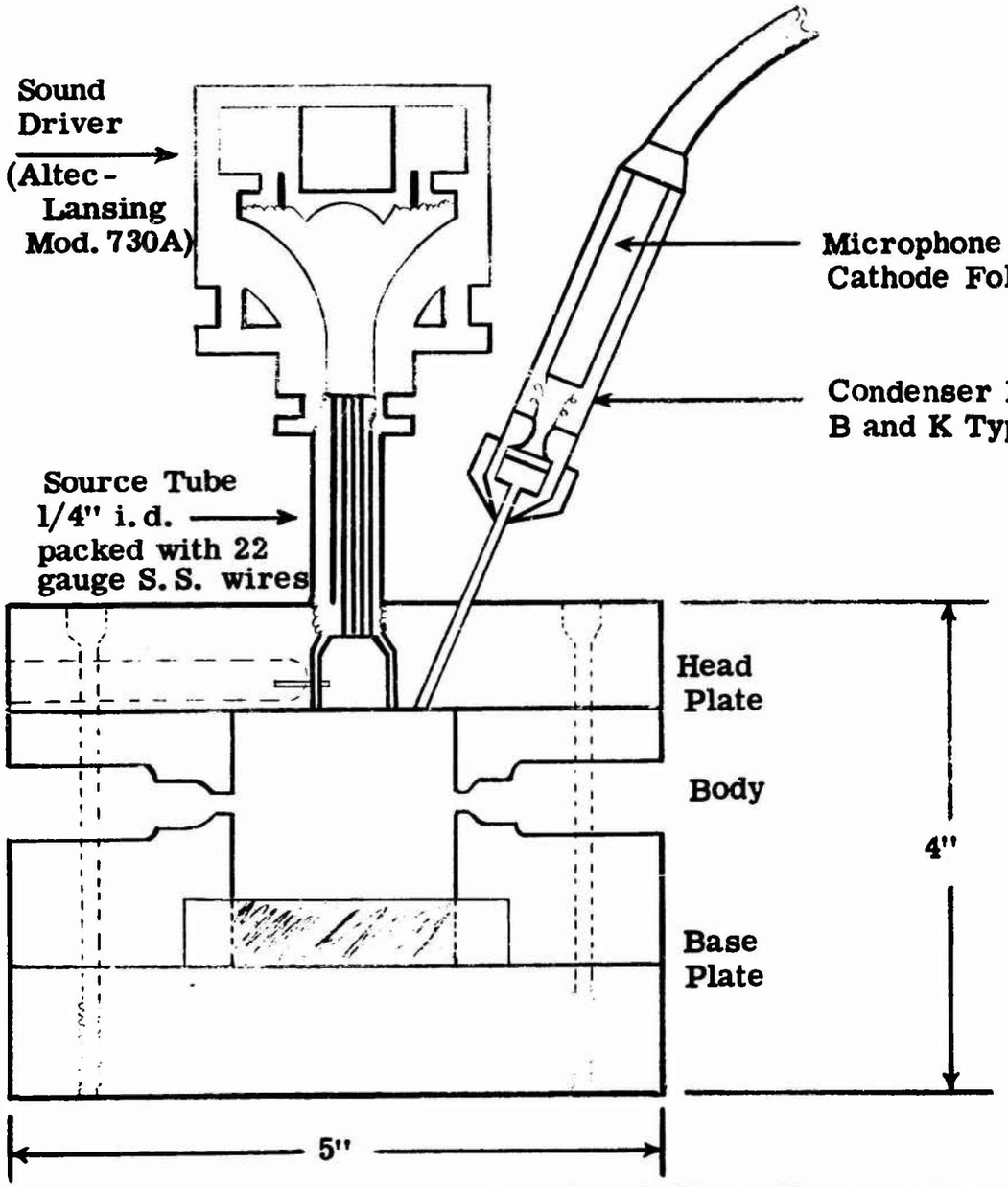

Annular opening around Spool (0.027") Packed with 22 gauge S.S. Wires

Chamber Dimensions:	20 cc	40 cc
Height	0.598"	1.196"
Diameter	1.625"	1.625"
Area	2 in.	2 in.^{2}

Propellant Sample Thickness 1/2".

9 Radially distributed exhaust ports with 1/8" openings.

Fig. 1. MODIFIED MAWARDI IMPEDANCE MEASUREMENT CHAMBER

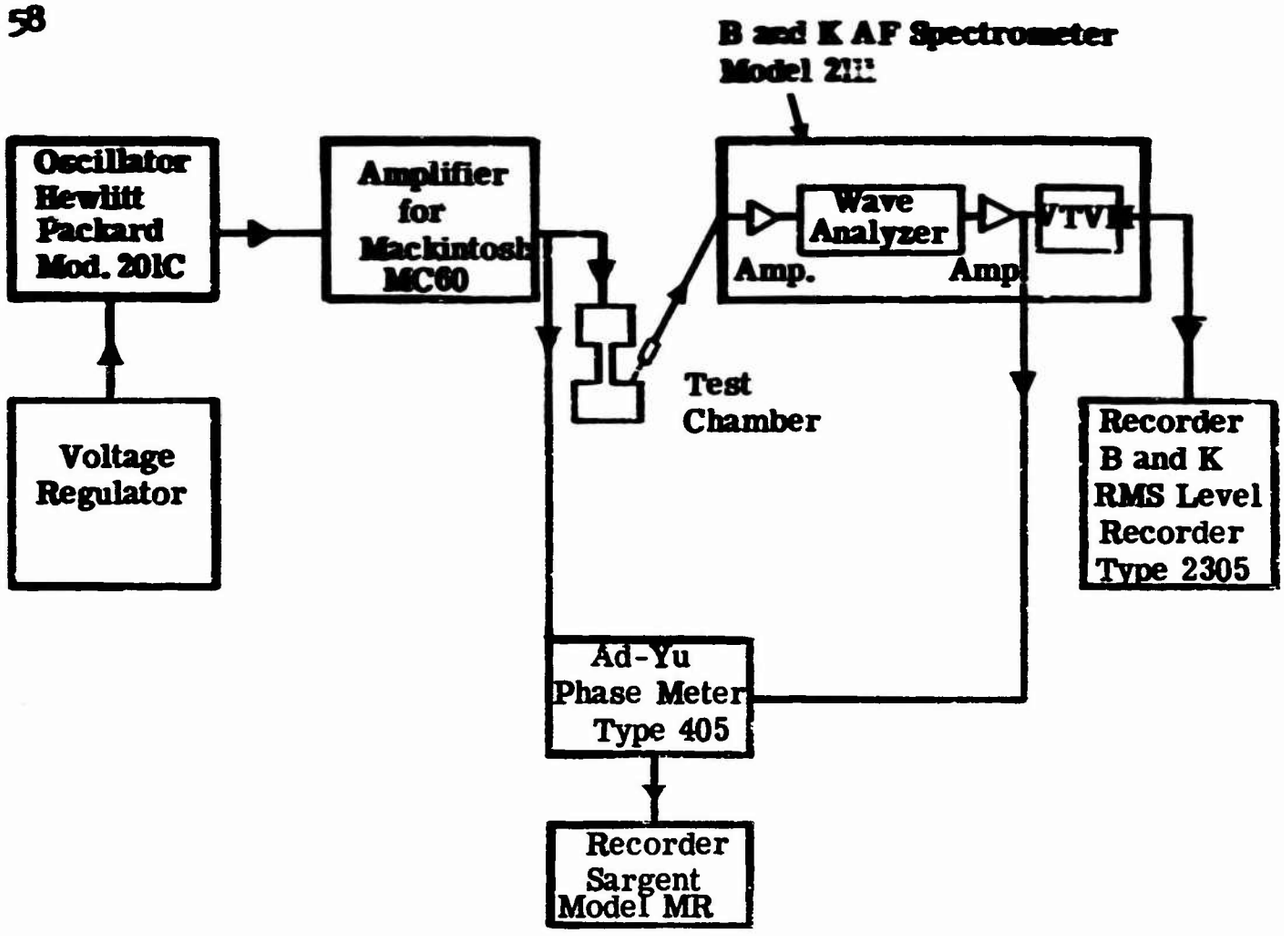

Fig. 2. BLOCK DIAGRAM OF INSTRUMENTATION FOR ACTIVE TESTS

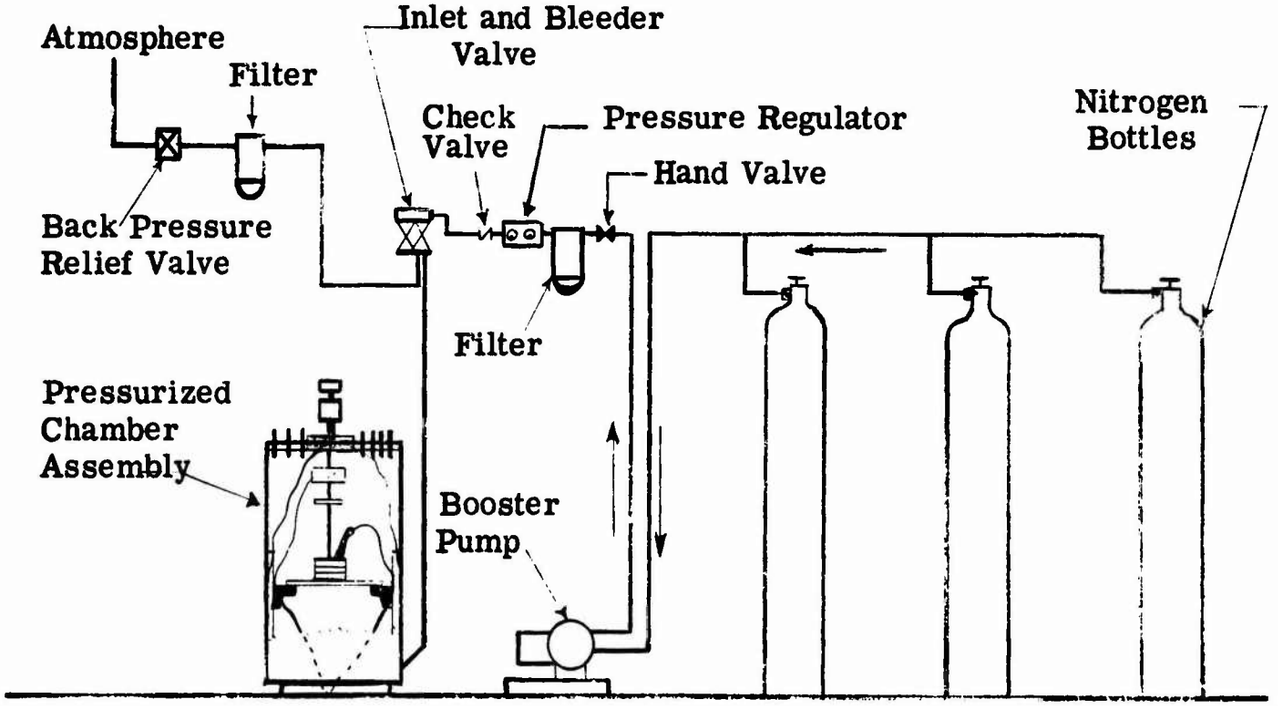

Fig. 3. SCHEMATIC OF PRESSURE SYSTEM

ACOUSTIC WAVE BURNING ZONE INTERACTION IN SOLID PROPELLANTS*

H. F. Calcote
AeroChem Research Laboratories, Inc.
Princeton, New Jersey

The main objective of this research was to measure the acoustic admittance of a solid propellant flame. The unique feature of this experiment was the passage of the acoustic wave through the propellant and thence through the combustion zone. This phase of the program has been completed. Work of a preliminary nature has also been done on the noise spectra produced by such flames. Preliminary experiments on measuring the acoustic absorptivity of propellant gases issuing from aluminized propellants have been performed, and more accurate measurements of the acoustic attenuation of aluminum oxide particles in the gas phase from solid propellants employing aluminum are being made.

Acoustic Admittance

The apparatus employed in the measurement of acoustic admittance is presented in Fig. 1. This involves a wave analyzer coupled to a signal generator from which the driver signal activates two 60 watt horn driver units which are coupled to the propellant through a 93-inch long tube, 1 1/8" i.d. The propellant is burned at one atm. in an anechoic chamber which is 10' x 10' x 14'. This allows operation at frequencies above 500 cps. The frequency range of the Hewlett-Packard model 302A wave analyzer and signal generator is from 500 to 15,000 cps. The output of the acoustic sound intensity after passing through the burning surface is detected by a microphone and fed to the wave analyzer. The output of the wave analyzer is recorded on an oscillograph. The minimum detectable db change in this experiment was - 1.3×10^{-3} rayls^{-1}. Since no absorption of the sound could be accredited to the presence of the flame, the admittance of the combustion zone must be less than - 1.3 x 10-3 rayls. This is consistent with an estimate of Hart (1). The prope lants used in these experiments were ammonium perchlorate composites. We feel we have gleaned as much from this experiment as is possible so the technique has been abandoned.

Flame Noise Spectra

Experiments were run to determine the spectral distribution of the combustion noise produced by the burning strands. Square strands

*The work reported on is that of Dr. D. W. Blair, who is currently on leave of absence with the Norwegian Defense Research Establishment. In his absence, this report was presented by Dr. H. F. Calcote. The work was sponsored by the Office of Naval Research, Contract Nonr-3477(00), ARPA Order No. 23-61.

3/8" on a side were burned in the anechoic chamber. The location of the strand and the microphone within the chamber were varied. The microphone signal after being amplified was sent to the wave analyzer which produced a dc signal proportional to the input amplitude. This signal was electrically integrated over a period of 52 seconds. Experiments were performed at several frequencies and the results reported as change in db relative to standard signal level. Some typical results are reported in Fig. 2. In this figure the effect of particle size for an ammonium perchlorate propellant is recorded as well as results from a double base propellant. The signal level is observed to peak at about 3,000 cycles independent of particle size, propellant type, and variation in propellant composition and aluminum content. The only change seems to be in signal amplitude. This similarity in sound spectra suggests that some property of the anechoic chamber is being measured. However, this possibility has been eliminated by shifting the positions of the strand and microphone and by replacing the strand with an electrical-mechanical sound source. It is possible that the sound is generated by the turbulent mixing between the propellant gases and the surrounding atmosphere (jet noise). It should be possible to demonstrate this by varying the strand diameter. This will be done in future experiments.

Acoustic Absorptivity of Aluminized Propellant Products

Some very preliminary work was carried out to determine the feasibility of measuring the acoustic absorptivity of the aluminum oxide particles in the combustion gases from a solid propellant. The experimental apparatus is sketched in Fig. 3. A metal tube was coupled to the acoustically driven air column through an asbestos diaphragm. In the middle of this tube a microphone was connected through a glass wool packed T-tube. The propellant was burned in a connecting tube near the diaphragm such that the combustion gases flowed through the main tube and out an open end into the anechoic chamber. The propellant strands consisted of layers of non-aluminized and aluminized propellants, thus the change in the microphone signal could be recorded as the combustion gases changed from products without aluminum to products containing aluminum oxide. The results of this work are presented in the table. The experiment demonstrated a definite change in sound level with the addition of aluminum.

Acoustic Frequency (cps)	Acoustic Pressure Ratio, Aluminized to Nonaluminized Propellant (db)
2% aluminum:	
290	- 1.5
1400	- 1.1
4% aluminum:	
250	- 2.5
475	- 5.0
1425	- 0.83

Proposed Measurement of Acoustic Absorptivity

It is proposed to measure the acoustic absorptivity by a method based upon experiments recently reported by Parker (2). In essence, this measurement consists of determining the "half power point" of gases contained in a rigid walled cylindrical tube. Since a tube of this type will show resonance at a series of harmonic frequencies, the experiment is performed by driving the tube at the several harmonics and observing the difference in frequency at which the power is one half the maximum. The basic equation is:

$$\Delta f = \frac{c\sigma}{\pi}$$

where Δf is the frequency difference at the half power point,

c is the velocity of sound which must be measured separately or obtained from two measurements at the half power point,

σ is the acoustic absorptivity.

Experiments are being designed to make these measurements.

REFERENCES

1. Hart, R. W., Eighth Symposium (International) on Combustion, Williams and Wilkins Company, Baltimore, Maryland , p. 917, 1962.

2. Parker, J. G., J. Chem. Phys. 34, 1767 (1961).

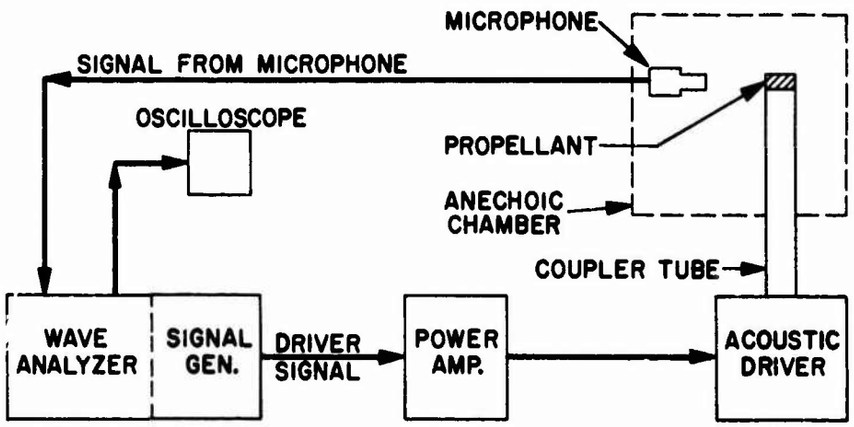

Fig. 1. FLOW DIAGRAM FOR SOLID PROPELLANT ACOUSTIC INTERACTION EXPERIMENT

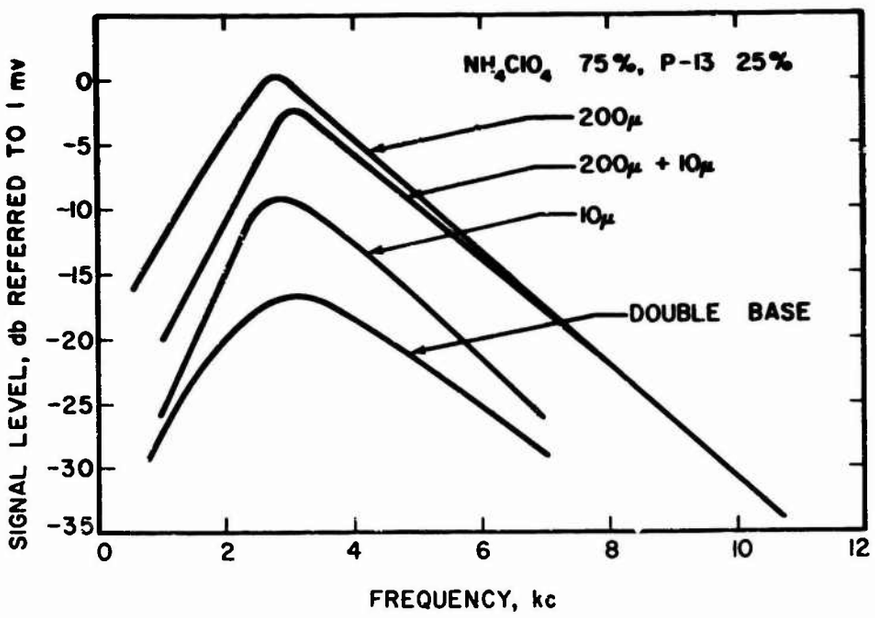

Fig. 2 FLAME NOISE SPECTRA

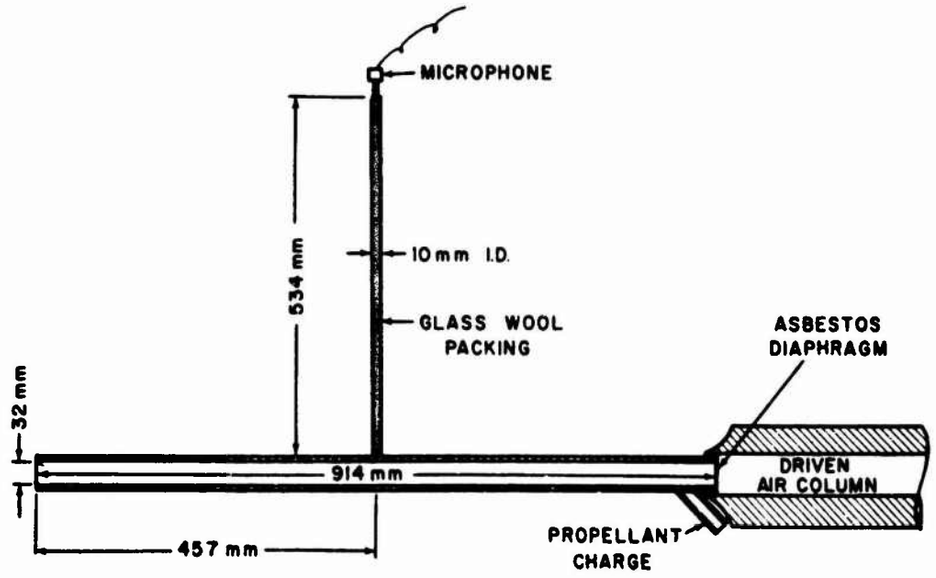

Fig. 3 EXPERIMENTAL APPARATUS FOR DETERMINING ACOUSTIC ABSORPTIVITY OF PROPELLANT COMBUSTION GASES

CARDE EXPERIMENTS ON NONLINEAR AXIAL COMBUSTION INSTABILITY

W. G. Brownlee*
Canadian Armament Research and Development Establishment
Valcartier, P.Q.

INTRODUCTION

A systematic investigation of finite wave axial combustion instability was undertaken at CARDE in 1960. To date some 200 experimental motors have been fired using polyurethane ammonium perchlorate (CARDEPLEX) propellants. The primary aim of the firings has been to determine the gross dependence of the unstable process on motor operating parameters. The results obtained have been applied to motor design programs (1) [superscript numbers refer to footnotes; numbers in parentheses are references] and are now incorporated in CARDE motor development procedures.

Nonlinear axial combustion instability occurs when one or more strong compression waves propagate axially within a motor cavity. The resulting unsteady flow field interacts with the combustion process, derives energy from the interaction and causes an increase in the time-average burning rate of the propellant. Thus the flow field is nonlinear in the usual sense; furthermore, the experimental results indicate that the process is linearly stable and nonlinearly unstable with respect to initiation. Therefore a triggering flow disturbance is required to produce instability. This trigger was provided in the experimental firings by means of the pulse technique originated by Dickinson (2).

The single "sonance-tube" system reported in Ref. 2 was modified by the author (3,4,5) so that several flow disturbances are now injected directly into the motor cavity as shown in Fig. 1. Pressure time traces from a typical firing[1] with pulse initiation are shown in Fig. 2. The increase in space-time average burning rate associated with the instability is evident in the low frequency response pressure recording. The traces labelled "interval A,B" are piezo (Kistler) gauge pressure recordings taken at the head end of the motor. The steep fronted compression wave has a pressure ratio at reflection of approximately 1.4. Application of one-dimensional theory for reflection of a plane shock wave (γ=1.24)

1. This motor was 8 inches in diameter x 80 inches in length. The propellant was Type A3, nonaluminzed, 25% polyurethane binder, 75% ammonium perchlorate. The propellant grain was case-bonded and cylindrically perforated with a 4-inch port diameter. The grain ends were restricted. For brevity the motor will be coded as A3 x 4 x 8 x 80 in. Future references to motors will employ this coding. For other propellant formulations see Table I.

*Major, Royal Canadian Artillery, Seconded to Canadian Armament Research and Development Establishment, Defence Research Board, Quebec.

leads to a propagation Mach number of 1.08. The frequency of oscillation is approximately 250 cps.

Similar results have been obtained with motors as large as Star x 17 x 180 in. and as small as 1 x 2 x 10 in. Typical results are shown in Fig. 3.[1] It may be seen that the frequency range for finite wave axial combustion instability extends from at least 100 cps to 2 Kcs.

The experimental firings exhibited a remarkable degree of reproducibility. The observed operational trends lead to an approximate criterion for stability which can be obtained experimentally. Certain salient features of the results are described in the present summary. A more complete description is given in Ref. 5.

TABLE I

Propellant Data

Formulation Code No. 4760/	A3	A5	A12	B7	C2
Polyurethane fuel, % by weight	25	25	25	25	25
Ammonium perchlorate (150 μ), % by weight	75	70	70	70	56
Aluminum, % by weight					
SAX-3 (40μ, 6% Mg)	-	5	-	5	-
SA-24 (7 μ)	-	-	5	-	-
SAX-9 (40μ, 12% Si)	-	-	-	-	19
LiF, added parts	-	-	-	1.8	-
Flame temperature, °K	2288	2460	2460	2350	2677
Mean molecular weight (gas)	22.49	20.99	20.99	21.06	17.85
Burning rate at 1000 psia, in./sec	0.19	0.20	0.22	0.15	0.14

Case-bonded grain cross-sections of tubular, opposed slab, star and two and three arm modified cloverleaf designs were used in the test motors.

NONLINEAR AMPLIFICATION AND INITIATION

Motor response to a flow disturbance depends on the net amplification or gain of the system. The response is nonlinear in that the gain is a function of disturbance amplitude. This may be seen clearly in Fig. 4, where pressure traces are shown for an A5 x 1 x 2 x 20 in. firing. On the second pulse the motor seemed marginally

1. The 17 in. firing was not pulsed. Instability was initiated by a small flow disturbance of unknown origin. The motor casing burst on the fiftieth cycle of oscillation.

stable as evidenced by the decaying amplitude of the compression wave. Nevertheless the motor became fully unstable on arrival of the strong third pulse at a time when the weaker wave was damping out. Similar nonlinear effects have been observed in many firings. On the other hand no instances of amplification from the 'noise' level have been encountered.

An immediate consequence of nonlinear amplification is that motors capable of the most catastrophic unstable behavior will repeatedly operate in a stable manner provided that no triggering flow disturbance occurs. This inherent capability of unstable operation will be referred to here as incipient instability. A measure of the degree of incipient instability is the relative jump in average pressure which occurs on transition from stable to unstable operation. Motors which are incipiently unstable to a high degree require only a small flow disturbance in order to transition, as for example in the case of the 17 in. motor shown in Fig. 3.

To ensure positive testing of development motors the pulses used are larger than any natural disturbances likely to occur. The same is true of the experimental firings for in the latter case interest has centered on the behavior of fully excited motors. The purpose has been to determine the conditions under which any given motor is incipiently unstable.

DEPENDENCE OF AXIAL INSTABILITY ON THE AREA RATIO K_n

The effect of varying the motor geometry has been investigated with a large number of firings. The most crucial result is that the degree of instability (for a given propellant and motor scale) is almost entirely dependent on the ratio of burning surface area to throat area, K_n. Pressure time curves obtained from a series of A5 x 1 x 2 x 20 in. motors are shown in Fig. 5. The traces are arranged in ascending order of the initial value of the area ratio, K_{ni}. Motors with successively smaller throat sizes became progressively more unstable and at earlier times until at $K_{ni} = 392$ instability began on ignition. This behavior pattern has been observed in all unstable firings regardless of propellant type, grain cross-section, grain temperature and motor size or scale.

Pressure data from a similar series of A3 x 1 x 2 x 20 in. motor firings is plotted logarithmically versus log K_n in Fig. 6. All values are head end pressures taken at a time when the fraction of the web burnt, f_w, was 0.8.[1] The curves labelled 'peak' and 'minimum' refer to the maximum head end pressure at reflection and the minimum pressure just prior to reflection, respectively. Average pressures were obtained from a low frequency response pressure recording system.

1. For CARDEPLEX propellants the constants in the non-erosive rate law, $r=\alpha p^n$, are weak functions of the web fraction. At constant pressure the rate increases until $f_w=0.5$ and then decreases to burnout. The value of r at $f_w= 1.0$ exceeds that at $f_w=0$. Maximum deviation from the ideal law is about 15 to 20%. This effect is reflected somewhat in the unstable pressure values. Therefore, wherever possible, data has been compared to a fixed value of f_w.

The peak, average and minimum pressures lie on parallel straight line segments in the log p - log K_n plane. It follows that the ratio of peak to minimum pressure (i.e. the compression wave strength) is independent of port-to-throat ratio, 1/J. More generally, results at other values of f_w show that the ratio is independent of K_n. Again, the time average unstable pressure, P_{cus}, plots linearly. This pressure will be reached only if the instability is triggered. For example, a motor operating stably at P_{cs} = 610 psia (i.e. $K_n \approx 400$) is capable of unstable operation at $\bar{P}_{cus} \approx 1300$ psia. The relative jump in pressure decreases with K_n. In fact, the oscillating flow field produces an effect equivalent to an increase in n and decrease in α in the stable burning rate law. Consequently the plot of $\bar{P}_{cus}$ intercepts that of P_{cs} at a particular value of K_n, say K_n^*, which in the present instance is about 220. If a motor operating at $K_n < K_n^*$ is pulsed, the injected compression wave is attenuated in successive cycles and the average pressure returns to the stable value. Since K_n increases with time for tubularly perforated motors it is possible for them to be inherently stable during an early portion of a firing and incipiently unstable at a later time when K_n has become greater than K_n^*. Also, it is clear that if the throat size is decreased in successive firings, then K_n^* will be reached at correspondingly earlier times. This trend is apparent in the firings shown in Fig. 5.

In view of the above it is obvious that K_n^* can be used as a stability criterion[1] provided that linear scale-up, change in grain cross-section, or change in motor length does not affect the correlation of P_{cus} with K_n. In order to determine the effect of scaling up, a series of A3 x 4 x 8 x 80 in. motors was fired. Results are given in Fig. 7. The P_{cus} vs K_n correlation method remained valid but the degree of instability was reduced so that K_n^* increased to 270. Thus, the larger motor may be considered less prone to instability. Other results (5) show that this improvement does not continue proportionally for still larger motors. Firings of 17 x 180 in. motors show that they are at best only slightly more stable than the 8 x 80 in. size.

Further tests were made to determine the influence of motor length and grain cross-section. Complete firing traces from B7 x 3 x 8 x 80 and 120 in. motors are compared in Fig. 8. It is clear that a length increase of 50% does not seriously affect the correlation. Similar results were obtained from A3 x 1 x 2 x 20 and 30 in. motors as may be seen in Fig. 9. On the other hand, shortening the length to 10 inches reduced the degree of instability. At the same time, the latter motors were not very reproducible as may be seen in Fig. 9 and it was difficult to initiate instability.

---

1. For CARDEPLEX propellants the dependence (noted earlier) of the stable rate law constants on web fraction leads to a corresponding shift in K_n^*. This effect is easily accounted for in prediction.

A number of motors were fired with the non-tubular grain cross-sections shown in Fig. 10. The change in grain cross-section did not affect the $\bar{P}_{cus}$ vs K_n correlation obtained from tubular firings. As an example, in Fig. 11, data from A3 x 2 Arm x 8 x 80 in. motors is compared with tubular results.

Summarizing, it appears that $\bar{P}_{cus}$ is a function of K_n only, for given case diameter, propellant, and propellant temperature provided that L/D is sufficiently large. A critical value of restriction ratio, K_n^*, exists such that motors operating at $K_n < K_n^*$ remain axially stable.

EFFECT OF VARIOUS PROPELLANT ADDITIVES

The dependence of motor stability on propellant formulation has not been investigated in depth. However, results obtained so far show that aluminum additive is not nearly as effective a suppressant of finite axial instability as it has proven to be for the transverse modes. This may be seen in Fig. 12 where 4 x 8 x 80 in. firing data is plotted for propellants A3, A5, A12, C2 and B7. The estimated intersections of $\bar{P}_{cus}$ with P_{cs} are marked with solid circles in each instance. The associated K_n^* values are given in Table II.

TABLE II

Propellant	K_n^*	Additive
A3	270	-
A5	430	5% Al (40 μ, 6% Mg)
A12	500	5% Al (7 μ)
C2	310	19% Al (40 μ, 12% Si)
B7	350	5% Al (40 μ, 6% Mg) + 1.8 added parts LiF.

It is immediately evident that substitution of 5% SAX-3 aluminum alloy for the equivalent amount of oxidizer (propellant A5) is beneficial in that K_n^* increases from 270 to 430. Therefore, while an A3 motor operating at say, P_{cs} = 700 psia would be incipiently unstable to a high degree, the equivalent A5 motor at the same chamber pressure would almost certainly be inherently stable. A further gain was made on substituting fine pure aluminum rather than SAX-3 (propellant A12).

Propellant B7 presents an interesting situation. The formulation is identical with that of propellant A5 except for the addition of 1.8 parts LiF which serves to reduce the stable burning rate by about 25 percent. The stability characteristics are adversely affected since K_n^* decreases from the A5 value of 430 to 350. Suppose that the burning time of an A5 motor is to be increased by substituting propellant B7. Assume further that a stable chamber pressure of 700 psia is to be maintained by decreasing the throat area. The required value of K_n for the B7 motor is 540 which corresponds to

an unstable chamber pressure of about 1500 psia. The design change thus leads to a motor which is inherently unstable to a high degree. The ill-fated 17 in. firing shown earlier in Fig. 3 resulted from just such a seemingly innocuous redesign. Needless to say, current information was not available at the time.

A low burning rate may also be obtained by increasing the aluminum loading as in propellant C2. Preliminary data points from 4 x 8 x 80 in. and Star x 17 x 180 in. firings are given in Fig. 12. It appears that there is no great difference in the behaviour of the two motors. The degree of instability is low and the gaseous compression waves are very weak and not steep fronted. In fact they have the same highly damped aspect as the decaying waves that are present during tail-off of an unstable motor using nonaluminized propellant. Whether this is due to decreased propellant response or increased particle damping is not yet clear.

The information given in Fig. 12 may be cross plotted ($\bar{P}_c$ vs P_{cs}) as in Fig. 13. The line at 45 degrees corresponds to stable operation for all propellants; that is, the time average pressure equals the stable pressure. The oblique lines give the incipient unstable average pressures, $\bar{P}_{cus}$ as functions of the corresponding stable pressure P_{cs}. The relative stability of the propellants with respect to P_{cs} is B7$\longleftrightarrow$C2, A3, A5, A12. These are ordered in the same way as the burning rate as may be seen on reference to Table I. Thus is appears that low-burning-rate propellants become unstable at low operating pressures and high rate propellants at high pressures. It seems likely that this behavior can be associated with the erosive burning characteristics of the propellants. However, the latter characteristics are not yet available in detail.

INFLUENCE OF INITIAL GRAIN TEMPERATURE

As might be expected, the propellant grain temperature has an important influence on unstable motor behavior. Firings with an A12 x Star x 10 x 120 in. motor show that with fixed geometry, stability decreases with initial grain temperature. This does not appear to be due to an increase in $\bar{P}_{cus}$ at given K_n as may be seen in Fig. 14.[1] Rather, the onset of instability at low temperature can be associated with the shift in K_n* arising from temperature displacement of the P_{cs} plot.

FURTHER OBSERVATIONS

Several interesting operational features were noted during the course of the experiments. It is possible for two compression waves to exist simultaneously at undiminished strength. When this occurs $\bar{P}_{cus}$ increases only slightly. During single shock wave instability

---

1. All values of K_n are referred to the best estimate for the 72°F firing at the time when the fractional pressure integral, ϕ , reached a value of 0.6 in each instance. Hence the positions of the data points relative to each other are probably correct although the 72° base point may be somewhat mislocated.

the wave is attenuated when propagating from head to nozzle and amplified when moving upstream.

The nonaluminized propellant A3 occasionally exhibited transverse tangential instability. In a few instances the onset of high frequency instability occurred when the motor was fully excited in the finite axial mode. The average burning rate then increased a further 50 to 70 % while the axial mode was immediately suppressed. A plausible explanation follows if we assume that the rate increases associated with both types of instability are largely due to induced tangential gas particle velocities (6,7). The space average excitation should be greater for the transverse mode. If a limit to the rate increase due to gas velocity is assumed, then the axial wave may be unable to sustain itself on the grounds that locally it can produce no rate increase over that arising from the fully developed tangential wave.

The very small 1 x 2 x 20 in. motors are unsuitable for evaluating the stability characteristics of propellants. Aside from the large scaling effect noted for the nonaluminized A3 propellant, it was found that aluminized propellants behaved anomonously. The average unstable pressure, $\bar{P}_{cus}$, for propellants A5 and B7 was essentially identical with that for A3; that is while stable burning rates were normal the unstable rate was not influenced by the presence of aluminum or lithium fluoride. It has been shown that this was not true for the larger 8 x 80 in. motors.

Finally, while the experiments were conducted using polyurethane propellants it appears that nonlinear axial instability is by no means limited to this class. The same phenomenon has been observed in a CARDE firing of a 5 x 50 in. motor with plastic propellant (8). Triggering occurred when an injected graphite sphere produced momentary, partial nozzle blockage.

ACKNOWLEDGEMENTS

Prosecution of the investigation reported here obviously required the cooperation, ingenuity, and concerted efforts of a large number of people. The author wishes to acknowledge the direct and indirect contributions of all concerned.

The larger test motors were cast by the Process Engineering Section under the direction of Mr. B. J. Holsgrove. The Propellant Group, Rocket Engine Development Section, filled the subscale motors. All firings, development of firing facilities, and the preparation of raw data for reduction were carried out by Test and Evaluation Section under Mr. C. D. Martin. Digital computer analysis of firing data was provided by Systems Wing.

The program was greatly aided by the enthusiastic support of Mr. L. A. Dickinson, until recently head of the Rocket Engine Development Section. Furthermore, his pioneering work with the pulse method of initiation of axial instability provided the essential technique which made the investigation possible.

Within the Rocket Engine Development Section most people were directly involved in some aspect of the program. Mr. F. Jackson, now Section Leader, was Ballistic Group Leader during most of the investigation. The author is particularly indebted to him for his patient, generous support as a friend and as a scientist.

Finally, the author especially wishes to thank Mr. A. K. Roberts, who scheduled the trials of the 10 x 120 in. and 17 x 180 in. motors, for his unselfish view that certain preliminary results should be included in the present report.

REFERENCES

(1) [redacted]

(2) [redacted]

(3) Dickinson, L.A. "Command Initiation of Finite Wave Axial Combustion Instability in Solid Propellant Rocket Motors", ARS Journal, April 1962.

(4) Dickinson, L.A., Brownlee, W.G., and Jackson, F., "CARDE Investigations of Finite Wave Axial Combustion Instability (U)", CARDE Tech. Note 1459/62.

(5) Brownlee, W.G., "An Experimental Investigation of Finite Wave Axial Combustion Instability"(U), CARDE Tech. Memo No. 660, UNCLASSIFIED. In process of publication.

(6) Brownlee, W.G. and Marble, F.E., "An Experimental Investigation of Unstable Combustion in Solid Propellant Rocket Motors", Academic Press, Progress in Astronautics and Rocketry, Vol. 1: Solid Propellant Rocket Research, 1960, pp. 455-494.

(7) Price, E.W., "Combustion Instability in Solid Propellant Rocket Motors", NAVORD Report 7023 (NOTS TP 2389), 1959, UNCLASSIFIED.

(8) Morris, E.P., Test and Evaluation Section, Propulsion Wing, CARDE. Personal Communication.

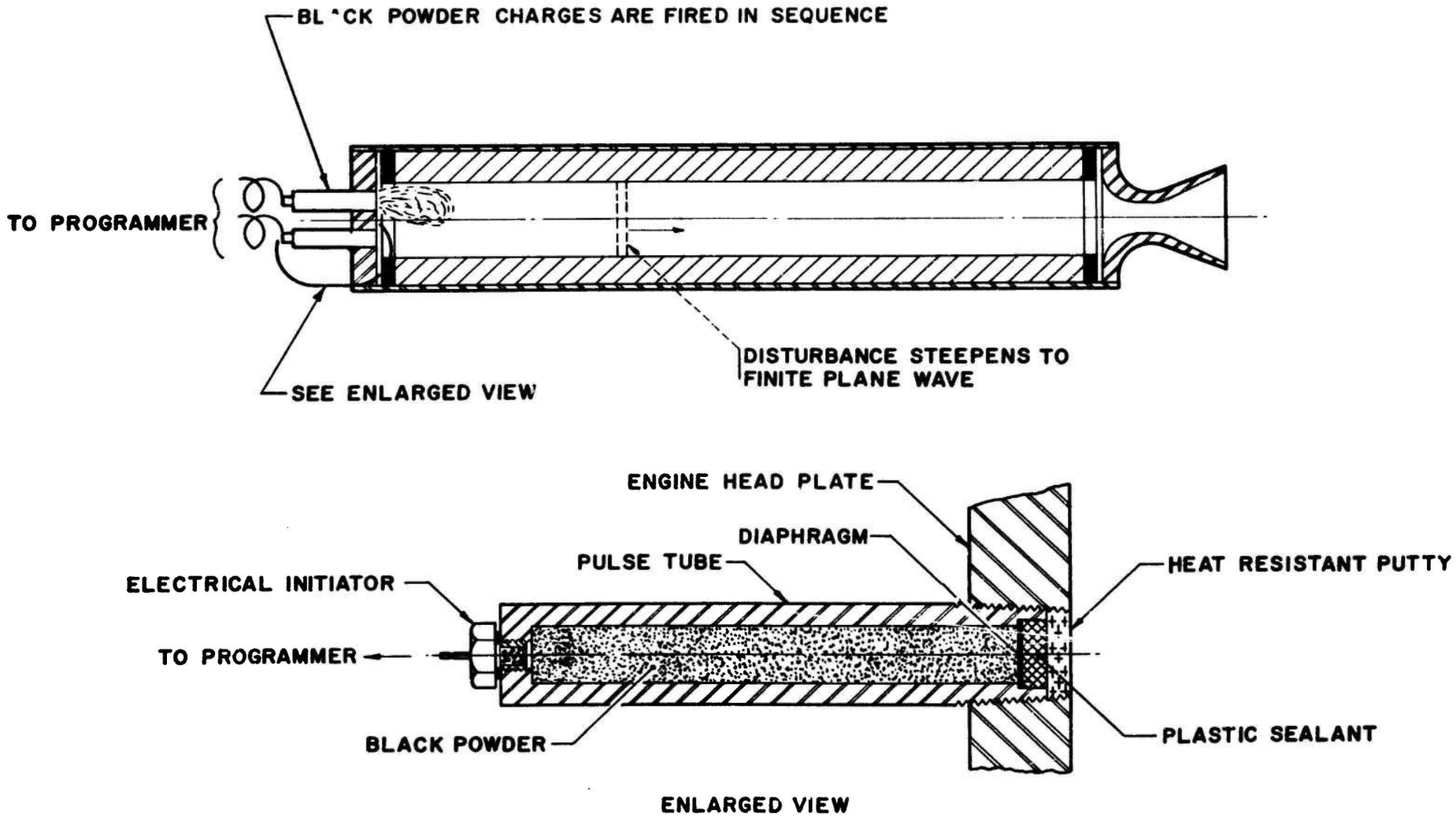

Fig. 1 PULSE TUBE LAYOUT

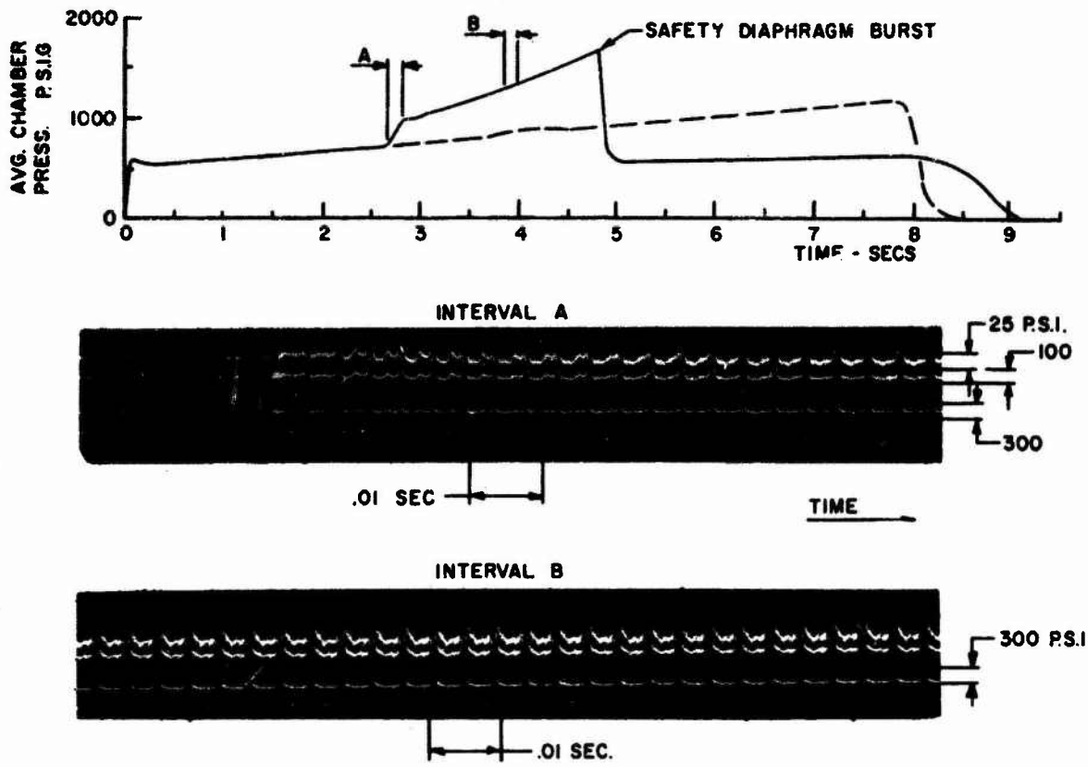

Fig. 2. PRESSURE-TIME HISTORY OF A TYPICAL A3 x 4 x 8 x 80 in. UNSTABLE FIRING AT 70°F; PULSE INITIATION

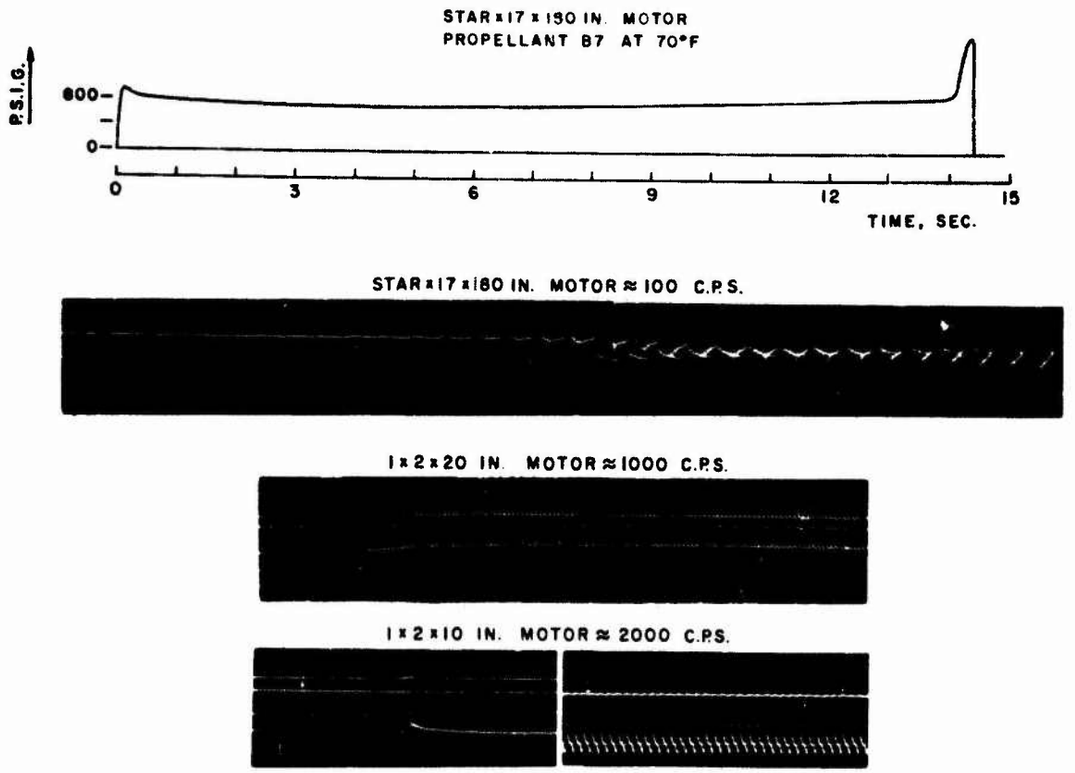

Fig. 3 TYPICAL HIGH FREQUENCY PRESSURE RECORDINGS IN THE FREQUENCY RANGE 100 cps to 2 Kc

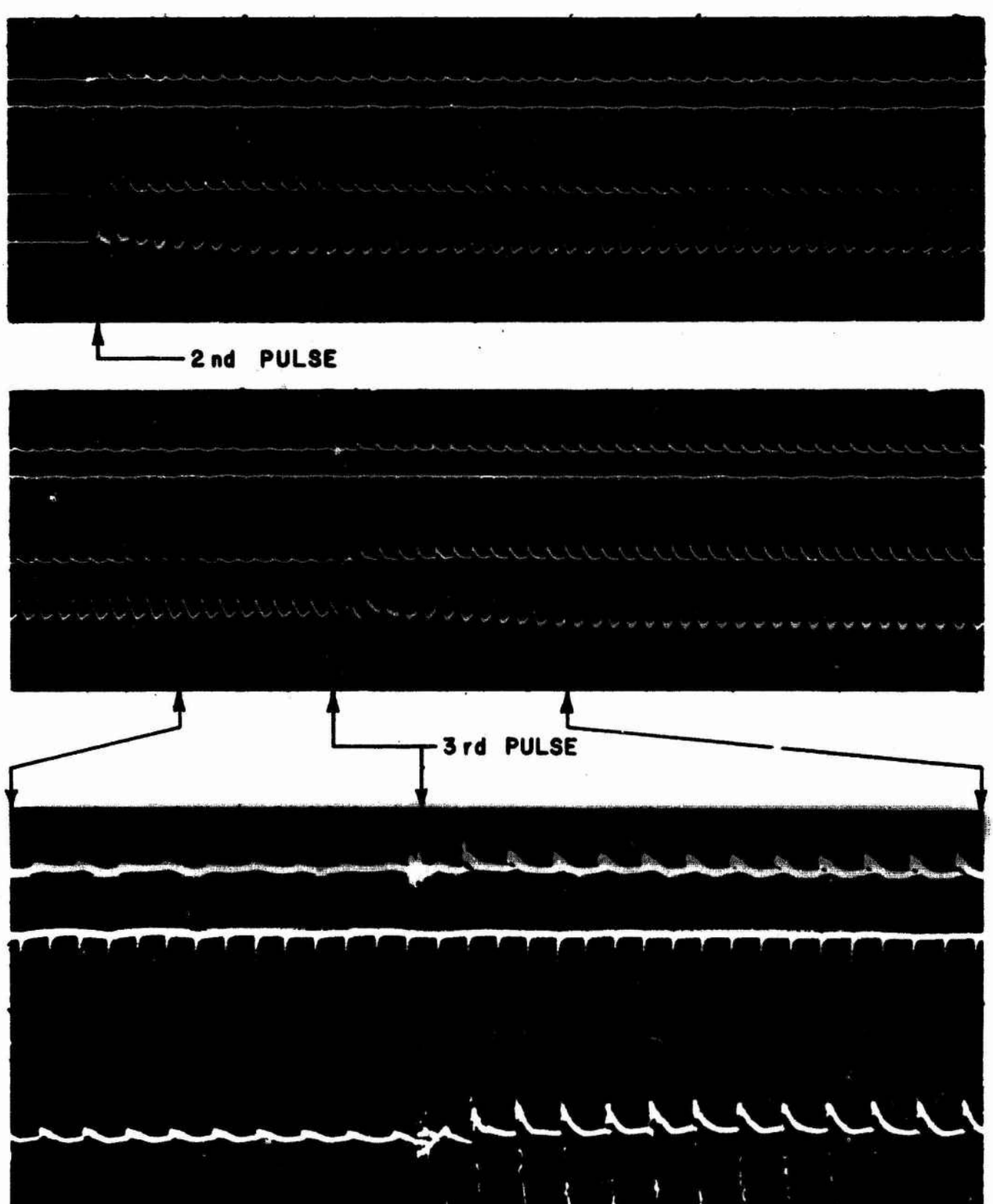

Fig. 4 NONLINEAR AMPLIFICATION OF FLOW DISTURBANCES IN AN A5 x 1 x 2 x 20 in. MOTOR

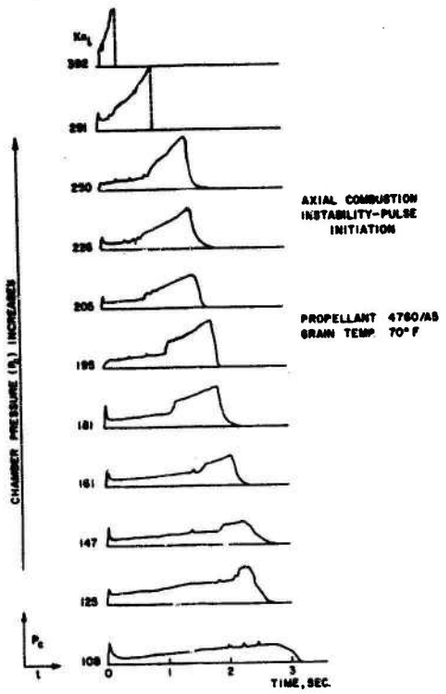

Fig. 5 EFFECT OF VARYING THE INITIAL THROAT DIAMETER; A5 x 1 x 2 x 20 in. MOTORS AT 70°F; P_c versus t

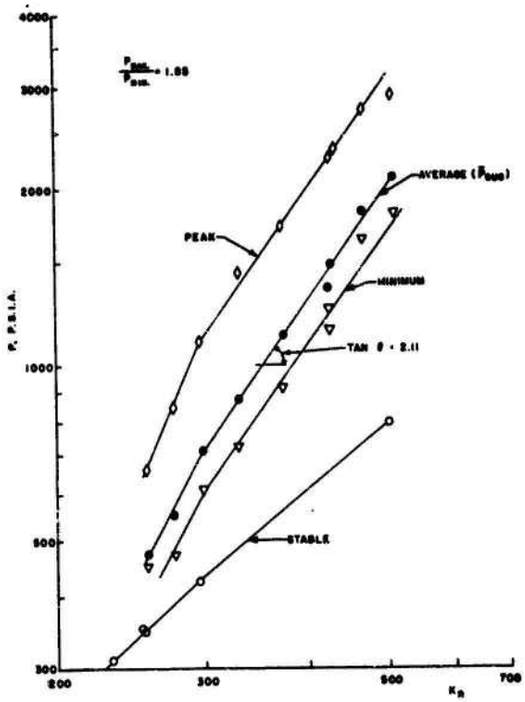

Fig. 6 PEAK, AVERAGE AND MINIMUM PRESSURES DURING INSTABILITY VERSUS AREA RATIO, K_n; WEB FRACTION, f_w = 0.6; A3 x 1 x 2 x 20 in. MOTORS AT 70°F

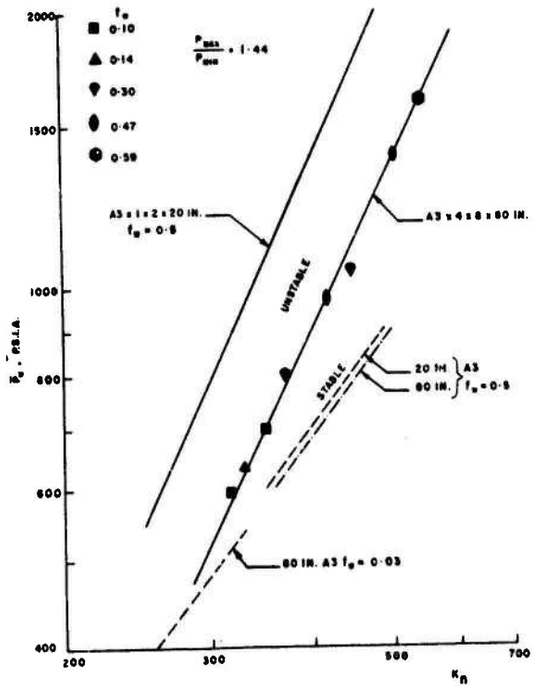

Fig. 7 EFFECT OF A LINEAR SCALE-UP; $\bar{P}_{cux}$ versus K_n FOR A3 x 4 x 8 x 80 in. MOTORS AT 70°F; f_w = 0.1 to 0.59

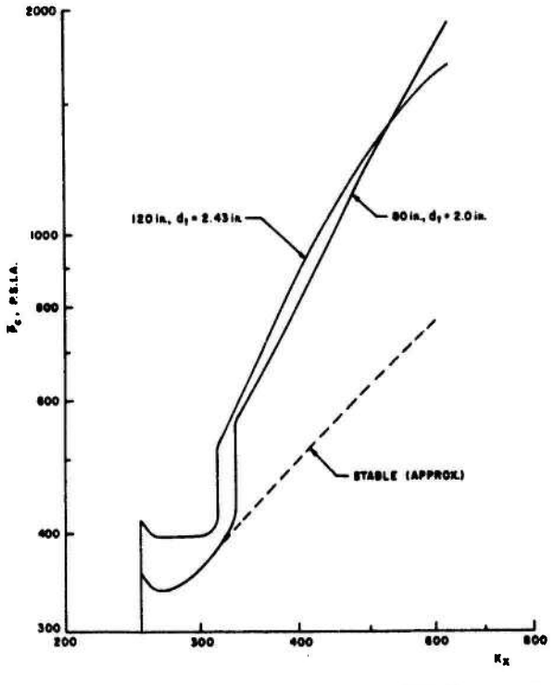

Fig. 8 EFFECT OF CHANGING THE MOTOR LENGTH; $\bar{P}_{cux}$ versus K_n for B7 x 3 x 8 x 80 and 120 in. MOTORS AT 70°F

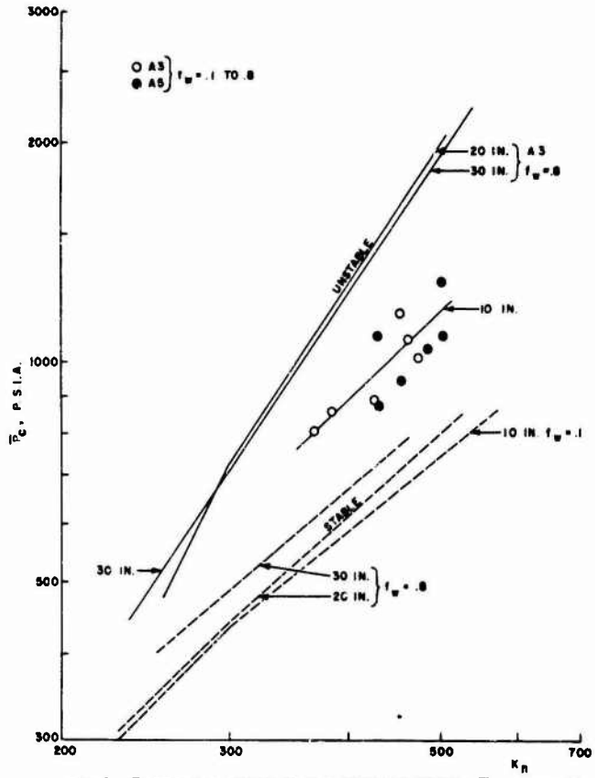

Fig. 9 EFFECT OF CHANGING THE MOTOR LENGTH; $\bar{P}_{cus}$ versus K_n for A3 x 1 x 2 x 10, 20, and 30 in. MOTORS AT 70°F; f_w = 0.8

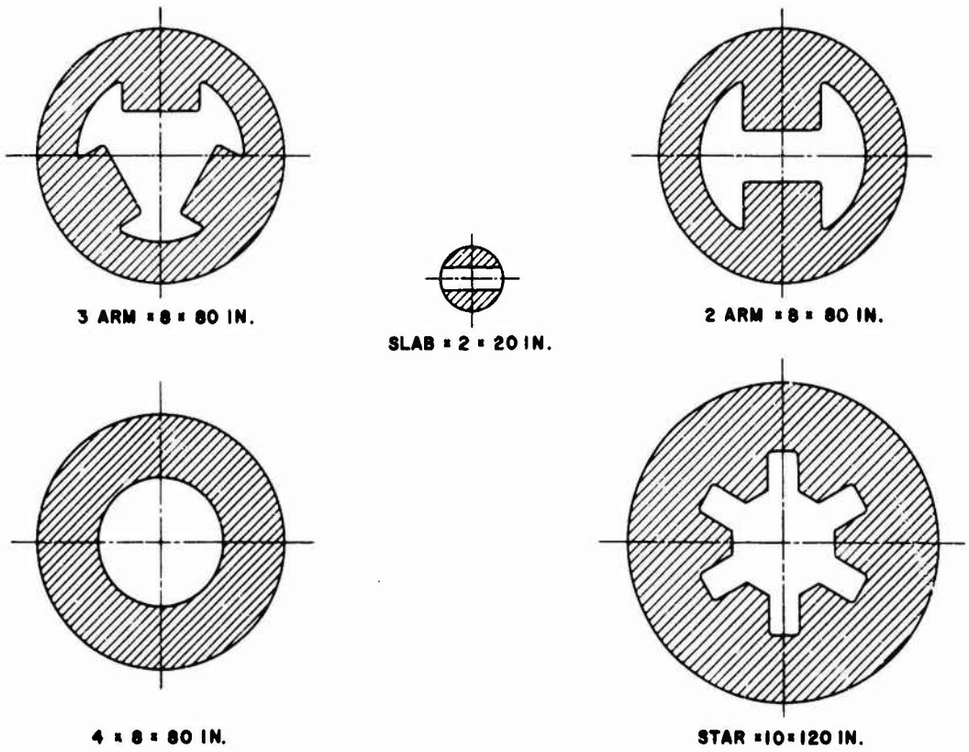

Fig. 10 GRAIN CROSS-SECTIONS

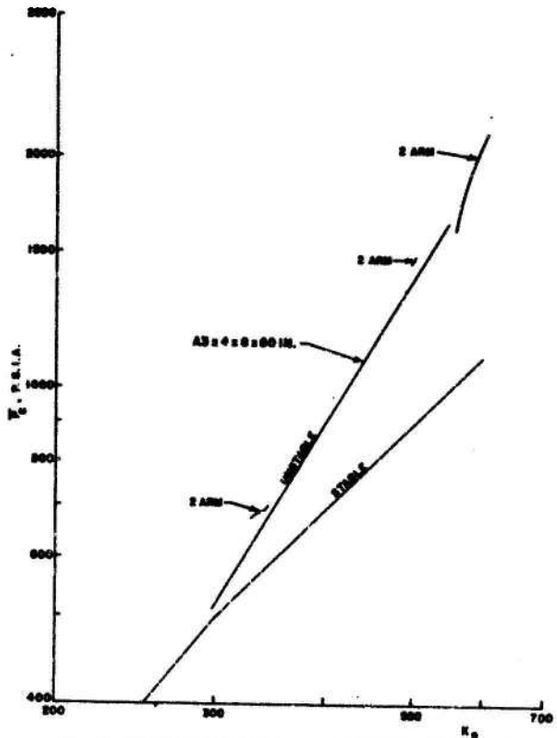

Fig. 11 EFFECT OF CHANGING THE GRAIN CROSS-SECTION; P_{cus} versus K_n for A3 x 2 Arm x 3 x 80 in. MOTORS AT 70°F

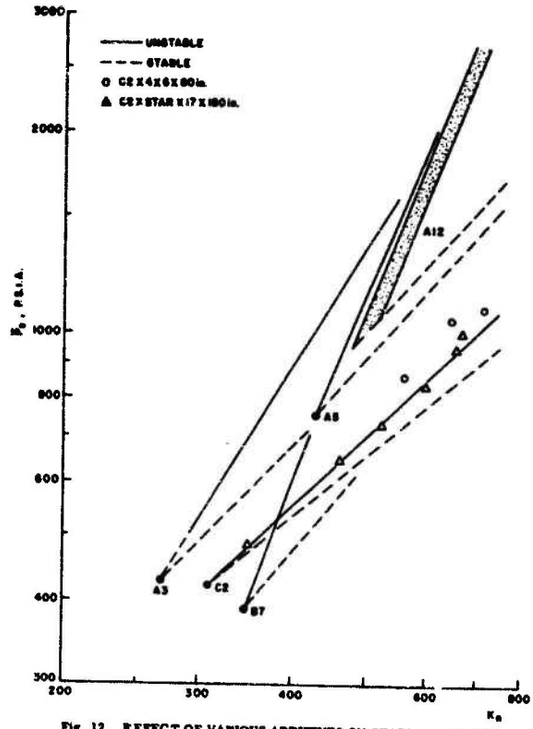

Fig. 12 EFFECT OF VARIOUS ADDITIVES ON STABILITY OF THE 4 x 8 x 80 in. MOTORS: P_{cus} and P_{cs} versus K_n FOR PROPELLANTS A3, A5, A12, B7 and C2 at 70°F

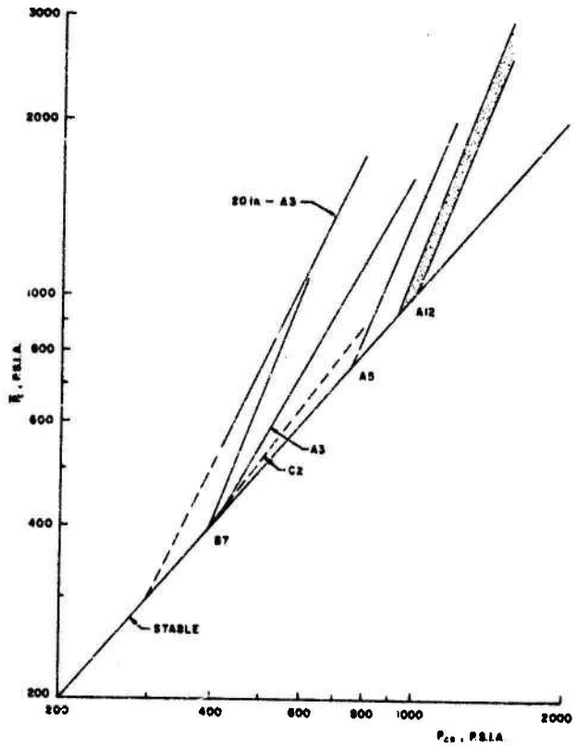

Fig. 13 EFFECT OF VARIOUS ADDITIVES ON STABILITY OF THE 4 x 8 x 80 in. MOTOR; P_c versus P_{cs} FOR PROPELLANTS A3, A5, A12, B7 and C2 at 70°F

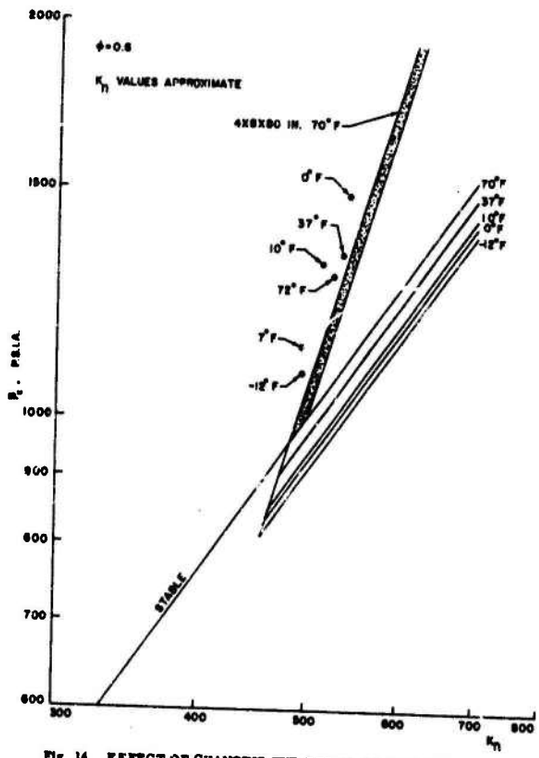

Fig. 14 EFFECT OF CHANGING THE INITIAL GRAIN TEMPERATURE; P_{cus} versus K_n for A12 x Star x 10 x 120 in. MOTORS

EXPERIMENTAL INVESTIGATIONS OF LOW FREQUENCY COMBUSTION INSTABILITY*

E. W. Price
U. S. Naval Ordnance Test Station
China Lake, California

Occurence of oscillatory behavior in the 1-100 cps frequency range has become increasingly common as the size of rocket motors has increased, as the operating pressure has been reduced, and as the variety of propellants has increased. The oscillatory behavior in this frequency range is usually (but not always) in nonacoustic modes of the combustion chamber, and is usually (but not always) obtained with propellants using metal fuel ingredients. The unstable behavior includes not only periodic oscillations, but also self-quenching and chuffing. Because no well-established laboratory or theoretical tools were available for elucidation of the phenomena, progress in achieving understanding or rational control of such instability has been slow.

During the past year two experimental techniques have been applied to the study of low frequency instability. One consists of a double-ended burner with propellant discs having burning surfaces facing each other (Fig. 1). The reaction products are vented through a hole in the center of one of the propellant discs, leading to a sonic nozzle. In this configuration, the stay time of material in the combustion chamber flow is varied by varying the distance between the two burning surfaces. This system was tested 75 times, with several propellant-nozzle size-stay time combinations.

A typical oscillatory test is shown in Fig. 2. All classes of behavior from steady high pressure burning to oscillatory behavior to chuffing to spontaneous quenching after ignition were observed, with all propellants exhibiting such anomalous behavior under some conditions at low pressure. While the behavior was not correlated with any quantitative arguments, it was observed that the limiting conditions for stable behavior with each propellant could be correlated with the L^* of the combustion chamber. At pressures below 100 psi, unstable behavior of some kind was generally encountered for L^* below the critical value noted in the table on the following page.

*This work was sponsored by NASA.

Propellant Type	Minimum L* For Stable Behavior
PBAA-ammonium perchlorate	10 in.
Polyurethane-ammonium perchlorate-15% aluminum	200 in.
Double-base with MG-Al alloy	200 in.
Double-base	2,000 in.

The correlation between the limiting L*'s and the known combustion rates (i.e., completeness of combustion of ingredients) of the propellants at low pressure supports the argument that pressure-dependent combustion efficiency is a factor in the stability of the combustor (as argued in an accompanying article). Work is continuing on this investigation, with particular emphasis on low pressure combustion rates and on accumulation, shedding, and combustion of metal fuels during propellant burning. Also, a few firings of the burner have been made with glass walls; the results indicate that photographic methods hold considerable promise.

A second experimental technique used for low frequency investigations consists of a six-inch-diameter burner with lengths up to 60 feet. The purpose of this burner is to permit investigations in acoustic modes at frequencies down to 10 cycles per second. The configuration was described in last year's report: the burner provides for a propellant slab at each end and for either no vent or a nozzle midway between the ends. The system oscillates spontaneously with some propellants in the axial mode. With "stable" propellants, the relative stability can be determined by measuring the decay rate of a pressure oscillation induced by a small black powder charge. To date this system has been used to compare stability of about 15 propellants in a series of 35 firings. While the technique appears to be useful for comparing propellants with respect to low frequency pressure-coupled instability, further experience is required to evaluate the effects of heat loss, to determine how to control the mean pressure level, and how to obtain decisive ignition and pressurization of this high-free-volume system. While the present performance is adequate for comparing the relative stability of propellants, quantitative data such as that obtained by Horton in smaller burners at higher frequency may not be attainable.

Aside from obtaining comparative data on different propellants, the low frequency investigations to date have served primarily to show how varied and complex the LFI behavior is. While enough is known about the behavior to warrant speculative interpretation of results, data to verify the speculations is still lacking and will be slow to "emerge" because of the experimental difficulties. Probably the most intriguing result to date is the evidence that a propellant may have a preferred frequency

for low frequency instability, i.e., a frequency at which it is prone to burn in an oscillatory fashion. This idea has been suggested by results reported by Angelus in previous Technical Panel meetings, and is implied in the analytical results of Dennison and Baum. It has even been suggested that some propellants will burn in an oscillatory manner in a constant pressure vessel. While the results of investigation of one particular propellant during the present program (Fig. 3) support the concept of a preferred frequency, it does not seem likely that any inherent capacity of a propellant to burn in an oscillatory manner can lead in itself to rocket motor instability. Instability of the "combustor" as a whole can occur only if the oscillatory combustion of the propellant at various locations in the combustor is brought into some suitable phase relation characteristic of the particular mode of oscillation. It is hard to see how such "coherence" of the oscillatory combustion behavior could occur unless there is some measure of responsiveness of the combustion oscillations to the oscillating state of the combustor as a whole. The "preference" of some propellants for oscillations at particular frequencies in burners and motors thus may reflect a high susceptibility to oscillatory behavior in a particular frequency range, but cannot possibly be construed as inherent instability of the propellant independently of the oscillating environment produced in the burner (assuming the propellant sample size is large compared to the thickness of the combustion zone). This thesis is supported in the results of the "big pipe" tests summarized in Fig. 3. During these tests, the burner would not oscillate except at times during the test when the frequency-pressure conditions in the figure were satisfied for natural acoustic mode of the burner, i.e., when the combustor was able to exert a feedback to the combustion at the frequency "preferred" by the propellant.

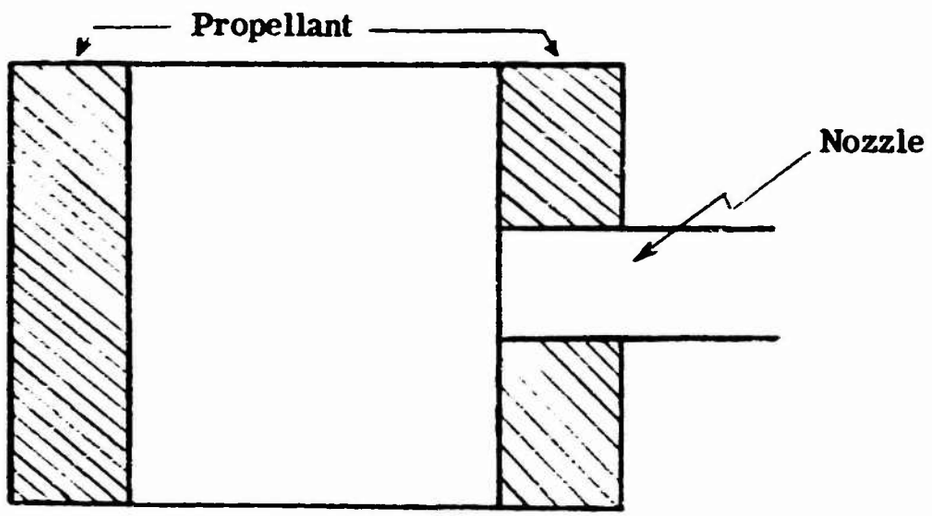

Fig. 1 SCHEMATIC OF L* BURNER

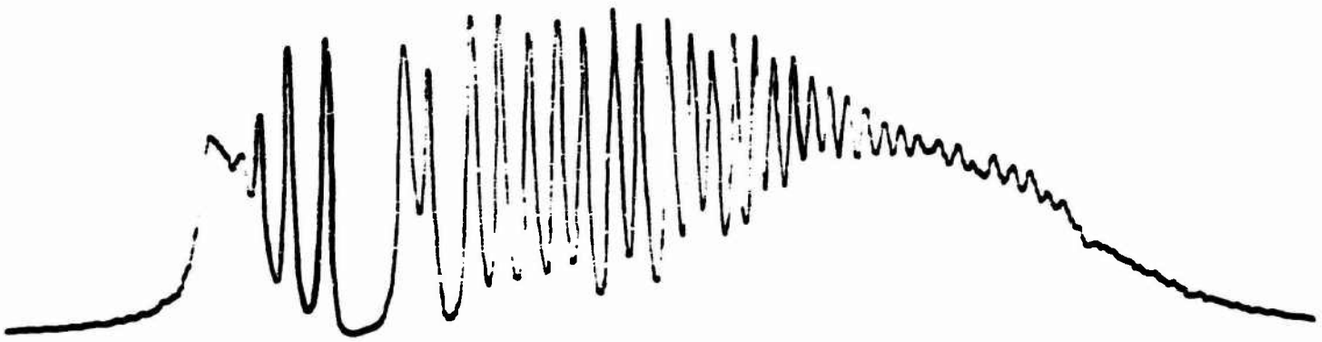

Fig. 2 OSCILLATORY BEHAVIOR OF THE L* BURNER
(pressure-time record)

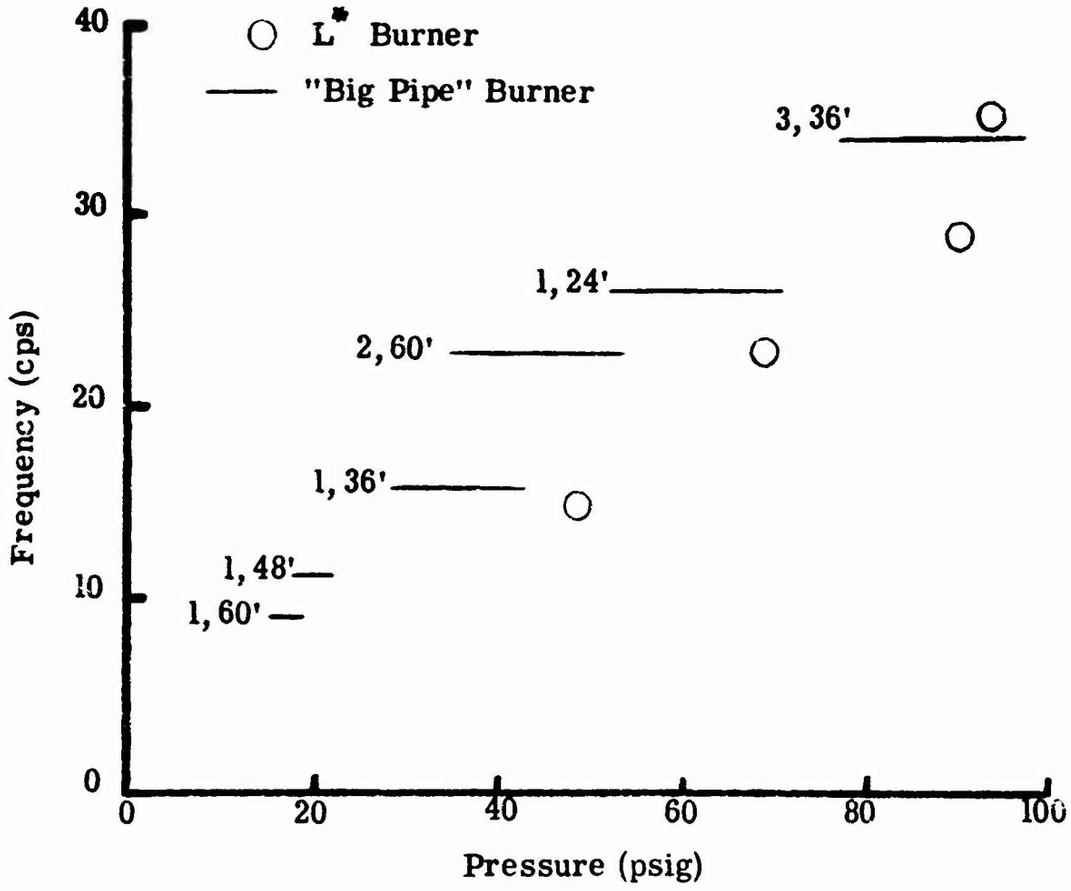

Fig. 3 FREQUENCY OF OSCILLATIONS WITH A CAST DOUBLE-BASE PROPELLANT CONTAINING 4% MAGNESIUM-ALUMINUM ALLOY ADDITIVE. NUMBERS IN THE FIGURE IDENTIFY THE UNSTABLE AXIAL MODE AND LENGTH OF THE BURNER

PROGRESS REPORT ON SOLID PROPELLANT COMBUSTION INSTABILITY STUDY*

A. O. Converse and G. K. Klinzing
Carnegie Institute of Technology

INTRODUCTION

Our studies of combustion instability are carried out in a 1 1/2" diameter pipe which is open at one end and closed with a reciprocating piston at the other. The propellant is attached to the piston and is ignited while the piston is in oscillatory motion. The combustion, therefore, takes place in an oscillating pressure field. The pressure is measured at the piston end of the pipe under resonant conditions. As indicated in the section on the mathematical analysis this allows one to evaluate the dynamic burning rate-pressure response. The combustion products are vented through the open end and, at present, the static pressure is one atmosphere. The piston is driven by a variable speed electric motor through a scotch yoke. The piston motion, therefore, contains no harmonics. With the present equipment the frequency can be varied from 4 to 25 cps and the amplitude of the oscillating pressure between 0 and 0.5 atmosphere.

This sytem was chosen for the following reasons:

a. At very low frequency one can assume that at each instant the pressure dependency of the burning rate is the same as the static pressure dependency. This pseudo steady-state assumption which must begin to apply at some sufficiently low frequency allows one to calculate the pressure amplitude to be expected. This allows one to verify the experimental results. At higher frequency both the measurement and the calculation may be subject to question and there is somewhat of a dilemma.

b. With piston driver it is possible to have much larger pressure amplitude than can be obtained with acoustic equipment. This is an advantage in distinguishing the signal from combustion noise. Although the amplitudes may be large the reflection conditions at the open end of the pipe prevent large distortion of the desired sinusoidal pressure wave forms. This allows the investigation of the nonlinear response of the combustion without the complications of extreme nonlinearities (e.g. shock waves) in the pressure wave forms.

c. And, of course, the low frequency region is of interest itself.

---

*This work is supported by the Army Materiel Command at the Ballistic Research Laboratory, Aberdeen Proving Ground, Maryland. Contract No. DA-36-034-AMC-3797(R).

EXPERIMENTAL RESULTS

In order to evaluate our ability to analyze the effect of time-average flow on the pressure oscillations, some non-combustion experiments have been run.[1] In these experiments air is admitted at the piston end of the pipe through a critical flow orifice. Thus the mass flow rate can be maintained constant, independent of the pressure oscillations in the tube. The effect of mean flow on the pressure oscillations at the piston end of the tube is shown in Fig. 1. The effect is most pronounced where $M < 0.035$. In connection with this, it is interesting to consider the effect of steady state Mach number on the gas velocity. With no mean flow ($M = 0$) the gas velocity reverses direction during a period, at every point in the tube. As mean flow is introduced, the gas flow ceases to reverse its direction first at the piston end of the tube, and then progressively throughout the tube as the Mach number is increased. Under the conditions corresponding to the data in Fig. 1, flow reversal ceases at $M = 0.03$. Hence is appears that the damping of the pressure oscillations is greater when there is no flow reversal, and the rate of change of pressure amplitude with increasing mean flow is greatest when the flow reversal is being destroyed. This should be considered to be a preliminary remark; greater verification is obviously needed.

THEORETICAL RESULTS

At present inorder to simplify the analysis we consider a purely hydrodynamic model. That is, the propellant is considered merely as a source of gas, the flux of which depends on the pressure.

Two methods of analysis have been applied. In the first method the continuity and motion equations have been linearized permitting an analytical solution. Although momentum transfer between the gas and tube is considered, heat transfer is not. However, this omission is corrected empirically by using a measured damping coefficient. The damping coefficient is evaluated in the experiment where $M = 0$.

In the second method the nonlinear equations were applied. This required numerical integration using the method of characteristics (1) [superscript numbers refer to footnotes; numbers in parentheses are references]. Two assumptions were made, however:

a. There is no heat transfer between gas and tube due to the variation in gas temperature during compression and rarefaction. This again was compensated by choosing the friction factor f so that computed and experimental amplitude agreed at $M = 0$.

---

1. In the combustion runs the pressure oscillations are also presumably affected by the temperature gradients as well as the flow. Combustion runs are now being started.

b. It was also assumed that the heat generated by friction at the wall was absorbed by the wall and was not transferred to the gas. Thus the entropy of the gas could be considered constant.

A. Linearized Analysis.

The following linearized wave equation can be derived (2):

$$\frac{\partial^2 \mu}{\partial \theta^2} - (1 - M^2)\frac{\partial^2 \mu}{\partial \varphi^2} + 2M\frac{\partial^2 \mu}{\partial \varphi \partial \theta} + MB\frac{\partial \mu}{\partial \varphi} + B\frac{\partial \mu}{\partial \theta} = 0 \quad . \tag{1}$$

The boundary conditions are

$$\pi(1) = 0 \qquad \text{at open end} \tag{2}$$

$$\mu(0) = \epsilon + \alpha\pi(0) \qquad \text{at piston end} \tag{3}$$

where $\alpha = M(N\gamma - 1)$; $\epsilon = V/\bar{c}$. (4)

The boundary condition at the piston end is the essential one and it is obtained from a sample mass balance

$$\rho u = V\rho + Kp^N\rho_P \tag{5}$$

total mass flux = mass flux due to piston motion + mass flux due to propellant combustion .

The pressure is measured at resonance at the piston end. Under these conditions and with $M < 1$ we get

$$\frac{\pi(0)}{\epsilon} = \frac{(2/B)\cos(\eta\theta)}{1 - (2\alpha/B)} \quad . \tag{6}$$

The above equation is in agreement with our physical intuition. As B, the damping factor, goes to 0, the pressure amplitude becomes infinite, which is to be expected at resonant conditions. When N becomes larger, which is to say that the burning rate pressure exponent becomes larger, the pressure amplitude also increases.

From Eq. (6), α can be determined from the measured pressure π and the damping factor B.

Since

$$\alpha = M(N\gamma - 1) \quad , \tag{7}$$

one can evaluate the effective pressure exponent N because γ and M are known. Since this is a steady state experiment, the damping factor B must be obtained from other sources.

In the actual experimental results reported in Fig. 1, the mass flow into the tube was independent of pressure, hence N = 0 and α becomes - M. With this slight alteration, Eq. (6) becomes

$$\frac{\pi(0)}{\epsilon} = \frac{2}{B}\frac{\cos(\eta\theta)}{1 + (2M/B)} \quad . \tag{8}$$

Values of $\pi(0)/\epsilon'$ computed from Eq. (8) are compared to the experimental values in Fig. 1. The value of B was calculated from the no-flow experimental data; hence the theoretical and experimental curves are forced to agree at M = 0. The inability of the linearized analysis to predict the observed behavior is apparent. The calculated values were refined by allowing for the fact that B is a function of $\pi(3)$. The improvement was negligible. The reason why the linearized analysis breaks down is not known at present.

B. Nonlinear analysis.

Following the development of Shapiro (1) the equations upon which the analysis is based are

$$\left(\frac{dx}{dt}\right)_{I,II} = u \pm c \tag{9}$$

$$\left(\frac{du}{dt}\right)_{I,II} = \mp \frac{2}{\gamma-1}\left(\frac{dc}{dt}\right)_{I,II} - F\left(1 \mp \gamma \frac{u}{c}\right) \quad . \tag{10}$$

These equations are integrated numerically, using the method of characteristics. Here the agreement with experiment is quite good as shown in Fig. 1.

CONCLUSION

The effect of mean flow on the pressure oscillations in a gas-filled tube has been studied under a limited set of conditions. Whereas the linearized analysis failed to predict the observed behavior, a well known nonlinear analysis did succeed. Thus it appears that the effect of the mean flow caused by a burning propellant can be taken into account. It is suggested that this method of analysis should be employed in the study of unstable combustion in rocket motors if the flow can be considered to be one-dimensional.

NOMENCLATURE

B = damping factor

c = velocity of sound

$\bar{c}$ = time average velocity of sound

D = pipe diameter

f = Fanning friction factor

$F = (fu^2)/D\ (u/|u|)$

K = a constant in the burning rate expression

L = pipe length

M = $\bar{u}/\bar{c}$, Mach number

$n = \omega L/\bar{c}$

p = pressure

t = time

u = gas velocity

V = piston velocity

α = defined by Equation (7)

γ = Cp/CV

$\epsilon = V/\bar{c}$, dimensionless piston velocity

ϵ' = amplitude of ϵ

$\theta = t\bar{c}/L$ dimensionless time

$\pi = p/\gamma\bar{p}$ dimensionless oscillatory pressure

ρ = gas density

ρ_p = propellant density

$\varphi = x/L$ dimensionless distance

ω = angular frequency

REFERENCES

1. Shapiro, A.H., "Dynamics and Thermodynamics of Compressible Fluid Flow," Ronald Press (1954), Vol. II, 976-977.
2. Converse, A. O., "Research Study on Solid Propellant Instability," Quarterly Progress Report No. 1(12/31/62), Carnegie Institute of Technology
3. Converse, A. O. and R. L. Pigford, "Pulsating Gas Flow in Pipes," S.P.E. paper No. 106, Oct. 1961.

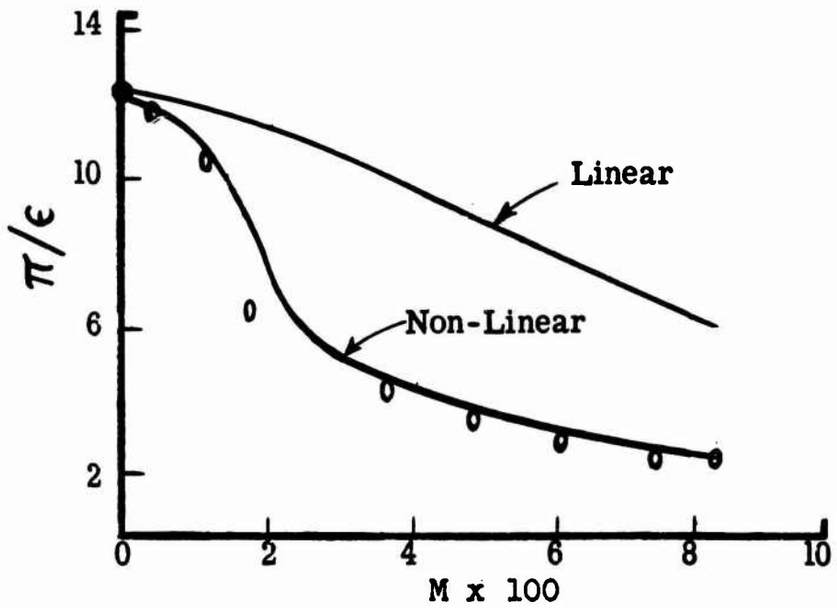

Fig. 1 EFFECT OF MEAN FLOW ON PRESSURE OSCILLATIONS AT PISTON END OF TUBE

LOW FREQUENCY (NON-ACOUSTIC) INSTABILITY STUDIES FOR THE PERIOD MARCH 1, 1962 to MARCH 1, 1963

R. A. Yount and T. A. Angelus
Hercules Powder Company
Allegany Ballistics Laboratory
Cumberland, Maryland

Current trends in solid propellant motor systems are toward large motors and low operating pressures. At low operating pressures, achieving and maintaining equilibrium operation may become difficult due to the danger of hangfires and periodic combustion phenomena, such as chuffing and low frequency (non-acoustic) instability (LFI). For large motors, the acoustic modes of the system may be of such low frequency that coupling may occur between these modes and periodic combustion phenomena which may be inherent in the propellant. Thus, it is important that a fundamental knowledge of these phenomena be obtained.

Results of work prior to this period suggested that the phenomena of LFI and possibly chuffing were intrinsic propellant properties rather than a coupling between combustion and some other mechanisms of rocket motor operation. During this period, further work was done to determine if LFI was a coupling between propellant combustion and rocket motor parameters. High impulse, heavily metallized propellant systems were also examined for susceptibility to chuffing and LFI, and a fundamental investigation into the nature of these low pressure phenomena was begun.

The effect of residence time on LFI was studied by comparing data from standard motor firings in which the free volume was systematically changed. All firings were otherwise identical relative to A_p/A_t, operating K and propellant. The propellant was a double base system containing 5 per cent of a Mg-Al alloy. LFI was observed in all cases, the frequency being independent of free volume, and the amplitude change being inversely proportional to the free volume. This indicates that the residence time, by itself, at least, is not a strong controlling factor in LFI. A double length grain-double length motor firing was also compared with the standard motor firing. This firing was identical in all respects except for A_p/A_t ratio. The frequency of oscillation did not change, but a marked decrease in amplitude occurred, indicating a possible relationship between driving force and velocity (or possibly pressure drop) within the port. The addition of a reaction catalyst, which had been known to increase the combustion efficiency of some propellants at low pressures, increased the frequency but did not affect the amplitude of LFI.

Highly aluminized composite modified double base propellant systems were observed to exhibit chuffing and LFI in motor firings at low operating pressures. The pressure-frequency-amplitude

relations for LFI were similar to those observed earlier for systems containing small amounts of metal additives (1). The frequency increased as the operating pressure increased; the amplitude decreased with increasing operating pressure and with increasing free volume. Strands of these propellants were also burned in a combustion bomb. This was done to determine if LFI was related to rocket motor geometry or an intrinsic property of the propellant. Movies of the burning strands showed the periodic build-up and ejection of aluminum globules and also "shedding" of layers of condensed phase material at the burning surface. The frequency of this process appeared to increase with increasing operating pressure, and the order of magnitude of the frequency was comparable to that of LFI observed in the motor firings. This gives added support to the previously proposed theory (1) that LFI is associated with the periodic accumulation of some oxidative resistant species, in this case the metal particles, at the burning surface.

The facts that chuffing and LFI often occur simultaneously, are both low pressure phenomena, and show similar dependence on operating pressure, suggest that they may be related. The amplitude of chuffing has been observed to decrease as the pressure associated with the base pressure between the chuffs increases. This "base" pressure was also found to depend inversely on the pressure decay rate of the prior chuff. The time between chuffs showed an inverse dependence on this pressure for a CMDB propellant containing different types of aluminum (Fig. 1).

The sharp transition from the low pressure dark zone reaction to a chuff suggests an explosion mechanism. Furthermore, experimental evidence shows that this may be thermal in nature (2). If such a mechanism is involved, one should be able to correlate the time between chuffs, t_i, with the induction time, τ, for thermal explosion. Analysis involving a time-dependent form of the heat flow equation (3) and an Arrhenius-type equation to represent the propellant surface temperature (4) has been made. An equation of the form $\ell n\ t_i = C - D\ \ell n\ P_i$ relating the induction time of a chuff to the pressure (P_i) of the quasi-steady reaction prior to the chuff is obtained. The constants C and D depend upon thermodynamic properties of the propellant and the kinetics of the combustion process. The data from Fig. 1 plotted in this way (Fig. 2) give reasonably good straight lines, thus indicating the possibility of a thermal explosion mechanism.

Laboratory apparatus has been built to determine experimental induction times for thermal explosion. Preliminary results indicate that a relation of the type given by Cook (3) is obeyed for the propellant studied (a highly aluminized system).

Work will also continue in attempts to gain further insight into the mechanism of LFI and chuffing. Specifically, studies will be oriented toward determining if the building up and discharging of metal agglomerates observed at the surface of burning propellant

strands is the cause of LFI in rocket motors using these propellants. According to this theory, a correlation between LFI and various properties of the metal additive should exist. The effect of LFI on the reactivity of the metal additive as determined by its composition, particle size, melting point, boiling point, properties of its oxide, and concentration will be determined by strand burning and, if necessary, motor firing experiments.

REFERENCES

1. Angelus, T.A., "Solid Propellant Combustion Instability," Eighth Symposium (International) on Combustion, The Williams and Wilkins Company, 1962, pages 921-924.

2. Huffington, J.D., Trans. Faraday Society 50, 942 (1954).

3. Cook, G.B., "Some Developments in the Theory of Thermal Explosions," Sixth Symposium (International) on Combustion, Reinhold Publishing Corporation, 1957, pages 626-631.

4. Wilfong, R.E., Penner, S.S., and Daniels, F., J. Phys. Chem. 54, 863 (1950).

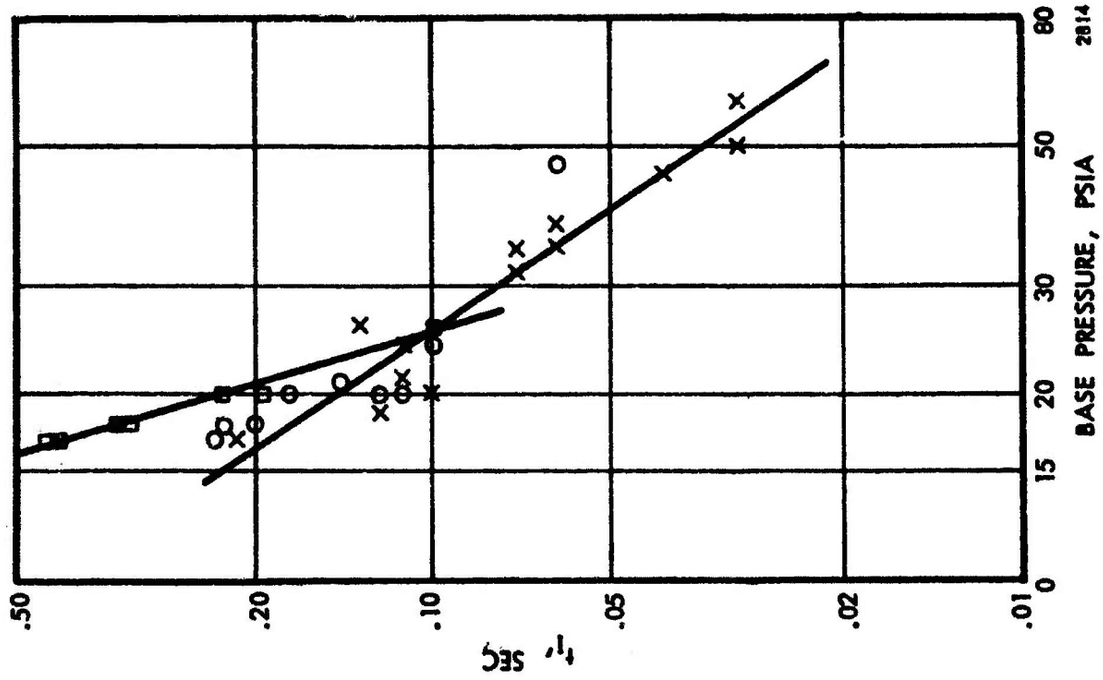

FIGURE 2
Log-Log Plot of Figure 1

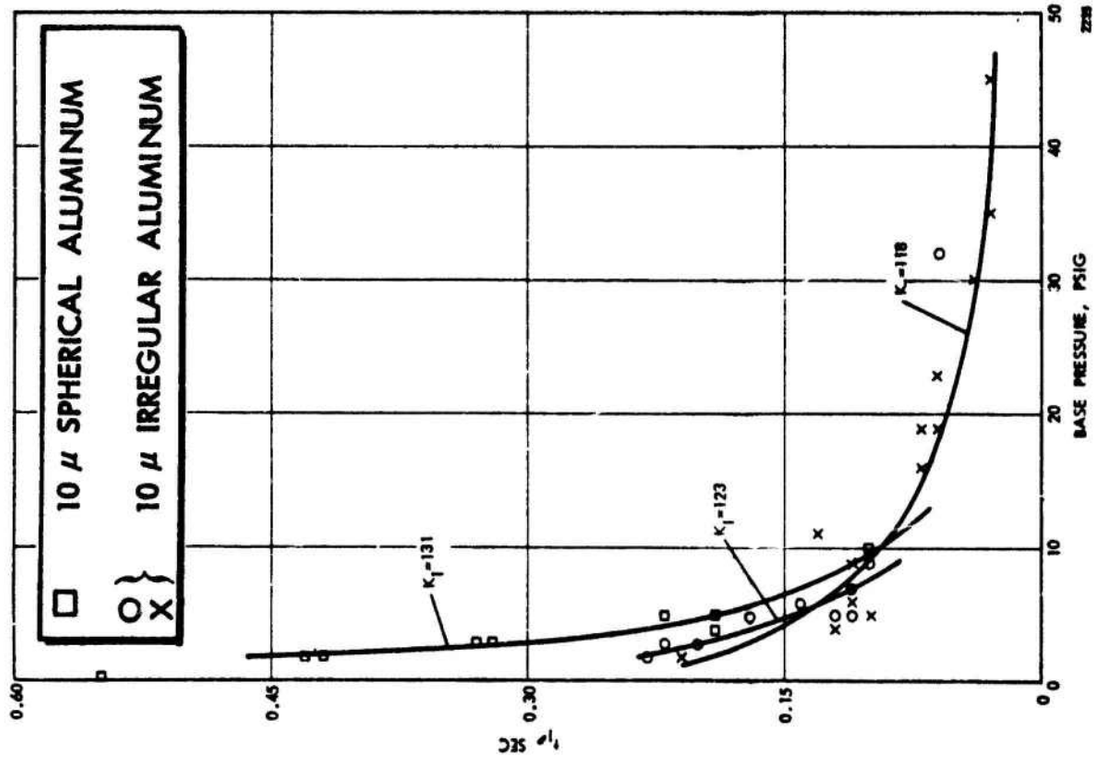

FIGURE 1
Time Between Chuffs vs. Base Pressure (Prior to Chuff) for Various Surface to Throat Area (K_1) Ratios

ENTROPY WAVES GENERATED BY COMBUSTION UNDER OSCILLATORY PRESSURE*

R. H. W. Waesche, J. Wenograd, and M. Summerfield
Guggenheim Aerospace Propulsion Laboratories
Princeton University
Princeton, New Jersey

INTRODUCTION

This report describes progress made during the past year in a program designed to investigate the physico-chemical aspects of combustion instability through a study of the interaction between the solid propellant flame zone and an oscillating pressure field. Particular attention has been devoted to the nature of the boundary condition describing the flame zone - pressure field.

In their treatment of combustion instability, Hart and McClure (1) have assumed that a gas particle traversing the flame is subject to adiabatic compression leading to a time-varying temperature at the edge of the flame zone. An alternative point of view (2) describes a situation which might prevail with low frequency oscillations. In this case, the transit time of a gas packet is short compared to the period of oscillation and the flame is essentially isothermal due to the weak dependence of flame temperature on pressure. The isothermal assumption leads to the expression $Y = - v/p\ (\mu/\epsilon - 1)$ for the acoustic admittance, where μ is $d\dot{m}/\dot{m}$, ϵ is dp/p and v and p are the velocity and pressure respectively. This differers from the result of Hart and McClure's assumption which leads to an expression $Y = - v/p\ (\mu/\epsilon - 1/\gamma)$ for the acoustic admittance. The $1/\gamma$ factor has been re-analyzed in detail by Hart and Cantrell in a recent paper (3).

THEORETICAL BASIS OF EXPERIMENTAL PROGRAM

A significant feature of the isothermal boundary condition assumption is the prediction of the existence of entropy waves at low frequencies in the gases flowing from a propellant burning under oscillating pressure conditions. With an isothermal flame, gas packets emitted at low pressure will have a temperature higher than or equal to the adiabatic flame temperature since they immediately experience a compression, while gas packets emitted at high pressure will suffer a subsequent rarefaction and a resulting lowering of temperature. These entropy waves will have a wavelength much shorter than the acoustic wavelength (Fig. 1).

A straightforward analysis, assuming low frequency, gives the following expression for the entropy of the gas as a function of distance x (from the burning surface) and time:

$$s(x,t) = \zeta + \epsilon \frac{\gamma-1}{\gamma} C_p \sin[\omega (t - \frac{x}{v}) - \pi] \qquad (1)$$

where $\epsilon = \Delta p/p$, $\bar{v}$ = ave. gas velocity, and the other symbols have their usual meaning. This entropy equation is immediately convertible to a temperature equation:

$$\frac{T(x,t)}{\bar{T}} = 1 - \epsilon \frac{\gamma-1}{\gamma} \left\{ 2 \sin \frac{1\omega x}{2\bar{v}} \cos \left(\omega t - \frac{1\omega x}{2\bar{v}}\right) \right\} . \qquad (2)$$

It can be seen from this expression that temperature waves should exist in the burnt gases. It is these temperature waves which are observable and manifest the existence of entropy variations.

From the equation, it should be noted that temperature nodes should exist when $\omega x_n/2\bar{v} = n\pi$ and antinodes when $\omega x_n/2\bar{v} = (n + 1/2)\pi$. The temperature nodes under the conditions outlined in Fig. 1 should be at $x = 0$, 7.5 mm, 15 mm, 22.5 mm, etc. In addition, it should be noted that the phase relation between temperature and pressure depends on position, and that, at the antinode for $\eta = 1$, the pressure is out of phase with temperature by 180°.

EXPERIMENTAL OBSERVATIONS

The existence of waves emitted from a propellant burning under oscillating pressure was first observed in movies taken by W. A. Wood of the Rohm and Haas Company, who was studying the combustion of metal additives in solid propellants. A careful examination of these films at this laboratory showed that the products emitted from the flame had a fluctuating luminosity. It was also noted that the spacing between the luminous bands varied as the pressure changed. However, the interpretation of these films was confused by the presence of metal, since it was possible that the waves observed were due to smoke. In addition, no simultaneous synchronized pressure record was available. Consequently, to obtain definite proof of the entropy wave hypothesis, an experimental program under way at Princeton on unstable burning in solids was pointed toward a study of entropy waves.

The source of oscillating pressure used here is a T-burner, shown in Fig. 2. This driver has been used at frequencies ranging from 280 cps to 1600 cps. Most firings have been made at 430 cps for handling ease. The observation of entropy waves at higher frequencies approaches a dual barrier: first, the decrease in period might cause it to be comparable to the flame transit time, and second, an analysis of decay by one-dimensional heat conduction shows that the temperature waves persist best at low frequencies. The disappearance of entropy waves at higher frequencies can probably be used as an indication of the flame zone residence time.

Firings have been made with seven different drivers at pressures from 150 psi to 700 psi, and it has been found that the T-burner is quite reproducible in the amplitude of oscillation attained for a given driver at a given pressure. Typical experimental

conditions are:

$$\text{observed pressure amplitude} = \frac{100 \text{ psi}}{400 \text{ psi}} = 25\%$$

$$\text{theoretical temperature amplitude} = \frac{\gamma-1}{\gamma}\frac{\Delta p}{p} \approx \frac{112°K}{2800°K} = 4\% \ .$$

Initially, high speed movies were taken to determine whether waves did indeed occur for non-metallized composite propellants. Initial attempts to photograph the temperature waves were thwarted by soot deposition on the windows within 0.1 second after ignition. A large number of attempts were made to alleviate these conditions, and these are described in greater detail in a progress report (4). It appears that use of a polyurethane-based ammonium perchlorate propellant as the driver has cured the difficulty, and movies have been taken which show waves emitted by a non-metallized propellant.

Although the presence of the waves is an encouraging factor, the entropy wave hypothesis can only be proved or disproved by measurement of the gas stream temperature as a function of position and time for comparison with Equation [2]. The temperature of flame gases is best measured by optical means, since no disturbance occurs from probes inserted in the flow. To make the variations in temperature more marked, flames may be colored by the addition of small amounts of sodium to the test propellants, and a brightness-emissivity method used in the region of the "D" lines. The emissivity of the flame can be varied to optimize the temperature sensitivity of the method by varying the sodium concentration and thickness of the flame.

In order to determine the optimum parameters, the amount of broadening of a sodium line for a thick flame at elevated pressures was calculated. It was assumed that all NaCl molecules yield Na atoms, and that all Na atoms were thermally excited. As a result mainly of pressure and absorption broadening, it was found that at the normal operating pressures an emissivity of 1 was attained over a spectral region broader than 100 Å, for a propellant containing less than 1/2% of NaCl. This means that such a flame would have a black body character when viewed through a standard interference filter.

Thus, temperature can be measured directly by measuring the intensity of radiation emitted by the flame gas. The 4% temperature variation mentioned previously leads to a total radiation amplitude variation of 17% over the entire spectrum, assuming a uniform grey body emissivity. However, the variation of the radiation intensity using a "D" line filter, for the same 4% temperature change, is 44%. This should be measurable with precision.

The experimental arrangement is shown in Fig. 3. Since the micrometer slit is fixed and the sample surface regresses, the photocell records the luminosity at a continuously increasing distance from the surface. The test time is of the order of 600 msecs. In Fig. 4,

a segment of the oscilloscope record obtained in a typical run by a strip camera is shown. The bottom trace is the output of a 1P42 photocell viewing the flame through a pair of 1 cm high slits, 1 mm wide, with a 5890 AU interference filter interposed which has a 100 AU band width and 40% maximum transmission. At the time this segment was recorded, x (the distance from the surface) was such that $\omega x/2\bar{v} = \frac{3}{2}\pi$, i.e., the antinode for $\eta = 1$. The sinusoidal form of the pressure record should be noted, as should the pressure-temperature phase relation. Furthermore, temperature nodes were observed earlier in the same luminosity trace. All these observations are in qualitative accord with the predictions of the previously mentioned analysis.

DISCUSSION AND FUTURE PLANS

The results shown are, of course, only preliminary. Tests will be run with narrower slits, which will require the use of a photomultiplier tube to give higher outputs. In addition, absolute temperature measurements will be made. These will necessitate a calibration as well as some means of determining the changing transmissivity of the viewing windows. The latter will involve the use of a source at some wavelength other than the "D" line, while the former will be done using a standard black body.

The quantitative measurements of temperature and phase relations will give an indication of the validity of the isothermal boundary condition, and the mechanism of combustion under oscillating pressure. Some knowledge of reaction times might be obtained by varying the frequency and noting at what point the reaction time becomes an appreciable part of the oscillation period. In addition, the waves might be used as tracers to obtain gas velocity. If this were done, admittance could be determined from a simultaneous measurement of the pressure and velocity at the same plane.

REFERENCES

1. Hart, R.W. and McClure, F.T., J. Chem. Phys. 30, 1501 (1959).

2. Waesche, R.H.W., Wenograd,J., and Summerfield, M., "Research on Solid Propellant Instability," Second Progress Report No. 564b, Princeton University, Department of Aeronautical Engineering, 20 December 1961.

3. Hart, R.W. and Cantrell, R.H., AIAA Journal 1, 398 (1963).

4. Waesche, R.H.W., Wenograd, J., and Summerfield, M., "Research on Solid Propellant Combustion Instability," Technical Summary Report No. 635a, Princeton University, Department of Aeronautical Engineering, 29 January 1963.

---

*This work supported by Advanced Research Projects Agency (ARPA).

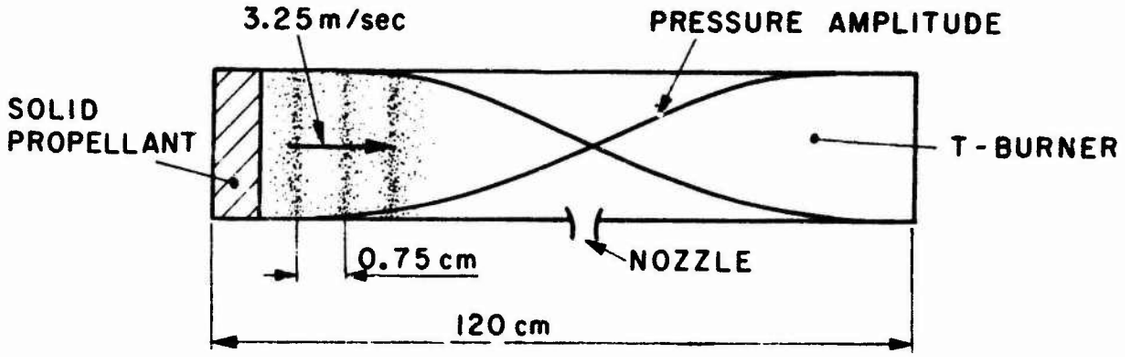

	ENTROPY WAVES	ACOUSTIC WAVES
FREQUENCY	430 cps	430 cps
VELOCITY	3.25 m/sec	1030 m/sec
WAVE LENGTH	0.75 cm	240 cm

Fig. 1 ENTROPY WAVE PROPERTIES IN AN ACOUSTIC FIELD

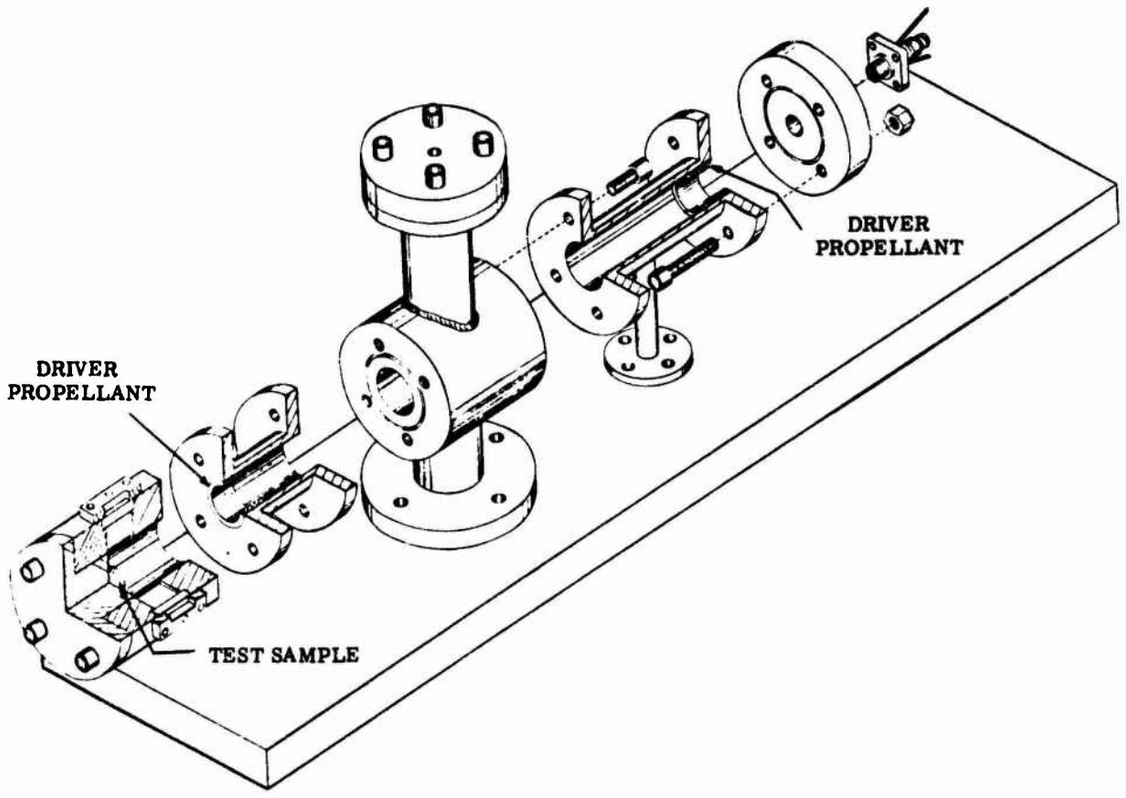

Fig. 2 ASSEMBLY VIEW OF OSCILLATOR

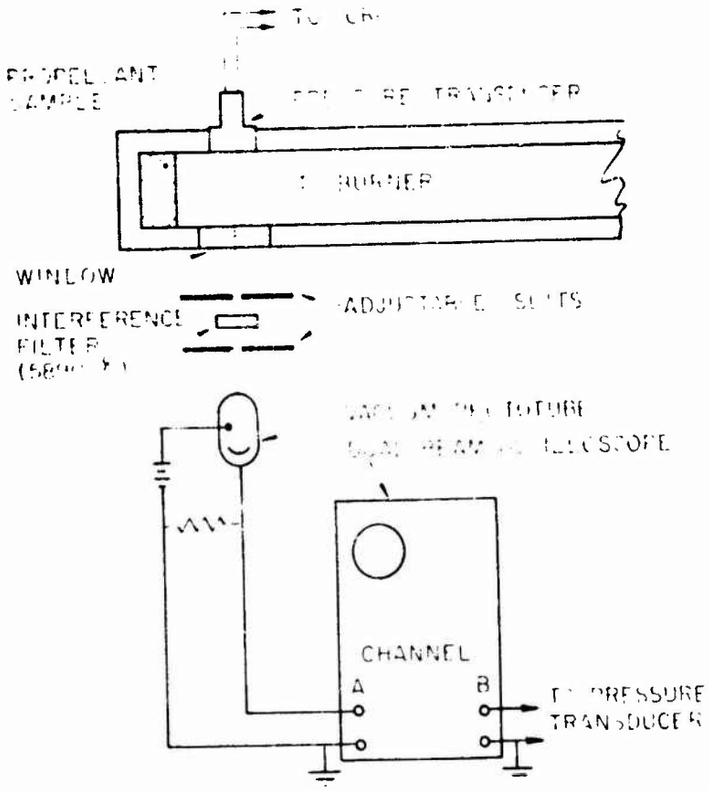

Fig. 3 PHOTOMETRIC TEMPERATURE MEASURING APPARATUS

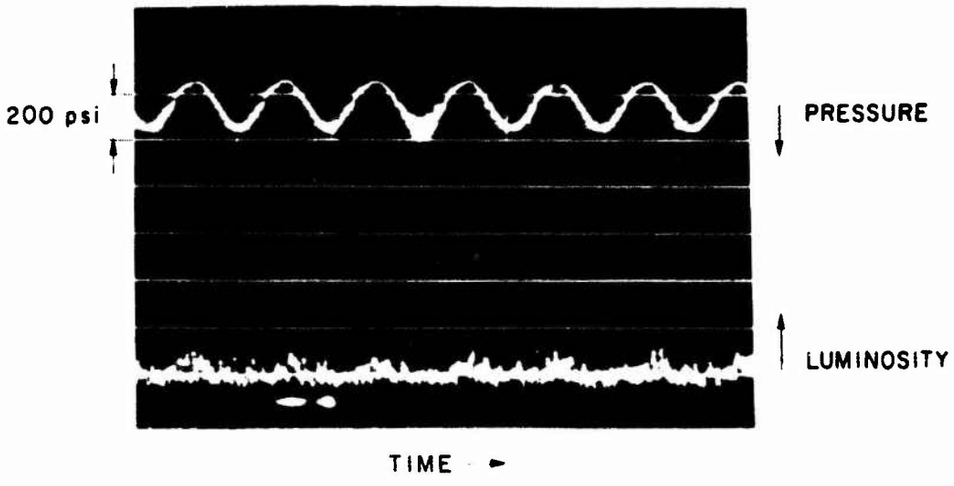

Fig. 4 PRESSURE AND LUMINOSITY TRACES

(Portion of Record approximately 3/2 entropy wavelengths from propellant surface; note phase difference between luminosity and pressure maxima.)

EXPERIMENTS ON ACOUSTIC EROSIVITY EFFECTS ON PROPELLANT BURNING RATES

Leland A. Watermeier, William P. Aungst, and
Richard C. Strittmater
Ballistic Research Laboratories,
Aberdeen Proving Ground, Md.

Late in 1961, McClure, Bird, and Hart published a report (1) in which they "investigate an interesting non-linearity arising from acoustic erosivity, i.e., the dependence of the burning rate on the magnitude (but not the direction) of the fluctuating gas velocity parallel to the transpiring surface. This non-linearity is of first order in the acoustic amplitude, and so can be significant even when higher-order effects are negligible." They presented simple calculations of the stability in axial modes to illustrate this phenomenon and they showed that a motor stable at low acoustic amplitudes could be unstable at moderate amplitudes due to the non-linearity of erosion.

In August 1952, Murphy of Purdue published a very complete review (2) of the current status of erosive burning in solid propellant rocket motors. The fact remains, however, that very little effort has been made to measure acoustic erosivity effects on propellant burning rates. Probably the most precise measurements to date have been made by Price (3) on extinguished grains.

The objective of the program underway in the Interior Ballistics Laboratory is to measure instantaneous burning rate variations. These variations are to be determined as functions of frequency and amplitude of the acoustic environment. This is to be accomplished by using an adaptation of the resonant tube technique developed for acoustic admittance studies (4).

Figure 1 shows a schematic drawing of the test chamber. The chamber has a square cross-section which is 2" x 2" and it is centrally vented. A single exhaust port will be used for initial experiments with an eventual changeover to a multi-nozzle system if it proves advisable. The tube length can be varied from 10" to 8' which permits a frequency range capability of approximately 1700 to 200 cps, respectively.

Two chambers are to be used. One will be lined with a 0.006" thick sprayed coating of zirconium oxide. The other chamber will be left uncoated for use in comparative studies.

---

*This program is supported by the Army Materiel Command.

Both single and double-ended propellant "driver" systems will be used. The propellant samples under study will be of the same composition as the driver propellant. They will be located near the exhaust plane (velocity antinode) of the chamber. Lucite windows provide a means of photographing the regressing propellant surfaces. Pressure gages are located near both ends and at the middle of the chamber. Two more gages will be added later half-way between each end and the exhaust port.

Thermocouple measurements of the wall surface temperature during each run are also planned.

Acoustic damping will be provided either by the Helmholtz cavity technique discussed by Ryan or by a series of screens near the passive end of the chamber. This will be varied so as to determine the burning rate variation dependent upon acoustic amplitude.

The entire chamber system (test section and dump tanks) will be pre-pressurized with nitrogen prior to each run. The pressure range of approximately 100 to 1500 psi will be investigated. The test chamber is attached to the top of one of two 2 ft^3 dump tanks. It is also in line with a Schlieren system as shown in Fig. 2. The strong backlighting from the mercury lamp provides a sharp outline of the propellant samples. By means of high speed photoggraphy the regression rate of the samples can be followed. It is anticipated that the burning rate change per cycle of oscillation may be extremely small in some cases. That is why we are resorting to low frequencies and high camera framing rates initially. This should provide maximum experimental conditions for film recording of any changes. If the cycle to cycle variation is impossible to follow (beyond film resolution, etc.) it is hoped that, at least, a specific period of time can be isolated where the chamber conditions will be fairly well-known. In this case, an average effect would have to be accepted.

The Schlieren system may provide additional information on gas density gradients during oscillatory operation if suitable standards can be established and the gas temperature can be determined.

Eventually it is planned to try the Weinberg "inclined-slit" technique (Fig. 3) for measuring temperature profiles above the burning propellant surface. Again, as in the case of the Schlieren system, this type of information should be quite valuable if it can be obtained.

The primary objective of the program, i.e., determination of burning rate variations under controlled acoustic erosivity conditions, should lead to determination of non-linear aspects as brought out in the McClure-Bird-Hart report.

REFERENCES

1. F. T. McClure, J. F. Bird, R. W. Hart, "An Erosion Mechanism For Non-Linear Instability in the Axial Modes of Propellant Rocket Motors", Applied Physics Laboratory, The Johns Hopkins University, Report TG 335-9, October, 1961.

2. J. M. Murphy, "Technical Memorandum on the Current Status of Erosive Burning in Solid Propellant Rocket Motors" Jet Propulsion Center, Purdue University, Report No. TM-62-6, August, 1962. (Report is Classified)

3. E. W. Price, Progress in Astronautics and Rocketry, Vol. I: Solid Propellant Rocket Research. New York Academic Press, Inc., 1960, pp. 561-602.

4. M. D. Horton and E. W. Price; N. W. Ryan, R. L. Coates and A. D. Baer; and R. Strittmater, L. A. Watermeier and S. Pfaff; The Ninth Symposium (International) on Combustion. New York Academic Press, Inc., to be published.

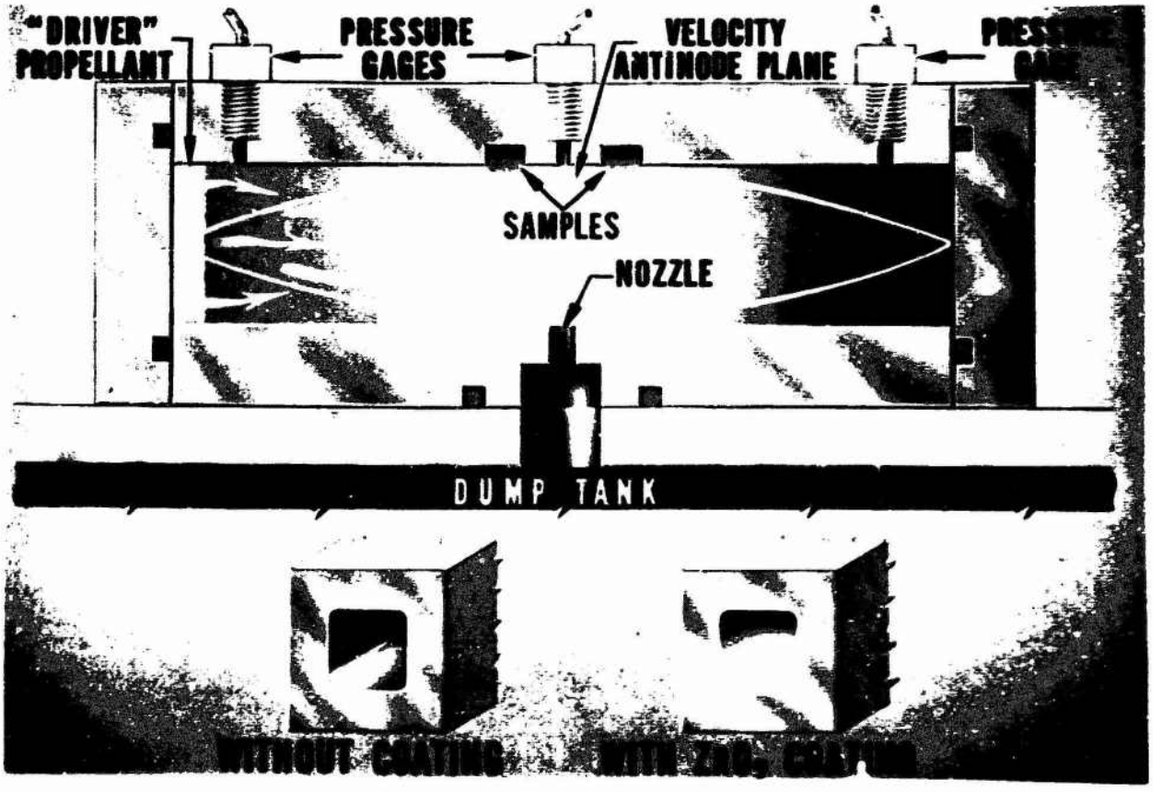

Fig. 1 SCHEMATIC DRAWING OF INTERNAL CHAMBER CONFIGURATION

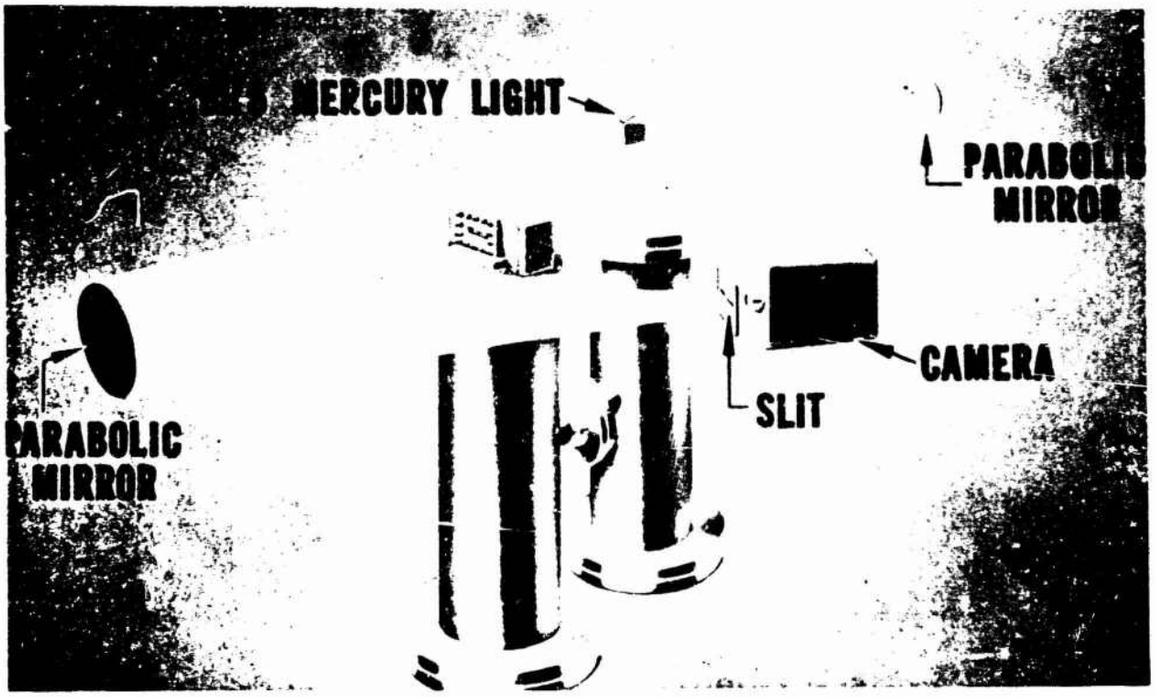

Fig. 2 SCHEMATIC DIAGRAM OF SCHLIEREN SYSTEM AND CHAMBER

Fig. 3 ADAPTATION OF F. J. WEINBERG "INCLINED SLIT" TECHNIQUE FOR TEMPERATURE PROFILES

EFFECT OF ACOUSTIC ENVIRONMENT ON PROPELLANT BURNING RATE*

E. W. Price
U. S. Naval Ordnance Test Station
China Lake, California

Earlier work continued on determination of the change in mean burning rate in the presence of large amplitude gas oscillations. It was previously reported (1,2) that with double-base propellants an acoustic velocity environment increased the burning rate, while an acoustic pressure environment decreased burning rate. Similar results have now been obtained also for a composite propellant. These results were obtained using the double burner described last year, consisting of coupled "T" motors discharging through the same nozzle, with one motor rigged for oscillatory combustion and the other for nonoscillatory combustion.

In addition, an extensive series of tests was made in the end-burner configuration (Fig. 1), where the oscillatory behavior is more nearly one-dimensional than in the tubular, double-burner configuration. This design is less versatile because it does not provide such severe oscillatory behavior and gives data only on acoustic pressure effects on burning rate. On the other hand, it is easier to obtain data at different frequencies by varying the burner length; and the mean pressure is more easily controlled because the burner is fired on a pre-pressurized surge tank. By measuring the burning time of pre-measured propellant discs in the end burner, the mean burning rate can be compared with the oscillatory behavior.

Tests were made on seven unmetallized propellants (composite and double base) at two frequencies and two pressures (Ref. 3), to determine the effect of acoustic pressure on burning rate. It was observed that the effect of acoustic pressure was always to decrease the burning rate, the effect being greater at a frequency of 10 kc than at 2 kc. With respect to mean pressure dependence, it appeared that in the double base propellants the effect was greater at low pressure than at high and in the composites the opposite was true. The different propellants behaved similarly with respect to the magnitude of the burning rate changes, with the exception of a cast double base formulation which exhibited changes about twice as great as those typical of other propellants. Typical results are indicated in Fig. 2.

*Sponsored by the Special Projects Office of the Bureau of Naval Weapons.

REFERENCES

1. Crump, J. E. and E. W. Price, "Effect of Acoustic Environment on the Burning Rate of Double-Base Solid Propellants," ARS Journal, 31, No. 7, pp. 1026-1029 (July 1961).

2. Price, E. W., "NOTS Research on Low Frequency Combustion Instability," Report to Second SPIC Technical Panel Meeting, Stanford Research Institute, Menlo Park, Calif., March 8-9, 1962.

3. Eisel, J. L., "The Effect of Acoustic Pressure on the Burning Rates of Solid Rocket Propellants," presented at fall meeting of the Combustion Institute, Western States Section, Sacramento, California, November 26-27, 1962 (WSS/CI Paper 62-23).

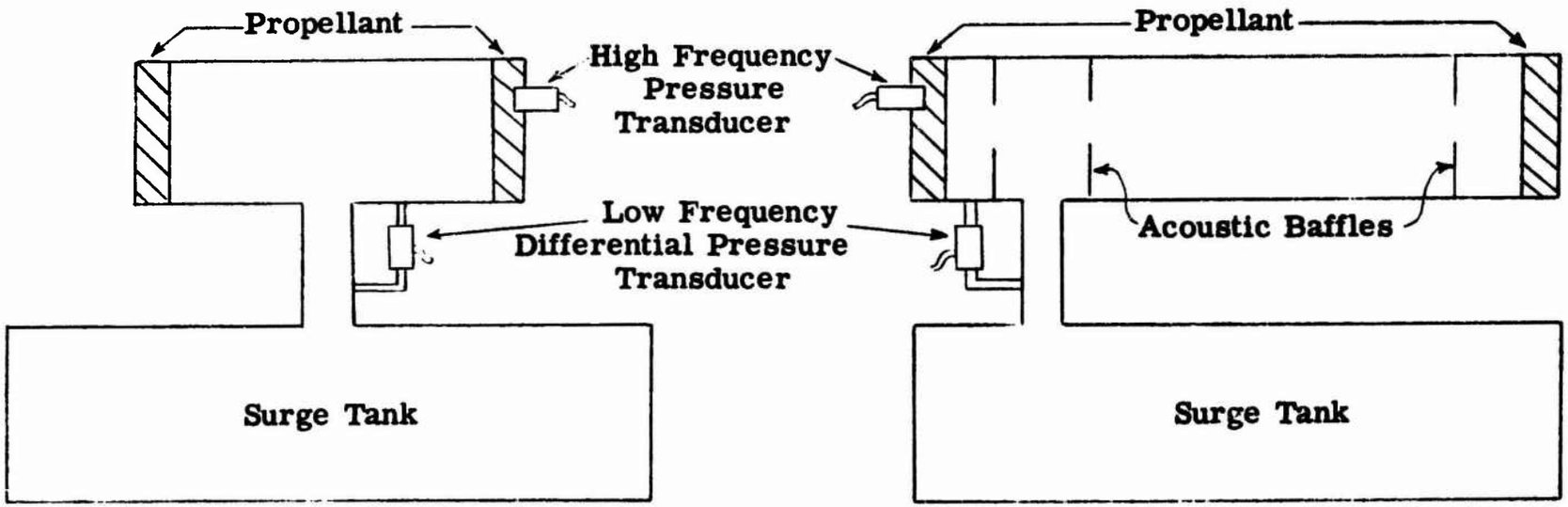

A. Mounted on Surge Tank for Constant Pressure

B. Rigged for Steady State Non-oscillatory Tests

Fig. 1 SCHEMATIC OF DOUBLE-ENDED OSCILLATORY BURNER

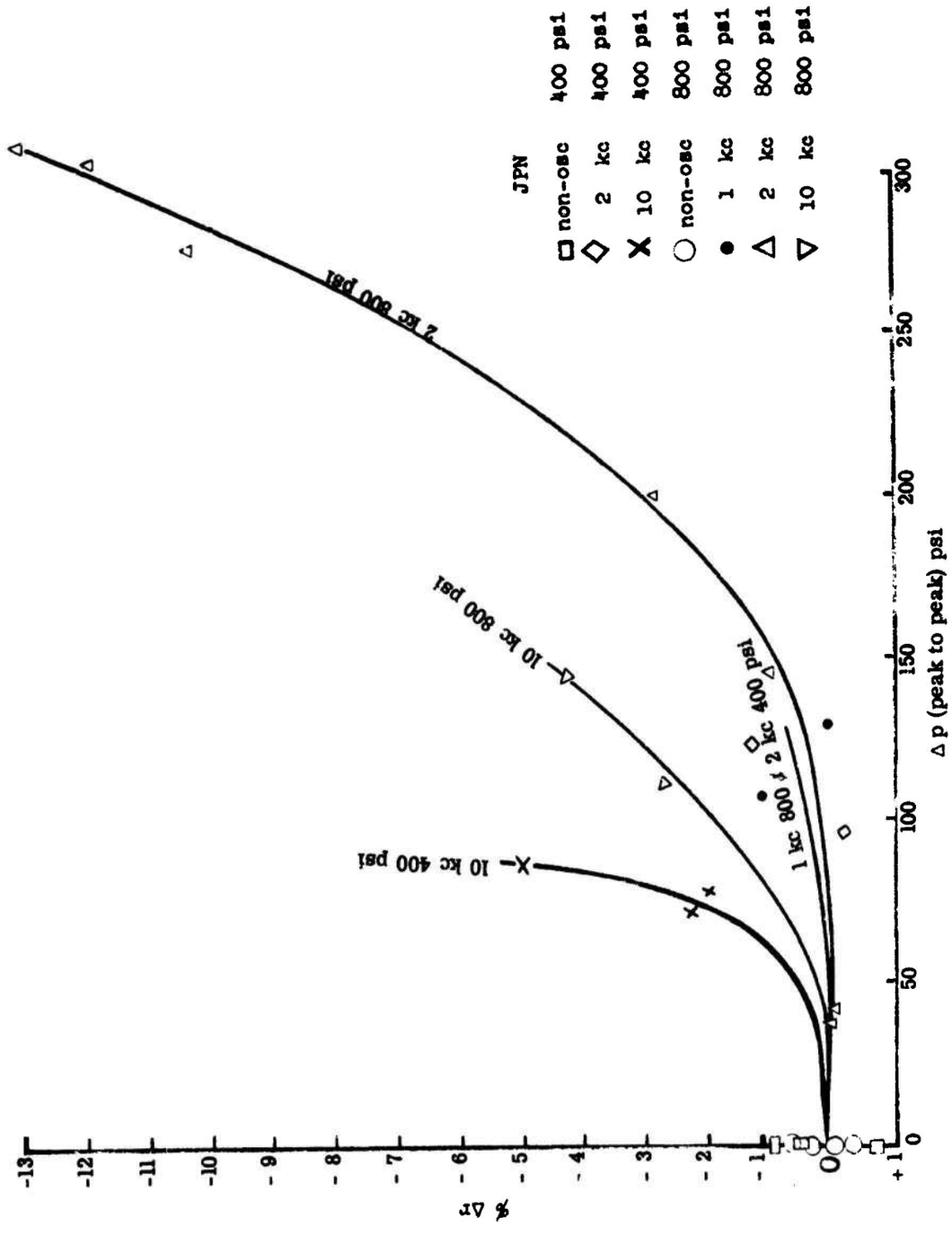

Fig. 2 EFFECT OF ACOUSTIC PRESSURE ON BURNING RATE OF JPN PROPELLANT

SCALING LAWS FOR COMBUSTION INSTABILITY*

E. W. Price
U. S. Naval Ordnance Test Station
China Lake, California

Investigation of the effect of size on the instability behavior in the NOTS T-burner continued with modifications of ANP 2639 AF propellant. Burner dimensions (inside) ranged from 1-inch diameter and 6-inch length to 10-inch diameter and 60-inch length. Aluminum concentrations from zero to 15% were tested, as well as 6% aluminum oxide. Results are summarized as follows:

1. With aluminum or aluminum oxide, high frequency oscillatory combustion occurred, in axial modes in small burners and transverse modes in large burners. The frequency range 1,000-4,000 cycles per second was favored.

2. With intermediate concentrations of aluminum (6% and 9%), only mild oscillatory behavior was observed which occurred sporadically in axial modes only over the whole frequency range 3,600-360 cps.

3. With high aluminum concentration (15%), significant oscillatory behavior occurred only in the 36-inch-long and 60-inch-long burners. In these burners, oscillatory behavior was severe at 100 and 360 cps respectively.

4. No oscillatory behavior was obtained in the formulation with 6% aluminum oxide.

The results of this investigation, interpreted in line with results available from other projects, indicate that aluminum and aluminum oxide suppress high frequency instability through the mechanism of acoustic damping of droplets in the combustion chamber gases. At lower frequencies this damping mechanism is believed to be marginally effective (below about 1,000 cps). There is increasing evidence that the combustion of the aluminum enhances axial mode instability in the frequency range below about 800 cps. The mechanism is believed to involve periodic "shedding" of aluminum from the propellant burning surface, coordinated by acoustic velocity (periodic fluctuations in gas velocity parallel to the burning surface). Since such velocity-coupled combustion disturbances require a time lag between the velocity-induced disturbance of the burning surface and the resulting combustion disturbance, the ignition-combustion time

*Sponsored by Special Projects Office of the Bureau of Naval Weapons.

of the aluminum droplets appears to be crucial to this type of instability. Current information on these combustion time constants is not adequate for correlation of motor firing data, but the effect of initial aluminum particle size (observed in other projects) seems consistent with the erosive-coupled mechanism in which aluminum combustion can contribute to instability.

DEPENDENCE OF ACOUSTIC LOSSES ON MOTOR DIMENSIONAL VARIABLES*

E. W. Price
U. S. Naval Ordnance Test Station
China Lake, California

Because of combustion problems in a motor development program, an experiment was set up to simulate axial mode oscillations with a cold-flow system in a quarter-scale model of the rocket motor. Flow simulation was accomplished by gas injection at the head-end of the combustion chamber through a high impedance porous plate. The inflow of air included an oscillating component at controlled frequency. Running at resonant frequency with constant amplitude oscillations, the acoustic power level in the motor is compared with the acoustic power input (which equals the acoustic losses under the steady oscillatory conditions prevailing). The model of the motor was made up from interchangeable components permitting systematic changes in internal dimensions. Repeated tests with different dimensional combinations permitted a correlation of acoustic loss levels with motor geometry. Results in this particular investigation correlated with qualitative arguments regarding loss mechanisms, and the technique appears to be widely applicable to measurement of the effect of geometry on acoustic loss in axial modes, particularly losses by radiation from the nozzle.

*Sponsored by Special Projects Office of Bureau of Naval Weapons.

AXIAL MODE INSTABILITY IN THE INTERMEDIATE FREQUENCY RANGE

E. W. Price
U. S. Naval Ordnance Test Station

The observation of axial mode instability with heavily aluminized propellants in development programs led to a survey program with a specially designed burner to compare the behavior of the various classes of commercially available propellants. The T-burner configuration was used with a 5-inch diameter and 72-inch length, yielding axial mode oscillatory behavior at about 240 cycles per second. During this year the design and fabrication of the burner and loading hardware was completed, and 14 firings were made with E 107 propellant (25% polyurethane, 57% ammonium perchlorate, 18% aluminum). All firings showed severe oscillatory combustion with major increases in burning rate accompanying oscillatory combustion (Fig. 1). Oscillations developed without finite initiating pressure pulses (Fig. 2) and initiated in the pressure range 500-1,500 psi. Methods for delaying the onset of oscillatory behavior using tuned acoustic filters were explored as a means of minimizing the higher acoustic modes in the burner (to permit comparison of the behavior of various propellants at the same frequency later in the program). A method for introducing a pressure pulse into the burner to test nonlinear instability was incorporated in the design, but has not been used because the system has oscillated without pulsing.

Negotiations were initiated for loading of ten additional propellants from various suppliers. Pending availability of these loadings, testing is continuing on E 107 propellants and modifications involving changes in aluminum particle size.

*Sponsored by Advanced Research Projects Agency.

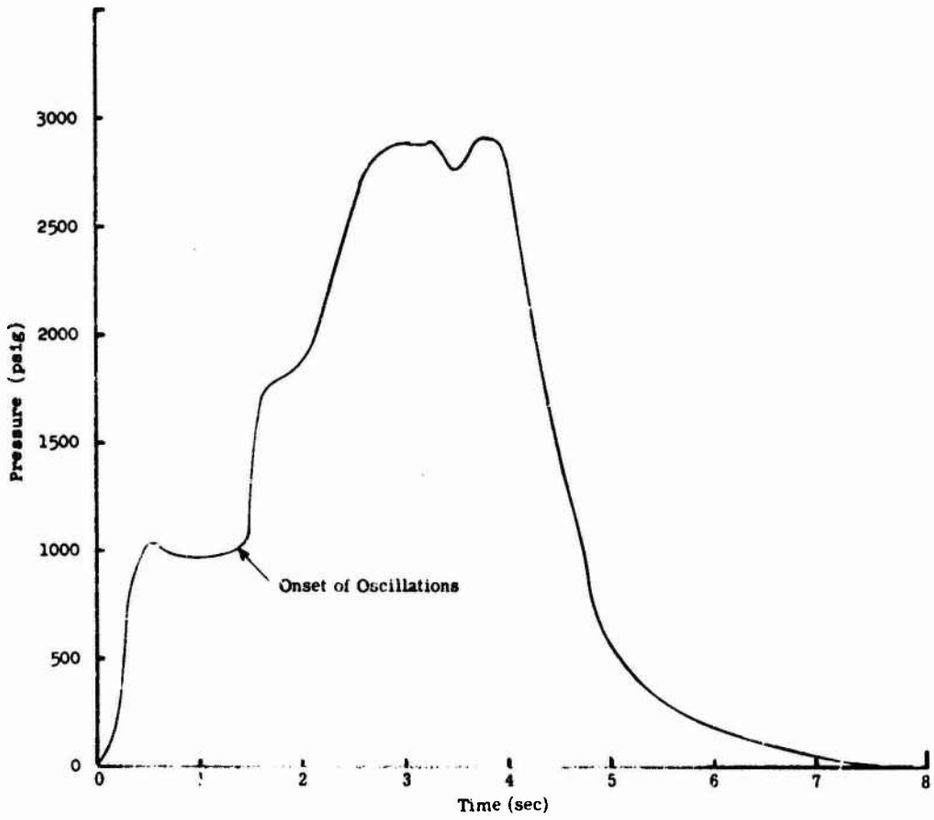

Fig. 1 PRESSURE-TIME CURVES SHOWING PRESSURE AT THE ONSET OF OSCILLATIONS

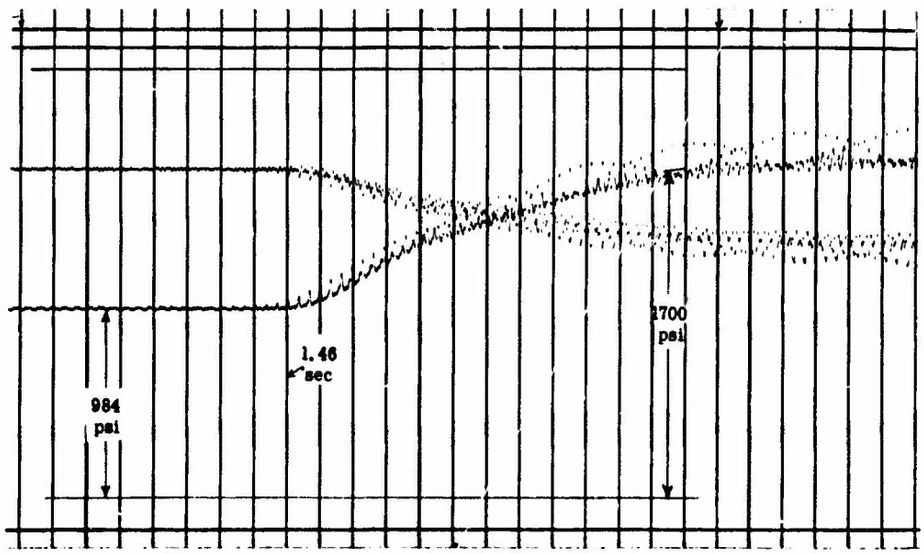

Fig. 2 ONSET OF OSCILLATORY BEHAVIOR

SOME NOTES ON THE EXPERIMENTAL MEASUREMENT OF TRANSIENT COMBUSTION INSTABILITY PHENOMENA

F. F. Liu
Quantum Dynamics, Inc.
Tarzana, California

I.

The study of transient phenomena involved in combustion instability has gained increasing interest in recent years. The following factors are believed to be some of the principal background factors:

A. The need for increasing accuracy in the quantitative measurement of key instability parameters (e.g., acoustic admittance of the burning zone) following the theoretical postulation by McClure, Hart et al. Measurements of this type are often directed toward the transient part of burning process, for instance, the rate of growth and decay of acoustic oscillation (1).

B. Renewed interest in the role of combustion driven shock waves in instability and detonability investigations.

C. The search for additional insight on the fundamental instability mechanism.

D. The recent availability of instrumentation techniques having high transient/frequency response and the requisite cooling power (or heat transfer rate) for quantitative measurement in the combustion chamber.

For the sake of discussion, the measurements of a solid rocket unstable burning process are analyzed in the nature of a case study. Knowing the diversity and complexity of the problem, however, no attempt is made here to infer that the phenomena discussed are typical of all other unstable burning processes. The discussion only offers to illuminate a few phenomenological observations and pertinent methods for the interpretation of data which hitherto had not been seriously reported. Instrumentation-wise, the transient data shown in this paper were obtained simultaneously with (thermal) radiation measuring devices and pressure measurement instruments. Both of these are capable of accurate measurement of transient quantities up to the megacycle region (2).

The usefulness of the radiation measurement in rocket research has been reported on several previous occasions. In earlier deflagration-to-detonation transition investigations, for example, it was noticed that little significant pressure variations were detectable until the very last moment prior to detonation. However, radiation measurement was able to reveal precursory phenomena virtually from

the beginning. To some extent this also applies to instability research where the utilization of brightness temperature as a sensitive indicator of unstable burning was borne out by numerous experiments. Such observations have since been corroborated by the theoretical works of Agosta and McClure, who pointed out independently that pressure is often not the sensitive parameter under certain unstable conditions (3).

Figure 1 is a simultaneous oscillographic recording of the transient phenomena covering the period from the inception to the full development of the instability. The middle trace records the high frequency chamber pressure (P_c) versus time with the time scale provided by the 10 Kc timing marks in the lower trace. Shown in the upper trace is the brightness temperature (T_{br}) pattern inside the combustion chamber, and this information was obtained with a high frequency (water-cooled, gas-purged) radiation transducer in conjunction with its ancillary electronic units. Since the radiation inside the chamber approaches that of the blackbody condition, a measure of the oscillatory chamber temperature can be obtained. Thus, the simultaneous recording provides both the momentum transfer (pressure) and energy transfer (temperature) picture of the combustion instability process from the formative stage to the development of steady-state pressure, temperature and velocity oscillations. In this respect, it will be shown later that information on flow field can also be deduced objectively from the recorded data. Figure 2 shows the T_{br} vs time during the entire run.

It is interesting to note that vigorous buildup of the fluctuation in T_{br} occurred long before the appearance of any significant P_c variation: the latter effect became noticeable only after a sufficiently prolonged (in terms of milliseconds) oscillation in T_{br}. Then one notices that wavelets of higher harmonics began to superimpose on the T_{br} waveform, and concurrently pressure oscillation also developed in increasing intensity.

For some of the more interesting information, one should focus his attention on the "envelopes" of the T_{br} oscillations. Initially, the T_{br} variation was confined to a single trace of lower frequency (ω_t^T); gradually it assumed the form of upper and lower boundaries of a higher frequency($\omega_{t,r}^T$) oscillation. These envelopes are referred to recently in the works of Summerfield and Waesche as "entropy waves" (4). In the beginning, both the peak and trough of the lower envelope appeared to be in phase with their respective counterparts in the upper envelope. But then an abrupt discontinuity took place: one of the enveloping waves suddenly shifted approximately 180° so that the peak of the lower envelope became nearly in phase with the trough of the upper one. This, in effect, corresponds to a doubling of frequency from ω_c to ω_c'.

The frequency-doubling now signifies a new phase of combustion oscillation, and it appears to be a phenomenon which separates the buildup and the intensified stages of combustion instability. Such a transitional pattern has been confirmed repeatedly in many unstable

rocket tests, when it was noted that the sudden 180° phase shift was generally, if not invariably, followed by more intense high frequency oscillations.[1] Moreover, such frequency-doubling behaviors are known in acoustical and shock wave theories; for under certain conditions of imposed discontinuity, the frequency and phase of the wave solution must satisfy a given set of secular equations (5).

Perhaps of no less fundamental significance is the stipulation that this sudden phase transition which marked the near superposition of a temperature peak and trough is actually the near coincidence of a compression and rarefaction wave; in which case, one must conclude that a combustion driven shock wave has been generated at this moment.

The aforementioned observation may now be briefly recapitulated into the following set of conclusions for the sake of conciseness:

a) That shock wave appears to be a principal coupling mechanism between different modes of oscillatory combustion.

b) That the conversion of thermal energy into acoustic energy is greatly facilitated by severe temperature gradients.

c) That the transition from one stage of combustion instability to another, e.g., from the buildup to a more intensified stage, is often accompanied by a sudden 180° phase-shift and/or doubling of frequency.

While these statements may appear to be qualitative, they are actually arrived at through careful quantitative measurements made possible by the use of powerful instrumentation and electronic technique of proven reliability (6). In the subsequent part of the paper, we shall discuss the possibility of extracting more quantitative information from combustion instability test data.

At the instant of shock passage, for instance, the Riemann invariant can be used to calculate the velocity of the shock characteristics which, as is well known, is the sum of the particle velocity (u) and the speed of sound (a). The relation may be expressed as follows (7):

$$u + a = \frac{2}{\gamma-1} a_o \left[\frac{\gamma+1}{2} \left(\frac{p}{p_o} \right)^{\frac{\gamma-1}{2\gamma}} - 1 \right] .$$

With the instantaneous pressure and temperature quantities measurable, one is greatly facilitated in the choice of realistic values for many other factors, for example: the ratio of specific heat (γ) and sound velocity (a). In this particular test, γ was determined to be 1.26; the absolute pressure values of p and p_o were measured as 60 and 120 psi. From these, it is readily calculated that

$$u + a / a_o = 1.69 .$$

1. Based on the analyses of the previously shown data of E. W. Price and N. W. Ryan.

In the above calculations, the effect of viscosity on transient phenomena is assumed to be small. Despite this simplification, however, the calculated velocity of the characteristics is shown to be considerably higher than the steady state velocity of the flow field as estimated from pertinent parameters (5). It is apparent that, in order to conserve the momentum, other modes of combustion oscillation such as the tangential and transversal modes, would have to be generated. The observation is then in accord with conclusion (a) mentioned above.

As further examples, additional estimates of sound velocity (a) may be obtained from the measured frequencies and the known geometrical configurations of the rocket chamber, using the following familiar relations:

$$\omega = \pi a_o/L; \qquad a_o = C^* \qquad\qquad a_o^2 = \frac{\partial P}{\partial \rho}\Big)_s = \gamma \frac{P}{\rho} \quad .$$

Experiences have shown that through successive calculations and approximations of this nature, sufficiently realistic estimates of the interesting thermodynamic quantities can be made, and which are obviously to be preferred over intuitive guesses. In the case of gas density ρ , methods for its direct and indirect determination are available although they have not been put into intensive use in rocket instability research.

In general, more quantitative information on instability can actually be extracted from accurately made measurements than ordinarily is believed possible. By means of such techniques, theoretical postulates can be verified or refined. For instance, in the McClure-Hart theory, the following relations on the amplitude of tangential velocity was given as

$$\frac{\Delta U}{a} = \frac{1}{1.84\gamma} \frac{\Delta P}{\overline{p}} \quad .$$

Since the values shown above are determinable either directly or indirectly, it would be instructive to compare the steady-state of value with its corresponding transient values as given by the velocity of the characteristics.

Accurate determination of γ, or its related parameters $(\gamma-1)/\gamma$ and $1/\gamma$, has important bearing on instability investigation, for the evaluation of such quantities leads directly to the assessment of the instability criteria

$$\left(\frac{\tilde{\mu}}{\tilde{\epsilon}} - \frac{1}{\gamma}\right) > 0 \; ; \quad \left(\frac{\tilde{\mu}}{\tilde{\epsilon}} - \frac{1}{\gamma}\right) < 0 \quad ,$$

where $\tilde{\epsilon} = \dfrac{\tilde{p} - \overline{p}}{\overline{p}}$ is immediately determinable from measurements, $\tilde{\mu} = \dfrac{m_1 - \overline{m}}{\overline{m}}$ and can also be computed indirectly from measured data. Moreover, if the instability criterion of Hart and Cantrell is

applicable, a reasonable estimate of the parameter $(\gamma-1)/\gamma < n \simeq 0.2$ should be useful in the study of low frequency combustion instability (8).

II.

The aforementioned observations, and the methods outlined above, are presented with the full knowledge that data on oscillatory pressure, even those so-called "high frequency" pressure oscillations, have appeared in abundance among existing literature; to a lesser extent, even data on radiation intensity have been previously reported. Most of these dealt with steady-state processes, whereas the present note has its main interest in transient phenomena, which appears to be less understood at present. In doing so, it is the intention of this work to suggest that, insofar as transient investigation is concerned, the merit of evaluation may indeed differ widely between a casually conducted "pressure" measurement, and a set of objectively directed quantitative measurements consisting of relevant values. Pressure measurement is by no means synonymous with the mere installation of pressure transducers; nor is pressure measurement alone adequate for the study of complex transient phenomena, particularly when it may not be a sensitive indicator of instability under many circumstances. To illustrate the point, Fig. 3 shows that in the presence of high chamber temperature and fast transients, there can be pronounced difference between an accurate dynamic measurement (lower trace), and other distorted indications on the same phenomena (other traces); dynamic errors can result due to the choice of transducers, method of mounting, quality and sophistication of electronic instrumentation, etc. Since they may affect the validity of experimental findings in instability research, and since a growing amount of quantitative data are required, such problems have lately become a matter of growing concern. In this we include a wide range of instrumentation problems, besides the more familiar pressure measurement.[1]

III.

Among the recent works on combustion instability, some studies have appeared on the subject of shock interaction with combustion zone and propellant burning surfaces. Theoretical treatment of this nature, for instance, has been advanced by Agosta and others (3). This addition of shock considerations has plunged us deeper into the regime of nonlinear instability studies, thus promising to further complicate the status of instability theories. Consequently, objective experimental investigations are looked upon to provide the necessary information. But at the same time, and for lack of actual observations, a number of experimentalists contend that shock waves are not ever-present in combustion instability, and therefore they are of minor or no importance. Such opinion, of course, is conditional

1. Some limited evaluation programs on pressure "transducers" (not pressure instrumentation systems) had been conducted previously by JPL, but this is now being actively pursued at Guggenheim Laboratory, Princeton University, under a NASA program.

upon the adequacy of measurement techniques. For instance, an examination of the lowest trace in Fig. 3 would easily convince an investigator that steep shock fronts and "spikes" of oscillating shocks are present; on the other hand, one could not readily indentify the presence of shock from the other traces, mainly due to lack of transient response of the transducers. Thus, in the latter case, the distorted data might conceivably prevent one's gaining a proper perspective of the process, and could perhaps lead one to believe that "high frequency" oscillations rather than shocks are involved. Thus, the conclusion drawn from distorted data can be a different one.

It is questionable that one could safely dismiss the effects of shock wave on combustion instability, particuarly in the case of very large solid or liquid rockets. Crocco and Cheng, for instance, have mentioned several phenomena which, they believe, are involved in nonlinear type combustion instability. Among these are the generation of shock waves due to coalescence of compression waves in the combustion chamber, and the exponential dependence of certain rates on temperature(9). The mechanism due to a shock wave's direct action on chemical reaction rates has received particular attention, and they consider that such effects can be larger than the combined effects of the pressure and temperature increases through the shock itself. These observations are believed to be essentially valid, for we have noticed through numerous rocket tests that the interaction between fluctuation in the chamber and burning rate is noticeably amplified by the appearance of shock. The data shown in this paper are sufficiently convincing to support this contention. The rapid increase in the propellant's heat release rate is evidenced by the sharp spikes and steep gradients shown in the T_{br} or radiation intensity recordings (Figs. 1 and 2). Even the high frequency oscillations are characterized by sufficiently steep fronts to be considered shock waves. Since the chemical reaction rate figures importantly in shock interaction studies, the data presented here are especially pertinent. The signals shown are actually indications of the propellant's heat release rate, which is given by $\bar{m}RT/M$, where $\bar{m}$ is the mass rate of burning per unit surface, and M is the molecular weight of the propellant gas, R_g is the gas constant, and T is the usual gas temperature.

Possibly the effect of shocks on heat release rate can be further examined analytically. Before attempting this, it is instructive to point out (see Figs. 1 and 2) that the accompanying change of density ρ across the shock front is sufficiently drastic and discontinuous. As such, the gas traversing such discontinuity would experience an entropy increase which, for weak shocks, is given by (10)

$$\Delta S = \frac{\gamma(\gamma+1)}{12} R_g \left(\Delta\rho/\rho\right)^3 .$$

The amount of heat release per unit time and unit area is thus $T\Delta S$, which can be evaluated since T is obtainable from measurements and ΔS can be derived from measured values. Some sample calculations have been done during the past on the time-varying pattern of $T\Delta S$.

In the steady-state case, this parameter has important significance in the "entropy wave" concept. However, with the presence of shocks, this entropy parameter wave has been found to be significantly different. Although both tend to raise the gas temperature, the entropy increase in the shock wave equation involves a third order effect. This involves formation of curved shock, which is often characterized by a substantial temperature gradient throughout its cross-section. When this occurs, according to the Crocco theorem (11), the gas in the combustion chamber is highly susceptible to vortex-type spinning. In fact, such rotating vortex phenomena have since been noticed independently this this author, and by Jenkins, Swithenbank, and Trubridge, of Britain (12).

REFERENCES

1. McClure, F.T., Hart, R.W., and Bird, J.F., "Solid Propellant Rocket Motors as Acoustic Oscillators," Solid Propellant Rocket Research, Vol. I., (M. Summerfield, Ed.), Academic Press (1960), pp. 295-358; Hart, R.W. and McClure, F.T., "Combustion Instability: Acoustic Interaction with a Burning Propellant," J. Chem. Phys. 30, 1501-1514 (1959); Price, E.W., "Combustion Instability in Solid Propellant Rocket Motors," Astronautica Acta, V, 63-72 (1959); also, see recent works of M.D. Horton and E.W. Price.

2. Liu, F.F. "Verbesserung des Uebergangsverhaltens elektromechanischer Messumformer durch elektronische Kompensation der Verzerrung," (in German), Archiv. Tech. Messen, 174R, 145-164 (November 1958); Liu, F.F. and Berwin, T.W., Rev. Sci. Instr. 29, 14-22 (1958); Liu, F.F., "Measurement of High Temperature in Rocket Propulsion Development," Contract N123(60530)23247A(FBM) submitted to Special Projects Office (1961).

3. Agosta, V., "Shock Interaction with Burning Surface," This volume. Paper delivered at 3rd Meeting, Combustion Instability Panel, Applied Physics Laboratory, The Johns Hopkins University (March 4-5, 1963); McClure, F.T., "Comments, 4th March, 1962", at 3rd Meeting, SPIC.

4. Summerfield, M. and Waesche, R.H.W., "Entropy Waves Produced at Burning Solid Propellant Surface under Oscillatory Pressure," paper presented at 2nd Meeting, Panel on Solid Propellant Combustion Instability, March 7-9, 1962, at Stanford Research Institute, Menlo Park, California.

5. Betchov, R., "Nonlinear Oscillation of a Column of Gas," Physics of Fluids 1, 209 (1958).

6. See, for instance, Knauer, R.C. and Layton, J.P., "Transient Pressure Measuring Method Research, etc. ...", Princeton University, Aero. Eng. Dept., Report No. 595C (May 1962).

7. Glass, I.I. and Patterson, G.N., "A Theoretical and Experimental Study of Shock Tube Flows," J. Aero. Sci. 22, 73-100 (1955); Laderman, A.J., Urtiew, P.A., and Oppenheim, A.K., "Measurement of Pressure Field Generated at the Initiation of Explosion," Symposium on Measurement in Unsteady Flow, the Amer. Soc. of Mech. Engr. (1962).

8. McClure, F.T., Hart, R.W., and Bird, J.F., see Ref. 1, p. 321; Hart, R.W. and Cantrell, R.H., "On Amplification and Attenuation of Sound by Burning Propellants," Applied Physics Laboratory, The Johns Hopkins University, Rept. TG 335-11; McClure, F.T., Hart, R.W., and Cantrell, R.H., "Interaction between Sound and Flow Stability of T-burners,", Applied Physics Laboratory, The Johns Hopkins University, TG 335-12 (July 1962).

9. Crocco, L. and Cheng, S.I., Theory of Combustion Instability in Liquid Propellant Rocket Motor, AGARDOGRAPH No. 8, London: Butterworths, 1956, p. 7.

10. Betchov, R., Ibid, pp. 209-210.

11. Shapiro, A.H., The Dynamics and Thermodynamics of Compressible Flow, Vol. I, New York: Ronald Press, 1953, pp. 281-282.

12. Liu, F.F., "Comparative Analysis and Interpretation of High Speed Experimental Data on Instability and Detonation Phenomena in Solid Combustion Chamber," Applied Physics Laboratory, The Johns Hopkins University, TG 371-4B (May 1962). Presented before the 2nd Meeting, Combustion Instability Panel, at Stanford Research Institute, Menlo Park, California, March 7-9, 1962.

Jenkins, J.M. and Swithenbank, J., "Cyclic Combustion Driven Shocks in a Compressible Vortex," Rept. No. 8, Department of Fuel Technology and Chem. Eng., Sheffield University, England, 1962-1963.

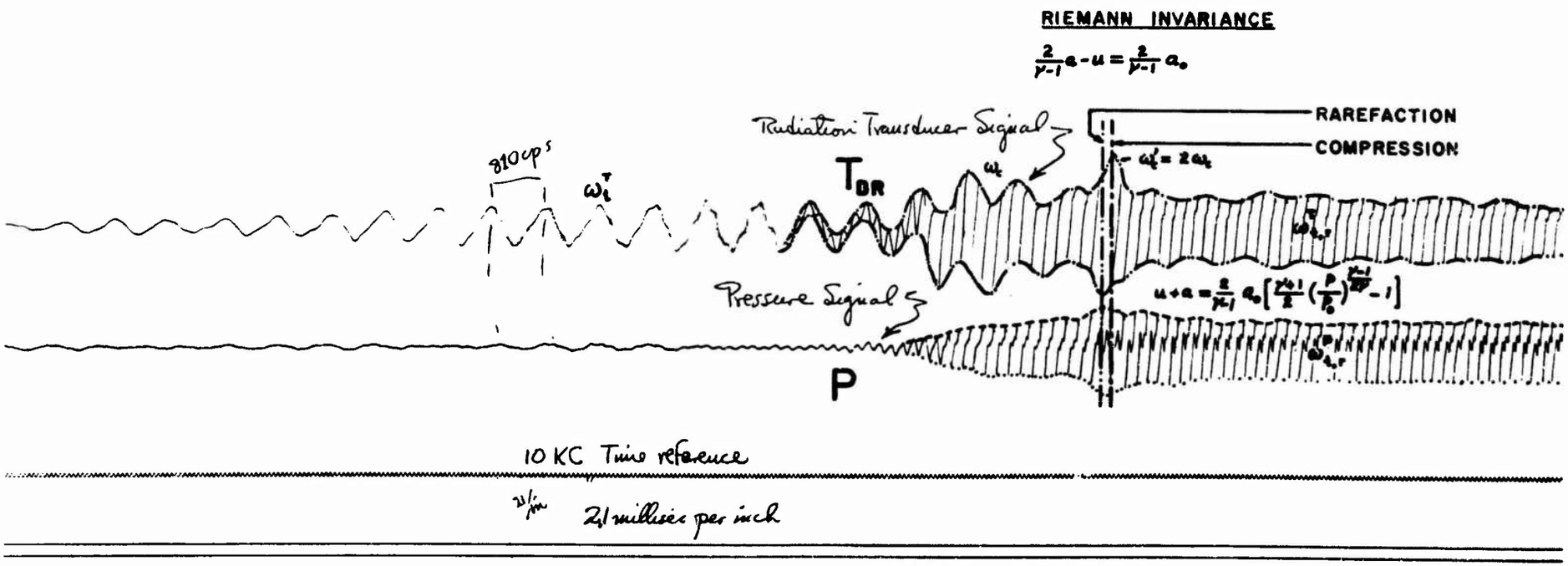

Fig. 1 SIMULTANEOUS PRESSURE AND BRIGHTNESS TEMPERATURE RECORDING OF SOLID ROCKET COMBUSTION INSTABILITY TRANSIENT PHENOMENA

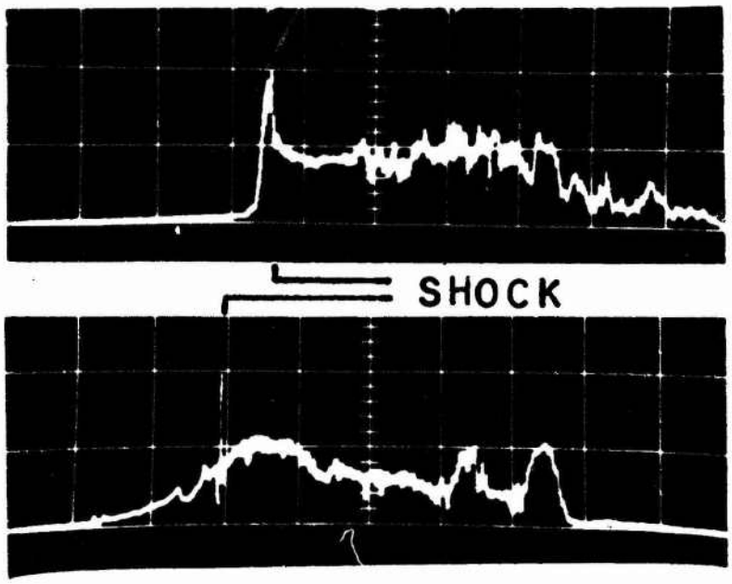

Fig. 2 SHOCK WAVE IN COMBUSTION INSTABILITY PROCESS

RESPONSE OF LIU GAGE AND PHOTOCON (DYNAGAGE) TO OSCILLATIONS IN THE N.O.T.S. 6" UNSTABLE BURNER

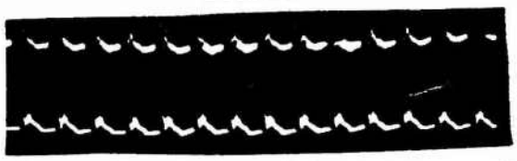

Liu Gage: Two tests with gage mounted behind 3/16" x 1/2" grease line (D-C 11).

Liu Gage: Mounted behind hole without grease. 60 psi water cooling.

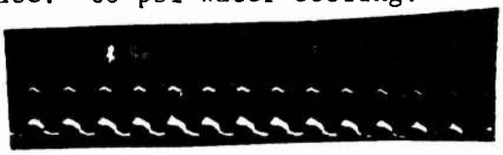

Photocon Gage: Mounted behind grease line as above. (top trace)

Liu Gage: Flush mount. 200 psi water cooling. (bottom trace)

Fig. 3 COMPARATIVE PERFORMANCE OF DYNAMIC PRESSURE MEASUREMENT DEVICES

RESPONSE OF PROPELLANTS TO DIFFERENT TYPES OF MECHANICAL EXCITATION

Thor L. Smith
Stanford Research Institute
Menlo Park, California

INTRODUCTION

A program[1] is being conducted whose primary objective is to characterize the response of propellants to different types of mechanical excitation within the range of linear viscoelastic behavior. Secondary objectives are to determine propellant response to large deformations and to consider ways in which propellant mechanical properties depend on such factors as mechanical history. The information should assist in relating certain aspects of combustion instability to the mechanical characteristics of the propellant grain.

By way of review, the response of a linear elastic material to various stress or strains can be represented in terms of certain elastic constants which are independent of the magnitude of the stress and strain. In an analogous way, a linear viscoelastic material can be characterized by certain time-dependent quantities which are independent of the magnitude of the stress-time (or strain-time) history. For example, we can define a tensile modulus $M(t) = \sigma/\epsilon$ where $M(t)$ is the time-dependent modulus, σ is the stress, and ϵ is the strain. If at zero time the material is subjected to a strain which remains constant during the determination of the stress, the time-dependent modulus obtained from the data is called the relaxation modulus $E(t)$. If the material is subjected to a strain which increases linearly with time, the resulting stress-strain data give the so-called (1) constant-strain-modulus $F(t)$ Further, if the material is subjected to a sinusoidally varying strain, the response can be described by a complex modulus $E^*(\omega) = E'(\omega) + iE''(\omega)$ where $E'(\omega)$ and $E''(\omega)$ are the storage and loss moduli, respectively, and ω is the circular frequency. However, the moduli $E(t)$, $F(t)$ and $E^*(\omega)$ can be interrelated by equations from the theory of linear viscoelasticity. In principle, if one of the moduli of a material is known over an extended range of time (or frequency), its response to any arbitrarily selected type of mechanical excitation can be calculated provided the response is in the linear range.

[1]The program, "Viscoelastic Properties of Solid Propellants and Propelland Binders," is administered by the Bureau of Naval Weapons under Contract NOw 61-1057-d and is funded by the Advanced Research Projects Agency.

The linear viscoelastic properties of many materials can be specified in terms of their shear and dilatational (bulk compressional) behavior. For rubbery materials, including propellants, under sufficiently small strains, Poisson's ratio is essentially 0.50. In other words, the bulk modulus is large compared to the shear modulus, and as a result, the tensile modulus is three times the shear modulus.

In the remainder of this paper, we shall consider briefly the bulk modulus of propellants and how it depends on temperature and mechanical history. Then, we shall present some tensile data determined at various strain rates and temperatures on a polyurethane propellant and the complex shear modulus derived from these data.

Before considering illustrative data, a few remarks should be made about the propellants being studied and how their properties may differ from those of a grain in a rocket motor. The propellants now being studied are dried for several weeks before being used. This procedure has been adopted because certain mechanical properties of propellants depend on the moisture content. In a rocket motor, the moisture content of a grain undoubtedly is not uniform and depends on a variety of factors. Even in the absence of moisture, the properties of certain propellant grains are not uniform because the binder properties may depend on the temperature history both during and after cure and on other factors which are difficult to control. In addition, even for so-called well consolidated propellants, the surface area of filler particles apparently is not completely wetted by the binder because the repeated application of pressure changes the compressibility of the propellant and probably other mechanical properties.

BULK MODULUS

The bulk modulus of a propellant depends on pressure, temperature, and time. The time-dependence may result either from viscoelastic relaxation or from certain structural charges, of a more or less permanent nature, produced by pressure.

Although no determination apparently has been made of the complex bulk modulus of a propellant, our knowledge of rubbery polymers indicates that the storage bulk modulus of a propellant should vary by a factor of two or less as the frequency is varied over 6-8 decades. On the other hand, the equilibrium bulk modulus in both the rubbery and glassy regions is quite dependent on temperature. Also, the repeated application of pressure to a propellant can change significantly its static bulk modulus. Because of these characteristics, it is desirable to obtain static compressibility data over a wide temperature range before a concerted

attempt is made to determine the complex bulk modulus as a function of frequency, temperature and pressure.

Static compressibility data are being obtained by placing a specimen and a confining fluid (Dow Corning 330 silicone fluid) in a glass dilatometer. The dilatometer is placed in a pressure vessel equipped with a window to permit observation of the meniscus in the dilatometer when pressure is applied. Some typical data for a polyurethane propellant containing 70% solids are shown in Fig. 1. (See Ref. 2 for a detailed discussion.) Before data were recorded, the dilatometer was subjected to one pressure cycle during which the pressure was increased up to 1500 psig. Data from the second, third, and fourth pressurization cycles are those shown in Fig. 1 plotted as pressure vs. $\Delta V/V_0$, where ΔV is the volume change and V_0 is the specimen volume at -10°C at atmospheric pressure. (The arbitrary constant A on the abscissa is used to displace for clarity the data from the second pressurization cycle.) The P vs. $\Delta V/V_0$ data from the second and third pressurization cycle yield a curve, although data from depressurization yield a straight line which intersects the abscissa at a finite value of $\Delta V/V_0$. Also, the width of the hysteresis loop for the third cycle is less than for the second one. On the other hand, neither nonlinearity nor hysteresis was observed during the fourth pressure cycle. These changes are believed to result from the compaction of the propellant during the repeated application of pressure.

The bulk modulus, from data obtained during depressurization, increases from 7.6×10^5 to 8.4×10^5 psi in going from the second to the fourth pressurization cycle. On the other hand, the initial slope of the P vs. $\Delta V/V_0$ curve for the second pressurization cycle gives a modulus of about 4×10^5 psi.

An equation has been presented (3) for estimating the % voids in a propellant from the shape of the curved portion of a P vs. $\Delta V/V_0$ curve. By use of this equation, it is estimated that the propellant at the beginning of the second and third pressurization cycles contained 0.14% and 0.09% voids, respectively. Apparently, no voids existed at the beginning of the fourth pressurization cycle because $\Delta V/V_0$ increased linearly with pressure.

After completing the work at -10°C, the specimen was tested at temperatures between 45 and -17°C. On the second pressurization cycle at each temperature (the first cycle for which data were recorded), the resulting P vs. $\Delta V/V_0$ curve was nearly linear and no hysteresis was observed. Values of the bulk modulus are shown in Fig. 2 plotted against temperature. Preliminary data from earlier experiments on another specimen are also shown along with modulus data for the silicone oil used as the confining fluid in the dilatometer.

The data in Fig. 2 show that the modulus increases from about 5.4×10^5 psi at 50°C to about 8.7×10^5 psi at -20°C. As the

velocity v for the propagation of bulk compressional waves is given by the equation $v = (K/\rho)^{1/2}$ (provided the shear modulus is small compared to the bulk modulus), where K is the modulus and ρ is the density, the velocities are about 1.48×10^5 and 1.89×10^5 cm/sec at 50 and -20°C, respectively. However, because the modulus of a propellant before being pressurized repeatedly may be lower by a factor of 2 than the values given, the velocity of propagation of sound in a rocket grain may be in the vicinity of 1×10^5 cm/sec at temperatures somewhat above ambient.

COMPLEX SHEAR MODULUS

Tensile stress-strain curves have been determined over a range of strain rate at temperatures between 70 and -20°C on a polyurethane propellant (AEBA-10) which contains 80% solids. The methods for obtaining and analyzing the data are described in detail elsewhere.(4). In brief, all data for strains up to 10% yielded a single curve on a plot of log F(t) 298/T vs log t/a_T, where F(t) is the constant-strain-rate modulus defined as $(1 + \epsilon)\sigma/\epsilon$ where σ is the stress and ϵ is the strain, T is the test temperature in °K, t is the time which equals $\epsilon/\dot{\epsilon}$ where $\dot{\epsilon}$ is the strain rate, and a_T is the temperature function, given by the Williams-Landel-Ferry equation, required to superpose data determined at different temperatures.

The data could be represented (5) by the equation

$$F(t) - 350 = 654t^{-0.25} \qquad (1)$$

where F(t) is in psi and t is in minutes. (This equation represents the behavior at 25°C over an extended range of time; a_T equals unity at this temperature.) By applying certain approximation methods, which are discussed in Ref. 5, it was found that

$$\log G'(\omega) - G_e = 0.25 \log \omega + 7.545 \qquad (2)$$

$$\log G''(\omega) = 0.25 \log \omega + 7.163 \qquad (3)$$

where $G'_a(\omega)$ and $G''(\omega)$ are the storage and loss shear moduli in dynes/cm^2, $G_e = 8.05 \times 10^8$ dynes/cm^2, and ω is the circular frequency in radians/second. Plots of log G' and log G" against log ω are given in Ref. 5 along with corresponding plots of $j'(\omega)$ and $J''(\omega)$ which are the storage and loss compliances.

Values of $J'(\omega)$ and $J''(\omega)$ have been measured on the same propellant with the Fitzgerald Apparatus by workers at the Atlantic Research Corporation (6) (ARC). From their data at temperatures between 25 and 45°C, reduced plots were made of log J'T/298 and log J"T/298 against log ωa_T. The resulting curves are compared in Fig. 3 with those given by Eqs. (2) and (3) over a limited frequency range. Equations (2) and (3) should be applicable down to very low frequencies; the highest frequency at which they apply is not known. The shortest value of reduced time t/a_T at which $F(t)$ was obtained corresponds to an ω of about 100 radians/second at 25°C.

Figure 3 shows that $G'(\omega)$ calculated from tensile stress-strain curves are in close agreement with values obtained from the ARC data; agreement between calculated and experimental values of $G''(\omega)$ is relatively poor. At the present time, it is not possible to state which values of $G''(\omega)$ are most reliable. However, the results presented in this section indicate that reasonably reliable values for the complex shear modulus can be obtained from tensile data determined at various strain rates and temperatures.

REFERENCES

1. Smith, T. L., Trans. Soc. Rheology 6, 61 (1962).
2. Smith, T. L. and Smith, J. R., "Viscoelastic Properties of Solid Propellants and Propellant Binders," Stanford Research Institute, Quarterly Technical Summary Report No. 4, July 31, 1962. Prepared for BuWeps, Contract NOw-61-1057-d.
3. Milloway, W. T., Surland, C. C., and Skulte, I., "The Effect of Initial Voids on the Bulk Modulus and Void Formation on Uniaxial Extension", Solid Propellant Information Agency, Bulletin of the 20th Meeting of the JANAF Panel on the Physical Properties of Solid Propellants, SPIA/PP14u, October 1961.
4. Smith, T. L., and Smith, J. R., "Viscoelastic Properties of Solid Propellants and Propellant Binders," Stanford Research Institute, Quarterly Technical Summary Report No. 5, October 31, 1962. Prepared for BuWeps, Contract NOw-61-1057-d.
5. Smith, T. L., Hiam, L. E., and Smith, J. R., "Viscoelastic Properties of Solid Propellants and Propellant Binders," Stanford Research Institute, Quarterly Technical Summary Report No. 6, January 31, 1962. Prepared for BuWeps, Contract NOw-61-1057-d.
6. "Dynamic Mechanical Properties of Propellants," Atlantic Research Corp., Quarterly Technical Summary Report, 31 December 1962. Prepared for BuWeps, Contract NOw 61-1054-c.

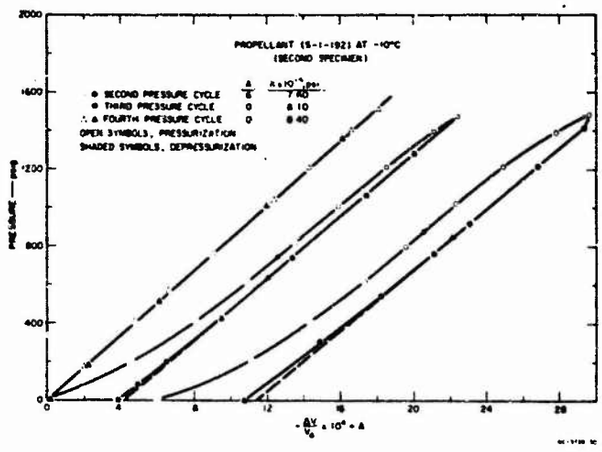

Fig. 1 ISOTHERMAL COMPRESSIBILITY DATA AT -10°C ON POLYURETHANE PROPELLANT CONTAINING 70% SOLIDS

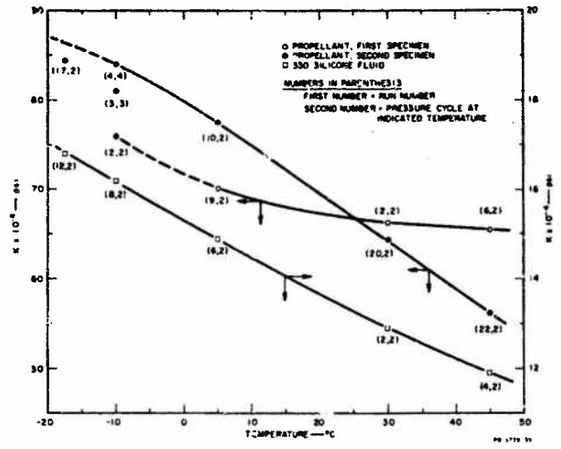

Fig. 2 TEMPERATURE DEPENDENCE OF THE ISOTHERMAL BULK MODULUS OF POLYURETHANE PROPELLANT AND DOW CORNING 330 SILICONE FLUID

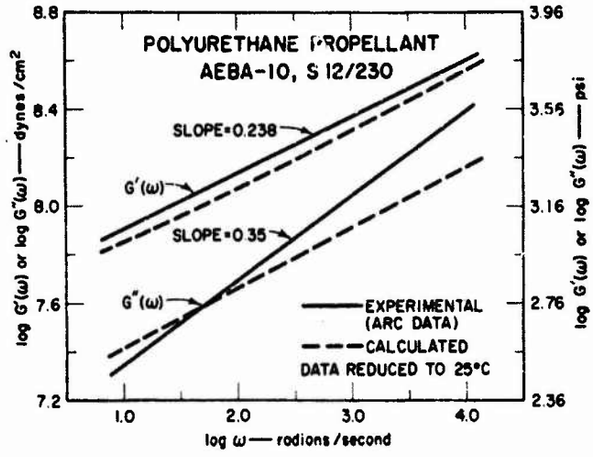

Fig. 3 G'(ω) and G"(ω) CALCULATED FROM CONSTANT-STRAIN-RATE DATA COMPARED WITH VALUES DERIVED FROM DATA REPORTED BY ATLANTIC RESEARCH CORP.

MEASUREMENT OF THE COMPLEX DYNAMIC SHEAR COMPLIANCE OF COMPOSITE SOLID PROPELLANTS*

C. N. Robinson**
Atlantic Research Corporation

INTRODUCTION

This paper presents results of an experimental program to define dynamic shear properties of two composite solid propellants at frequencies between 25 cps and 5000 cps within the temperature range of -50°C and +75°C, and at pressures from ambient to 1000 psig. This program is intended to further the study of combustion instability in rocket motors by providing dynamic shear compliance data for calculating dissipation of energy when the propellant is periodically deformed(1).

Measurements are made on a Fitzgerald Apparatus which has been described previously (2). Disc-shaped samples are held between two parallel metal surfaces, under slight compression to prevent slippage. The sinusoidal shearing force applied to the sample normally has an amplitude of about 2000 dynes. Stress amplitude, depending on the area of the sample, is about 5000 dynes per cm^2 or less. The data given herein are the two components of the complex dynamic shear compliance for two propellants. Other pairs of quantities used to describe the dynamic mechanical properties of a viscoelastic material can be computed from the components of compliance.

The application of sinusoidal shear stress to a linear viscoelastic material induces strain response which is sinusoidal and of the same frequency, but which is displaced in time. Two quantities, each a function of temperature and frequency, are used to define this stress-strain relationship. The real component J', and the imaginary component J'', are related to the complex shear compliance J^* and to the loss angle a as follows:

$$J^* = J' - iJ''$$

$$\tan a = J''/J' \quad .$$

Energy stored in the displaced material per unit volume per cycle is $2S^2J'$, while energy dissipated per unit volume is $2\pi S^2J''$,

*This work supported by the Advanced Research Projects Agency (ARPA).
**Presented by R. Friedman

where S is the rMS value of the sinusoidal stress.

Because of the energy relationship, J' is termed the storage compliance, while J" is the loss compliance. The two quantities are utilized subsequently to describe experimental results in units of dynes/cm^2. Compliance is the reciprocal of complex shear modulus, G*.

MEASUREMENT OF DYNAMIC SHEAR COMPLIANCE

Effect of Temperature and Frequency. The effects of temperature and frequency on the real and imaginary components of the dynamic shear compliance of a PBAA solid propellant (TPH-1001) are shown in Table I and displayed graphically in Figs. 1 and 2. Similar data for a polyurethane propellant (AEBA-10) are shown in Tables II through VI, and Figs. 3 and 4. It can be seen that for a given temperature for the PBAA propellant, the real component, J' of the dynamic shear compliance decreases with increasing frequency while the imaginary component J" increases. For the polyurethane propellant, both components of the dynamic shear compliance tend to decrease with increasing frequency at a constant temperature.

Measurements of the polyurethane propellant produced results unexplained in the runs conducted above 45°C. Data of the first two series of measurements showed inconsistent values of compliance as temperature varied between 45°C and 55°C. A source of uncertainty existed insofar as the moisture content of the transducer atmosphere was uncontrolled due to a leak in the system during the first series of measurements. It was estimated that the dew point was probably in the region of -17°C. The second series of measurements was made under closely controlled humidity conditions. The average dew point for these measurements was -45°C. Figure 4 compares the results of these two sets of data at two frequencies (320 cps and 800 cps). While the samples having the lower moisture content were slightly more compliant, it is apparent that moisture content of the samples is not the controlling parameter at the levels that existed.

A third set of measurements from 25°C to 65°C have recently been completed with propellant from a different batch. These data, which are not included in this paper, have compliance versus frequency curves which are smooth and regular as would be expected. No explanation has yet been developed for the anomalous behavior during the first two series of measurements.

Time-Temperature Superposition. One of the objectives of this program is to provide a test of applicability of the method of reduced variables (time-temperature superposition) to solid propellants. Measurements at closely spaced frequencies and temperatures are required for this purpose. The data mentioned above provide such a set of measurements.

Measurements are reported for frequencies from 320 cps to 2000 cps. In testing the method of reduced variables, it is desirable to extend measurements to lower frequencies. However, the range of frequencies over which accurate measurements can be made for any one sample depends on the mechanical impedance of the sample. This, in turn, depends upon the compliance of the material and the sample dimensions. For compliance in the range of 10^{-9} cm^2/dyne to 10^{-10} cm^2/dyne, measurements at low frequencies are not possible.

The trend of the data as frequency and temperature are changed is such that the temperature-shift required to superpose the real component data is not the same as the factor required to superpose the imaginary component data. This is contrary to the results found by Landel (3) in his study of polyisobutylene-glass beads systems.

Effect of Cure Time on Aging. Previously published data on dynamic shear compliance of TPH-1001 solid propellant, cured 48 hours at 40°F (60°C) showed that dynamic mechanical properties of this material increased with time (4). This aging effect has been further investigated using propellant cured 80 hours and 186 hours.

Measured values of the real components of the dynamic shear compliance of the two samples are given in Tables VII and VIII, and shown graphically in Figs. 5 and 6. Sample #46 was cured 180 hours at 140°F and Sample #47 was cured 80 hours at 140°F. The sequence of measurements was as follows: one run at room temperature; one run at high temperature; one run at room temperature; two runs at high temperature; one run at room temperature; several runs at low temperatures; and finally, one run at room temperature. The final run at room temperature was made about one month after the first.

Examination of the data shows that the change of dynamic properties with age is less for the material having the longer cure time. This difference probably indicates that the short cure time does not afford complete reactivity of the binder components. Accordingly, long-cure materials were used in this program when aging effects were to be minimized.

Effect of Compression of Sample by the Transducer. Two series of tests were made to determine the effect of sample compression on the dynamic shear compliance of TPH-1001 propellant.[1] Compliance was measured on a sample under 2 per cent compression after which the compression was increased in per cent steps to 4 per cent without removing the sample, and the run repeated. Some erratic operation of the electrical portion of the equipment,

1. 2 per cent compression is the smallest practicable value for the sample dimensions being used.

due to a malfunction in the amplifier, occurred during these tests. Although the measured compliance values were correspondingly erratic, the general trend of the data is still evident as shown in Figs. 7 and 8.

In one case, decreasing the thickness of a sample from a compression of 2 per cent to a compression of 4 per cent increased the sample constant[1] by about 4 per cent, but decreased the real component of the compliance by about 20 per cent. The imaginary component was decreased by about 35 per cent. Some uncertainty exists concerning the shape of the sample under compression, and hence a small possible error in the sample constant. Visual inspection has failed to show any evidence of sample bulging in the installed sample. Further investigation of this effect is warranted, particularly in conjunction with tests at elevated pressures.

Effect of Pressure on the Dynamic Shear Compliance. One major objective of this program is to determine the effect of pressure (up to 1000 psi) on the dynamic shear compliance of the selected propellants. A high pressure chamber has been constructed and associated modifications to the Fitzgerald Apparatus were made at the time of this writing.[2] No data are available as yet.

---

1. Sample constant, $C = 2A/h$, where A is the cross sectional area and h is the thickness of the sample.
2. The Fitzgerald Apparatus and the high pressure chamber are shown in Fig. 9.

REFERENCES

1. Hart, R. W., and McClure, T.T., "Combustion Instability: Acoustic Interaction with a Burning Surface," J. Chem. Phys. 30, 1501-1514 (1959).
2. Fitzgerald, E.R., and Ferry, J.D., "Method for Determining Dynamic Mechanical Behavior of GELS and Solids at Audio Frequencies; Comparison of Mechanical and Electrical Properties," J. Colloid Sci., 8, 1-34 (1953).
3. Landel, R.F.,"The Dynamic Mechanical Properties of a Model Filled System: Polyisobutylene-glass Beads," Trans. Soc. Rheology, Vol. II, 53-75 (1958).
4. Bryant, R.C., "Preliminary Measurements of the Dynamic Shear Compliance of a Solid Propellant," presented at Technical Panel on Solid Propellant Combustion Instability, Stanford Research Institute, March 8-9, 1962.

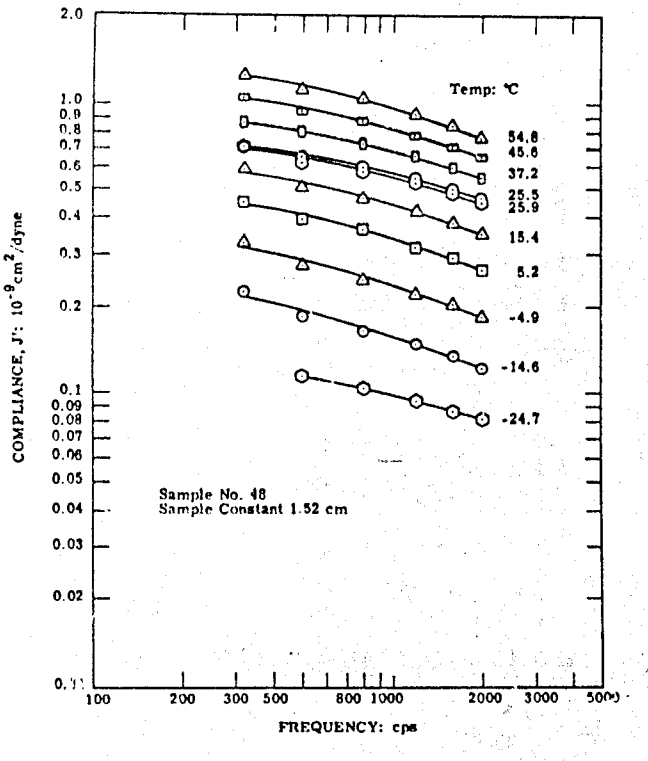

FIGURE 1. VARIATION OF THE REAL COMPONENT J' OF THE DYNAMIC SHEAR COMPLIANCE WITH FREQUENCY, TP-H-1001.

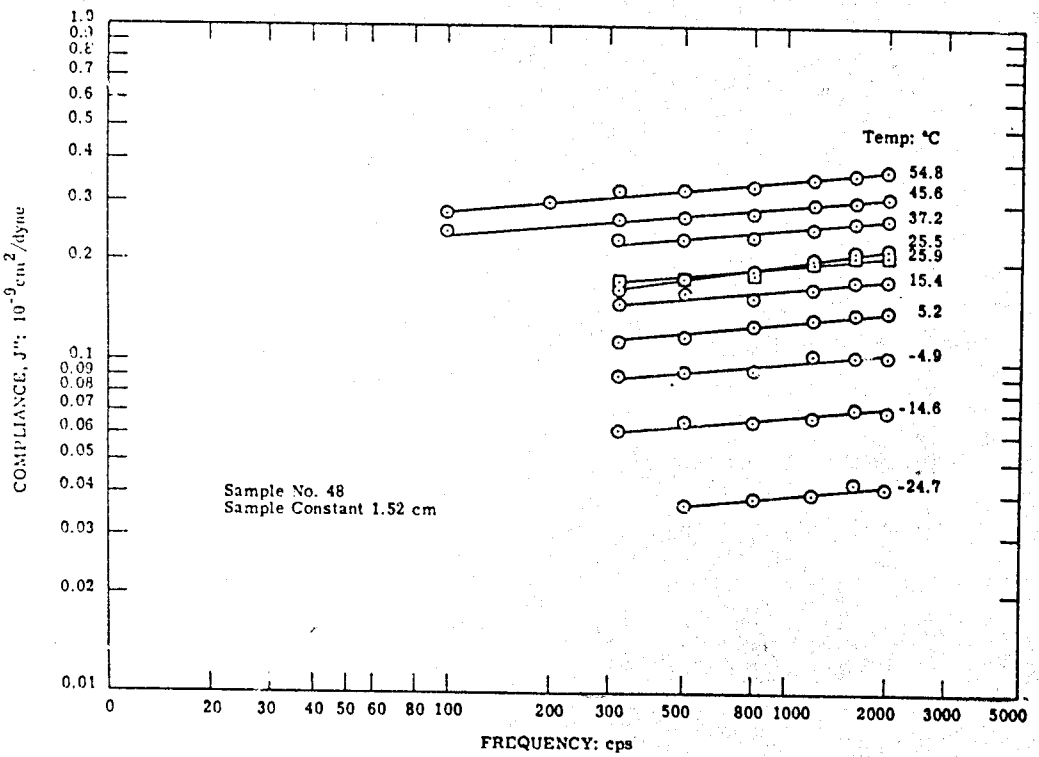

FIGURE 2. VARIATION OF THE IMAGINARY COMPONENT J" OF THE DYNAMIC SHEAR COMPLIANCE WITH FREQUENCY, TP-H-1001.

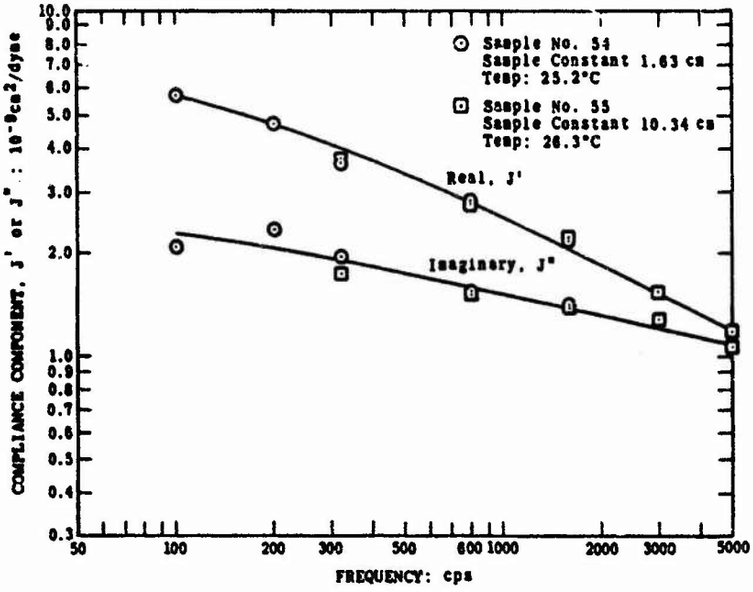

FIGURE 3. VARIATION OF THE REAL COMPONENT J' AND THE IMAGINARY COMPONENT J" OF THE DYNAMIC SHEAR COMPLIANCE WITH FREQUENCY, AEBA-10.

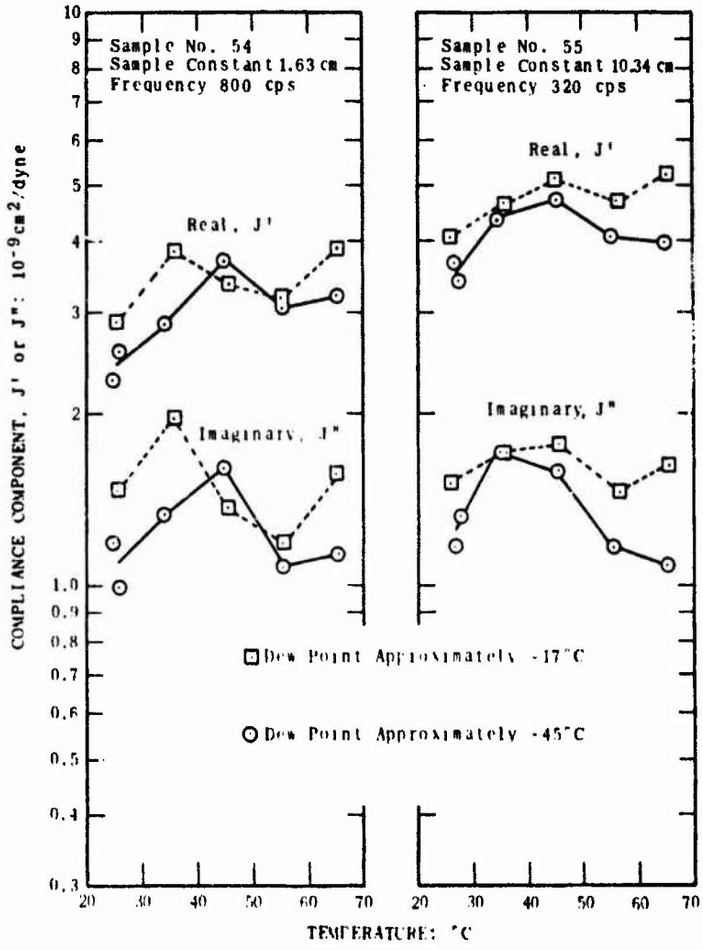

FIGURE 4. EFFECT OF TEMPERATURE AND MOISTURE ON THE DYNAMIC SHEAR COMPLIANCE OF POLYURETHANE PROPELLANT, AEBA-10, AT 800 CPS AND 320 CPS.

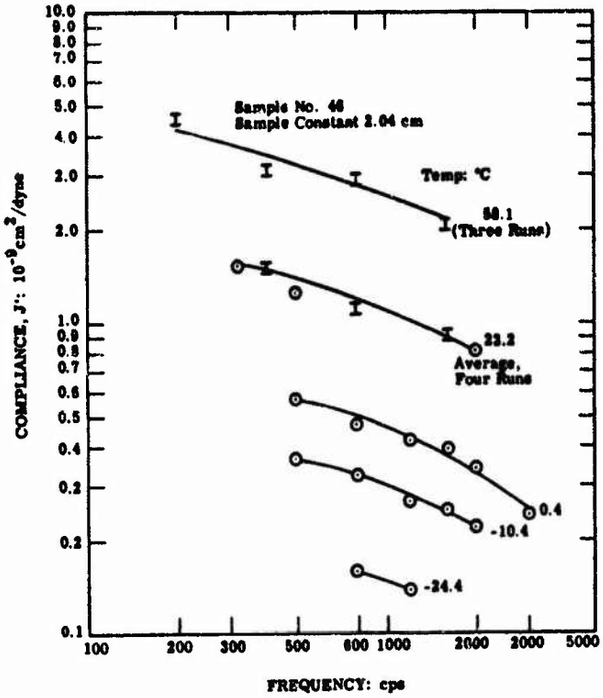

FIGURE 5. VARIATION OF THE REAL COMPONENT J' OF THE DYNAMIC SHEAR COMPLIANCE WITH FREQUENCY, TP-H-1001, LONG CURE.

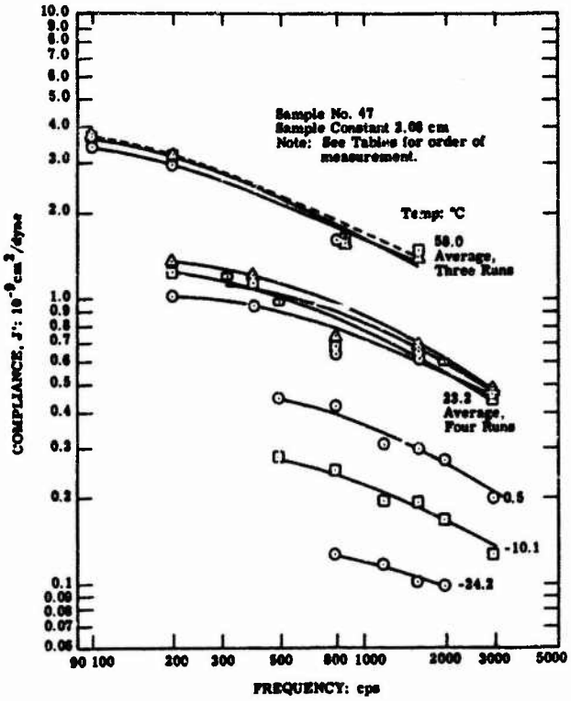

FIGURE 6. VARIATION OF THE REAL COMPONENT J' OF THE DYNAMIC SHEAR COMPLIANCE WITH FREQUENCY, TP-H-1001, NOMINAL CURE.

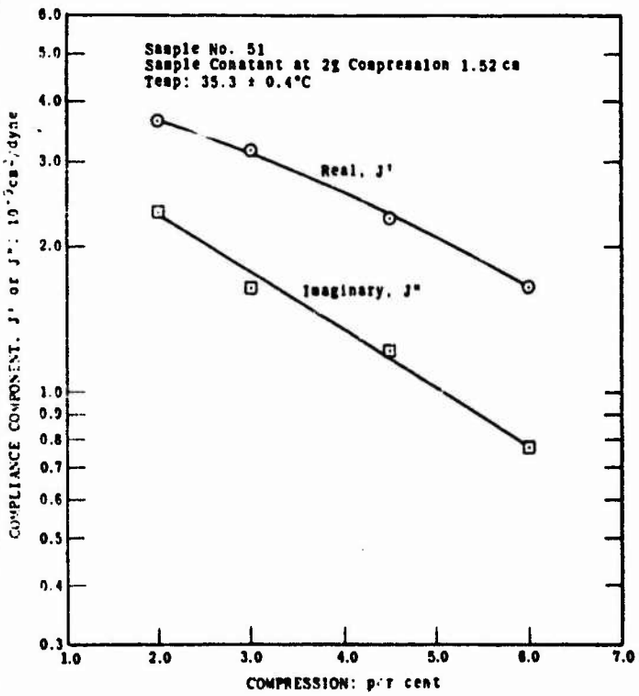

FIGURE 7. EFFECT OF COMPRESSION ON THE DYNAMIC SHEAR COMPLIANCE OF TP-H-1001 AT 800 CPS.

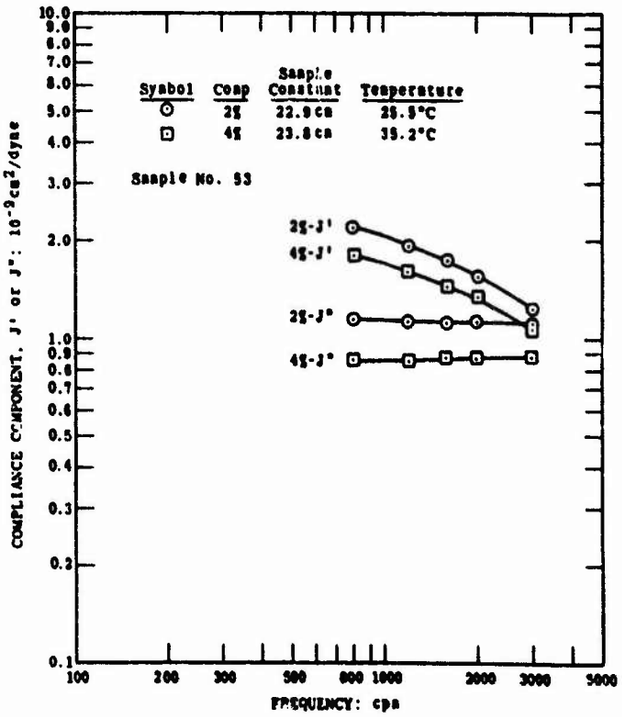

FIGURE 8. EFFECT OF COMPRESSION, TP-H-1001.

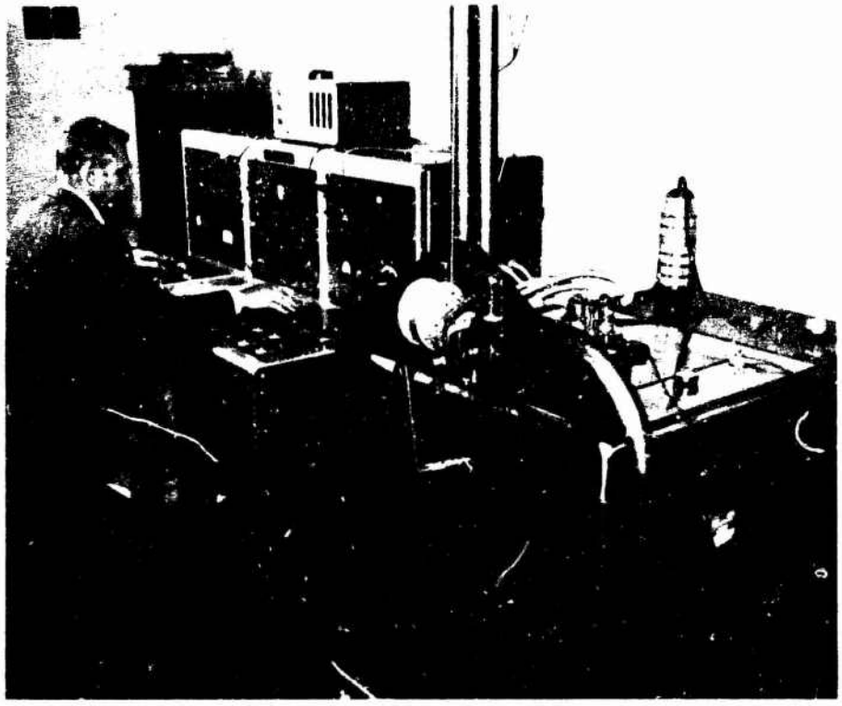

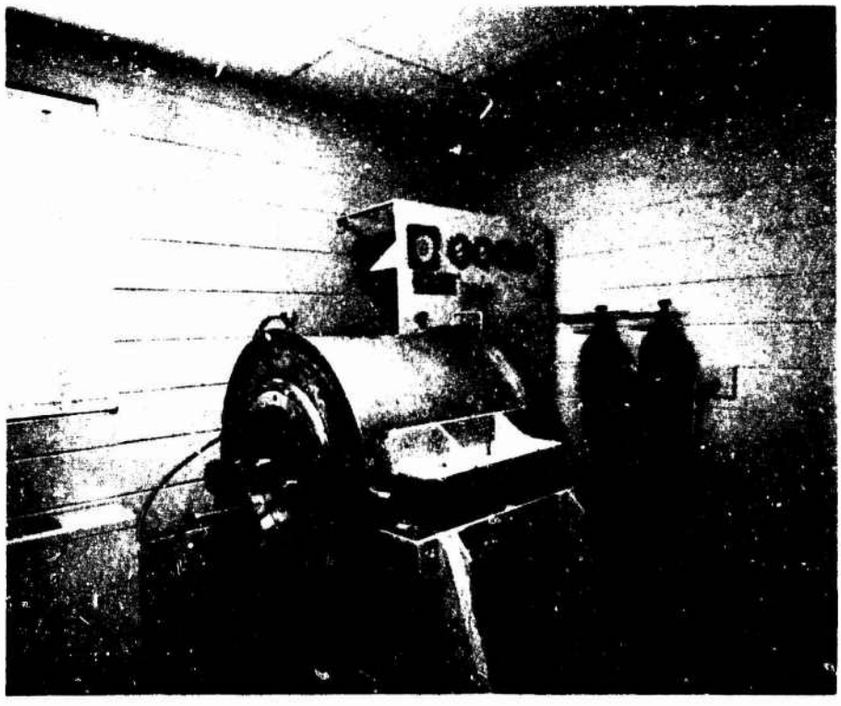

Fig. 9 FITZGERALD APPARATUS

TOP: Operating Console and Temperature Bath Containing Sample Transducer

BOTTOM: High Pressure Chamber and Accessory Equipment

Table 1. DYNAMIC SHEAR COMPLIANCE, TP-H-1001, Sample No. 48

Sample: Area 0.274 cm^2. Thickness 0.361 cm. Constant 1.52 cm.

Date	Temp (°C)	Frequency (cps)	Compliance (10^{-9} cm^2/dyne) J'	J"
3-7-62	25.5	320	.71	.164
		500	.65	.179
		800	.60	.187
		1,200	.55	.202
		1,600	.50	.215
		2,000	.465	.216
3-9-62	5.2	320	.450	.114
		500	.393	.119
		800	.364	.129
		1,200	.317	.134
		1,600	.291	.140
		2,000	.263	.142
3-13-62	- 4.9	320	.329	.091
		500	.277	.094
		800	.248	.095
		1,200	.220	.106
		1,600	.203	.105
		2,000	.183	.105
3-14-62	-14.6	320	.227	.062
		500	.184	.066
		800	.165	.066
		1,200	.149	.068
		1,600	.135	.072
		2,000	.121	.071
3-15-62	-24.7	500	.113	.0371
		800	.103	.0388
		1,200	.095	.0395
		1,600	.087	.0430
		2,000	.082	.0417
3-20-62	15.4	320	.59	.150
		500	.51	.162
		800	.462	.157
		1,200	.421	.167
		1,600	.387	.177
		2,000	.351	.177
3-21-62	25.9	320	.71	.174
		500	.63	.178
		800	.58	.185
		1,200	.53	.199
		1,600	.49	.210
		2,000	.449	.211
3-27-62	37.2	320	.87	.232
		500	.80	.234
		800	.73	.237
		1,200	.66	.252
		1,600	.60	.263
		2,000	.55	.270
3-29-62	45.6	100	1.20	.245
		320	1.05	.269
		500	.94	.272
		800	.87	.280
		1,200	.78	.298
		1,600	.71	.303
		2,000	.65	.311
4-2&3-62	54.8	100	1.46	.279
		200	-	.300
		320	1.26	.325
		500	1.12	.330
		800	1.03	.339
		1,200	.92	.354
		1,600	.84	.368
		2,000	.76	.378

Table II. DYNAMIC SHEAR COMPLIANCE, AEBA-10

Sample No. 54: Area 0.300 cm^2. Thickness 0.369 cm. Constant 1.63 cm.
Sample No. 55: Area 1.943 cm^2. Thickness 0.376 cm. Constant 10.34 cm.

Sample No.	Date	Temp (°C)	Frequency (cps)	Compliance (10^{-9} cm^2/dyne) J'	J"
54	6-29-62	25.2	100	5.7	2.09
			200	4.79	2.34
			320	3.64	1.95
			800	2.88	1.55
			1600	2.19	1.41
55	6-27-62	26.3	320	3.75	1.73
			800	2.82	1.52
			1600	2.22	1.40
			3000	1.54	1.28
			5000	1.19	1.07

Table III. DYNAMIC SHEAR COMPLIANCE, AEBA-10, Sample No. 54

Sample: Area 0.300 cm^2. Thickness 0.369 cm. Constant 1.63 cm.

Date	Temp (°C)	Frequency (cps)	Compliance (10^{-9} cm^2/dyne) J'	J"
6-29-62 (Note: taken from Table 4 of previous Quarterly Report)	25.2	100	5.7	2.09
		200	4.79	2.34
		320	3.64	1.95
		800	2.88	1.55
		1600	2.19	1.41
7-02-62	35.9	25	9.5	-
		50	7.8	3.05
		100	7.1	2.62
		200	5.9	3.08
		320	4.81	2.20
		800	3.84	1.96
		1600	2.56	1.70
7-06-62	45.5	50	6.2	-
		100	5.7	1.59
		200	4.97	1.95
		320	4.04	1.58
		500	3.89	1.40
		800	3.37	1.37
7-10-62	55.7	50	5.6	-
		100	5.2	1.36
		200	4.54	1.53
		320	3.80	1.40
		800	3.19	1.18
7-27-62	26.3	100	5.6	1.75
		200	4.78	2.13
		320	3.68	1.81
		800	3.02	1.44
		1000	2.22	1.47
8-03-62	65.2	25	8	-
		50	7	2.26
		100	6.4	1.91
		200	5.5	2.18
		320	4.90	1.86
		800	3.89	1.56

Table III (Cont.)

DYNAMIC SHEAR COMPLIANCE, AEBA-10, Sample No. 54

Date	Temp (°C)	Frequency (cps)	Compliance (10^{-9} cm²/dyne) J'	J''
8-06-62	25.8	100	5.5	1.73
		200	4.78	2.08
		320	3.54	1.71
		800	3.03	1.45
		1600	2.03	1.42
8-10-62	15.1	100	5.0	1.96
		200	4.26	2.25
		320	2.83	1.89
		800	2.38	1.39
		1600	1.64	1.25
8-13-62	5.3	100	3.31	1.60
		200	2.44	1.54
		320	1.78	1.69
		800	1.19	0.93
		1600	0.79	0.77
		2000	0.65	0.68
8-14-62	-4.5	200	0.82	0.64
		320	0.78	0.65
		800	0.388	0.393
		1600	0.299	0.265
		2000	0.264	0.258
		3000	0.168	0.208
8-15-62	-15.1	320	0.244	0.120
		800	0.188	0.108
		1200	0.122	0.087
		1600	0.127	0.073
		2000	0.126	0.072
		3200	0.088	0.069
		5000	0.049	0.059
8-20-62	24.9	100	5.8	2.15
		200	4.90	2.71
		320	3.41	2.02
		800	2.58	1.40

Table IV. DYNAMIC SHEAR COMPLIANCE, AEBA-10, Sample No. 55

Sample: Area 1.943 cm². Thickness 0.376 cm. Constant 10.34 cm.

Date	Temp (°C)	Frequency (cps)	Compliance (10^{-9} cm²/dyne) J'	J''
6-27-62 (Note: taken from Table 4 of previous Quarterly Report)	26.3	320	3.75	1.73
		800	2.82	1.52
		1600	2.22	1.40
		3000	1.54	1.28
		5000	1.19	1.07
7-03-62	35.4	320	4.62	1.72
		800	3.26	1.56
		1600	2.72	1.46
		3000	1.90	1.67
7-05-62	45.3	200	4.92	1.87
		320	5.1	1.77
		800	3.84	1.61
		1600	3.36	1.64
7-09-62	56.3	200	4.75	1.49
		320	4.68	1.47
		800	3.71	1.37
		1600	3.24	1.43
7-27-62	26.0	200	4.45	-
		320	4.19	1.42
		800	2.58	1.64
		1600	2.34	1.38
		3000	1.64	1.32
8-02-62	65.3	200	5.2	1.73
		320	5.2	1.63
		800	4.09	1.53
		1600	3.59	1.62
		2000	3.34	1.68
8-06-62	25.6	200	4.43	-
		320	4.21	1.40
		800	2.42	1.63
		1600	2.39	1.30
		3000	1.67	1.30

Table V. DYNAMIC SHEAR COMPLIANCE, AEBA-10, Sample No. 54

Sample: Area 0.300 cm^2. Thickness 0.369 cm. Constant 1.63 cm.

Date	Temp (°C)	Frequency (cps)	Compliance (10^{-2} cm^2/dyne) J'	J''
11-08-62	24.8	100	4.66	1.60
		200	3.98	1.86
		320	2.54	1.81
		500	2.64	1.27
		800	2.29	1.19
		1200	1.93	1.17
11-12-62	34.2	25	7.4	-
		50	5.9	2.09
		100	5.7	2.01
		200	4.99	2.45
		320	3.42	1.79
		800	2.88	1.34
		1200	2.56	1.49
11-14,15-62	45°C*	25	8.5	2.96
		50	7.2	2.60
		100	6.5	2.20
		200	5.6	2.46
		320	4.54	1.83
		800	3.70	1.61
		1200	2.96	-
11-19-62	55.7	50	5.2	1.46
		100	4.88	1.28
		200	4.24	1.36
		320	3.50	1.24
		800	3.05	1.08
		1200	2.58	-
11-20,21-62	65.3	25	7.1	-
		50	5.7	1.45
		100	4.94	1.28
		200	4.31	1.34
		320	3.67	1.23
		800	3.21	1.14
		1200	2.82	-
12-03-62	26.0	50	4.75	1.42
		100	4.56	1.26
		200	4.16	1.59
		320	2.46	1.53
		800	2.58	1.00
		1200	2.18	1.06

Table VI. DYNAMIC SHEAR COMPLIANCE, AEBA-10, Sample No. 55

Sample: Area 1.943 cm^2. Thickness 0.376 cm. Constant 10.34 cm.

Date	Temp (°C)	Frequency (cps)	Compliance (10^{-9} cm^2/dyne) J'	J''
11-06-62	27.4	300	3.80	-
		320	3.41	1.32
		500	3.16	1.43
		800	2.13	1.83
		1200	1.96	1.15
		1600	1.86	1.15
		2000	1.71	1.17
11-09-62	34.3	100	5.3	-
		200	4.51	-
		320	4.40	1.71
		800	2.46	1.76
		1600	2.35	1.33
		2000	2.16	1.38
11-14-62	45.3	100	5.8	-
		200	4.53	1.99
		320	4.72	1.57
		800	3.66	1.62
		1200	2.88	1.25
		1600	2.56	1.18
		2000	2.31	1.14
11-15,16-62	55.2	100	5.3	-
		200	3.99	-
		320	4.07	1.17
		800	3.02	1.32
		1200	2.99	1.14
		1600	3.20	1.44
		2000	3.08	1.51
11-23,24-62	65.0	100	4.82	-
		200	3.78	-
		320	3.98	1.09
		800	3.02	1.21
		1200	2.98	1.07
		1600	2.87	1.15
		2000	2.70	1.20
11-30-62	26.7	300	3.89	-
		320	3.64	1.17
		500	3.46	1.26
		800	1.77	2.11
		1200	2.03	0.99
		1600	2.03	1.02
		2000	1.94	1.08
		3000	1.45	1.17

Table VII. DYNAMIC SHEAR COMPLIANCE, REAL COMPONENT, TP-H-1001, Sample No. 46, Long Cure

Sample: Area 0.172 cm^2. Thickness 0.169 cm. Constant 2.04 cm.

Date	Temp (°C)	Frequency (cps)	Compliance (10^{-9} cm^2/dyne) J'
1-23-62	23.4	400	1.46
		800	1.15
		1,600	.93
1-25-62	58.1	200	4.42
		400	3.08
		800	2.86
		1,600	2.09
1-29-62	22.9	400	1.54
		800	1.14
		1,600	.94
1-30-62	58.1	200	4.61
		400	3.15
		800	2.92
		1,600	2.16
2-1-62	58.1	200	4.57
		400	3.05
		800	2.86
		1,600	2.16
2-5-62	23.1	400	1.54
		800	1.12
		1,600	.93
2-15-62	0.4	500	.57
		800	.472
		1,200	.418
		1,600	.388
		2,000	.341
		3,000	.239
2-20-62	-10.4	500	.366
		800	.322
		1,200	.267
		1,600	.250
		2,000	.220
2-21-62	-24.4	800	.159
		1,200	.138
2-26-62	23.6	320	1.51
		500	1.24
		800	1.09
		1,600	.89
		2,000	.80

Table VIII. DYNAMIC SHEAR COMPLIANCE, REAL COMPONENT, TP-H-100i, Sample No. 47, Nominal Cure

Sample: Area 0.224 cm^2. Thickness 0.215 cm. Constant 2.08 cm^{-1}.

Date	Temp (°C)	Frequency (cps)	Compliance (10^{-9} cm^2/dyne) J'
1-23-62	23.4	200	.99
		400	.91
		800	.62
		1,600	.59
		3,000	.438
1-25-62	58.1	100	3.26
		200	2.87
		800	1.54
		1,600	1.37
		3,000	1.02
1-29-62	22.8	200	1.21
		400	1.10
		800	.66
		1,600	.64
		3,000	.444
1-30-62	57.9	100	3.49
		200	3.05
		860	1.57
		1,600	1.42
		3,000	1.02
2-1-62	57.9	100	3.51
		200	3.06
		860	1.54
		1,600	1.37
		3,000	.94
2-5-62	23.1	200	1.32
		400	1.17
		800	.72
		1,600	.67
		3,000	.463
2-15-62	0.5	500	.427
		800	.402
		1,200	.297
		1,600	.288
		2,000	.261
		3,000	.194
2-20-62	-10.1	500	.270
		800	.241
		1,200	.189
		1,600	.186
		2,000	.162
		3,000	.122
2-21-62	-24.2	800	.121
		1,200	.112
		1,600	.098
		2,000	.095
2-26-62	23.6	320	1.16
		500	.94
		800	.70
		1,600	.65
		2,000	.58
		3,000	.449

CURRENT WORK ON VISCOELASTIC PROPERTIES

A. S. Elder
Ballistic Research Laboratories
Aberdeen Proving Ground, Maryland

A theoretical and experimental program on the mechanical properties of solid propellants is in progress at BRL. Current theoretical work concerns the development of integral equation methods of solving quasi-static stress analysis problems in viscoelasticity. Methods of calculating constants for a viscoelastic model from experimental data have also been derived. The experimental program has been concerned mainly with the development of apparatus for measuring the bulk modulus and shear modulus of solid propellants. Only certain topics will be discussed in this paper, as a complete review of the work at BRL has been published elsewhere (1).

A study at BRL has shown that the stress functions of classical elasticity can be used for quasi-static problems in linear viscoelasticity (2). This theory has led to the formulation of problems involving moving boundaries in terms of Volterra integral equations of a very general type. A detailed analysis of a rocket motor containing a viscoelastic propellant grain which is subjected to the combined effects of pressure, thrust, and an eroding inner boundary is in progress. The formulation of this problem has been completed for an elastic motor case (3); recently it has been found possible to extend the analysis to include cases of viscoelastic material.

The modulus of the propellant in shear and under hydrostatic pressure are used as kernals of the Volterra integral equations mentioned above. As the burning time of the rockets to be used in the experimental work is about a second, an apparatus for measuring the shear modulus accurately in this short interval of time was required. A high-speed stress relaxation device has been developed at BRL for this purpose. This device consists essentially of a specimen, gage, and spring-loaded actuating mechanism. The specimen is a hollow cylinder which is subjected to a shearing force between a fixed inner rod attached to the gage and a concentric outer cylinder linked to the actuating mechanism. A tapered beam of high strength steel is used for the spring. The time to full load is less than a millisecond for an axial displacement of 0.1 in. Transient vibrations are insignificant after about ten milliseconds. A report dealing with the design and development of this apparatus is being prepared.

*This program is supported by the Army Materiel Command.

Approximately a year ago, N. C. Wogsland developed an apparatus for measuring the equilibrium bulk modulus of solid propellants and other viscoelastic materials (4). Hydrostatic pressure is applied to a test sample in the high-pressure chamber of a pressure intensifier. Measurement of the volume displaced by the low pressure end of the double piston provides high sensitivity in measurement of the volume change in the high-pressure chamber. The isothermal bulk modulus is obtained by making measurements after temperature equilibrium of the test sample has been attained. A thermocouple inserted in the test sample is used to measure the temperature of the sample during the test.

Although it is generally believed that viscoelastic materials should exhibit viscoelastic behavior when subjected to hydrostatic pressure, we have not attempted to measure the relaxation modulus under these conditions because of the difficulty in separating relaxation phenomena and thermodynamic phenomena associated with the equation of state. When the propellant is pressurized adiabatically, the temperature also increases. If the volume is then held constant, the pressure and temperature decrease until the specimen attains temperature equilibrium with its surroundings. The pressure-volume relation under equilibrium isothermal conditions appears to follow Tait's equation of state (5) with reasonable accuracy within the 0-2500 psi range over which measurements were made.

The Laplace transform provides an elementary method of solving quasi-static stress analysis in which boundaries do not vary with time and the load is applied over a fixed region of the boundaries (6). A limited number of dynamic problems also appear solvable by this method. In this connection, formulas for the free vibrations of a torsional pendulum have been derived at BRL. The pendulum consists of a circular, viscoelastic rod fixed at one end and attached to a rigid disc at the other end. However, detailed calculations require the solution of polynomial equations with complex roots. A code for calculating these roots is being programmed for the new BRLESC electronic computer at BRL.

The inversion of the Laplace transforms occurring in the analysis described above is facilitated if the mechanical properties of the viscoelastic material are represented by a spring-dashpot model. In this case, the transform to be inverted will generally be represented by a rational function, and the inversion is obtained through an application of residue theory. However, if the theoretical solution is to represent the behavior of a real system over a reasonable interval of time, the spring-dashpot model must also represent the measured mechanical properties over an adequate interval.

Methods of calculating viscoelastic model constants from experimental data have been under continuing study at BRL and North Carolina State College. In 1960, a method of calculating model

constants from complex compliance data was presented (7). This procedure was based in part on Zobel's method of network synthesis. At one stage of the analysis, the relaxation times were calculated as roots of a polynomial. Naturally, these roots would be obtained if the data varied rapidly with frequency, or if too many elements were assumed for the viscoelastic model.

In 1961, John T. Welch of North Carolina State College, under contract with BRL, showed how Baum's asymptotic method of network synthesis could be applied to this problem (8). In this method, response curves of the network plotted to a log-log scale are approximated by a series of straight lines. The network parameters are then calculated from the slopes and points of intersection of the line segments. In this method of graphical analysis, an adequate number of real, negative relaxation times are obtained. However, the accuracy of this method is limited.

The essential features of the two techniques have been combined by Goldberg and Dean of BRL (9). Their method has been applied to complex compliance data for N.B.S. polyisobutylene at 22 different temperatures. The calculated curves are generally within 5% of the experimental data, except at the extremes of frequency and temperature.

In addition, methods of model fitting based on inverted differences are being studied at BRL and North Carolina State College. The recursion formulas required by this method have been derived, and a program is now being written for the BRLESC electronic computer at BRL.

REFERENCES

1. Elder, A. S. and Gay, H. P. "Facility Report." Chemical Propulsion Information Agency, Bulletin of the First Meeting, Working Group on Mechanical Behavior, Dec. 1962. (This paper is Unclassified; the bulletin is classified Confidential.)

2. Elder, A. S. "General Solutions of Certain Integro-Differential Equations of Linear Viscoelasticity." Solid Propellant Information Agency, 20th Meeting Bulletin, Joint Army-Navy-Air Force-ARPA-NASA Panel on Physical Properties of Solid Propellants, Vol. I, Oct. 1961.

3. Elder, A. S. "Derivation of Equations for the Stresses and Strains in a Cylindrical Viscoelastic Case Bonded Grain." Aberdeen Proving Ground: BRL MR-1359, July 1961.

4. Wogsland, N. C. "An Apparatus for Measuring the Bulk Modulus of Solid Propellants." Solid Propellant Information Agency, 20th Meeting Bulletin, Joint Army-Navy-Air Force-ARPA-NASA Panel on Physical Properties of Solid Propellants, Vol. I, Oct. 1961.

5. Hirschfelder, J. O., Curtis, C. F., Bird, R. B. Molecular Theory of Gases and Liquids. John Wiley and Sons, Inc., New York, 1954. (Tait's Equation of State is given on Page 261.)

6. Lee, E. H. "Stress Analysis for Viscoelastic Bodies," in Viscoelasticity Phenemological Aspects, by Bergen, J. T., editor. Academic Press, New York and London, 1960.

7. Elder, A. S. "Calculation of Viscoelastic Model Constants from Complex Compliance Data." Solid Propellant Information Agency, Bulletin of the Joint Meeting JANAF Panels on Surveillance and Physical Properties of Solid Propellants, Sept. 1960.

8. Welch, John T. "Empirical Determination of Some Mathematical Models in Viscoelasticity." North Carolina State College Memorandum, Contract No. DA-01-009-ORD-991, August 1961.

9. Goldberg, W. and Dean, N. W. "Determination of Viscoelastic Model Constants from Dynamic Mechanical Properties of Linear Viscoelastic Materials." Aberdeen Proving Ground: BRL R-1180, November 1962.

DETERMINATION OF COMPLEX COMPLIANCE OF PROPELLANTS*

J. Edmund Fitzgerald
Lockheed Propulsion Company
Redlands, California

Rather than a technical presentation per sé, this paper is a report of research in progress relative to vibrational response of solid propellants.

While work has been in being for some years at our laboratory on the creep and relaxation phenomena of propellants, only recently have we become actively engaged in vibrational effects.

Pertinent points of interest toward the eventual application of our work to the oscillatory combustion - propellant response coupling are

1. The development and routing application of relaxation and retardation operators over an eighteen decade time domain. The results are generally expressed in finite linear differential operator form but, where more convenient for subsequent analysis, occasionally in hereditary integral form.

2. The development of routine procedures for the determination of complex compliance expressions from the above relaxation operators. It should be mentioned at this point that if the relaxation modulus plots as a straight line on log-log coordinates of E_{rel} vs reduced time that

   a) The real part of the complex compliance will be a straight line over the same range.

   b) The imaginary part of the complex compliance will be a straight line over the same range parallel to the first.

   c) The loss tangent will be a constant over the above range.

   This characteristic of power law relaxation moduli has frequently been overlooked.

   An example of a preliminary comparison of a PBAA propellant complex modulus as calculated from relaxation data and as determined experimentally elsewhere is given in Fig. 1.

3. The above results in conjunction with knowledge of the thermal properties of the propellant enable one to then calculate rather good estimations of the temperature rise in a vibrating propellant body. The rigorous solution to the problem involves non-linear mathematics even in

*Presented by Leon Green.

thermorheologically simple materials because of the resulting coupling of compliance and temperature change.

4. Experimental work is now in progress determining the complex compliance directly over a wide frequency and temperature range for both

   a) Complex shear modulus and

   b) Complex bulk modulus.

   It is felt that the bulk effects may demand considerably more attention for chamber pressure oscillation effects than bulk effects usually do with quasi-static problems where incompressibility is often assumed.

It is hoped that a detailed technical presentation on the above items with complete analytical and experimental correlations will be available at the next meeting of the Technical Panel.

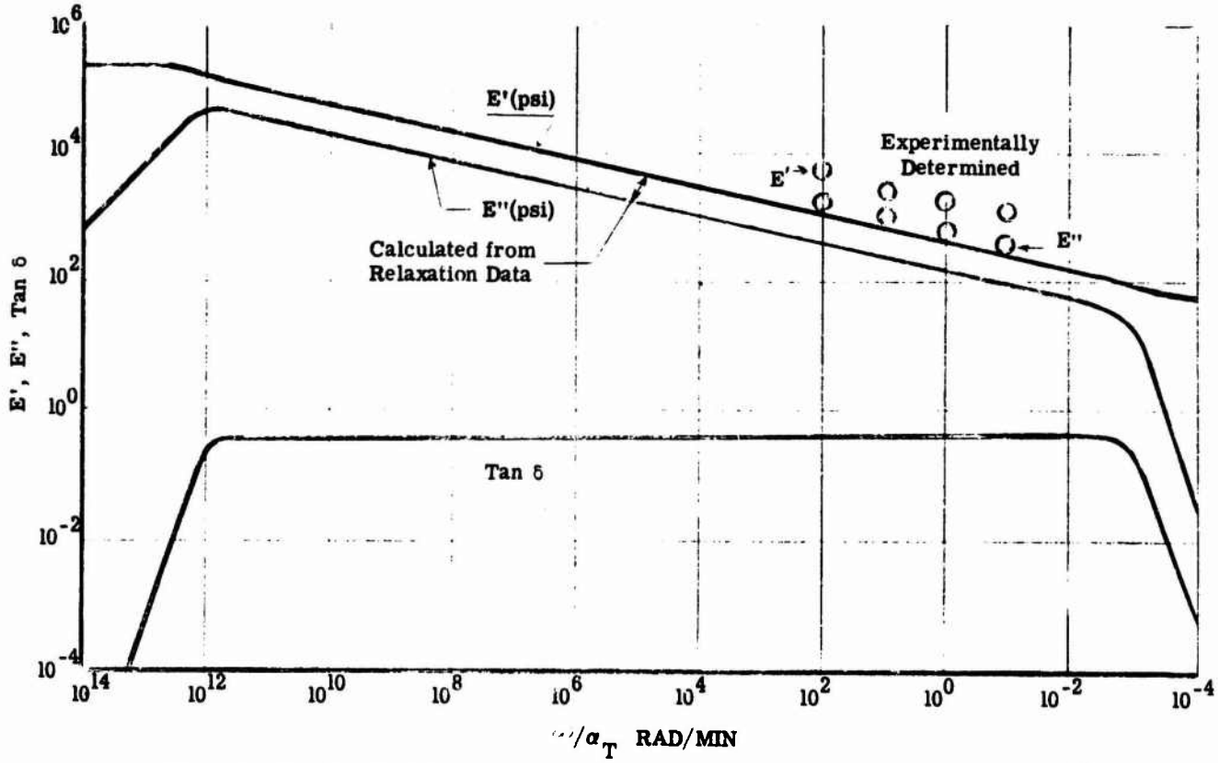

Figure 1. Complex Moduli and Loss Tangent, PBAA Propellant, at Temperature - 70°F

THE EFFECT OF FLOW ON BURNING INSTABILITY **

Ira Dyer
Bolt Beranek and Newman, Inc.
Cambridge 38, Massachusetts

I am pleased to be at this meeting, for I have much to learn about the acoustics of solid propellant instability. I am going to talk about a problem that I, for one, do not understand well. The purpose of a burning solid propellant is to evolve gas, and this it does. Although the gas is evolved at fairly low Mach numbers, I believe that the mean gas flow should be taken into account because it may have much to do with the details of energy balance, and hence the stability.

There are now at least three criteria available for deciding upon the instability of solid propellants. These criteria, cast in terms of the propellant response function μ/ϵ, are displayed in Fig. 1.[1] [Numbers in superscript are footnotes; numbers in parentheses are references.] To help set the stage, a response function calculated by Hart and McClure is also shown (1). The highest criterion, given by $\mathrm{Re}(\mu/\epsilon) > 1/\gamma$, was brilliantly suggested several years ago by McClure and his co-workers (1,2). This criterion ignores the presence of mean flow. Just a short time ago another criterion, considering mean flow, was derived by McClure and his co-workers (3). It is shown in Fig. 1 as the lowest criterion, given by $\mathrm{Re}(\mu/\epsilon) > 0$, which is the value obtained for very small values of the flow speed. Not long ago, I too had a try at it and arrived at the middle criterion, $\mathrm{Re}(\mu/\epsilon) > 1/(2\gamma)$.(4). Clearly these criteria can lead to greatly different conclusions on the frequency range of instability, as illustrated by Fig. 1. What can be said about these criteria, and which one, if any, is right?

Allow me to discuss the foregoing question initially in terms of energy flux in a one-dimensional situation. Imagine a burning solid propellant surface, located at $X = 0$, which evolves gas in the positive X direction. We may state that the acoustic intensity evaluated at $X = 0$ is the sum of the usual acoustic pressure-velocity product and a term representing the convection of kinetic and potential energy densities (4):

$$I = \overline{p_1 v_1} + v_o \left[\frac{\rho_o \overline{v_1^2}}{2} + \frac{\overline{p_1^2}}{2\rho_o c^2} \right] . \qquad (1)$$

With acoustic admittance of the burning surface defined by

$$Y = - \frac{v_1}{p_1} , \qquad (2)$$

we get

$$I = - \overline{p_1^2}\, \mathrm{Re}\, Y + \frac{1}{2} M_o\, \overline{p_1^2} \left[\rho_o c (\mathrm{Re}^2 Y + \mathrm{Im}^2 Y) + \frac{1}{\rho_o c} \right] . \qquad (3)$$

*See appendix for definition of symbols.

Equation (3) may be used to establish a criterion for instability, if we assume that the acoustic intensity represents the totality of energy flux available to overcome acoustic losses occurring elsewhere in the system. This assumption will be discussed later, for it is central to the problem of instability. For the moment, at least, grant it.

For a solid propellant to act as a sound source, the flux of energy must be positive, i.e., $I > 0$. By taking $M_o = 0$, Eq. (3) yields McClure's earlier result:

$$\text{Re } Y < 0 \ . \tag{4}$$

This may be transformed readily to[1]

$$\text{Re } \frac{\mu}{\epsilon} > \frac{1}{\gamma} \ . \tag{5}$$

On the other hand by taking $M_o << 1$, I have obtained

$$\text{Re } Y < \frac{M_o}{2\rho_o c} \tag{6}$$

which transforms to

$$\text{Re } \frac{\mu}{\epsilon} > \frac{1}{2\gamma} \ . \tag{7}$$

The difference in the criteria given by Eqs. (5) and (7) hinges on the added convection term in the intensity. This term is always positive; hence Eq. (7) predicts a greater range of $\text{Re}(\mu/\epsilon)$ for which the propellant acts as a sound source, i.e., is unstable.

Does the convection term actually represent an energy flux that is available to overcome acoustic losses, as assumed? It may be that the energy flux associated with convection merely disappears completely someplace else, without affecting the oscillations[2]. If so, then one might take Eq. (5) as a more appropriate criterion, even in the presence of flow. Since the convection term is positive, however, we might take refuge in the belief that the proper criterion is between $1/\gamma$ (corresponding to complete disappearance of the convected energy) and $1/(2\gamma)$ (corresponding to complete use of the convected energy in overcoming acoustic losses).

---

1. The thermoviscous nature of the burning gases is neglected, as well as the effects of diffusion of reactants as discussed by Williams (5).

2. For example, we may imagine the possibility of an open-ended one-dimensional tube (like an organ pipe) which is capable of supporting standing waves, but which may allow the convection of acoustic energy density out of the open end.

The uncertainty between $1/\gamma$ and $1/(2\gamma)$ stems from our inability at this point to give a clear physical interpretation of the convection term. It is apparent that a statement like Eq. (3) describing conditions at the face of a burning propellant is incapable of shedding light on the nature of sound-flow interaction in the remainder of the system. We may conclude that we must consider the entire system, including flow patterns, acoustic modes, and losses, before we can make headway with this problem.

In the recent work of McClure, Hart and Cantrell(3), account is taken of a complete system, namely a T-burner. Although the oscillation considered is primarily one-dimensional, the mean flow is not. Their results indicate that for $M_o << 1$, system instability may occur if

$$\mathrm{Re}\,\frac{\mu}{\epsilon} > 0 \quad . \tag{8}$$

In view of the range $1/\gamma$ to $1/(2\gamma)$ implied by Eqs. (5) and (7), this result may appear very surprising indeed! The implication is that some other part of the system may act as a sound source too. Unfortunately, McClure, Hart and Cantrell do not identify the part of the system or what mechanism is responsible for the generation of sound. Nevertheless, this possibility should not be discounted since many mechanisms exist for the conversion of flow energy to acoustic energy, particularly if rotational flows are considered. In any case, it is well to remember that Eq. (8) is a criterion relevant to the T-burner system, and may not be applicable to other systems.

Although I am not prepared to give general conclusions on the question of instability criteria, I am convinced that mean flow plays an important role. Flow may convect acoustic energy from one part of an oscillating system to another, it may enhance the ordinary acoustic loss mechanisms or bring into being new ones, and finally, it may cause sound to be generated quite apart from the action of the propellant. It is clear that much more needs to be accomplished, particularly along the lines of the McClure, Hart and Cantrell study, before we can resolve some of the issues raised herein. Only with a thorough understanding of the relevant physics will we have confidence in a general criterion for propellants.

REFERENCES

1. Hart, R.W. and McClure, F.T., "Combustion Instability: Acoustic Interaction with a Burning Propellant Surface," J. Chem. Phys. 30, 6, 1501-1514, June 1959.

2. McClure, F.T., Hart, R.W., and Bird, J.F., "Solid Propellant Rocket Motors as Acoustic Oscillators," Solid Propellant Rocket Research, Progress in Astronautics and Rocketry, Vol. 1, Edited by Martin Summerfield.

3. McClure, F.T., Hart, R.W.,and Cantrell, R.H., "Interaction between Sound and Flow Stability of T-burners," The Johns Hopkins University, Applied Physics Laboratory, TG 335-12, July 1962.

4. Dyer, I., "Acoustic Instability of Burning Gases," Fourth International Congress on Acoustics, Copenhagen, August 21-28, 1962.

5. Williams, F.A., "Response of a Burning Solid to Small-amplitude Pressure Oscillations," J. Appl. Phys., 33, 11, 3153-3166, November 1962.

Definition of Symbols

c	speed of sound
I	acoustic intensity
Im	imaginary part of
m	mass flow
M	Mach number
p	pressure
Re	real part of
v	velocity
Y	acoustic admittance of the propellant
γ	ratio of specific heats
ϵ	p_1/p_o
μ	m_1/m_o
ρ	density
o	mean quantities
1	fluctuating (acoustic) quantities

**This work supported by the Army Materiel Command, Contract DA-19-020-AMC-5755-R, and Advanced Research Projects Agency Order No. 357-62.

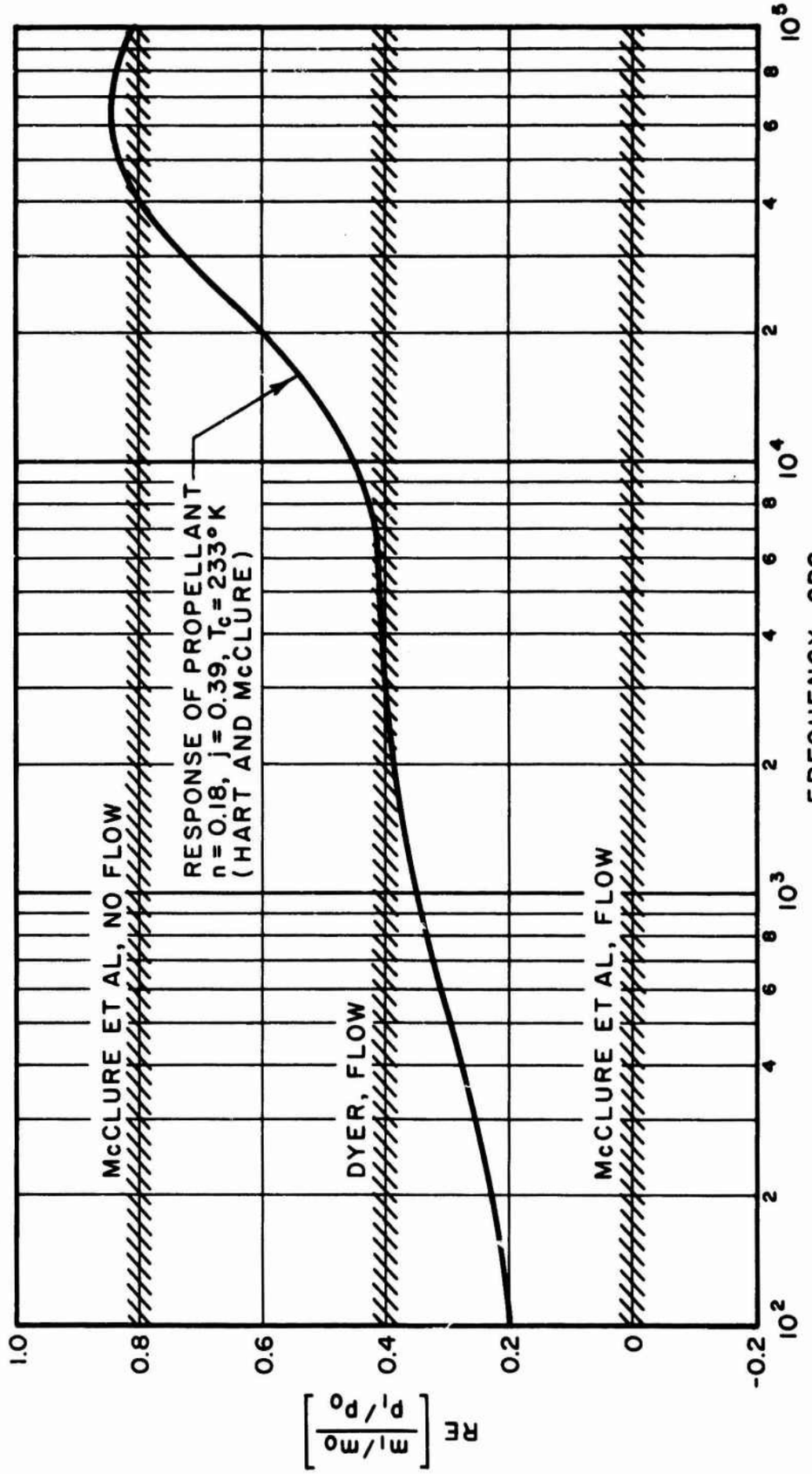

Fig. 1 THREE CRITERIA FOR INSTABILITY COMPARED WITH A CALCULATED RESPONSE FUNCTION

-7-

L* COMBUSTION INSTABILITY*

E. W. Price
U. S. Naval Ordnance Test Station
China Lake, California

INTRODUCTION

The pressure in the combustion chamber of a rocket motor is determined by the balance between the process by which mass is discharged from the chamber and the process by which mass is injected into the chamber. In transient situations, consideration must also be given to the intermediate processes following injection and preceding discharge, where significant mass accumulation may occur. For practical reasons, rocket motors are designed to assure that these mass rates converge rapidly after ignition to a desired equilibrium value yielding the desired combustion chamber pressure and thrust. However, this goal is not uniformly achieved, and a variety of unwanted classes of behavior occur, such as hard starts, chuffing, catastrophic pressure rises, hang-fires, and periodic pressure fluctuations. Periodic fluctuations are usually associated with the concept of "combustion instability," although in a scientific sense all of the classes of behavior referred to are unstable and it is difficult to define a decisive boundary for the concept. It has been observed that a small change in motor or propellant variables can lead to a series of instabilities ranging from periodic oscillatory behavior (Fig. 1a) to chuffing behavior (Fig. 1b) to quenching (Fig. 1c). These apparently different kinds of instability are all seen to be closely related.

The examples of instability noted in Fig. 1 are quite different from those discussed in recent literature involving interaction of combustion and acoustic behavior. The frequency of oscillation, when there is one, is relatively low (1-100 cps), and is not usually identifiable with any natural acoustic mode of the rocket motor. The prevalence of the behavior with propellants having slow-burning ingredients, and with low pressure operation where combustion is slow, suggests that low frequency instability is related to incomplete combustion and to factors governing reactant stay time in the combustion chamber. In a sense one might say that the problem involves a condition where the combustor volume is less than the volume of the combustion zone, the stay time is less than the reaction time (at least for some reactants), the combustion zone thickness is comparable to the combustor dimensions. These concepts are strange to the solid rocket propulsion scientist, who is used to the usual rapid reaction of solid propellants and to the usual large internal free volume of solid rocket motors. To the liquid propellant propulsion

*Sponsored by the National Aeronautics and Space Administration.

scientist, the problems of combustion volume and stay time are fundamental considerations in good design and are related experimentally to the concept of L*. A good engine design provides the lowest value of this ratio, $L^* = V_c/A_t$, consistent with efficient combustion. In the case of a solid propellant rocket, a low value of L* may be more tolerable because of more rapid combustion, but may be accepted even with slow combustion because the L* increases rapidly to acceptable values after burning starts. During the time that L* is low, the stability of the system depends upon the effects of incomplete combustion on the mass in-flow, out-flow, and accumulation in the system. The types of instabilities arising from this condition are referred to here as "L* Combustion Instability." The extent to which low frequency instability observed to date is "L* Instability" is not yet established, but it will be seen in the following that the concept fits the observed facts rather well.

MASS-BALANCE ARGUMENTS FOR PRESSURE DECAY

There is some reason to believe that the mechanisms governing the descending part of the pressure cycle are qualitatively different than the mechanisms governing the rising part of the pressure cycle. The descending part of the cycle can be explained in phenomenological terms by a quasi-steady model of mass rates as shown in Fig. 2. The graph shows what the mass burning rates and mass discharge rates would be at each pressure if the pressure were sustained at that value independently of combustion chamber mass-balance arguments. The solid curves represent the mass rates assuming large values of L* which allow complete combustion in the rocket motor and complete heat feedback to the propellant sample for normal burning rates. The broken lines represent mass rates at low values of L* here incomplete combustion leads to abnormally high nozzle discharge coefficients (low c*), particularly at low pressures. Burning rates may also be changed at low L*, either because of incomplete heat feedback to the propellant surface or convective encroachment of the chamber flow on the combustion zone near the propellant surface.

If one considers a motor design in which the value of L* is low (because of small free volume and/or large nozzle throat area), then it can be seen in Fig. 2 that the mass discharge rate is higher than the mass burning rate at normal rocket motor pressures. Thus the motor pressure, if raised to normal values by the igniter, would then drop off to the point where mass out-flow and mass burning rate are equal (e.g., point 1 in Fig. 2). From the figure, it is evident that such a motor pressure always exists if the propellant will burn at atmospheric pressure, because the mass discharge rate is zero at that pressure and an equilibrium must occur at some higher pressure.

Since the value of L* increases rapidly as the burning proceeds, the lower equilibrium noted above may not occur in practice. By the time the pressure has dropped off, L* may be enough larger to yield a higher equilibrium pressure (point 2 in Fig. 2). Thus the pressure may reach a minimum and then drift back to normal as L* increases towards values permitting complete combustion and heat feedback. It

should be emphasized that the drop-off in pressure after the ignition does not constitute incomplete ignition. Also, it should be noted that burning will be completely quenched by this drop-off behavior if the propellant will not burn at low pressures. This must still be regarded as combustion system instability rather than unsatisfactory ignition since the behavior is predicted even on the basis of steady-state burning rate data for the propellant.

THE LOW PRESSURE PART OF THE CYCLE

Very little data are available regarding burning characteristics of solid propellants at low pressures, so it is difficult to predict the behavior of the system after the pressure has dropped off. Partially reacted materials may accumulate in the combustion chamber, and the propellant surface may become covered with carbon or aluminum or other reactants and intermediate products. The gas flowing out of the nozzle may be only partially reacted, and may not have the same atomic composition as the propellant (because of selective accumulation processes in the combustion chamber). In addition, the temperature profile in the solid propellant surface may take some time after the pressure decay before it arrives at that profile normal for the low-pressure burning, and the burning will in the meantime be slowed by the excess heat flow into the solid. There seems to be little doubt that these effects are present, but their qualitative and relative importance has not been established. In spite of this ignorance of transient processes, some insight into the observed behavior during the low pressure part of the cycle in low-frequency instability can be obtained by use of steady-state arguments.

The region of pressure below 30 psia is one in which many propellants will not burn, and other propellants burn without a flame and with incomplete reaction. Thus the existence of a low-pressure equilibrium point in Fig. 2 is contingent on continued burning in the pressure range where the nozzle flow is subsonic and the discharge curve turns steeply down. The actual pressure range involved here is contingent on the external pressure (Fig. 3). If the external pressure is sufficiently low, the propellant mass burning rate curve may reach its low pressure limit before it intersects the mass discharge rate curve, and no low pressure equilibrium would be possible (case C in Fig. 3). Thus it would be expected that the character of the L* instability would be qualitatively different depending on the external pressure and on the low pressure deflagration limit of the propellant. This qualitative difference is predicted even by the steady-state theory, although such theory is not adequate for quantitative predictions. Provided this low pressure behavior is of practical interest, some determinations of low pressure deflagration limits would be instructive, as would be determinations of discharge coefficients and burning rates in the low pressure range above the deflagration limit.

To obtain a quantitative understanding of the low pressure part of the pressure cycle, it will be necessary to construct a very complicated transient model of combustion and gas discharge. For the

present it appears to be preferable to correlate obtainable behavior with the measurable steady-state burning and discharge characteristics and then assess the areas of inconsistency as a basis for future research if needed.

THE RISING PART OF THE PRESSURE CYCLE

A variety of arguments may be evolved to explain why the pressure doesn't remain at the low value dictated by the steady-state curves of Fig. 2 and Fig. 3. Since the pressure rise is not predicted by the steady-state curves, one cannot avoid reference to transient models in explaining the pressure rise. The most obvious explanation is the accumulation of partially reacted material in the motor in the presence of a progressive thermal environment leading to sudden burning of the accumulated reactants and heated propellant. The thermal explosion theory of Clemmow and Huffington is an example of such behavior, which may be relevant to some instances of LFI. However, it seems unlikely that the dominant contributions to the rising part of the pressure cycle are the same with all propellants at all temperatures, pressures, and combustion chamber cavity relaxation times. Consequently, the first problem is to identify the possible mechanisms, how they can be recognized or distinguished in practice, and when each becomes important. Since none of these things has been done, the present discussion will be restricted to comments on possible contributing mechanisms.

Thermal Lag. Heat stored in the thermal gradient of the solid propellant is greater at low pressure than at high pressure (in steady-state). Thus, when the pressure in the combustion chamber increases rapidly, the propellant at each instant has more heat content than normal and burns faster than normal. This condition does not induce pressure rise, but amplifies the effect of any rise that occurs for any other reason. In order to get an idea of the energies and times involved in the transient thermal adjustment during pressure changes, the relation between heat content, heat flux, and rate of pressure change was derived from the case of an isotropic propellant material

$$\left(\frac{dq_s}{dq_r} \Big/ \frac{dp}{dt}\right) = - \frac{n K T_m}{\rho C^2 (L + cT_m) p^{2n+1}}$$

where

dt = time interval for pressure to go from p to p + dp
dq_s = difference in heat content for steady-state burning at p and at p + dp
dq_r = heat transferred to the propellant from the combustion in the time dt under steady-state burning conditions
C = factor in the propellant burning rate rule $r = Cp^n$ (0.0446 cm·sec^{-1}· psi$^{-1/2}$)
c = heat capacity of the propellant (0.45 cal·gm^{-1}·°K^{-1})
K = heat conductivity of the propellant (2 x 10^{-3} cal·cm^{-1}·sec^{-1}·°K^{-1})

L = heat required for gasification of propellant after reaching the temperature T_m (100 cal·gm^{-1})

n = pressure exponent in the burning rate rule $r = Cp^n$ (.5)

T_m = surface temperature rise from ambient of burning propellant (400°K)

ρ = density of propellant (1.6 gm·cm^{-3})

Typical values of the parameters are noted in parentheses. For the values noted and for a pressure of 100 psi,

$$(dq_s/dq_r)\Big/(dp/dt) = 4.5 \times 10^{-5} \text{ sec/psi.}$$

This result can be used as a qualitative indication of the conditions under which significant deviation from steady-state behavior occurs. Thus, if a value of dp/dt leads to a value of dq_s/dq_r greater than about 0.1, it must be assumed that the burning rate will differ significantly from the steady-state value because a significant amount of the energy flux at the surface is going into accommodation of the temperature profile. In the case of rising pressure this is an energy excess (supplied from the temperature profile), which leads to increased burning rate. Taking this somewhat arbitrary criterion for "onset of transient response," in the example chosen, transient response occurs at rates of pressure change greater than 2,200 psi/sec. Thus one might anticipate that the thermal energy excess in the solid propellant acts to amplify a perturbing pressure disturbance with pressure changes of the order of 2 psi per millisecond (it should be noted that this result is applicable to both positive and negative pressure perturbations).

Thermal Explosion. With some propellants, exothermic reaction is believed to occur in the condensed phase. It was argued by Clemmow and Huffington that, following a pressure decline, the propellant temperature profile adjusted under the influence of external and internal heating until the condensed phase reactions "ran away" and rapidly consumed the heated surface layer of the propellant. Although the external heating conditions assumed in this theory were probably unrealistic, and the assumed condensed phase reactions are only vaguely established, the general mechanism is probably relevant to some double-base propellants. Furthermore, the mechanism draws not only on the thermal lag as a contributor to the pressure rise, but also provides an explanation for the onset of the pressure rise. However, it is significant that low-frequency instabililty similar to that observed by Huffington has also been observed with many solid propellants not exhibiting exothermic condensed phase reactions. Accordingly, it must be assumed that other transient processes can also be involved, and indeed may have been in Huffington's work also.

Surface Accumulation. Frequently it is observed that burning propellants have accumulations of carbonaceous or metallic material on the surface, which may act to aid or impede energy transfer to the surface. Although very little data are available on the rates of accumulation, manner of detachment, or manner of subsequent combustion of accumulated materials, the time constants are typically

in the frequency range 10 to 500 cps. So long as the detachment-combustion process is spatially uncoordinated, the accumulation processes do not contribute to oscillatory behavior. On the other hand, any degree of coordination must lead to fluctuations in mass combustion rate, and to fluctuations in composition and temperature of the exhaust jet and discharge coefficient. The coordination of detachment may be induced by already present pressure fluctuations, or by some "cascading" process in which detachment spreads from initiating sites. Knowledge of the processes involved in these surface accumulation and detachment phenomena is singularly lacking at present, so that their involvement in instability processes is largely speculative at present. However, the occurrence of surface accumulation processes and appropriateness of the time constants to low frequency instability are not in doubt, and the participation in oscillatory combustion is entirely plausible.

Volume Accumulation. During low frequency oscillatory behavior, the pressure during the low pressure part of the cycle is usually low enough so that incomplete reaction of the propellant may occur (i.e., even in steady-state). As a result, the combustion chamber may fill up with an explosive gas mixture, and the external jet may be both explosive and reactive with the atmosphere. The interplay of reaction processes and heat losses in this body of gas may give rise to a thermal explosion similar to that proposed for the solid propellant by Huffington. The "ignition" may occur either inside or outside the combustion chamber, and may provide the impetus for the pressure rise (external ignition will presumably be effective only at low pressures where the nozzle flow is subsonic). This impetus may be amplified by the thermal excess in the solid propellant and by coordinated detachment processes at the propellant surface.

Possibly the most significant aspect of the foregoing speculations about the rising part of the pressure cycle is the relative independence of the arguments on the value of L*. This seems consistent with the observation that, in the class of L* instabilities depicted in Fig. 1, the pressure rise rate is relatively independent of L*. Thus the distinctive features of L* instability will very likely emerge in the pressure decay, with the balance of the cycle being a sort of "recovery process."

SUMMARY

On the basis of steady-state arguments it is shown that the design equilibrium pressure may not be stable in solid rocket motors in which insufficient stay time for combustion of the propellant ingredients is provided. The instability arises from the pressure dependence of the combustion efficiency, with further contributions arising from anomalous burning rate of the propellant under conditions of incomplete combustion. The phenomenon is most likely to be observed in motors designed for low pressure operations and high loading density, characterized by low values of the free volume-to-throat area ratio, L*. The behavior occurs typically during the early part of burning when the free volume and stay times are small, and is more prevalent with propellants having either slow-burning ingredients, such as metal particles, or having incomplete reaction at low pressures.

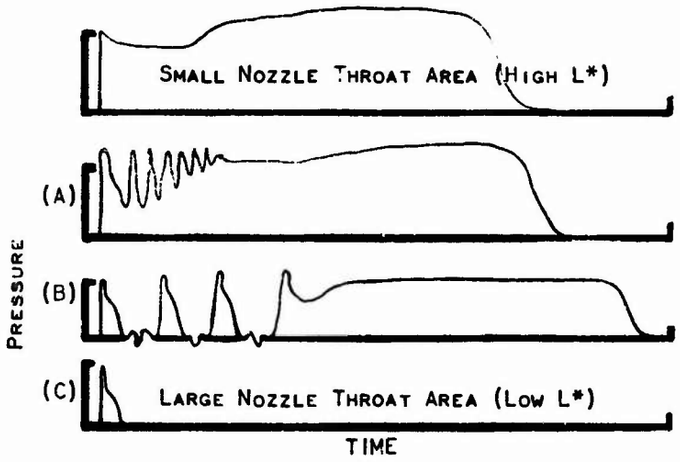

FIG. 1 SKETCHES OF TYPICAL ROCKET MOTOR BEHAVIOR WITH LOW FREQUENCY INSTABILITY, SHOWING THE EFFECT OF INCREASING NOZZLE THROAT AREA AND LOWERING OPERATING PRESSURE

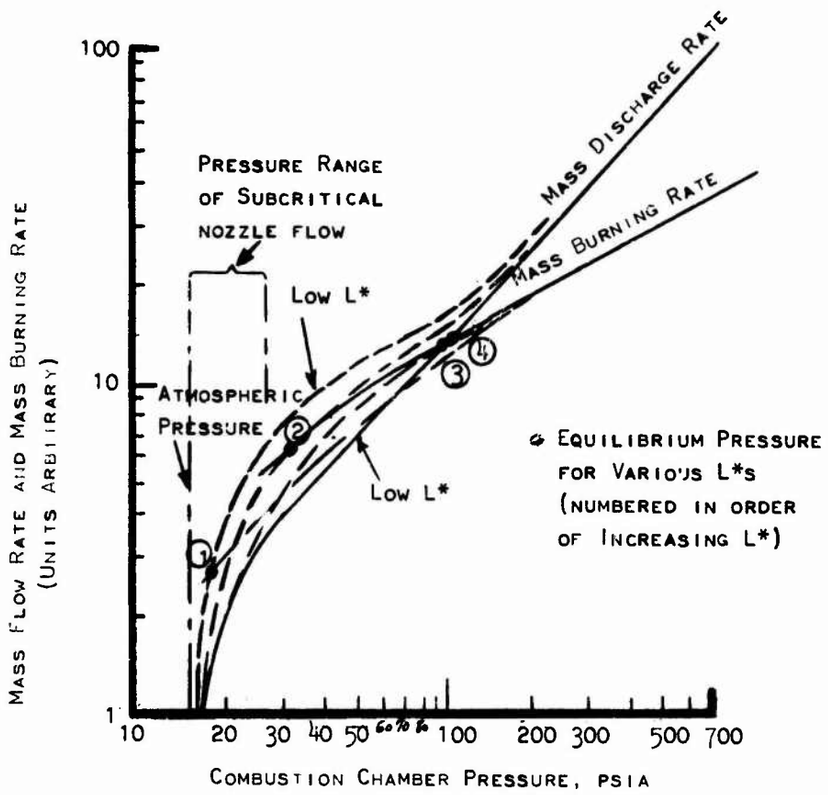

FIG. 2 SKETCH OF MASS RATE CURVES VERSUS PRESSURE ASSUMING QUASI-STEADY CONDITIONS. CURVES FOR LOW L* CORRESPOND TO CONDITIONS OF PRESSURE-DEPENDENT COMBUSTION EFFICIENCY

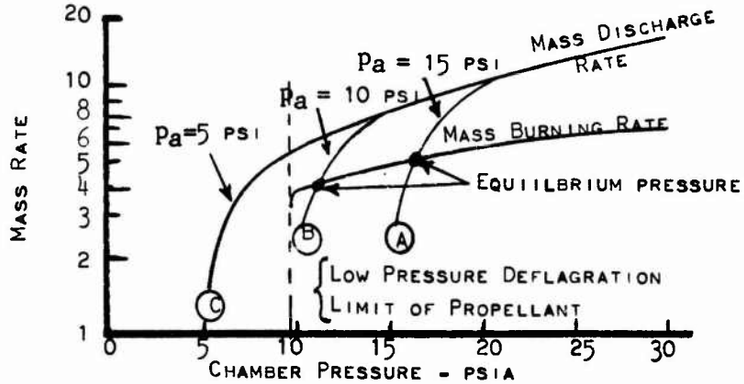

FIG. 3 CURVES OF MASS RATES AT LOW PRESSURES, SHOWING THE EFFECT OF ENVIRONMENTAL PRESSURE ON THE LOW-PRESSURE EQUILIBRIUM POINT

SHOCK WAVE INTERACTION WITH A BURNING PROPELLANT

Vito D. Agosta
Polytechnic Institute of Brooklyn

ABSTRACT

The interaction between a normal shock wave and an end burning solid propellant is analyzed to obtain the characteristics of the reflected shock wave and the attendant effects on the combustion process and heat transferred to the solid propellant. The equations and boundary conditions for shock wave reflection include a variable mass source represented as an exponential burning rate equation, the existence of a contact surface, and solid propellant compressibility, and gas pressure effects on the adiabatic flame temperature. The equations are solved, assuming a hypothetical propellant, for a particular set of initial conditions and a variation in the burning rate exponent.

It is found that the variation in reflected shock wave velocity, and in the pressure ratio across the reflected shock is quite small, about 0.2% and 0.5%, respectively. The greatest change (e.g., about 100%) occurs in the velocity of the contact surface, which as is known, follows particle paths. It is suggested that the contact surface propagation velocity is most suitable for instrumentation. Some phenomenological mechanisms are discussed concerning the value of the burning rate exponent under transient conditions. A short description of an end burning solid propellant rocket motor-shock tube is given.

INTRODUCTION

The purpose of this analysis is to investigate the interaction between a normal shock wave and a burning surface, such as can occur in an end burning solid propellant rocket motor. The single shock reflection problem is assumed since the steady state solution and the normal shock reflection from a plane wall solution offer a reference standard which can easily be verified experimentally. In addition, this analysis can be used as a point of departure for the more difficult cyclic and continuous wave propagation problems. Particular attention is focused on the gas dynamics at the expense of some of the transport processes with the objective of obtaining an insight on the governing mechanisms which influence shock wave behavior. The answers to three questions are sought: (a) What phenomena occur after shock wave reflection from a burning propellant surface; (b) Which of these predicted phenomena are most realistically amenable to instrumentation, and (c) What size equipment is required to observe these phenomena. Based on the theoretical results obtained, a rational approach is suggested in the design of test apparatus and instrumentation.

In general, the reflection of a shock wave from a burning solid propellant surface will affect the burning rate and hence the mass flux into the system. Thus the strength of the reflected shock wave, measured in terms of pressure ratio and wave velocity, will depend on the magnitude of the new burning rate, in addition to the initial shock conditions. The change in mass flux into the system gives rise to the formation of a contact surface, a discontinuity which delineates the higher density gas adjacent to the burning surface from the lower density gas existing behind the reflected shock. The theoretical analysis developed herein includes, in addition to the normal shock relations, the governing relationships across the contact surface, the compressibility and transport properties of the solid propellant, and some of the transport properties of the decomposition and burning zones adjacent to the propellant. Hence, all of these effects are coupled to give the reflected shock wave properties.

SHOCK REFLECTION FROM A BURNING SURFACE ANALYSIS

The introduction of a burning surface upstream of the incident shock is depicted schematically (Fig. 1). Under the conditions described, the upstream absolute gas velocity (u_1) must conform to continuity at the burning surface, namely,

$$\rho_1 u_1 = r_1 \rho_s \ , \tag{1}$$

where r_1 is the initial burning rate and ρ_s the propellant density. In order to solve this equation, a combustion analysis must be made to determine the adiabatic flame temperature. The energy equation is

$$h_s^o = h_1^o = h_1 + (u_1^2/2) \tag{2}$$

and the equations of state

$$P_1 = \rho_1 \frac{RT_1}{M_1} \ . \tag{3}$$

Implicit in these equations are the equilibrium equations required to determine the apparent molecular weight M_1 at the given pressure P_1. Thus, there are three equations and three unknowns (u_1, ρ_1, T_1) and this set can be solved.

The normal shock wave equations are

$$V_1 = u_1 + W_{12} \tag{4}$$

$$V_2 = u_2 + W_{12} \tag{5}$$

$$\rho_1 V_1 = \rho_2 V_2 \tag{6}$$

$$\rho_1 + \rho_1 V_1^2 = \rho_2 + \rho_2 V_2^2 \tag{7}$$

$$h_1 + \frac{V_1^2}{2} = h_2 + \frac{V_2^2}{2} \ . \tag{8}$$

List of Symbols

b	propellant burning rate constant	t	time
c	velocity of sound	t_d	delay time to attain steady-state conditions
c_p	specific heat at constant pressure	t_r	relaxation time for mass adjustment
g	gravitational constant	u	absolute gas velocity (relative to wall)
h	enthalpy	V	gas velocity relative to shock wave
J	mechanical equivalent of heat	$\bar{v}$	average molecular speed
L	heat of sublimation	W	shock wave velocity
M	Mach number	x	linear distance
$\bar{m}$	molecular weight	γ	ratio of specific heats
n	propellant burning rate exponent	θ	sublimation temperature
P	pressure	ρ	density
R	gas constant	ρ_s	propellant density
R_o	universal gas constant		
r	propellant linear burning rate		
T	temperature		

Subscripts

x	upstream of shock	3	downstream of reflected shock
y	downstream of shock	1s	sublimation zone - prior to shock reflection
1	upstream of incident shock	3s	sublimation zone-subsequent to attainment of steady-state conditions
2	downstream of incident shock or upstream of reflected shock		
2*	upstream of reflected shock		

Superscript

' properties behind the contact surface

The equation of state and enthalpy are, respectively,

$$P_2 = \rho_2(RT_2/M_2) \qquad (9)$$

$$h_1 = c_{p_1}T_1 \ (10a); \ h_2 = c_{p_2}T_2 \ (10b) \qquad (10a,b)$$

Finally, the pressure ratio across the shock wave is given:

$$r_p = P_2/P_1 \ . \qquad (11)$$

Thus, there are (V_1, W_{12}, V_2, u_2, ρ_2, P_2, h_1, h_2, T_2) nine equations (4-11) and nine unknowns, and the solution can be found. A knowledge of specific heats and species (via the equilibrium equations) is assumed.

The conditions upon shock reflection are illustrated in Fig.2 where

$$V_2^* = u_2 - W_{23} \qquad (12)$$

$$V_3 = u_3 - W_{23} \ . \qquad (13)$$

A solution to the physical problem requires the existence of a contact surface. A contact surface separates regions of different density and temperature, but equal pressure and velocities, and results from the change in mass flux into the system due to the adjustment in burning rate behind the shock reflection. The assumptions made here are:

1) The propellant burning rate is pressure dependent.
2) The propellant is homogeneous and the burning rate is uniform over the entire burning surface.
3) Adjustments due to transients resulting from shock interaction with the burning surface have occurred (i.e., in burning rate, gas velocity, pressure, etc.) and steady state conditions have been achieved.

The contact surface is parallel to the particle trajectory and originates at the propellant surface at some time $t = t_r$ (where t_r is the inner relaxation time for the start of contact surface formation). The base reference time $t = 0$ is taken when the incident shock strikes the propellant surface. For the properties across the contact surface we have

$$P_3' = P_3 \qquad u_3' = u_3 \qquad T_3' \neq T_3 \qquad \rho_3' \neq \rho_3 .$$

The continuity condition is employed to relate the adjusted burning rate after shock reflection to gas properties behind the contact surface, namely,

$$\rho_3' u_3' = r_3 \rho_s . \tag{14}$$

A burning rate equation for the conditions is assumed in the form

$$r = b p^n \tag{15}$$

where the exponent n is not necessarily related to that obtained from steady state tests due to different temperature history in solid propellant before and after shock wave reflection,

$$r_1 = b P_1^n \tag{16}$$

$$r_3 = b P_3^n . \tag{17}$$

Continuity at the burning surface and the burning rate equation is combined to relate the contact surface velocity u_3' $(= u_3)$ to the gas velocity upstream of the incident shock u_1. Hence, using Eqs. (1), (14), (16), and (17), we have

$$\frac{u_3'}{u_1} = \left[\left(\frac{P_2}{P_1}\right)\left(\frac{P_3}{P_2}\right)\right]^{n-1} \left(\frac{R_3'}{R_1}\right)\left(\frac{T_3'}{T_1}\right) . \tag{18}$$

Eq. (18) exhibits an interdependency between the velocities (u_1 and u_3) and the strength of both the incident and reflected shock.[1] Moreover, the solution for reflected shock strength will be dependent on the burning rate exponent n, the ratio of combustion flame temperature T_3'/T_1, and gas constant (or molecular weight) R_3'/R_1. For given incident shock conditions and a specified burning rate exponent n, the change in combustion flame temperature and gas constant must be estimated before these relations can be used.

In order to estimate T_3' it is assumed that an increase in stagnation emthalpy of the solid propellant occurs due to isentropic compression and is equal to the work of compression done by the combusting gas downstream of the reflected shock surface. Hence, for the solid we have:

$$Tds = dh - vdP = 0 \tag{19}$$

or

$$\Delta h^o_{solid} \cong \Delta h^o_{gas} = \frac{\Delta P^o}{\rho_s J} . \tag{20}$$

For the low absolute gas velocities encountered in regions 1 and 3' we further assume

$$\Delta h^o_{gas} \cong \Delta h_{gas} = \frac{\Delta P}{\rho_s J} . \tag{21}$$

The effect of pressure on combustion temperature and gas constant can be obtained from the above expression for enthalpy increase. With these parameters determined, the reflected shock pressure ratio, shock velocity, density ratio and gas velocity u_3' can be calculated as a function of the burning rate exponent n.

The equations to be solved reduce to the continuity equation:

$$\frac{\rho_3}{\rho_2} = \frac{W_{23} - u_2}{W_{23} - u_3} , \tag{22}$$

the continuity and momentum equation,

$$(u_2 - W_{23})^2 = \frac{P_2 g}{\rho_2} \left[\frac{\frac{P_3}{P_2} - 1}{1 - \frac{\rho_2}{\rho_3}} \right] , \tag{23}$$

the Rankine-Hugoniot equation,

$$\frac{\rho_3}{\rho_2} = \frac{\left(\frac{\gamma+1}{\gamma-1}\right) \frac{P_3}{P_2} + 1}{\frac{P_3}{P_2} + \left(\frac{\gamma+1}{\gamma-1}\right)} , \tag{24}$$

and Eq. (18).

For illustrative purposes the following set of initial conditions are specified for this investigation:

propellant composition - $CH_{48}N_{16}O_8$ (hypothetical)

propellant density (ρ_s) - 50 lb/ft^3

incident shock strength (P_2/P_1) - 1.50

specific heat ratio (γ) - 1.23

initial temperature (T_1) - 4320°R (2400°K)

initial pressure (P_1) - 300 psia

initial burning rate (r_1) - 0.3 inches/sec.

For a first approximation (in determining T_3'/T_1) we estimate that the strength of the reflected shock (P_3/P_2) is equal to the incident shock strength (P_2/P_1). Then,

$$P_3 \cong P_1(P_2/P_1)^2 = 300(1.5)^2 = 675 \text{ psia};$$

hence, from Eq. (21),

$$\Delta h_{gas} = \frac{P_3 - P_1}{\rho_s J} = 1.388 \text{ BTU/lb.}$$

From the Hottel Charts for $CH_{48}N_{16}O_8$ at $T_1 = 4320°R$ and $P_1 = 300$ psia,

$$h_{300}^{4320} = 7387.508 \text{ BTU/lb.}$$

Therefore,

$$h_{675}^{T_3'} = h_{300}^{4320} + \Delta h_{gas} = 7388.900 \text{ BTU/lb.}$$

Using linear interpolation in the tables of the Hottel Charts, we obtain the combustion temperature after shock reflection

$$T_3' = 4333°R,$$

which yields a temperature ratio

$$\frac{T_3'}{T_1} = 1.003.$$

The effect of the increased pressure behind the reflected shock on gas constant (or molecular weight) can also be obtained from the Hottel Charts, namely, at $P_3 = 675$ psia,

$$R_3' = 124.266 \text{ ft/°R},$$

which yields a gas constant ratio

$$\frac{R_3'}{R_1} = 1.004.$$

With the temperature ratio and gas constant ratio known, Eqs. (18), (22), (23), and (24) can be solved numerically to obtain the reflected shock conditions.

A result is the variation in reflected shock pressure ratio with the burning rate exponent. This variation is presented graphically in Fig. 3, together with the value for plane wall reflection and the incident shock pressure ratio. It can be seen that for $n > 0.92$ the reflected shock strength from the burning surface will exceed the value of reflected shock strength for plane wall reflections (note, from either a stationary or moving boundary). Indeed, for $n \geq 3.0$ the reflected shock pressure ratio is greater than the incident shock pressure ratio. Conversely, for $n < 0.92$, the reflected shock strength is less than the shock reflecting from a plane wall. Any set of conditions (i.e., P_2/P_1, P_3/P_2, n, T_3'/T_1, R_3'/R_1) which result in a velocity ratio u_3'/u_1 equal to unity, will yield a reflected shock strength equal in magnitude to a plane wall reflection. For a velocity ratio $u_3'/u_1 > 1$, a stronger shock reflection will be obtained, and for $u_3'/u_1 < 1$ a weaker reflection will result. It should be noted that for a burning rate exponent of unity, Eq. (18) becomes

$$\frac{u_3'}{u_1} = \left(\frac{T_3'}{T_1}\right)\left(\frac{R_3'}{R_1}\right) \qquad n = 1 \qquad (25)$$

and the strength of the reflected shock compared to the case of plane wall reflection is entirely dependent upon the combustion temperature and gas constant ratios. For the conditions specified in this investigation the product of $(T_3'/T_1)(R_3'/R_1)$ results in a one per cent change in velocity ratio u_3'/u_1. For stronger incident shock pressure ratios (and hence stronger reflected shocks) the effect of the combustion temperature and gas constant ratios on the velocity ratio u_3'/u_1 will be greater. It is apparent, however, that the magnitude of the reflected shock strength is determined primarily by the value of the burning rate exponent (for $n \neq 1$). Table 1 summarizes the results for various values of the burning rate exponent n between 0.3 and 3.0, and includes for comparison purposes the solution for plane wall shock reflection with initial conditions identical to those specified above. As Table I indicates, for n varying between 0.3 and 3.0, the velocity ratio u_3'/u_1 varies between 0.58 and 5.10, yielding considerably larger changes than that induced by the product of combustion temperature and gas constant ratios. While r_3 will always exceed the initial burning rate r_1(0.3 inches per second) for any $n > 0$, the absolute gas velocity downstream of the shock reflection (i.e., the contact surface velocity $u_3' = u_3$) can be less than the initial gas velocity u_1. This is explained by the increased density behind the contact surface (ρ_3') and conforms

to the continuity equation (14). Table I shows the variation in contact surface velocity from 8.92 fps to 78.90 fps as n varies between 0.3 and 3.0.

As in the case of plane wall reflections, the reflected shock velocity is less than the incident shock velocity. However, for all values of the burning rate exponent n, the reflected shock velocity is greater than the reflected shock velocity from a plane wall (stationary boundary). It should be noted that the incident shock approaches the burning surface at a lower velocity than the incident shock approaching the plane wall, that is:

$$W_{12_{\text{burning surface}}} < W_{12_{\text{plane wall}}} \tag{26}$$

but

$$W_{23_{\text{burning surface}}} > W_{23_{\text{plane wall}}} . \tag{27}$$

An x-t diagram for the case of a shock reflection from a burning surface is presented in Fig. 4.

In order to discuss the temperature distributions throughout the system a model of the combustion zone structure is first established. The propellant and combustion zone model chosen consists of four adjoining regions: 1) the solid propellant, 2) the sublimation zone, 3) the decomposition zone, and 4) the deflagration zone. These zones are illustrated schematically in Fig. 5 (not to scale). The temperature distribution as a function of linear distance before and after shock reflection is also presented qualitatively.

The increased combustion temperature in the deflagration zone after shock reflection is representative of T_3'. While the illustrative example examined in Fig. 5 yielded only a 13°R increase for an incident shock strength of 1.50, a larger increase should be expected for stronger incident shocks. Moreover, the magnitude of combustion temperature increase will be dependent on the propellant composition and density under consideration and the pressure effect on combustion (adiabatic flame) temperature. The temperature in the sublimation zone is affected by the sudden increase in pressure behind the shock reflection. Assuming that thermodynamic equilibrium exists, the change in the sublimation temperature due to the increased pressure can be obtained with the Clausius-Claperon relation,

$$\frac{dP}{d\theta} = \frac{L\rho}{\theta} , \tag{28}$$

where L is the heat of sublimation and ρ the density of the gaseous phase. Assuming $P = \rho R\theta$, Eq. (28) becomes

$$\frac{dP}{d\theta} = \frac{L P \bar{m}}{R_o \theta^2} . \tag{29}$$

Separating variables and integrating, we obtain

$$\int_{P_1}^{P_3} \frac{dP}{P} = \frac{L\bar{m}}{R_o} \int_{\theta_{1s}}^{\theta_{3s}} \frac{d\theta}{\theta^2}$$

or

$$\frac{1}{\theta_{1s}} - \frac{1}{\theta_{3s}} = \frac{\left\{ \ln\left(\frac{P_3}{P_2}\right)\left(\frac{P_2}{P_1}\right) \right\} R_o}{L\bar{m}} \quad . \tag{30}$$

For thermodynamic equilibrium the Clausius-Claperon equation relates the adjusted sublimation temperature after shock reflection to the initial sublimation temperature θ_{1s}, the propellant properties (i.e., heat of sublimation and molecular weight), and the strength of both the incident and reflected shocks. Thus, the analytical method described above for calculating the magnitude of the reflected shock strength also provides the means of obtaining the boundary conditions for the adjusted temperature distribution after steady-state conditions have been achieved. It should be noted that the temperature distribution in an opaque solid propellant is largely unaffected by the combustion process due to its poor thermal conductivity.

For large molecular weight gases, the specific heat ratio approaches 1.00; therefore the temperature ratio behind a strong shock approaches 1.00. It is assumed for the case where thermodynamic equilibrium exists at the sublimating surface that an increase in heat transfer rate is mainly due to the compression or greater density of the gases near the propellant surface, e.g., the temperature gradient near the surface increases directly vs. the density ratio (or pressure ratio) and exponentially due to the increase in the collision frequency term in the reaction rate equation. From this simple-minded consideration a conservative estimate can be made of the increased heat transfer to the wall and the subsequent burning rate exponent n. It can be found that the obtained heat flux does not permit thermodynamic equilibrium to exist at the wall. For this case the method for the propagation of a freezing surface can be applied.

The importance of the following consideration is to determine the physical size of test equipment required to observe the results predicted theoretically. The higher temperature distribution in the combustion zones is consistent with the increased burning rates experienced after shock reflection (see Table 1 - r_3/r_1). It is apparent, however, as is described in Fig. 6, that the burning rate does not adjust instantaneously to the disturbance caused by the shock reflection. While the burning rate relation $r = bP^n$ correlates burning rate and pressure adequately for steady state, it is assumed that it is essentially the increased temperatures that generate

higher reaction rates and mass decomposition. Indeed, as will be discussed later, not even the pressure behind the shock reflection (P_3) reaches its final steady-state value instantaneously. The pressure does, however, affect the temperature distribution by causing an increased heat transfer rate (i.e., by increasing the heat transfer coefficient due to the aforementioned density effects).

The variation in propellant burning rate with time is shown qualitatively in Fig. 6. Two distinct time intervals are indicated, namely, the relaxation time t_r and the delay time t_d. The relaxation time t_r is the time delay between the incident shock striking the propellant surface and the start of burning rate adjustment. This time is also indicative of the start of formation of the contact discontinuity. The delay time t_d is the time required for the system to attain steady-state conditions. Hence, as shown in Fig. 6, the propellant burning rate continuously varies between t_r and t_d.

To estimate an order of magnitude of the relaxation time t_r, it is assumed that no adjustment in burning rate can occur until a heat wave, subsequent to the shock reflection, reaches the solid surface (i.e., passes through the decomposition zone). It is further assumed that the wave propagates with a velocity equal to the average molecular speed as given by kinetic theory:

$$\bar{v} = \left(\frac{8}{\pi} RT\right)^{1/2} . \qquad (31)$$

The data from Denton, et al. (1) was utilized to obtain an estimate of the thickness of the decomposition zone and the distance downstream of the propellant surface where the adiabatic flame temperature is reached in the deflagration zone. These distances are 0.2 mm and 1.0 mm, respectively. This also provides a representative order of magnitude of temperature at the start of the deflagration zone of 720°R. Applying Eq. (31), a $\bar{v}$ = 470 fps is obtained at a distance 0.2 mm downstream of the propellant surface and a $\bar{v}$ = 6635 fps at a distance of 1.0 mm. Hence, two estimates of t_r are obtained, namely, 0.495 microseconds and 1.396 microseconds, respectively. It is significant that these values are of the same order of magnitude, as it is indicative that the start of burning rate adjustment will occur within 1/2 and 1 1/2 microseconds after shock reflection.

The delay time t_d to attain steady-state conditions is dependent upon flow field interactions, heat transfer effects, and thermochemical reactions, the analysis of which is beyond the scope of this discussion. However, the flow field transients occurring until steady-state conditions are achieved can be examined on an x-t plane. This will provide some insight into the mechanisms that determine the results obtained for the steady-state analytical solution. Figure 7a depicts the actual transient case while Fig. 7b illustrates a somewhat simplified model. During the transient time t_d (but after t_r) the burning rate is increasing from its initial value r_1 to its final or steady-state value r_3. With each incremental change in mass flux into the system a contact surface is formed. Hence, a contact zone rather than a single contact surface is created during the

transition to steady-state conditions (Fig. 7a). The model depicted in Fig. 7b assumes a coalescence of each individual contact surface within the zone, or more specifically, the formation of a single contact surface after the delay time t_d. The change in density and temperature across the single contact surface of Fig. 7b can then be considered equivalent to the summation of these property changes across each individual contact surface within the contact zone.

It was pointed out that for gas velocity ratios $(u_3'/u_1) > 1$, the reflected shock strength from a burning surface will exceed the value of reflected shock strength for plane wall reflections (note, from either a stationary boundary $u_3' = u_1 = 0$, or from a moving boundary $u_3' = u_1 \neq 0$). It is apparent that this reinforcement in shock strength is due to a series of compression waves interacting with the reflected shock during the period $t = t_r$ to $t = t_d$, as shown in Fig. 7a. While the actual process consists of a series of incremental amplifications, Fig. 7b depicts the overall amplification as a single reinforcement. Hence, the initial shock reflection at $t \cong 0$ will be equal in strength to a plane wall reflection and subsequently amplified by compression wave reinforcement. This also serves to explain the increase in reflected shock velocity compared to the plane wall case. Namely, each interaction between a generated compression wave and the reflected shock will amplify not only the shock strength, but also its velocity. This result is shown in Figs. 7a and 7b by the increased slope of the reflected shock trajectory.

In addition, it was observed that for velocity ratios $(u_3'/u_1) < 1$, the reflected shock pressure ratio was less than that which would result from a plane wall reflection. This relative attenuation in reflected shock pressure ratio is the result of interactions with rarefaction waves generated at the propellant surface and overtaking the initial shock reflection. Thus, as above, the initial shock reflection is equal in strength to a plane wall reflection, but for $(u_3'/u_1) < 1$ it is attenuated by being overtaken by rarefaction waves, rather than being amplified by compression waves. As the results of the illustrative problem indicated, although the pressure ratio is attenuated, the reflected shock velocity is not. That is, the reflected shock velocity was in all cases greater than the reflected shock velocity from the plane wall. It should be noted that the actual amplification or attenuation process will start some time after $t = t_r$, and will be a function of the time required for the compression of rarefaction waves to overtake the reflected shock. The process continues until $t = t_d$, where steady-state conditions are achieved, and no further adjustment in shock strength or burning rate is encountered.

An experimental test rig (see Fig.8), for the purpose of analyzing shock interactions with a burning propellant, is at present under construction at the Polytechnic Institute of Brooklyn Graduate Center facility in Farmingdale, New York. The shock tube is approximately five feet in length and 1.6 inches in inside diameter. Additional sections can be used to lengthen this chamber. An explosive charge, or gas driver, will generate the incident shock and drive it against an end burning propellant at the opposite end of the chamber. From the results of the illustrative problem (see Table 1) it can be

observed that for incident shock pressure ratios of 1.5 or less, standard pressure tap instrumentation will be insufficient. Under these conditions the difference in pressure behind the shock reflection between a burning surface and plane wall reflection are not discernible. Temperature probes and/or Schlieren photographic techniques will both afford the ability to detect the contact surface due to the large temperature and density changes across this boundary. With the contact surface velocity determined, the mass addition and shock velocity after shock reflection can be calculated and compared to the theoretical value predicted by the analytical techniques above. Finally, any change in shock velocity, pressure ratio, or temperature ratio subsequent to reflection would be indicative of the amplification or attenuation process described above. The chamber length to be used will provide a test duration of several milliseconds.

It is significant to observe the existence of contact surfaces and the concomitant small waves following the reflected shock wave as the theory herein predicts. It is noted that the contact surface will be generated within several microseconds after the shock wave reflection and, due to its low velocity, will be observable near the burning propellant. As it propagates downstream, diffusion effects will cause its boundaries to become undistinguishable. In addition, the determination of the relaxation time t_d, both theoretically and ultimately experimentally, will prescribe the minimum shock tube length required to observe changes in the reflected shock wave strength and, indeed, whether steady-state conditions can be attained in a reasonably-sized shock tube.

ACKNOWLEDGEMENTS

The author wishes to acknowledge with great pleasure the assistance of Mr. Sheldon Pinsley, who worked on the analysis of shock wave behavior; of Mr. Howard Schusterman, who carried out the design of the solid propellant rocket motor-shock tube and who checked it out experimentally, and of Mr. Gerald DiLauro, a participant in the National Science Foundation-Undergraduate Science Education Program, who assisted in the design of the shock tube.

REFERENCES

1. Denton, E., Needham, D., and Powling, J., "The Flame Decomposition of Ethyl Nitrate," Explosives Res. and Dev. Establishment, Rept. 7/R/53, Ministry of Aviation, United Kingdom, April 1953.

TABLE 1. Reflected Shock Characteristics as a Function of Burning Rate Exponent

Parameter	Units	n=0.3	n=0.6	Plane Wall Reflection	n=1.00	n=1.50	n=3.00
P_3/P_2	-	1.47561	1.47648	1.47767	1.47801	1.48079	1.50115
$\frac{P_3/P_2}{P_2/P_1}$	-	0.98374	0.98432	0.98511	0.98534	0.98719	1.00017
r_3	$\frac{in.}{sec.}$	0.3803	0.4833	--	0.6651	0.9930	3.4219
r_3/r_1	-	1.2677	1.6110	--	2.2170	3.3100	11.4063
W_{23}	$\frac{ft.}{sec.}$	4183.11 (+)→	4184.71 (+)→	4174.55 (+)→	4187.50 (+)→	4192.53 (+)→	4229.23 (+)→
W_{23}/W_{12}	-	0.75610	0.75639	0.75245	0.75689	0.75780	0.76444
u_3'	$\frac{ft.}{sec.}$	8.92 (+)→	11.33 (+)→	15.47	15.57 (+)→	23.21 (+)→	78.90 (+)→
u_3'/u_1	-	0.58	0.73	1.00	1.01	1.50	5.10
ρ_3/e_2	-	1.37021	1.37086	1.37175	1.37200	1.37407	1.38920
T_3/T_2	-	1.07692	1.07705	1.07722	1.07727	1.07767	1.08058
P_3	$P_{S_{I_A}}$	664.02	664.42	664.95	665.10	666.36	675.52
T_3	°R	5026.43	5027.04	5027.82	5028.05	5029.93	5043.51
e_3	$\frac{lb}{ft^3}$	0.15372	0.15379	0.15385	0.15392	0.15415	0.15585
e_3'	$\frac{lb}{ft^3}$	0.17764	0.17774	$= e_3$	0.17792	0.17826	0.18071

Initial Conditions

$P_2/P_1 = 1.50$
$T_1 = 4320°R$
$\gamma = 1.23$
$P_1 = 300$ psia
$e_s = 50$ lb/ft^3
$CH_{48}N_{16}O_8$
$R_1 = 123.789$ ft/°R
$r_1 = 0.3$ in/sec

Computed

$u_1 = 15.47$ ft/sec (+)→
$e_1 = 0.08081$ lb/ft^3
$u_2 = 1536.41$ ft/sec (-)←
$e_2 = 0.11219$ lb/ft^3
$T_2 = 4667.41°R$
$P_2 = 450$ psia
$W_{12} = 5532.49$ ft/sec (-)←
$W_{12} = 5547.96$ ft/sec (plane wall)← (-)
$T_3' = 4333°R$
$R_3' = 124.266$ ft/°R

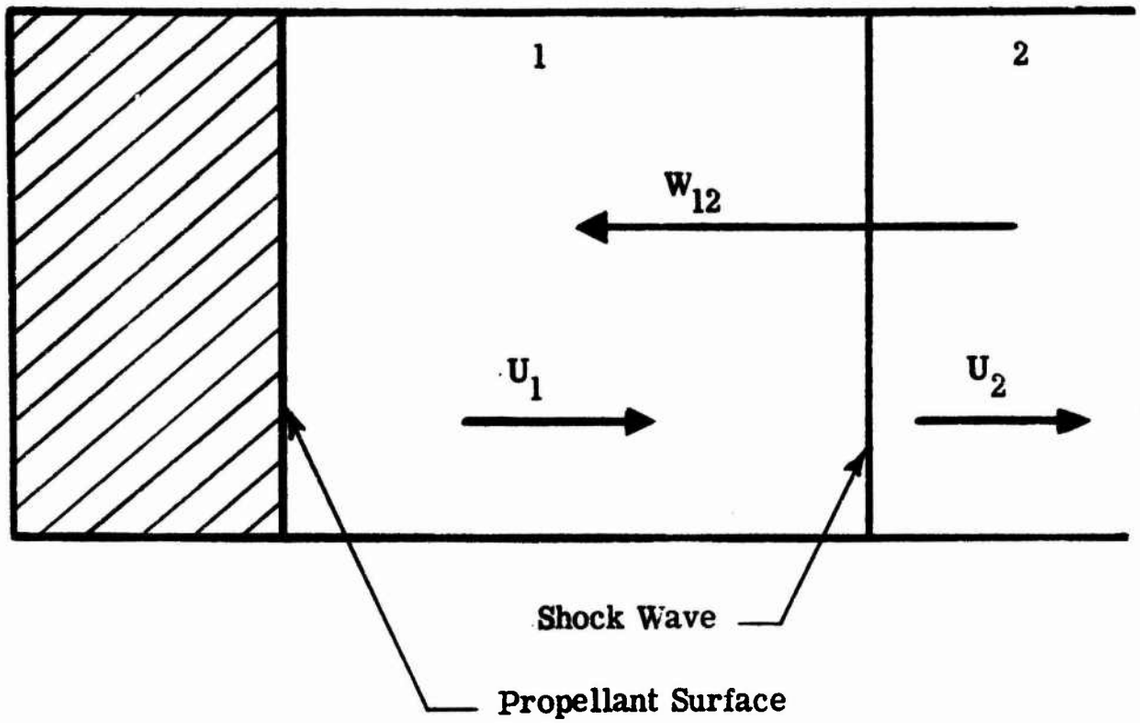

Fig. 1 INCIDENT SHOCK WAVE

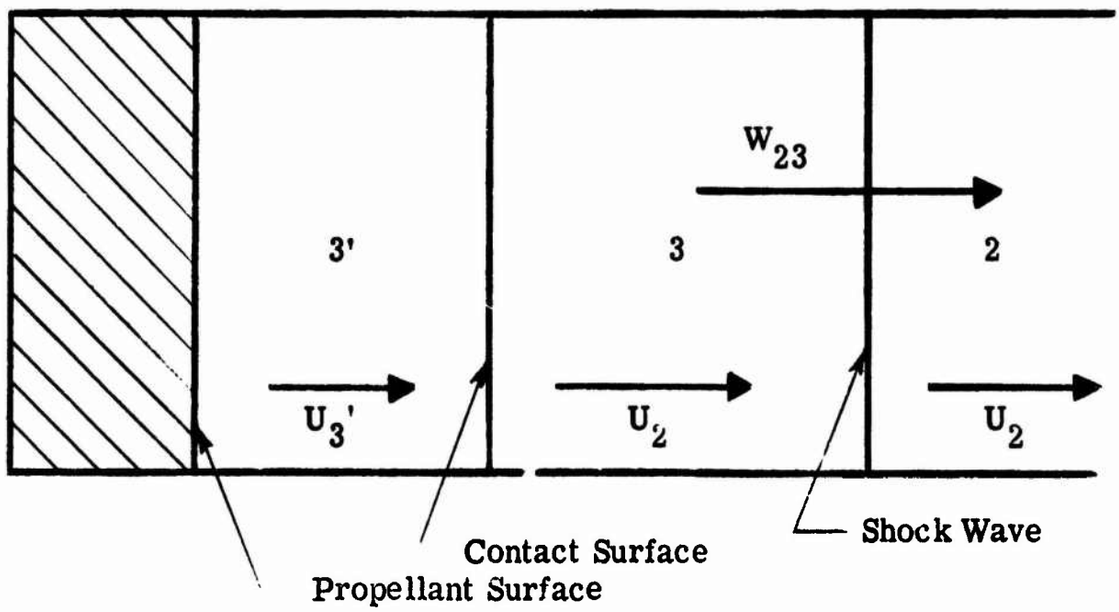

Fig. 2 REFLECTED WAVE

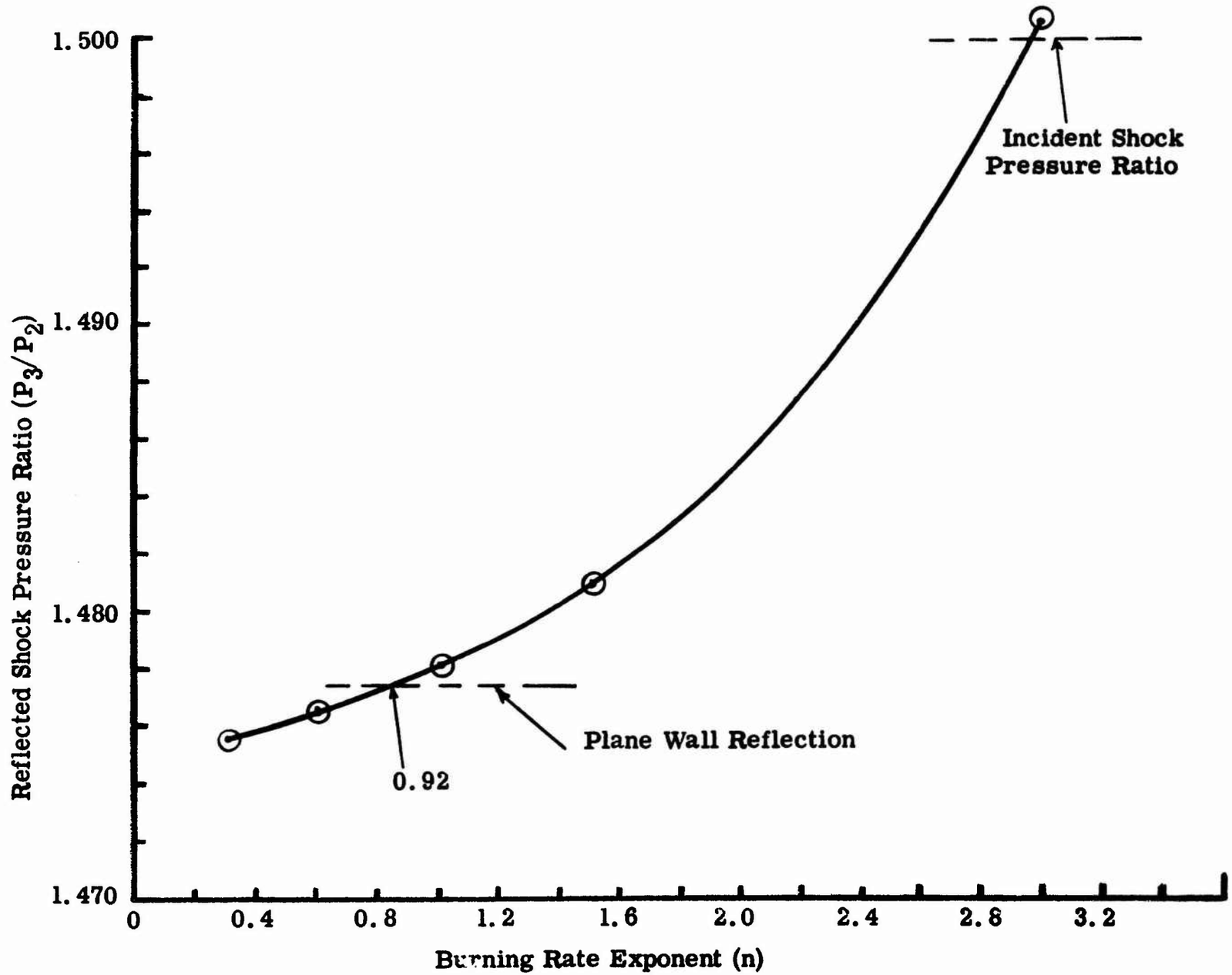

Fig. 3 REFLECTED SHOCK PRESSURE RATIO (REFLECTION FROM BURNING SURFACE)

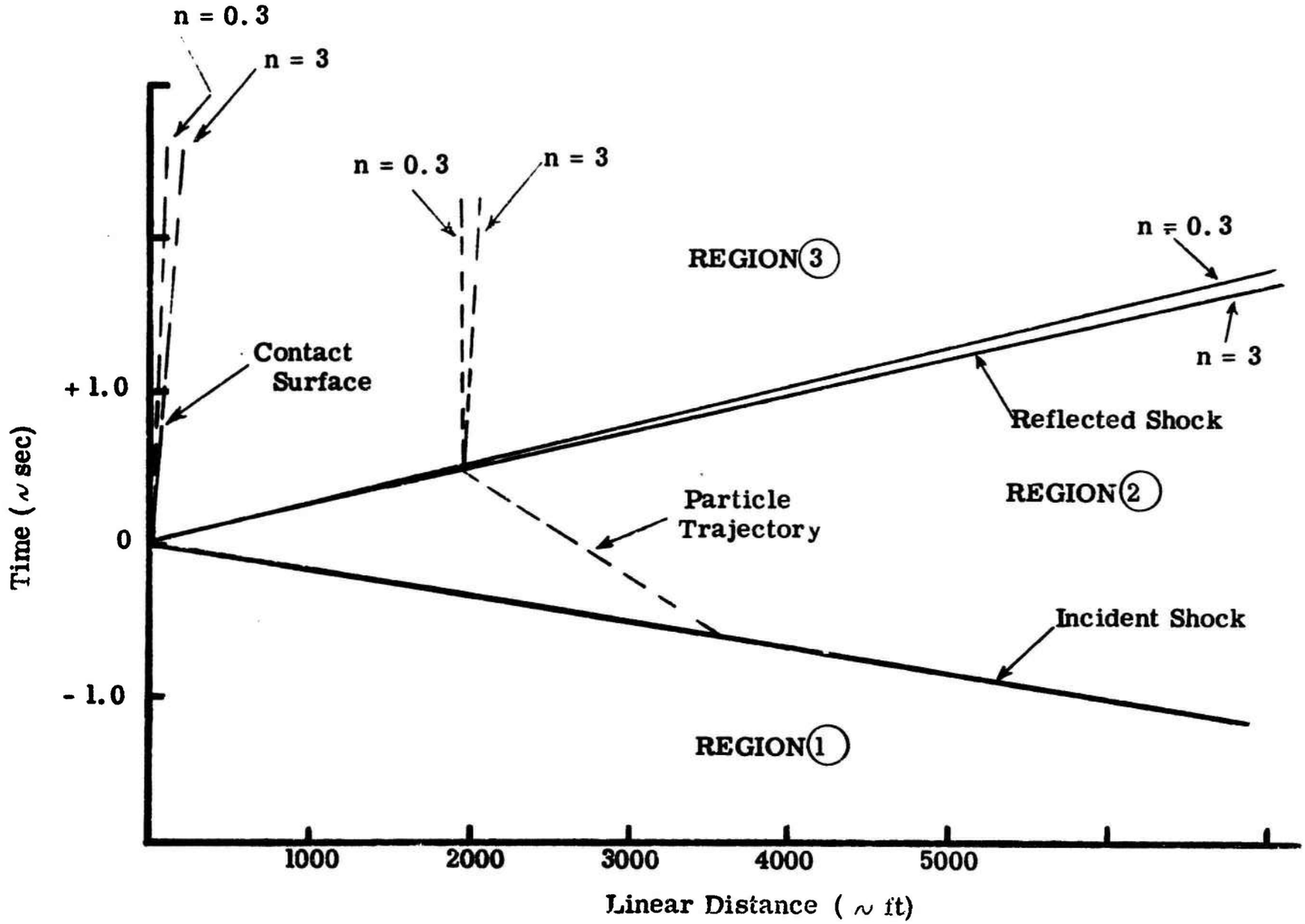

Fig. 4 x - t DIAGRAM FOR SHOCK REFLECTION

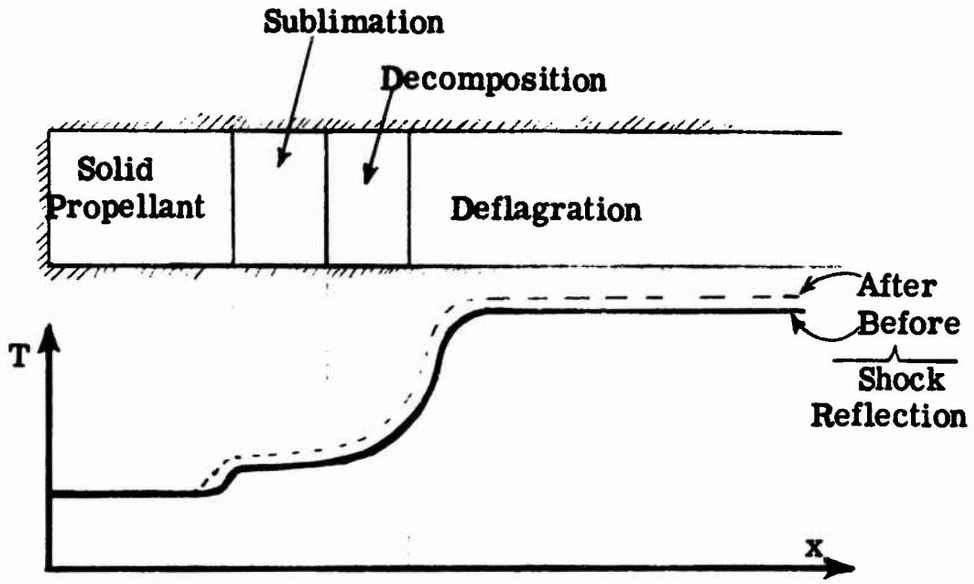

Fig. 5 COMBUSTION ZONES AND TEMPERATURE DISTRIBUTIONS

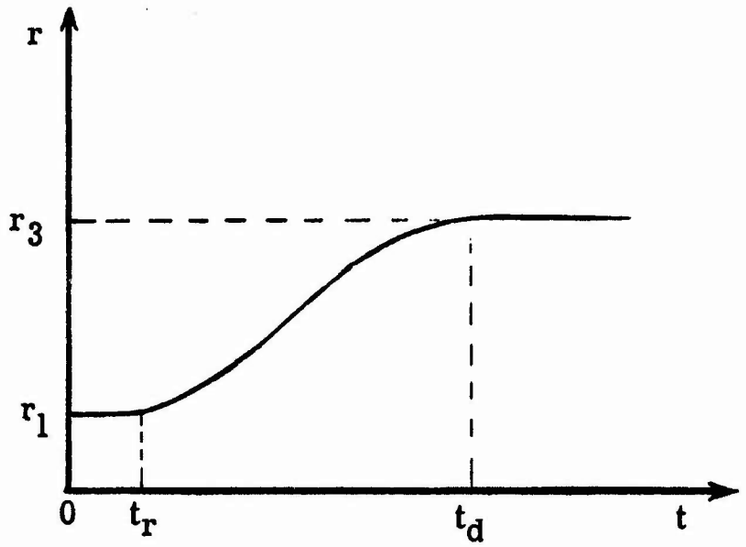

Fig. 6 VARIATION IN PROPELLANT BURNING RATE

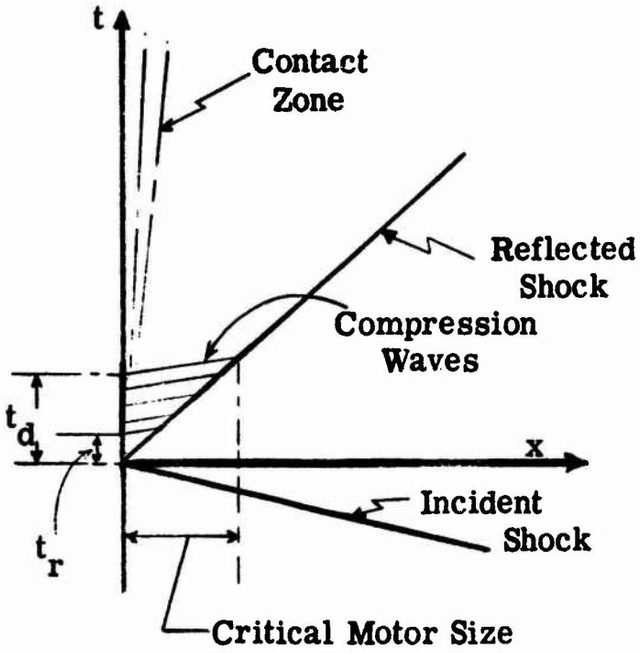

Fig. 7a TRANSIENT EFFECTS

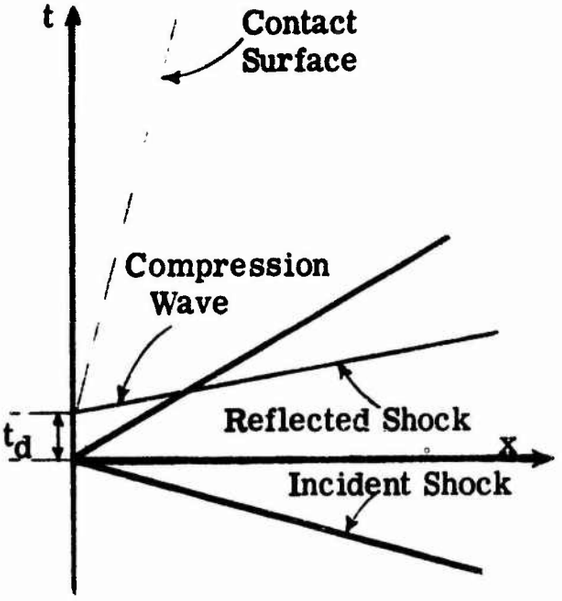

Fig. 7b TRANSIENT EFFECTS (Model)

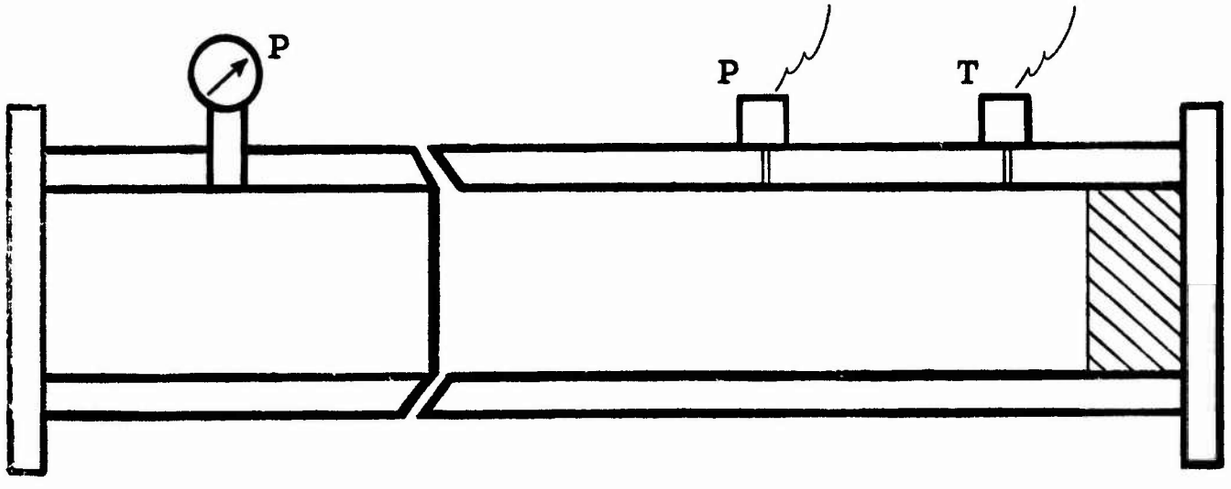

Fig. 8 SOLID PROPELLANT ROCKET MOTOR (SHOCK TUBE-END BURNING)

ANALYTICAL INVESTIGATION OF THE BURNING MECHANISM OF SOLID ROCKET PROPELLANTS*

T. Paul Torda, W. J. Christian, Fred L. Schuyler,
and
Richard H. Snow

Armour Research Foundation
of
Illinois Institution of Technology
Chicago, Illinois

FLUID DYNAMIC MODEL

(T. Paul Torda, W. J. Christian, and Fred L. Schuyler)

INTRODUCTION

The aims of these investigations are severalfold. They are first, to analyze existing theories of the burning mechanism of solid rocket propellants for the purpose of extending them to include non-steady phenomena, if such extension is possible, second, to extend these existing theories to include non-steady burning, and third, if such an extension is not possible, then to develop a steady-state analysis based on fluid dynamic principles and including thermochemical processes, with the ultimate aim of extension to include non-steady regression rate prediction.

Evaluation of available theories of burning mechanisms of solid rocket propellants has shown that due to the simplifying assumptions made, extension to include non-steady phenomena is not feasible. The efforts on this contract toward this first aim were discussed during the presentation at the Second Meeting of the Technical Panel. During this discussion, the model employed in our approach and also the basic equations, together with the method of solution, were discussed. A brief review will be helpful at this point.

It is important to bear in mind that our efforts to develop an analytical method for the investigation of the burning mechanism of solid rocket propellants have to be done in two phases. The first is to establish a steady-state model and analysis which describe in sufficient detail the fluid mechanics and thermochemical phenomena. Once this is successful, the extension of this approach to non-steady phenomena can be made. No proven method exists for the numerical solution of the non-linear set of second order partial differential equations involved. Initially (and for quite some time) we had difficulties with the stability of the solutions. However, this problem has been overcome and we have obtained smooth and reasonable results.

*This work supported by the Advanced Research Projects Agency (ARPA).

Last year, we presented the model (Fig. 1), and these figures are still valid with the possible modification that the temperature boundary layer or the concentration boundary layer may be much thinner than the momentum boundary layer. The conservation equations which represent the velocity, temperature, and concentrations for the two-dimensional flow of combustion products over a plane propellant surface are those originally presented (Eqs. 1-5). Equation (6) shows the boundary conditions at the solid gas interface, and Eq. (7) gives the expression of the propellant regression rate (i.e., an Arrhenius-type law). It should be noted that the radiative energy transfer to the solid is neglected, but this assumption may be removed if desired. The viscous energy dissipation is negligible and this term is not included in the energy equation.

Continuity:

$$\frac{\partial \rho u}{\partial x} + \frac{\partial \rho v}{\partial y} = 0 \tag{1}$$

$$\rho u \frac{\partial \alpha_i}{\partial x} + \rho v \frac{\partial \alpha_i}{\partial y} = \frac{\partial}{\partial y}\left[\frac{Le}{c_p} k \frac{\partial \alpha_i}{\partial y}\right] + w_i \tag{2}$$

Momentum:

$$\rho u \frac{\partial u}{\partial x} + \rho v \frac{\partial u}{\partial y} = -\frac{\partial p}{\partial x} + \frac{\partial}{\partial y}\left(\mu \frac{\partial u}{\partial y}\right) \tag{3}$$

Energy:

$$\rho\left(u\frac{\partial h}{\partial x} + v \frac{\partial h}{\partial y}\right) = \frac{\partial}{\partial y}\left(\frac{k}{c_p}\frac{\partial h}{\partial y} - \frac{k}{c_p}[Le-1]\sum_i h_i \frac{\partial \alpha_i}{\partial y}\right) \tag{4}$$

$$\dot{r}\frac{\partial T}{\partial y} + \alpha_s \frac{\partial^2 T}{\partial y^2} = 0 \quad . \tag{5}$$

Here, α_s is thermal diffusivity of the solid and $\dot{r}$ is the rate of recession of the burning surface. It is presumed here that the zone of phase change and chemical reaction in the solid is very thin and may be regarded as a surface heat sink insofar as the heat conduction in the solid is concerned. Accordingly, conditions at the solid-gas interface are described by the following heat balance:

$$k\left(\frac{\partial T}{\partial y}\right)_s = \left(k\frac{\partial T}{\partial y}\right)_g - \rho_s \dot{r} Q_p \Big|_{y=0} \tag{6}$$

$$\dot{r} = \left(Ae^{-B/T}\right)_{y=0} \tag{7}$$

where

c_p is constant pressure heat capacity of the mixture

h is enthalpy of mixture ($\sum_i \alpha_i h_i$)

h_i is enthalpy of i^{th} component

k is thermal conductivity

Le is Lewis number

p is pressure

Q_p is heat absorbed in gasification of the solid

$\dot{r}$ is regression rate

w_i is rate of production of i^{th} component by chemical reaction

α_s is thermal diffusivity of the solid

α_i is concentration of i^{th} component

μ is viscosity

ρ is density

and supscripts s and g refer to solid and gas, respectively.

In the two-dimensional steady-state boundary layer analysis, a number of questions concerning the numerical stability of the equations arise. In addition, the coupling between the chemical kinetics and the fluid flow presents the question of the minimum kinetic representation which will adequately describe the energy production process. In order to investigate these questions, a one-dimensional computer program was developed which represents the flow in the direction away from the surface only, and neglects any variation in the direction parallel to the surface. This approach is motivated by the fact that neglecting the variation parallel to the surface reduces the boundary layer equations to a set of ordinary differential equations for which adequate numerical methods are readily available. Although boundary-layer thicknesses cannot be determined, the questions mentioned above can still be investigated.

The program is initially coded using the identical formulation to that of the first annual report, except that all deviations with respect to x are set equal to zero.

Formulation of the computer code is sufficiently general that a large number of chemical reactions may be included. First results have been obtained for a one-step, second-order reaction in order to obtain some feeling for the kinds of solutions involved. Figure 2 shows temperature and concentration profiles obtained from the one-dimensional program. Rate expressions used here are based on estimates of frequency factors and activation energies for an ammonium perchlorate composite propellant. Figure 3 shows the results obtained using a lower activation energy in the solid phase.

These are just two examples of the results of the two-dimensional analysis. We shall use this analysis to discover as much as possible, concerning the effect of the various parameters on the burning rate and its pressure sensitivity. Ultimately, we shall

want to incorporate a chemical kinetic model for an actual propellant. Our investigation of the kinetics associated with nitrocellulose burning will provide the necessary input. Pending completion of that, however, we intend to utilize the kinetics of a well-known reaction, such as the hydrogen-oxygen reaction, to further study the character of the solutions to the one-dimensional system.

To increase the confidence in the results obtained, the two-dimensional computations have been made in two phases. The first computations have used the continuity, momentum, and energy equations to calculate the case for laminar boundary-layer development with constant property values for a porous wall with variable temperature and mass injection. However, no chemical reactions have been included. This was done because exact solutions for this case are available.

A comparison between the numerical solution obtained from the computer, and the exact analytical solution is shown in Fig. 4. The good agreement gives one confidence to proceed with solutions involving chemical reactions. A preliminary result of a two-dimensional calculation is shown in Fig. 5. Estimated kinetic expressions used in the one-dimensional calculations have been used here, and an erosion velocity of 200 ft/sec has been imposed.

It is emphasized that the results presented are of preliminary nature and serve only to indicate the general behavior of the numerical solutions. In the coming months extensive experimentation with the computer model will be undertaken.

PLANS

The one- and two-dimensional computations will be continued with successive refinements as the nitrocellulose combustion analysis progresses. With these results, which are discussed in Dr. Snow's paper, we hope to fulfill the first phase of our efforts, that is, the reliable analysis of a fluid mechanic process combined with chemical kinetic thermochemical processes. Thus, the erosion and pressure sensitivity of the regression rate will be established for the steady case. Immediately following will be the non-steady analysis, which is a modification of the two-dimensional analysis in that the time-dependent terms are included in the equation.

THEORY OF COMBUSTION INSTABILITY - CHEMICAL KINETICS

Richard H. Snow

The chemical kinetics of cellulose nitrate burning is being studied as a model for the investigation of solid rocket propellant combustion instability. These are two chemical problems: the partial decomposition of the solid to give gaseous products, and the burning of these gases in a flame above the surface. The solid decomposition is believed to be controlled by splitting off of nitrate groups. The products are oxides of nitrogen and aldehydes. Most

attention has so far been given to the gaseous reaction. A set of 46 simultaneous free radical reactions has been postulated, based on a study of published information on the types of reactions involved. A computer program is being developed to calculate reaction rate and products for any set of simultaneous reactions. It is currently being tested on a subset of 15 important reactions under constant temperature conditions. It will later be incorporated into the over-all combustion calculation scheme, including heat and mass transfer and fluid flow.

The following reactions comprise the proposed formaldehyde-nitrogen dioxide mechanism:

1) $HCHO + NO_2 \rightleftharpoons \dot{C}HO + HNO_2$

2) $\dot{C}HO + NO_2 \rightleftharpoons \dot{H} + CO$

3) $HNO_2 \rightleftharpoons \dot{O}H + NO$

4) $CC - \dot{O}H \rightleftharpoons CO_2 + \dot{H}$

5) $\dot{C}HO + NO_2 \rightleftharpoons CO + HNO_2$

6) $HCHO + \dot{O}H \rightleftharpoons \dot{C}HO + H_2O$

7) $HCHO + \dot{H} \rightleftharpoons \dot{C}HO + H_2$

8) $HNO_2 + \dot{O}H \rightleftharpoons H_2O + NO_2$

9) $NO_2 + \dot{C}HO \rightleftharpoons HC\dot{O}O + NO$

10) $HC\dot{O}O + NO_2 \rightleftharpoons HNO_2 + CO_2$

11) $HC\dot{O}O + \dot{C}HO \rightleftharpoons HCOOH + CO$

12) $NO_2 + \dot{H} \rightleftharpoons \dot{O}H + NO$

13) $\dot{C}HO + \dot{O}H \rightleftharpoons HCOOH$

14) $\dot{C}HO + \dot{O}H \rightleftharpoons CO + H_2O$

15) $\dot{C}HO + \dot{H} \rightleftharpoons H_2 + CO$

The mechanism involves the four radicals $\dot{C}HO$, $\dot{O}H$, $\dot{H}$, and $HC\dot{O}O$. Calculations show that steady state concentrations of these radicals are established. The last radical appears to be unimportant.

The more complete mechanism includes reactions of 2-carbon aldehydes. Particularly important are the reactions of the radicals $CH_3\dot{C}O$ and $\dot{C}H_3$, which are analogous to $\dot{C}HO$ and $\dot{H}$. An additional reaction sequence is

$$NO + \dot{C}H_3 \longrightarrow CH_3NO \longrightarrow CH_2NOH \longrightarrow HCN,\ CH_3CN.$$

This sequence explains the production of cyanides in cellulose nitrate combustion. The analogous sequence

$$NO + \dot{H} \longrightarrow NOH \longrightarrow \ldots$$

is also included.

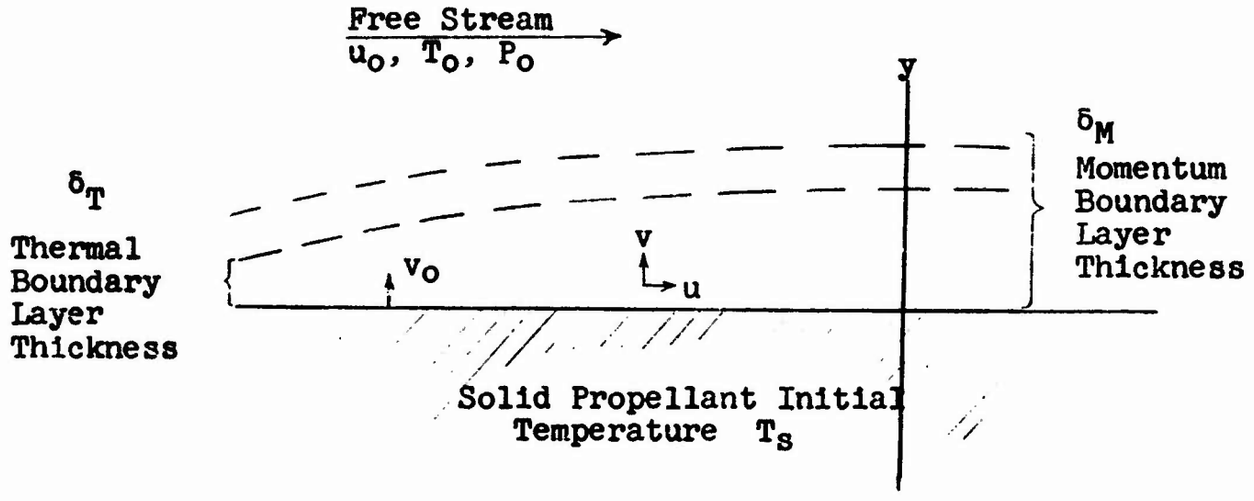

Fig. 1a. SCHEMATIC REPRESENTATION OF THE BOUNDARY LAYER CONTROL

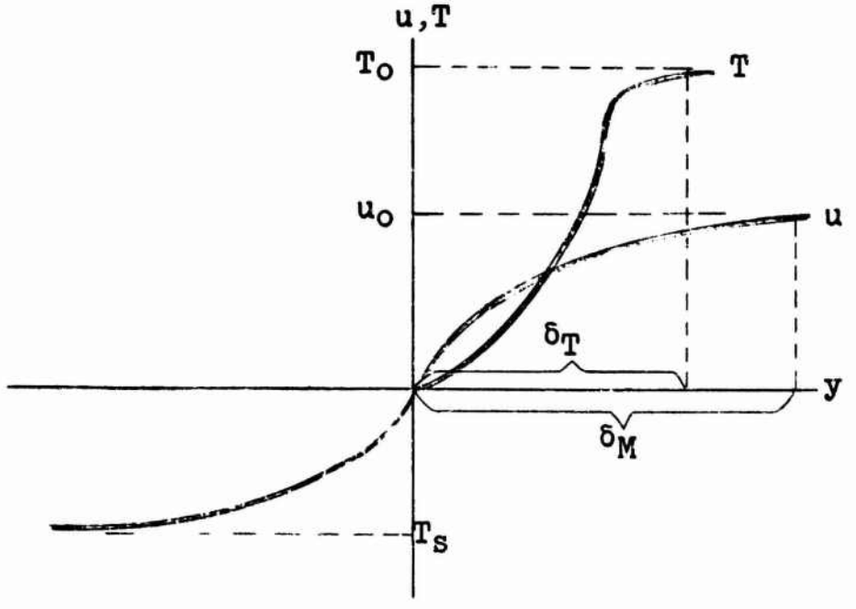

Fig. 1b. TYPICAL PROFILES OF TEMPERATURE AND VELOCITY

Fig. 2 PRELIMINARY RESULTS OF NUMERICAL SOLUTION FOR SOLID PROPELLANT COMBUSTION WITHOUT EROSION

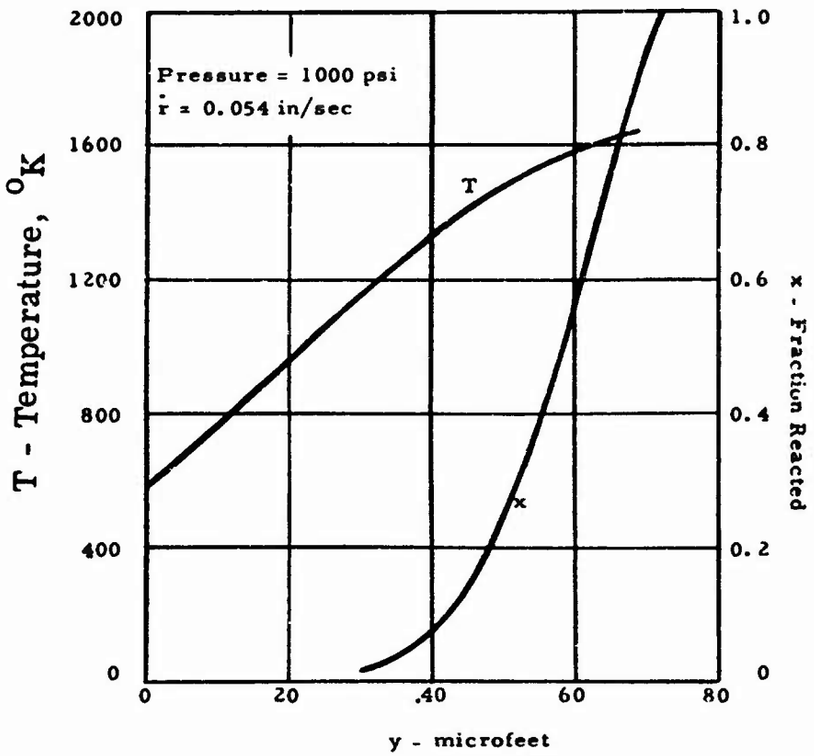

Solid Vaporization: $\dot{r} = 10 \exp(-8000/T)$
2nd Order Gas Reaction: $k_r = 3.1 \times 10^{12} \exp(-12,000/T)$

Fig. 3 PRELIMINARY RESULTS OF NUMERICAL SOLUTION FOR SOLID PROPELLANT COMBUSTION WITHOUT EROSION

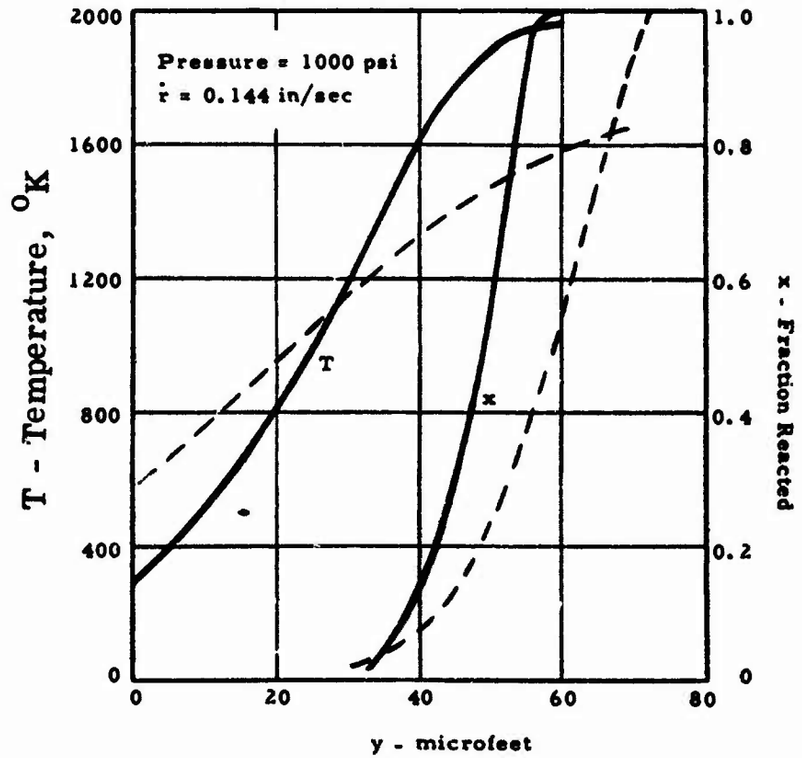

Solid Vaporization: $\dot{r} = 10 \exp(-3600/T)$
2nd Order Gas Reaction: $k_r = 3.1 \times 10^{12} \exp(-12,000/T)$

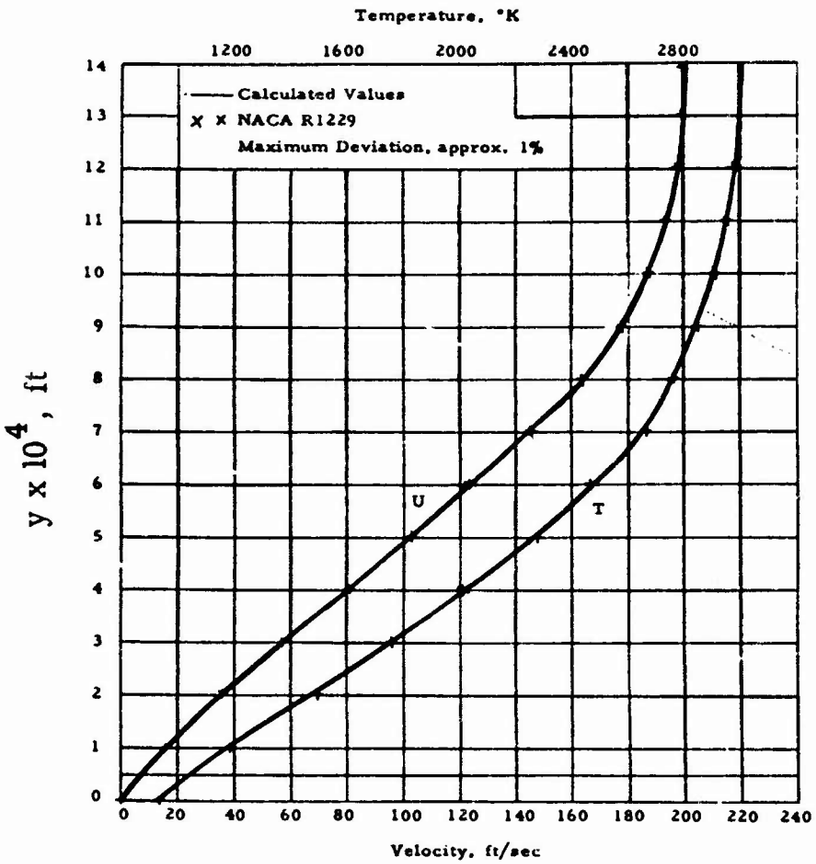

Fig. 4 COMPARISON OF NUMERICAL RESULTS WITH EXACT SIMILARITY SOLUTION FOR CONSTANT PROPERTIES BOUNDARY LAYER WITH HEAT AND MASS ADDITION.

Fig. 5 PRELIMINARY RESULTS OF NUMERICAL SOLUTION FOR TWO-DIMENSIONAL STEADY FLOW OVER BURNING SOLID PROPELLANT.

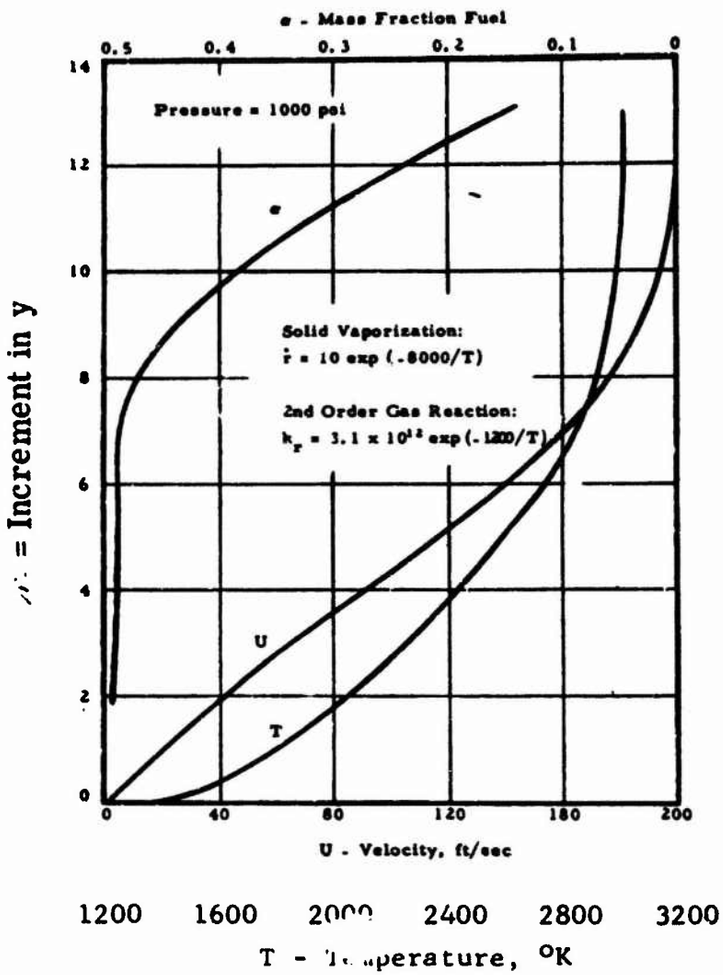

PROGRAM

3rd Meeting, Combustion Instability Panel
5th AFOSR Contractors' Meeting on Solid Propellant Combustion
March 4,5,6, 1963

March 4 (Classified Session) - 9:45AM

R. Lawhead (Rocketdyne)	-	Instabilities in Liquid Rocket Engines
J. B. Levy (ARC)	-	Research on the Deflagration of a High-Energy Solid Oxidizer
T. A. Angelus (ABL)	-	Studies of Low Frequency Instability in CMDB Propellants

(Unclassified Session)

W. Cohen (NASA)	-	The Large Solid Motor Program
M. D. Horton (NOTS)	-	Effect of Propellant Variables on Response Function
F. T. McClure (APL)	-	Comments on above
R. C. Strittmater (BRL)	-	Latest Experiments at BRL on Acoustic Admittance Measurements
N. W. Ryan (U. Utah)	-	Oscillatory Burning Studies
S. N. Foner (APL)	-	APL Experimental Program

March 4 (Unclassified Session) - 2:15PM

T. A. Angelus (ABL)	-	Acoustic Instability Studies
R. H. Cantrell (APL)	-	Acoustic Loss Theory
R. B. Lawhead (Rocketdyne)	-	Physical Processes of Solid Propellant Combustion
G. M. Muller (SRI)	-	Acoustic Admittance Measurements
G. R. Leader (Thiokol)	-	Experiments for the Measurements of the Acoustic Impedance of a Burning Solid Propellant
H. F. Calcote (AeroChem)	-	Acoustic Wave Burning Zone Interaction in Solid Propellants
W. G. Brownlee (CARDE)	-	CARDE Experiments on Non-Linear Axial Combustion Instability

March 4 (Unclassified Session) - 2:15PM (Continued)

E. W. Price (NOTS)	- Experimental Investigation of Intermediate and Low Frequency Combustion Instability
A. O. Converse (Carnegie Inst.)	- Dynamic Response in Presence of Low-Frequency Instability

March 5 (Unclassified Session) - (9:45AM)

G. P. F. Trubridge (ICI)	- Progress of Work at Summerfield Research Station and the University of Sheffield
I. Dyer (Bolt Beranek & Newman)	- The Effect of Flow on Burning Instability
E. W. Price (NOTS)	- Theory of L* Combustion Instability
V. D. Agosta (Brooklyn Poly.)	- Shock Interaction with Burning Surface
P. Torda (Armour)	- Theory of Combustion Instability
T. L. Smith (SRI)	- Response of Propellants to Different Types of Mechanical Excitation
R. Friedman (ARC)	- Measurement of Complex Dynamic Shear Compliance of Composite Propellants
A. S. Elder (BRL)	- Current Work On Viscoelastic Properties
L. Green (Lockheed)	- Determination of Complex Compliance of Propellants

March 5 (Unclassified Session) - 2:15PM

L. Watermeier (BRL)	- Experiments on Acoustic Erosivity Effects on Propellant Burning Rates
E. W. Price (NOTS)	- Effect of Acoustic Environment on Propellant Burning Rate
M. D. Horton (NOTS)	- Mechanism of Suppression of Oscillatory Burning by Aluminum Additives
W. Nachbar (Lockheed)	- Experiments with a Solid Propellant Acoustic Oscillator
M. Summerfield (Princeton)	- Solid Propellant Combustion Under Oscillatory Pressure
F. F. Liu (Quantum-Dynamics)	- Instrumentation Techniques for Solid Combustion Research

March 6 (Unclassified Session) - 9:45AM

C. Ciepluch (NASA)	-	Solid Propellant In-House Research at NASA Lewis Research Laboratory
W. Nachbar (Lockheed)	-	Steady and Unsteady Burning of Solids
S. Sibbett (Aerojet)	-	Investigations of the Mechanisms of Decomposition, Combustion, and Detonation of Solids
D. Fleischer (RMI)	-	Tracer Method for Determination of Solid Propellant Burning Rates
J. Osborn (Purdue)	-	Continuous Measurements of Solid Propellant Burning Rates
H. Wight (Aeronutronics)	-	Reflection and Scattering of Sound by Gaseous Flames

March 6 (Unclassified Session) - 2:15PM

M. Evans (SRI)	-	Detonation Characteristics of Low Density Granular Materials
R. Friedman & L. Fagg (ARC)	-	High-Pressure Plasma Production Technique
T. Acker (Radiation Applications)	-	Radiation Induced Solid Propellant Decomposition
A. Baer (U. Utah)	-	Ignition and Burning of Solid Propellants
M. Summerfield (Princeton)	-	Fluid Dynamic Aspects of Solid Propellant Ignition
M. Summerfield (Princeton)	-	Solid Propellant Ignition Transient

ATTENDANCE

Terese Acker
Radiation Applications, Inc.

*Vito D. Agosta
Polytechnic Inst. of Brooklyn

Ralph Anderson
United Technology Corp.

*T. A. Angelus
Allegany Ballistics Laboratory

A. Baer
University of Utah

*Walter G. Berl
Applied Physics Laboratory
The Johns Hopkins University

Joseph F. Bird
Applied Physics Laboratory
The Johns Hopkins University

David T. Blackstock
General Dynamics/Electronics

Carl Boyars
Naval Ordnance Lab., White Oak

Theodore Brownyard
Bureau of Naval Weapons

Maj. W. G. Brownlee
C.A.R.D.E., Quebec,
Canada

*H. F. Calcote
Aerochem Research Labs., Inc.

R. H. Cantrell
Applied Physics Laboratory
The Johns Hopkins University

Larry W. Carlson
Rocketdyne, Canoga Park

*S. I. Cheng
Princeton University

H. Cheung
Aerojet General Corp., Sacramento

H. C. Christensen
Naval Ordnance Test Station

William J. Christian
Armour Research Foundation

Ralph Coates
Hercules Powder Co.
Bacchus Works

*William Cohen
National Aeronautics and Space Administration

*A. O. Converse
Carnegie Inst. of Technology

Carl Ciepluch
National Aeronautics and Space Administration, Cleveland

R. Comer
Ballistic Research Labs.

Lionel Dickinson
Stanford Research Inst.

*Ira Dyer
Bolt, Beranek and Newman, Inc.

Gunther von Elbe
Atlantic Research Corp.

A. Elder
Ballistic Research Labs.

John F. Engler
Lockheed Missiles and Space Co.,
Palo Alto

Marjorie Evans
Stanford Research Inst.

D. Fleischer
Reaction Motors Div.
Thiokol Chemical Corp.

---

*Member, Panel on Solid Propellant Combustion Instability (SPIC)

ATTENDANCE (Cont'd)

S. N. Foner
Applied Physics Laboratory
The Johns Hopkins University

*J. H. Frazer
Ballistic Research Labs.

*R. Friedman
Atlantic Research Corp.

Winston Gin
National Aeronautics and Space Administration

*Leon Green, Jr.
Lockheed Propulsion Co.

*R. W. Hart
Applied Physics Laboratory
The Johns Hopkins University

*Robert J. Heaston
Advanced Research Projects Agency

M. D. Horton
Naval Ordnance Test Station

Roland Jackel
Office of Naval Research
Washington

Irving Jaffe
Naval Ordnance Lab., White Oak

Oliver H. Johnson
Bureau of Naval Weapons

*E. M. Landsbaum
Aerospace Corp.

Robert B. Lawhead
Rocketdyne, Canoga Park

Evan K. Lawrence
Naval Ordnance Lab., White Oak

*Gordon R. Leader
Thiokol Chemical Corp.
Elkton Division

Joseph B. Levy
Atlantic Research Corp.

*Frederick F. Liu
Quantum-Dynamics

Stanley Mathews
Allegany Ballistics Lab.

William J. Marciniak
Bureau of Naval Weapons

*Joseph F. Masi
AF Office of Scientific Research

Robert F. McAlevy
Stevens Inst. of Technology

*F. T. McClure
Applied Physics Laboratory
The Johns Hopkins University

George Muller
Stanford Research Institute

S. N. B. Murthy
Purdue University

*William Nachbar
Lockheed Missiles and Space Co.,
Palo Alto

Lt. Walter Niessen
AF Rocket Research Labs., Edwards

George Odian
Radiation Applications, Inc.

J. R. Osborn
Purdue University

Louis Povinelli
National Aeronautics and Space Administration, Cleveland

*E. W. Price
Naval Ordnance Test Station

*Ralph Roberts
Office of Naval Research,
Washington

ATTENDANCE (Cont'd)

*Norman W. Ryan
University of Utah

Karl Scheller
AF Aeronautical Research Lab.

Fred L. Schuyler
Armour Research Foundation

Robert Sehgal
Jet Propulsion Lab.

William E. Sheehan
Office, Secy. of Defense

D. J. Sibbett
Aerojet General Corp., Azusa

*Thor L. Smith
Stanford Research Institute

Richard Snow
Armour Research Foundation

J. G. Sotter
Sheffield University
England

R. Strittmater
Ballistic Research Lab.

*Martin Summerfield
Princeton University

*R. J. Thompson, Jr.
Rocketdyne, Canoga Park

*G. F. P. Trubridge
Imperial Metal Industries, Ltd.

Richard Waesche
Princeton University

*L. A. Watermeier
Ballistic Research Labs.

Joseph Wenograd
Princeton University

Peter Westervelt
Bolt, Beranek and Newman, Inc.

H. M. Wight
Aeronutronic

*G. H. Wolfhard
Reaction Motors Div.,
Thiokol Chemical Corp.

B. T. Wolfson
Air Force Office of Scientific Research

W. A. Wood
Rohm and Haas Co.

Raymond Yount
Allegany Ballistics Lab.

PANEL MEMBERS UNABLE TO ATTEND

David Altman
United Technology Corp.

J. A. Chalmers
Army Material Command

L. Crocco
Princeton University

J. Diederichsen
Rocket Propulsion Establishment
(U.K.)

H. W. Emmons
Harvard University

F. Jackson
Canadian Armament Research
and Development Establishment

PANEL MEMBERS UNABLE TO ATTEND (Cont'd)

G. Markstein
Cornell Aeronautical Lab.

P. L. Nichols
Aerojet General Corp., Sacramento

Dana Peckworth, USN
Special Projects Office

B. G. Sage
California Inst. of Technology

H. Shanfield
Aeronutronic

H. M. Shuey
Rohm and Haas Co.

Irving Silver
Bureau of Naval Weapons

Paul Torda
Armour Research Foundation

M. J. Zucrow
Purdue University